UNITED STATES
NUCLEAR REGULATORY COMMISSION
WASHINGTON, D. C. 20555

February 17, 1987

Docket Nos. 50-275/323

MEMORANDUM FOR: Document Control Desk

FROM: Hans Schierling, Project Manager
Project Directorate #3
Division of PWR Licensing-A

SUBJECT: DIABLO CANYON LONG TERM SEISMIC PROGRAM (LTSP)

The enclosed package of documents on the LTSP was received by the Project Manager on February 10, 1987 from Pacific Gas and Electric Company. The documents are identified an the enclosed list. Please place the documents and the list in the docket file for Diablo Canyon Unit 1, Docket No. 50-275, and arrange for a copy to be placed in the NRC PDR and the Local PDR.

for Paulette Smith
Hans Schierling, Project Manager
Project Directorate #3
Division of PWR Licensing-A

Enclosure:
As stated

cc: Reg File w/o enclosure

H001 Add: NSIC Ltr Encl
1 1
1/1 Hans Schierling 1 0

LIST OF PG&E LTSP-SSI DATA PACKAGES TRANSMITTED TO NRC

I. Data Package A - Additional Materials Presented at the NRC/PG&E LTSP-SSI Workshop on 12/10-12/86.

1. Comparisons of Results between CLASSI and SASSI Solutions

2. Summary of Description for Analyses of Recorded Earthquake Data and Correlation with Analytical Models.

3. Viewgraphs of presentation for Incorporation of Incoherent Ground Motions in SSI Analyses.

4. Viewsgraphs of presentation for Nonlinear SSI Analysis for Base Uplifting.

II. Data Package B - Structural and Foundation Model Properties for the DCPP Containment Structure used in the LTSP-SSI Parametric Studies

1. Fixed-Base containment structure model properties and natural vibration modal properties

2. CLASSI surface-supported foundation model and impedance functions for containment

3. SASSI surface-supported and embedded foundation models and impedance functions for containment.

4. Listing and diskette of the Hosgri time history used in the parametric studies for the containment structure.

III. Data Package C - References Requested by the NRC Consultants on the Studies of Incoherent Ground Motions.

1. Loh, C. H. and Penzien J., "Identification of Wave Types, Directions, and Velocities Using SMART-1 Strong Motion Array Data," The 8th World Conference of Earthquake Engineering, San Francisco, 1984.

2. Loh, C. H., Penzien, J., and Tsai, Y. B., "Engineering Analysis of SMART-1 Array Accelerograms," Earthquake Engineering and Structural Dynamics, Vol. 10, 1982.

3. King, J. L., "Observations on the Seismic Response of Sediment-Filled Valleys," Ph.D. Dissertation, University of California, San Diego, 1981.

4. Lilhanand, K., and Tseng, W. S., "Direct Generation of Probabilistic Floor Response Spectra," Bechtel Power Corporation Technical Report No. SFPD-C/S-83-07, December 1983.

COMPARISONS BETWEEN CLASSI AND SASSI SOLUTIONS

CONTAINMENT STRUCTURE

SURFACE FOUNDATION

- o VERTICAL SV - WAVE
- o INCLINED SV - WAVE 30° FROM VERTICAL

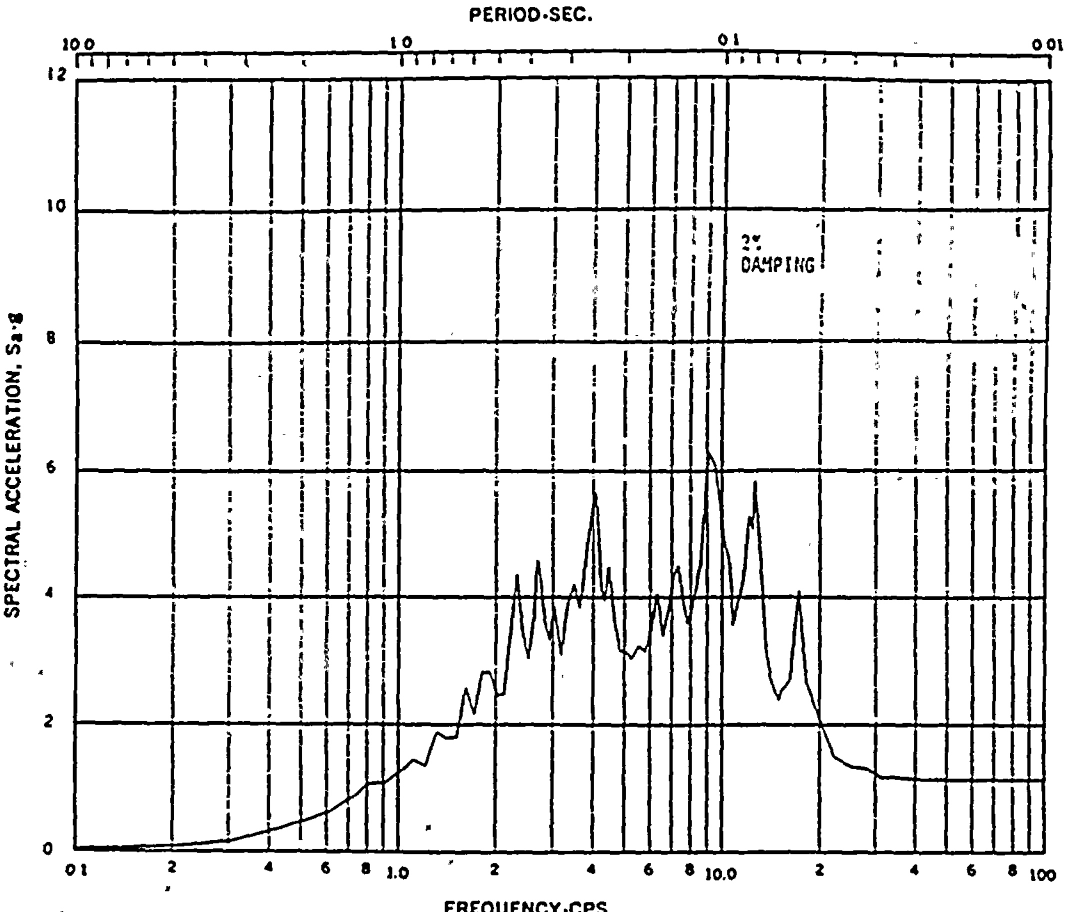

CONTAINMENT (TOP OF INTERNAL) - SURFACE FOUND. - VERTICAL SV
(CLASSI)

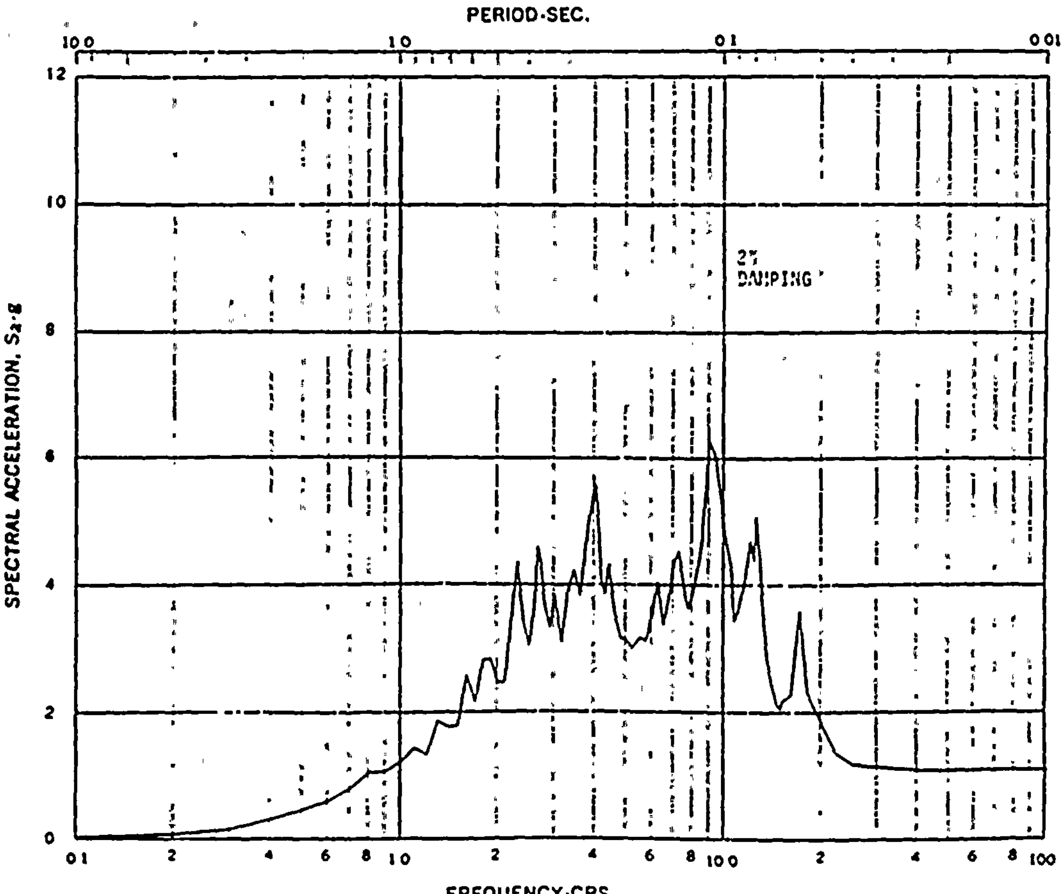

CONTAINMENT (TOP OF INTERNAL) - SURFACE FOUND. - VERTICAL SV
(SASSI CASE CSC1)

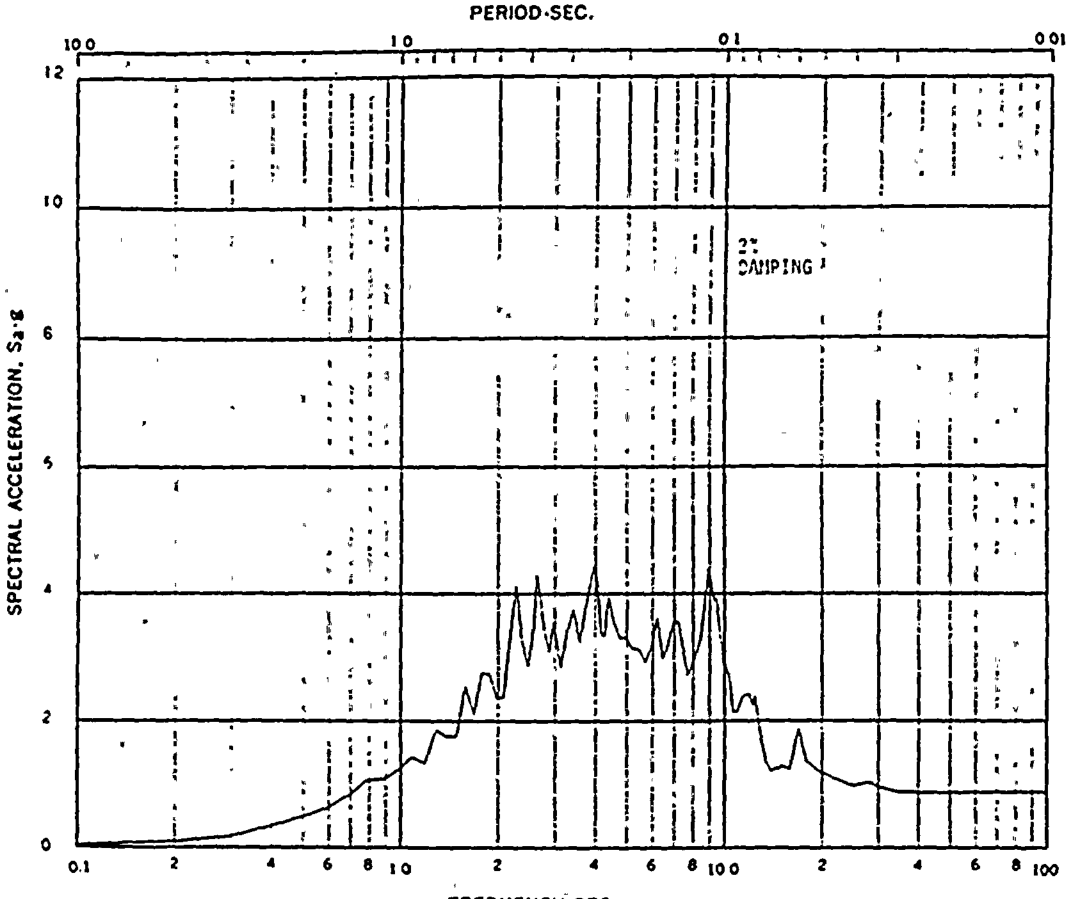

CONTAINMENT (BASE OF INTERNAL) - SURFACE FOUND. - VERTICAL SV
(CLASSI)

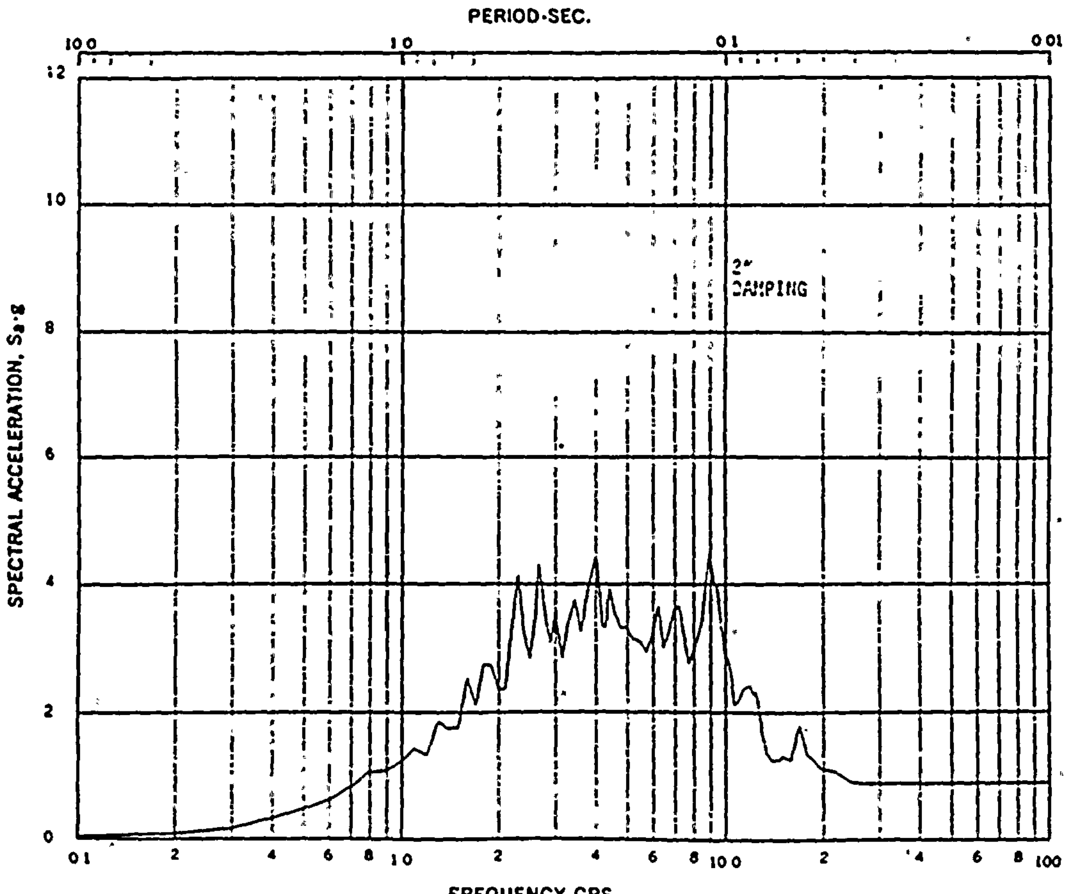

CONTAINMENT (BASE OF INTERNAL) - SURFACE FOUND. - VERTICAL SV
(SASSI CASE CSC1)

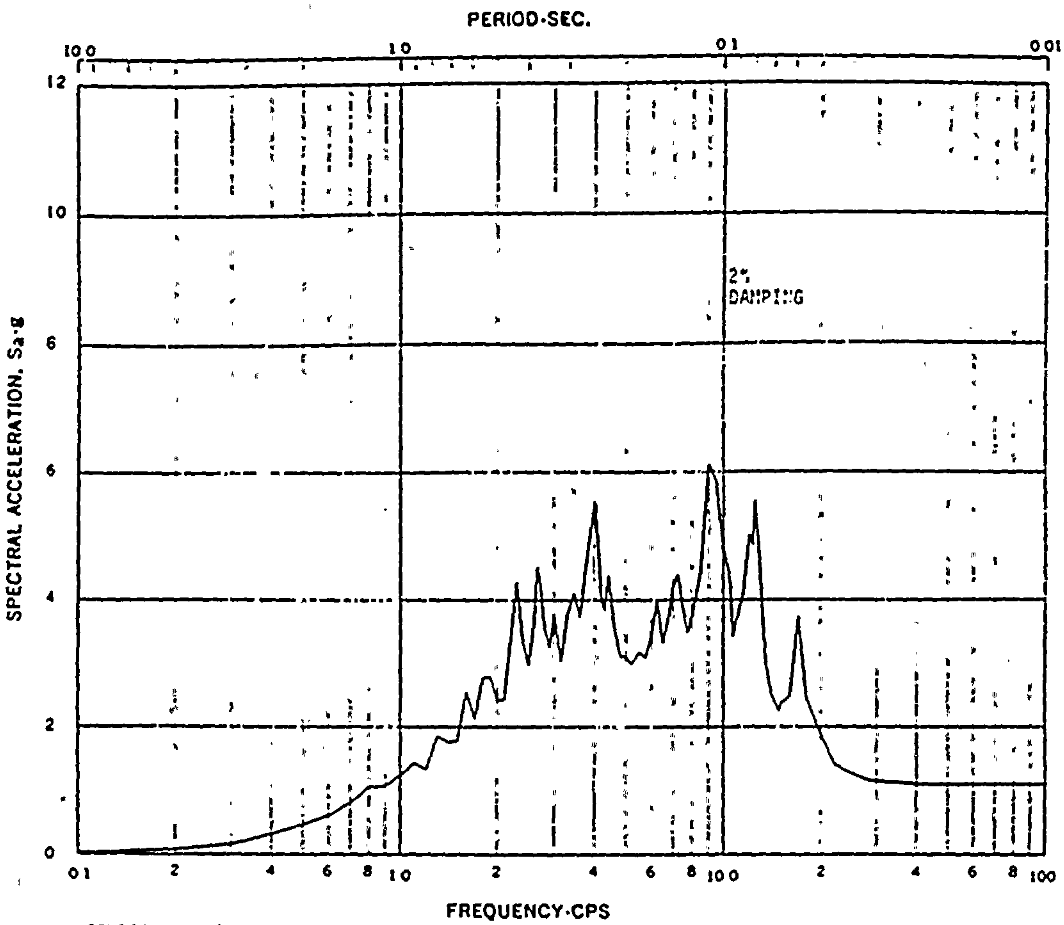

CONTAINMENT (TOP OF INTERNAL) - SURFACE FOUND. - 30 DEGREE SV
(CLASSI)

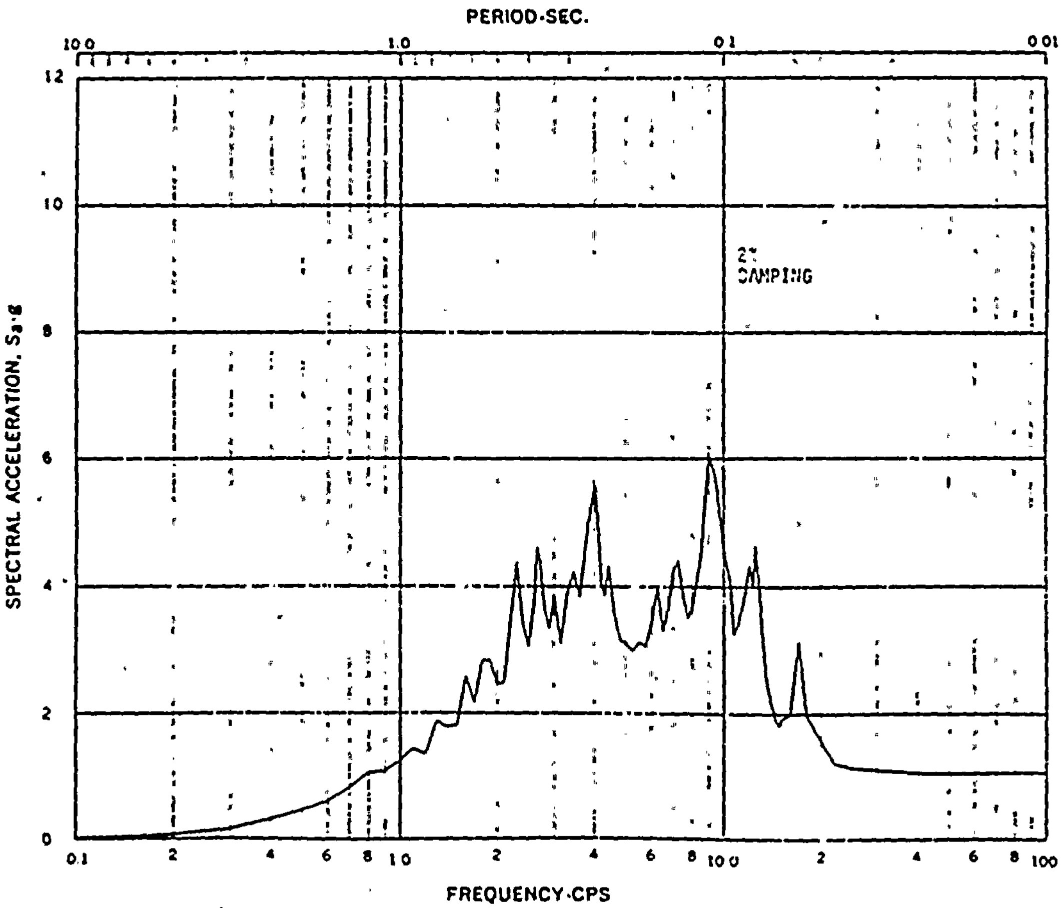

CONTAINMENT (TOP OF INTERNAL) - SURFACE FOUND. - 30 DEGREE SV
(SASSI CASE CSC2)

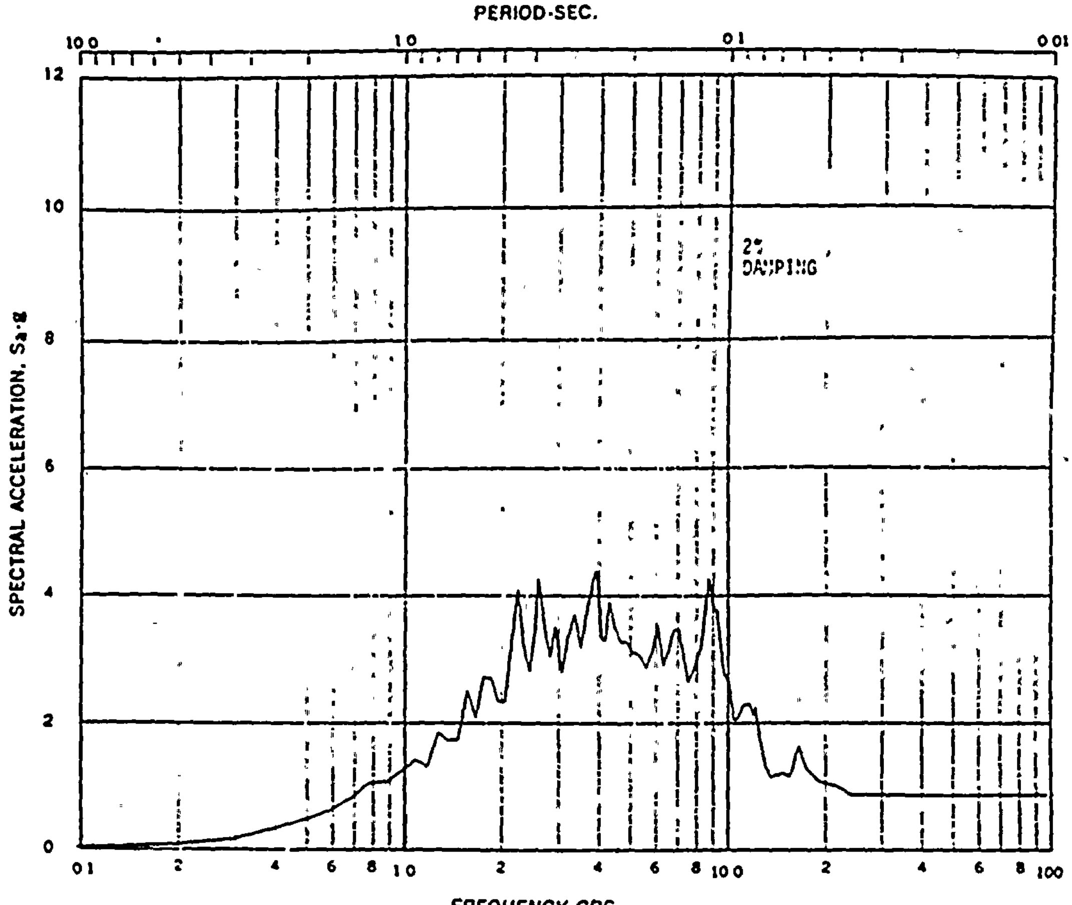

CONTAINMENT (BASE OF INTERNAL) - SURFACE FOUND. - 30 DEGREE SV
(CLASSI)

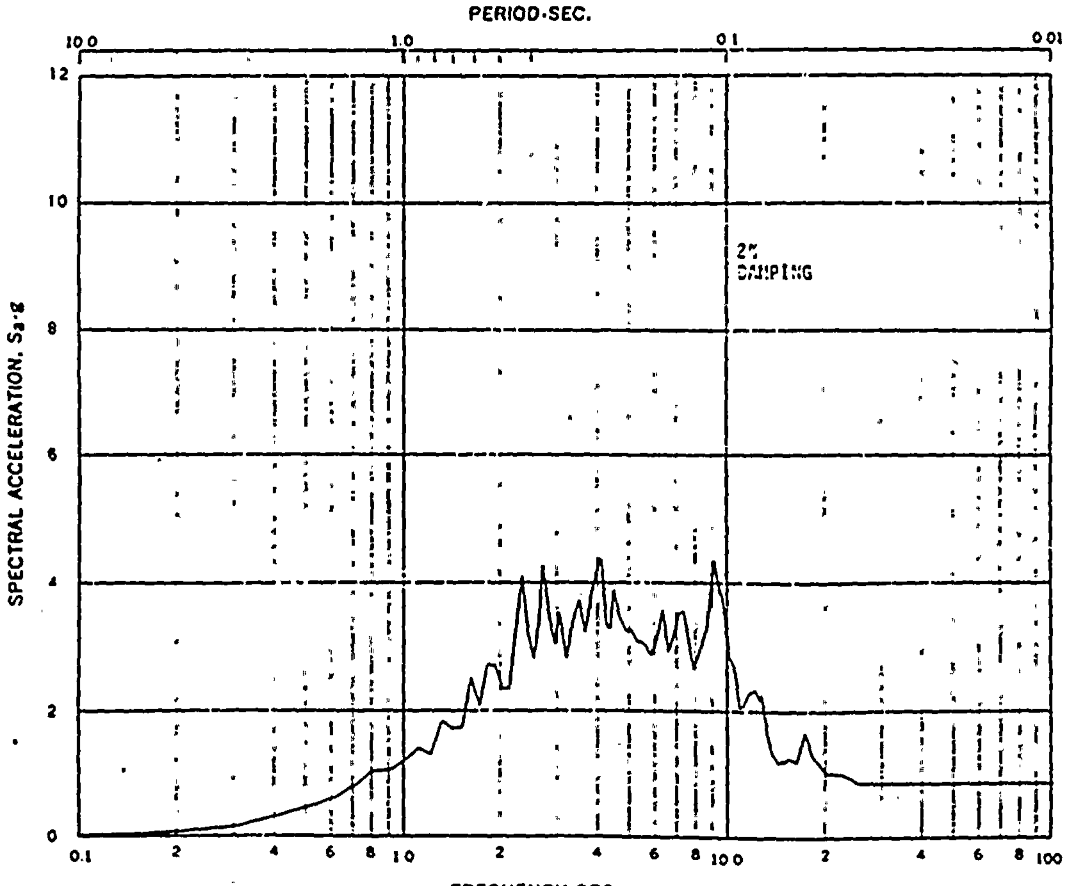

CONTAINMENT (BASE OF INTERNAL) - SURFACE FOUND. - 30 DEGREE SV
(SASSI CASE CSC2)

COMPARISONS BETWEEN CLASSI AND SASSI SOLUTIONS

AUXILIARY BUILDING

SURFACE FOUNDATION

- VERTICAL SV - WAVE
- INCLINED SV - WAVE 30° FROM VERTICAL

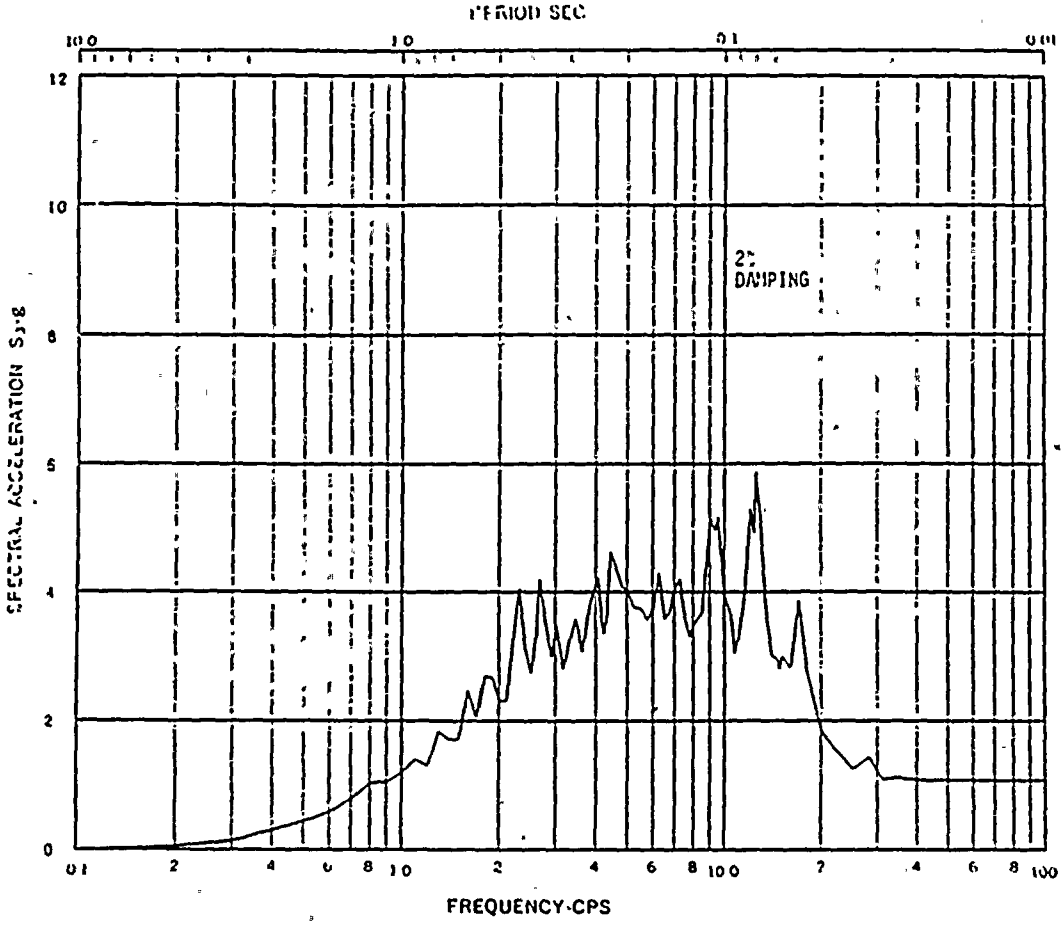

AUX. BLDG. (ELEV. 140) - SURFACE FOUND. - VERTICAL SV
(CLASSI)

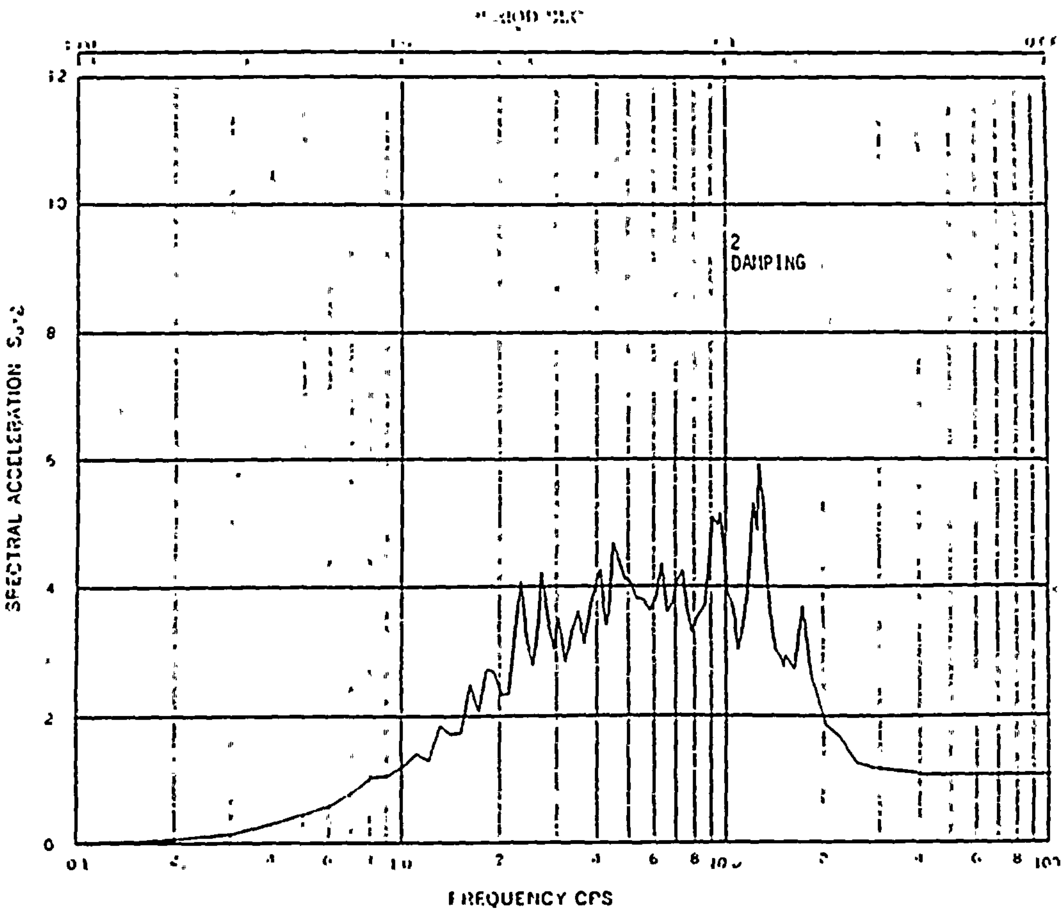

AUX. BLDG. (ELEV. 140) - SURFACE FOUND. - VERTICAL SV
(SASSI CASE ASC3)

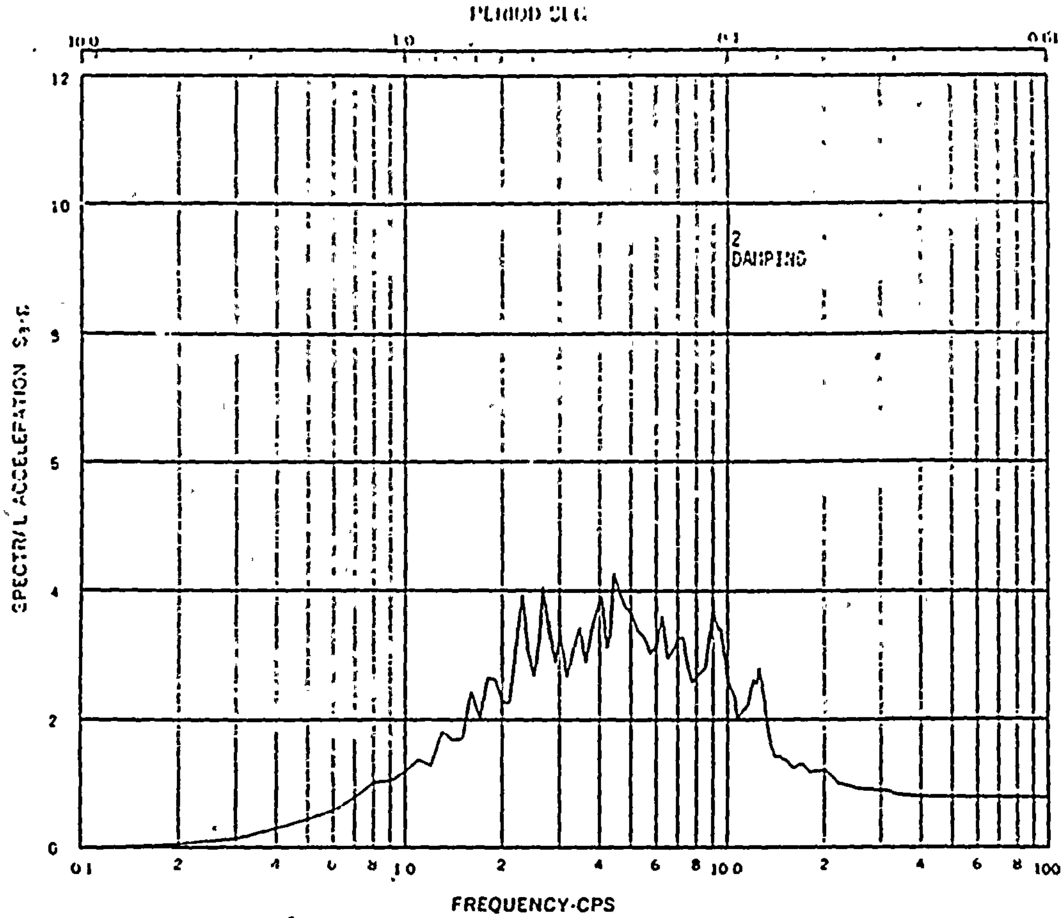

AUX. BLDG. (ELEV. 35) - SURFACE FOUND. - VERTICAL SV
(CLASSI)

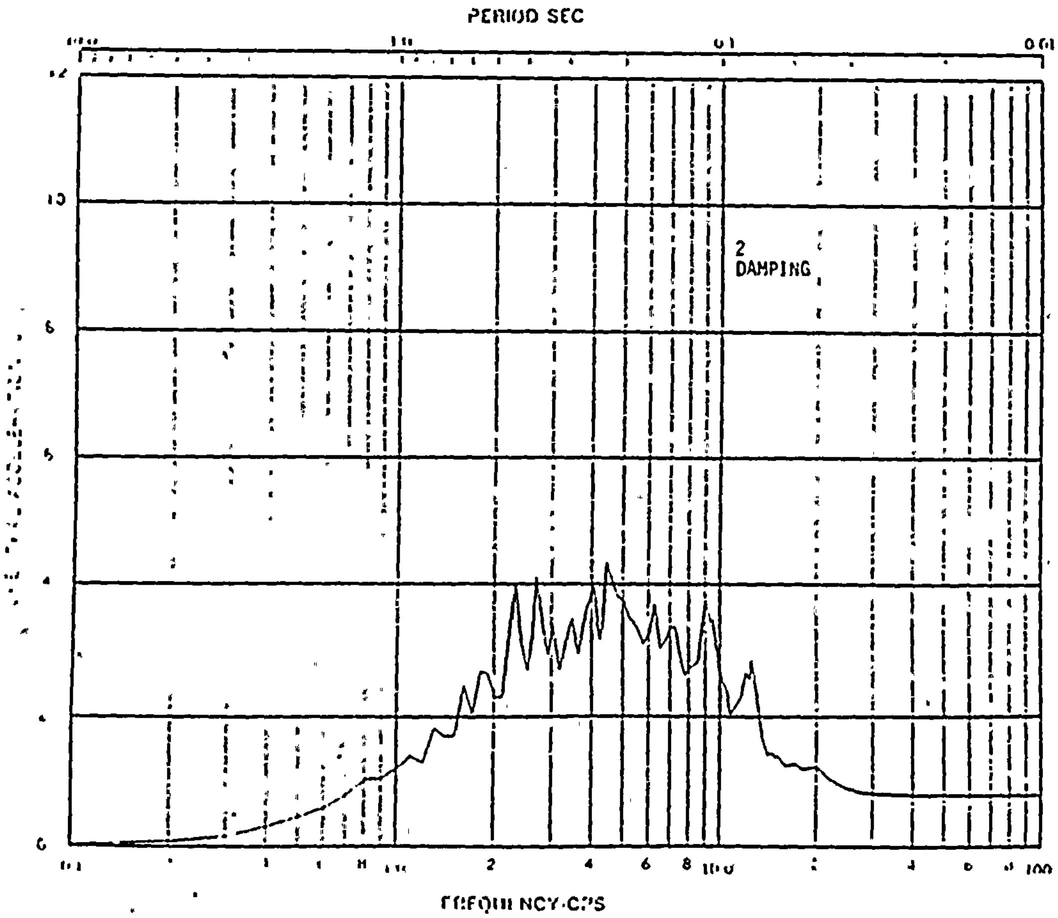

AUX. BLDG. (ELEV. 85) - SURFACE FOUND. - VERTICAL SV
(SASSI CASE ASC3)

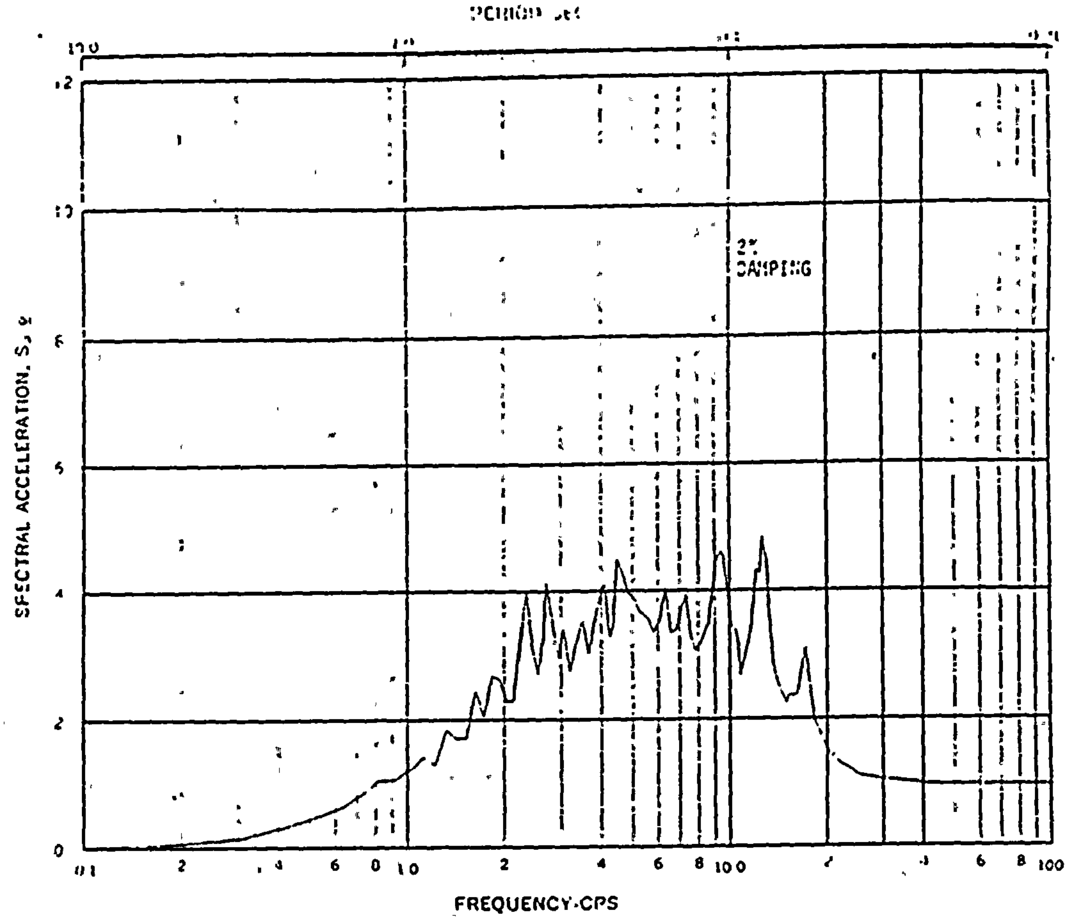

AUX. BLDG. (ELEV. 140) - SURFACE FOUND. - 30 DEGREE SV
(CLASSI)

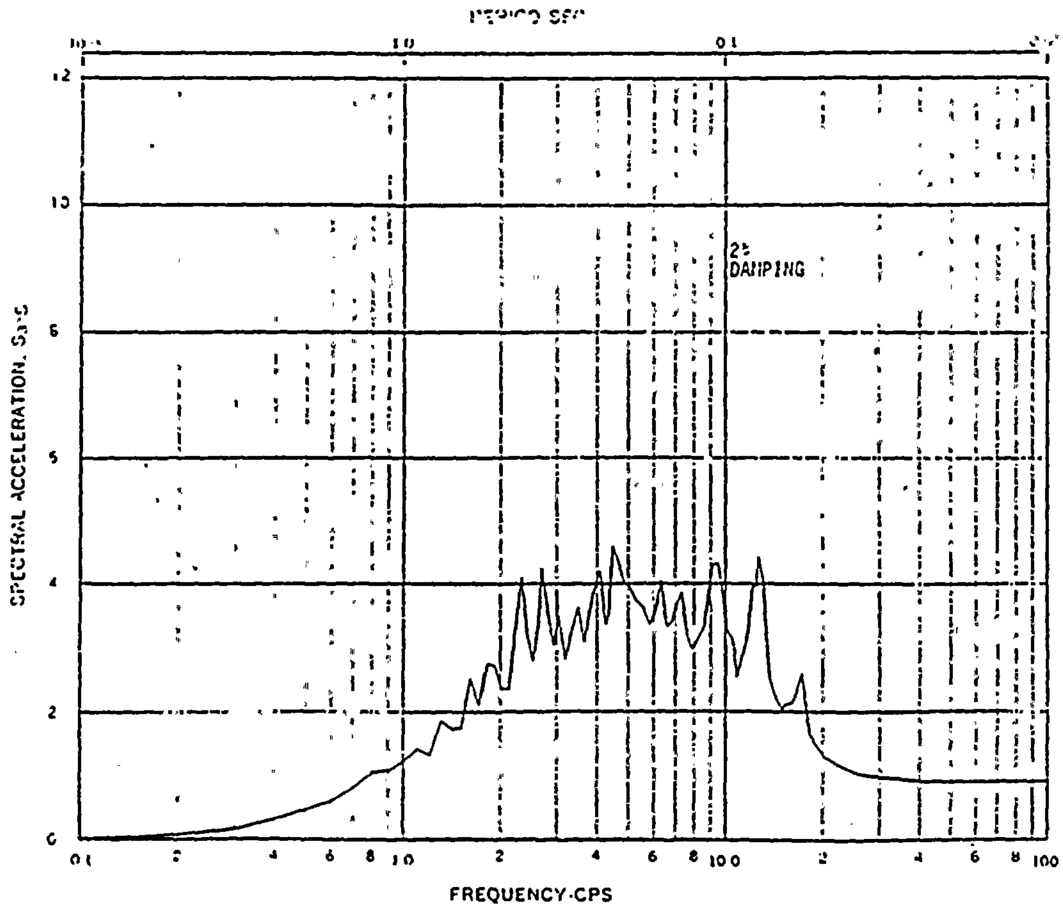

AUX. BLDG. (ELEV. 140) - SURFACE FOUND. - 30 DEGREE SV

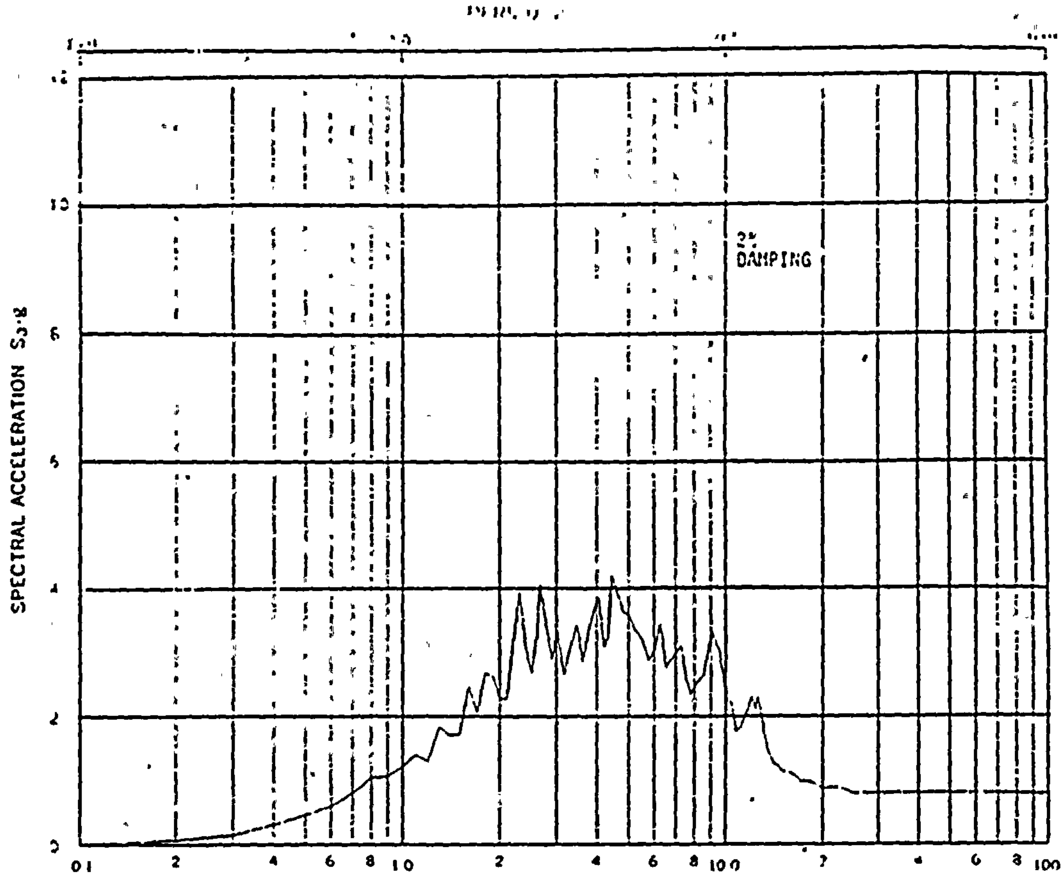

AUX. BLDG. (ELEV. 85) - SURFACE FOUND. - 30 DEGREE SV
(CLASSI)

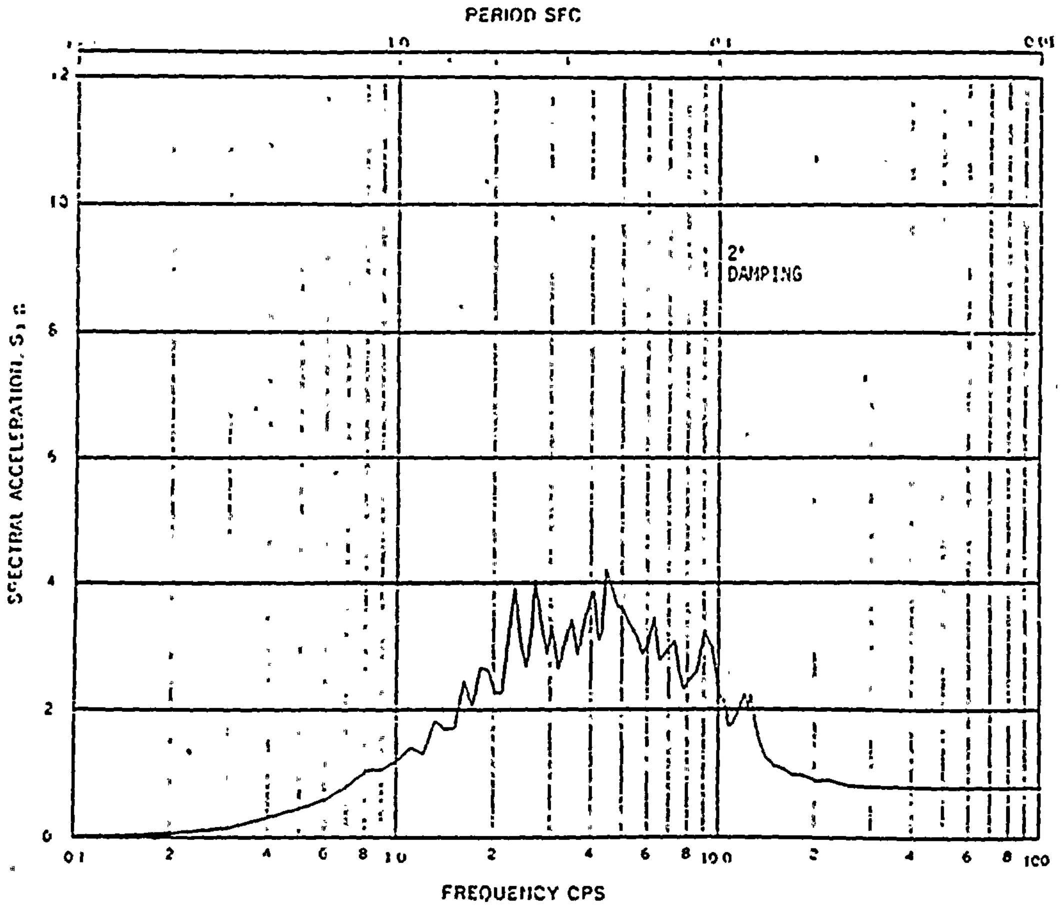

AUX. BLDG. (ELEV. 85) - SURFACE FOUND. - 30 DEGREE SV
(SASSI CASE ASC4)

COMPARISONS BETWEEN CLASSI AND SASSI SOLUTIONS

CONTAINMENT + AUXILIARY BUILDING

SURFACE FOUNDATION

- VERTICAL SV - WAVE

- INCLINED SV - WAVE 30° FROM VERTICAL

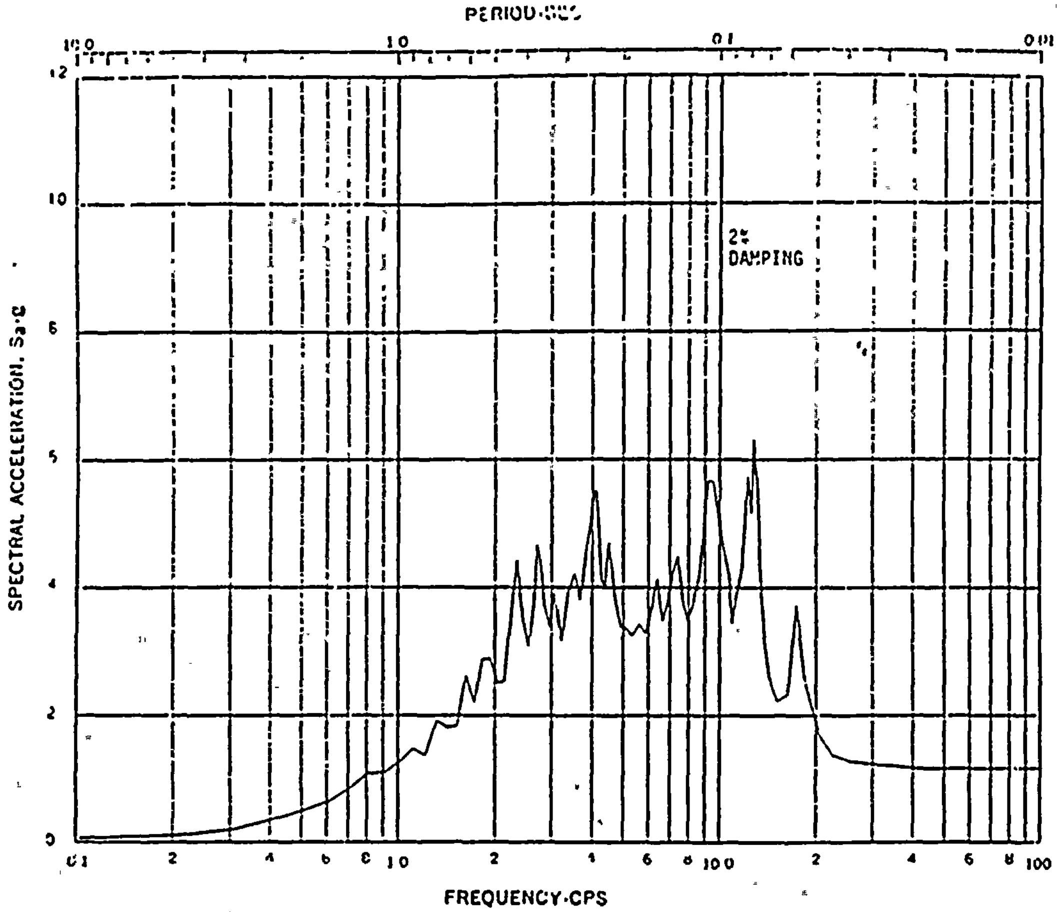

AUX. + CONT. (TOP OF INTERNAL) - SURFACE FOUND. - VERTICAL SV
(CLASSI)

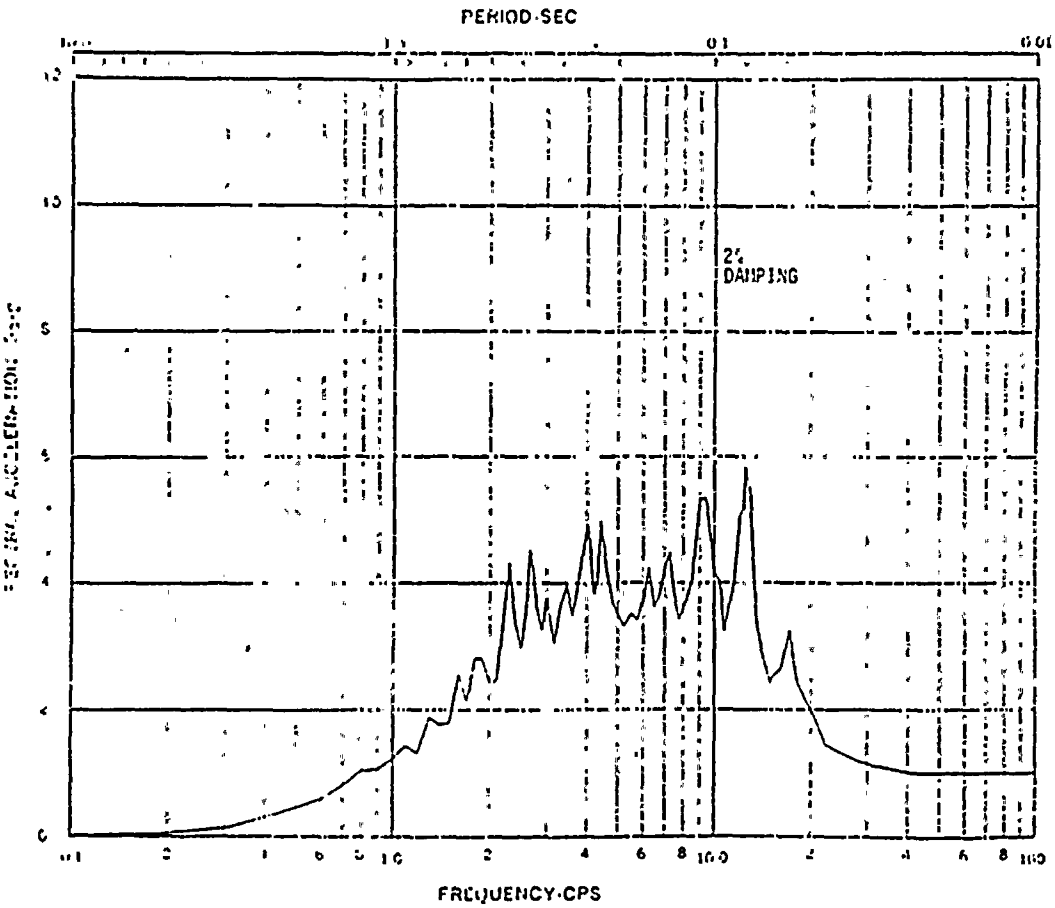

AUX. + CONT. (TOP OF INTERNAL) - SURFACE FOUND. - VERTICAL SV
(SASSI CASE ACS1)

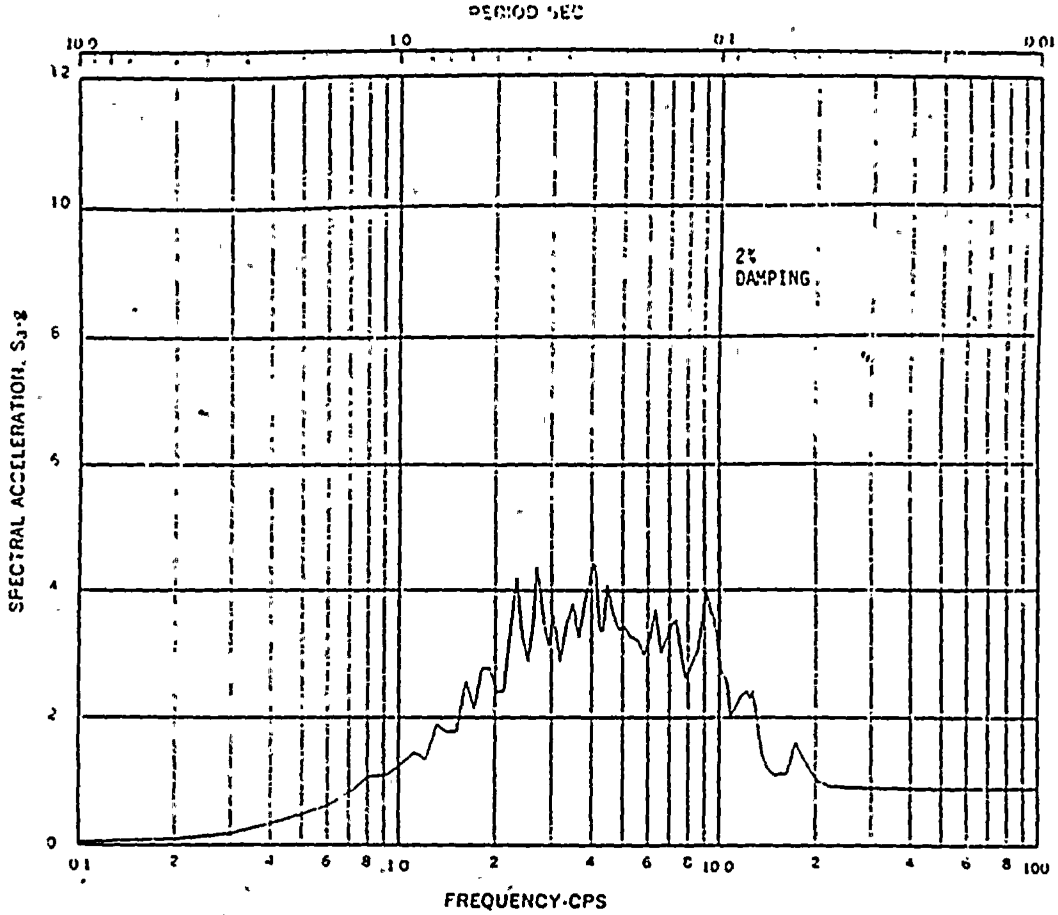

AUX. +-CONT. (BASE OF CONT.) - SURFACE FOUND. - VERTICAL SV
(CLASSI)

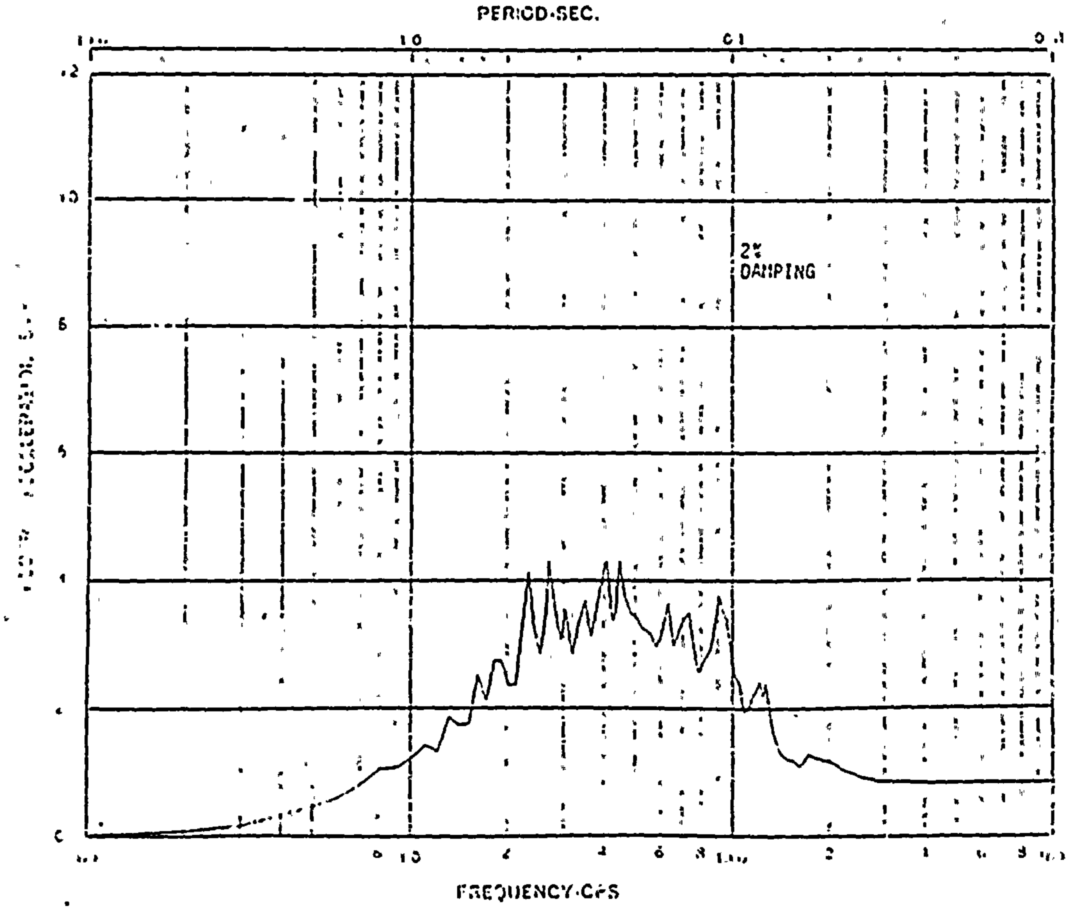

AUX. + CONT. (BASE OF CONT.) - SURFACE FOUND. - VERTICAL SV
(SASSI CASE AC3)"

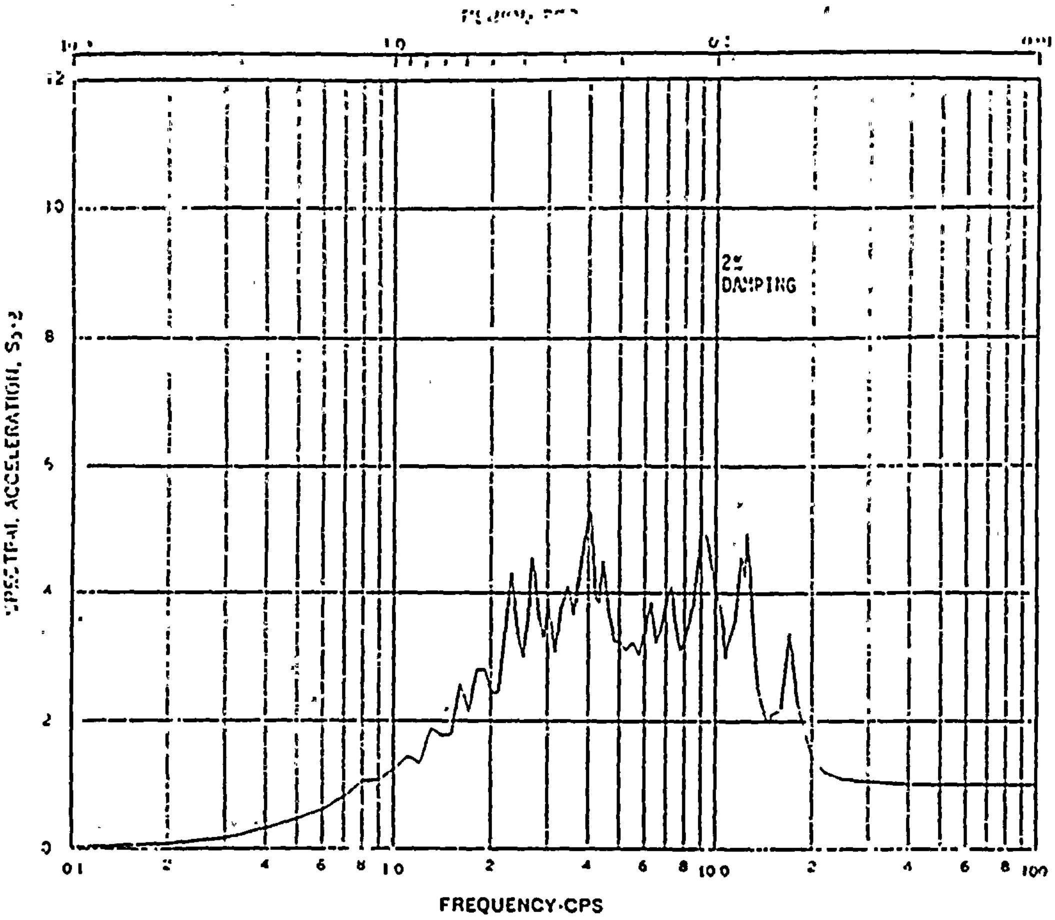

AUX. + CONT. (TOP OF INTERNAL) - SURFACE FOUND. - 30 DEGREE SV
(CLASSI)

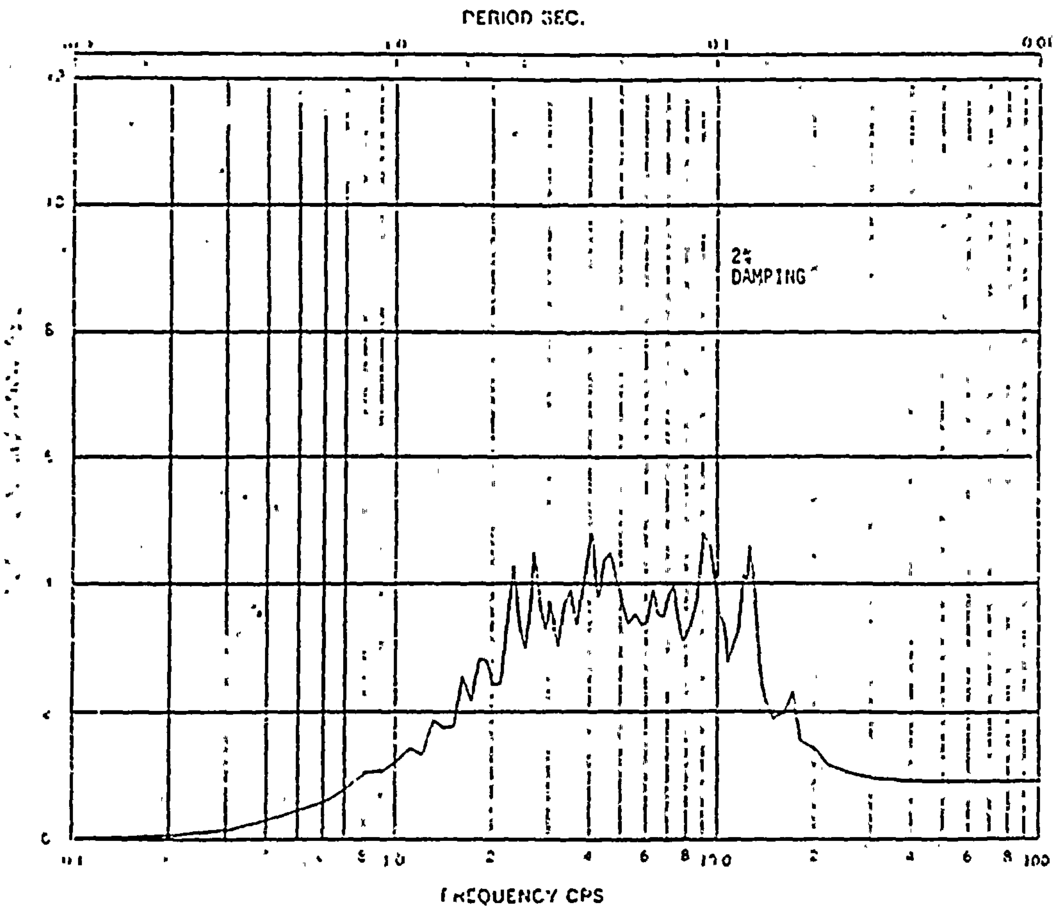

AUX. + CONT. (TOP OF INTERNAL) - SURFACE FOUND. - 30 DEGREE SV
(SASSI CASE RCS2)

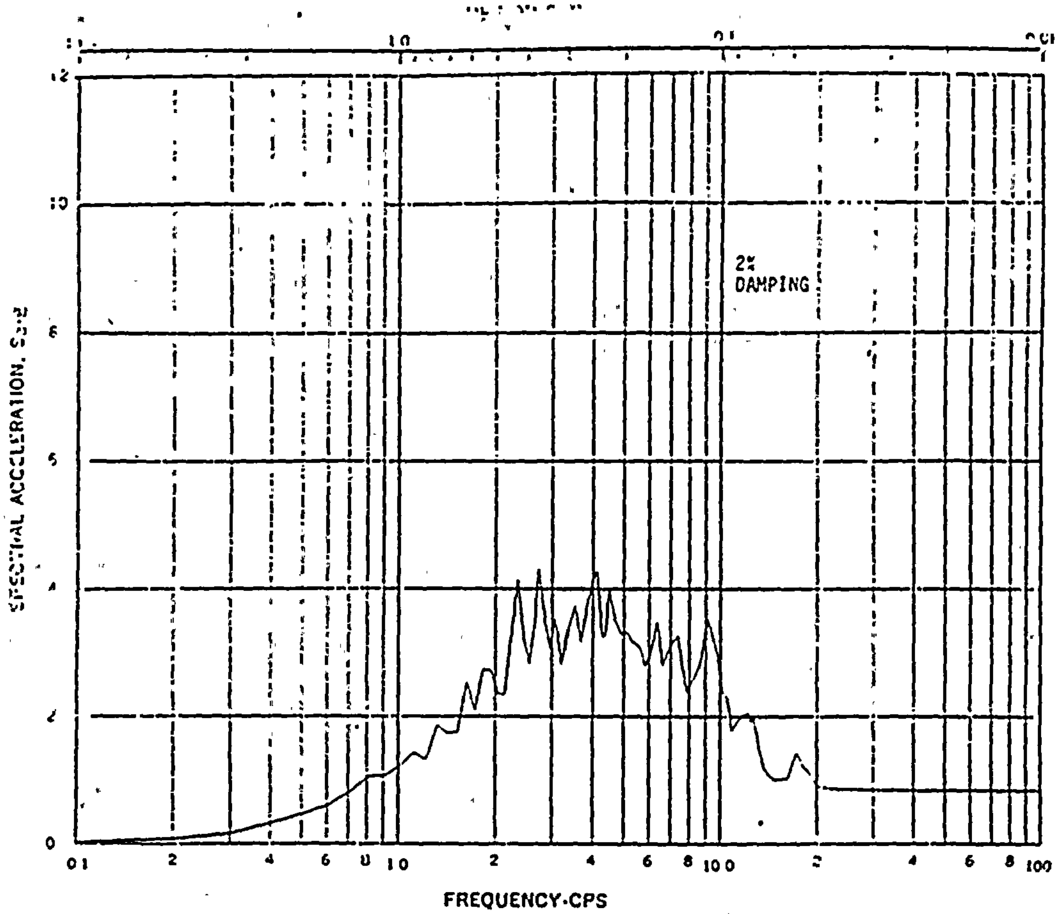

AUX. + CONT. (BASE OF CONT.) - SURFACE FOUND. - 30 DEGREE SV
(CLASSI)

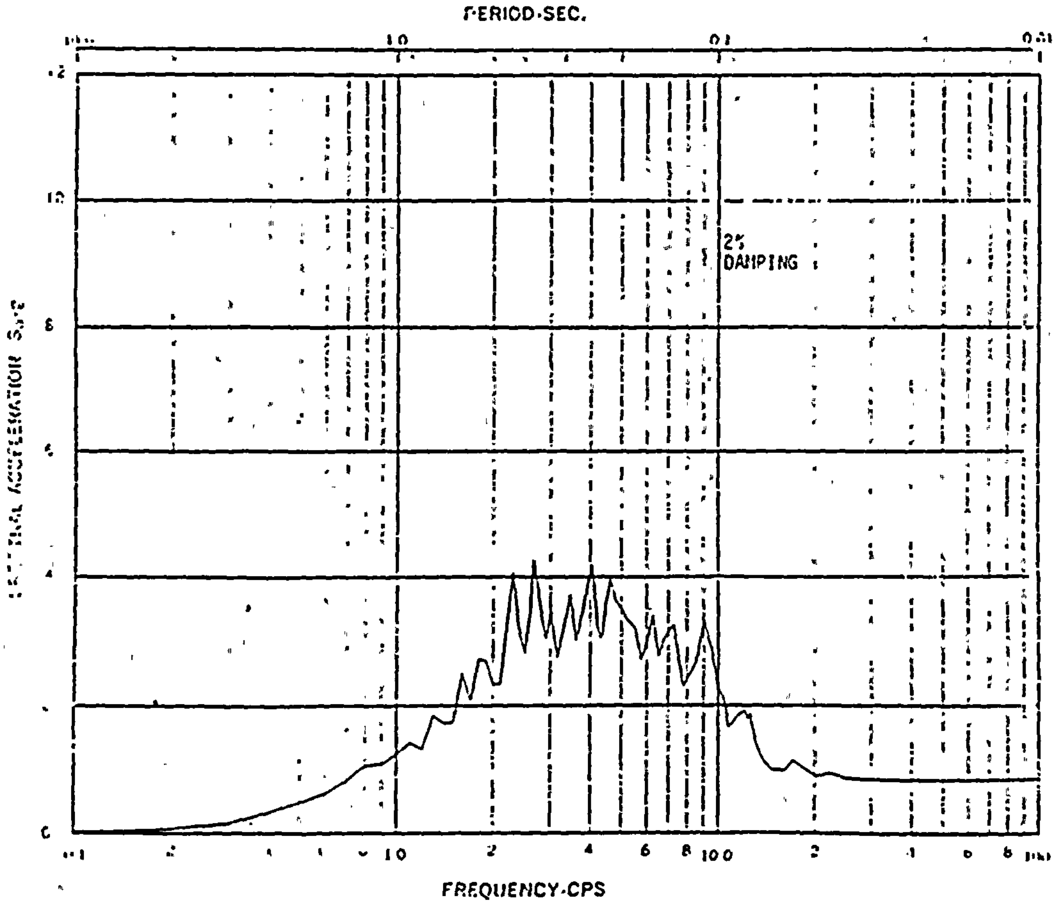

AUX. + CONT. (BASE OF CONT.) - SURFACE FOUND. - 30 DEGREE SV
[illegible]

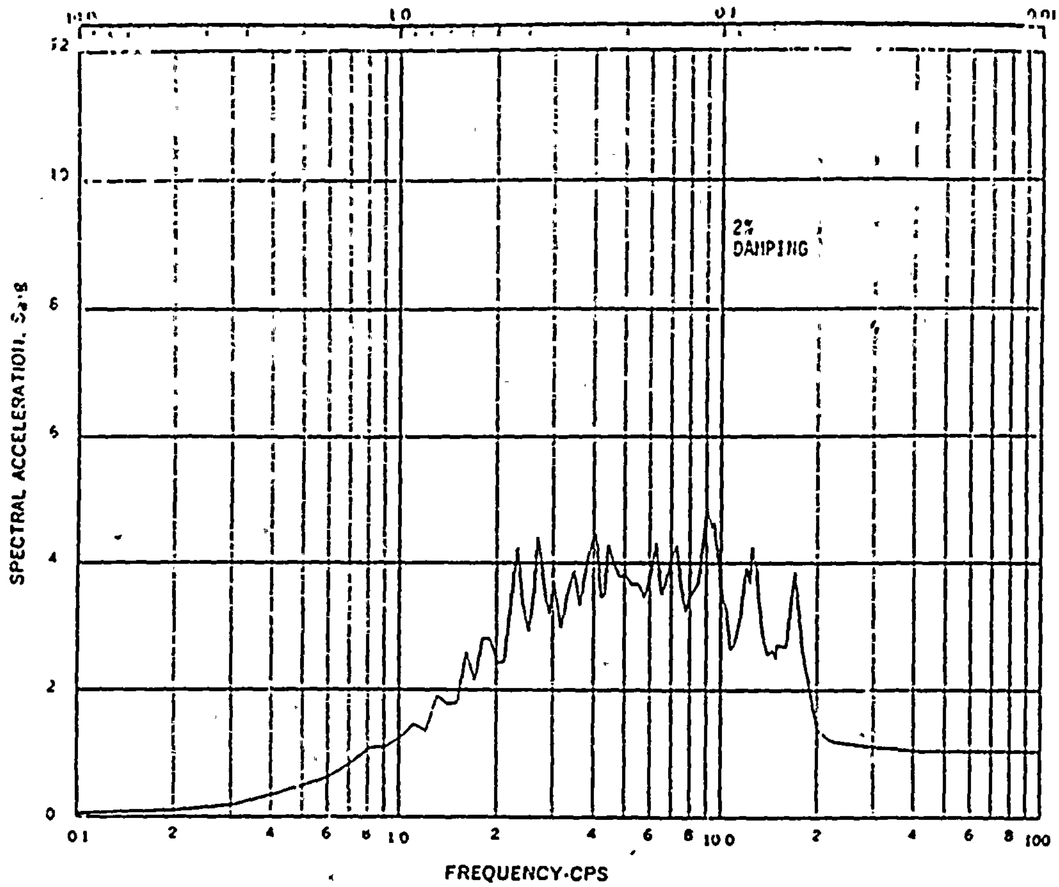

AUX. + CONT. (ELEV. 140 OF AUX.) - SURFACE FOUND. - VERTICAL SV
(CLASSI)

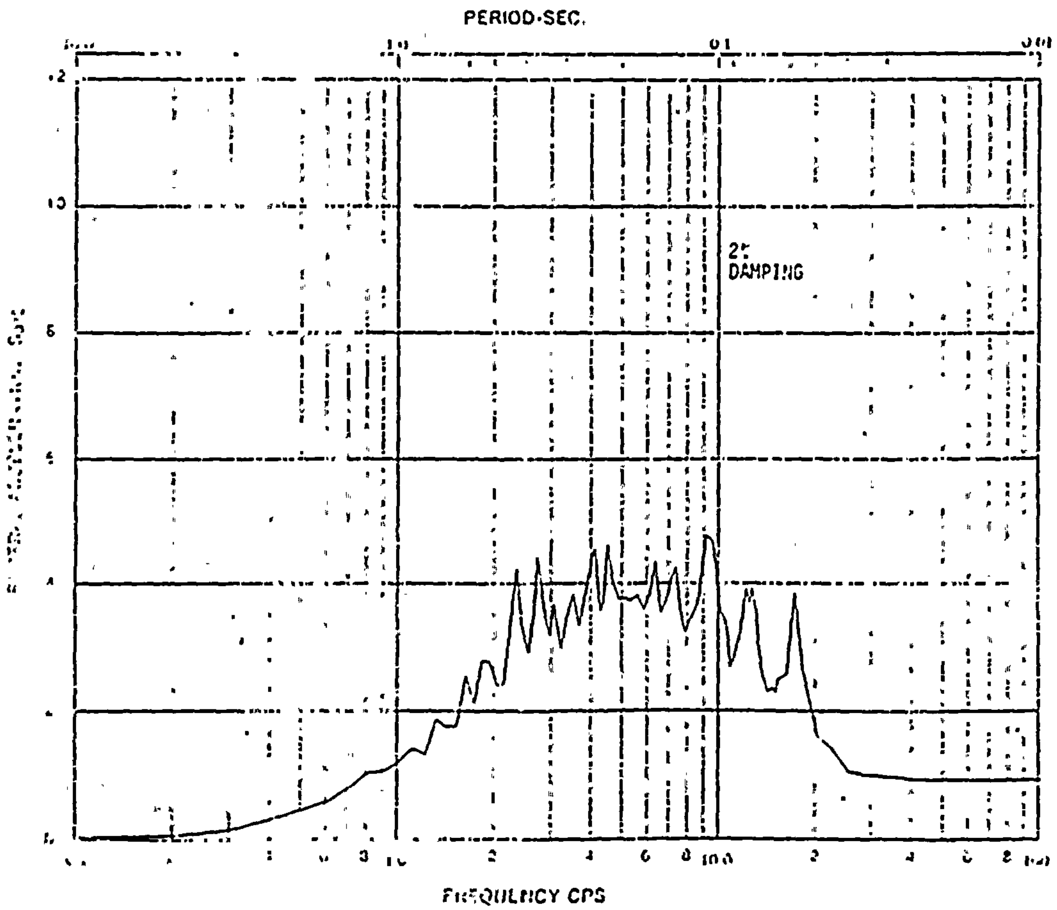

AUX. + CONT. (ELEV. 140 OF AUX.) - SURFACE FOUND. - VERTICAL SV
(SASSI CASE ACSI)

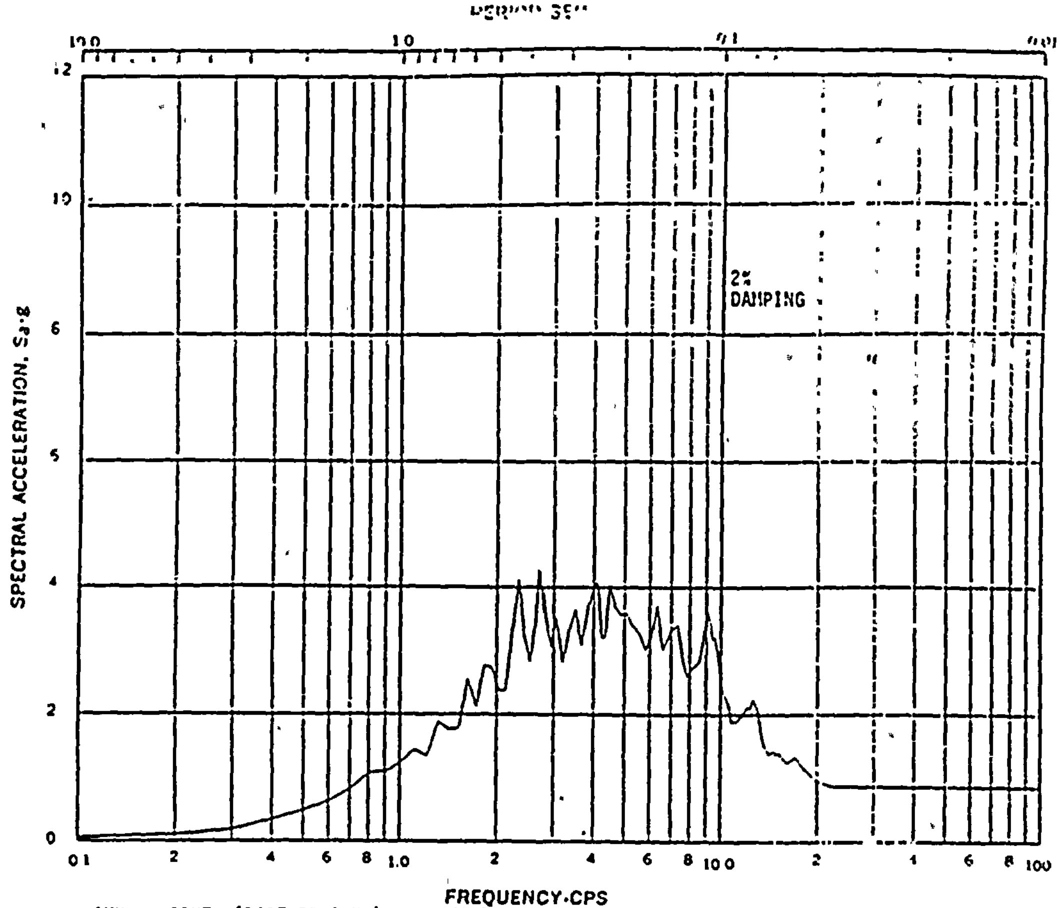

AUX. + CONT. (BASE OF AUX.) - SURFACE FOUND. VERTICAL SV
(CLASSI)

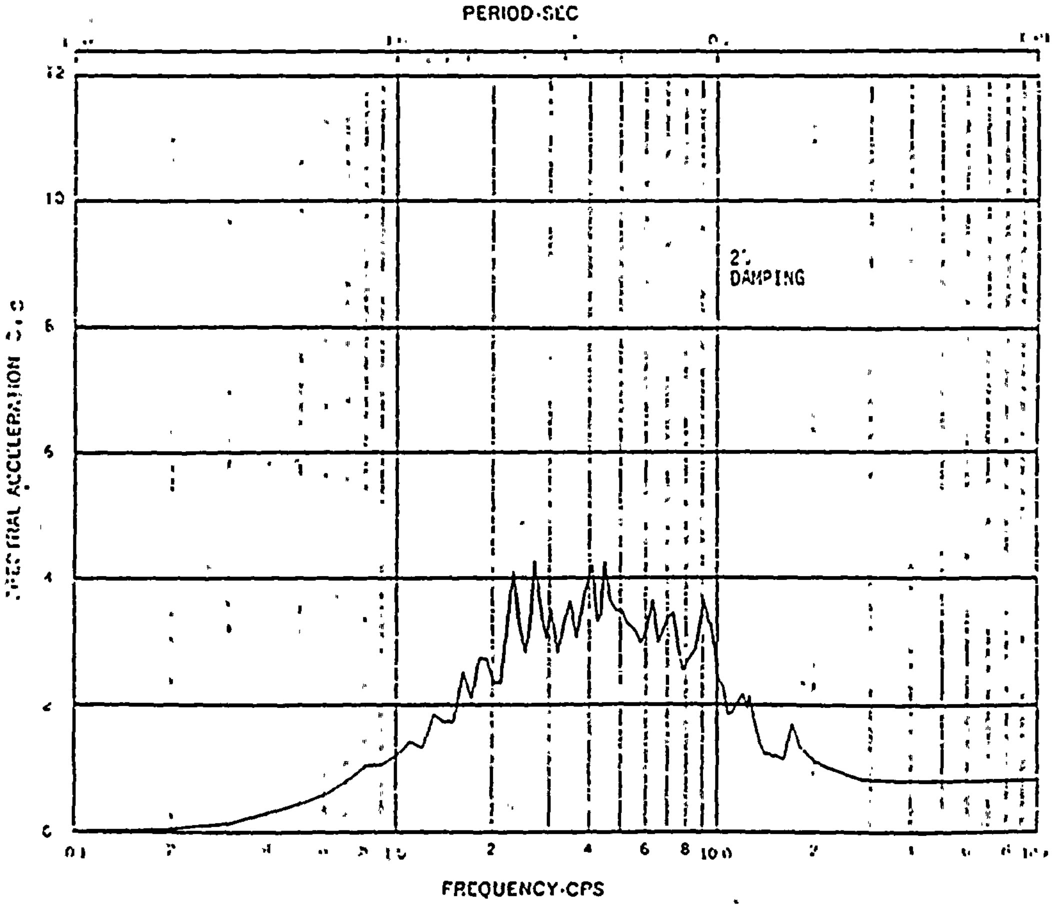

AUX. + CONT. (BASE OF AUX.) - SURFACE FOUND. - VERTICAL SV
(SASSI CASE ACS1)

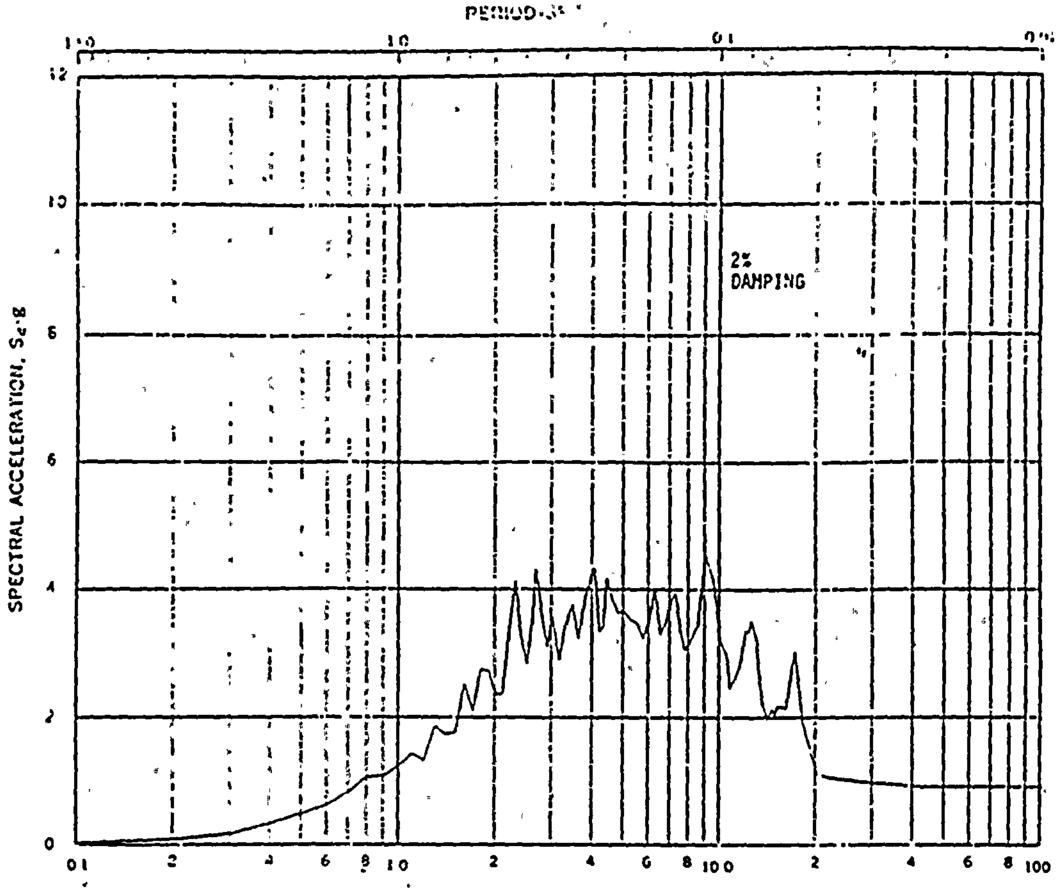

AUX. + CONT. (ELEV. 140 OF AUX.) - SURFACE FOUND. - 30 DEGREE SV
(CLASSI)

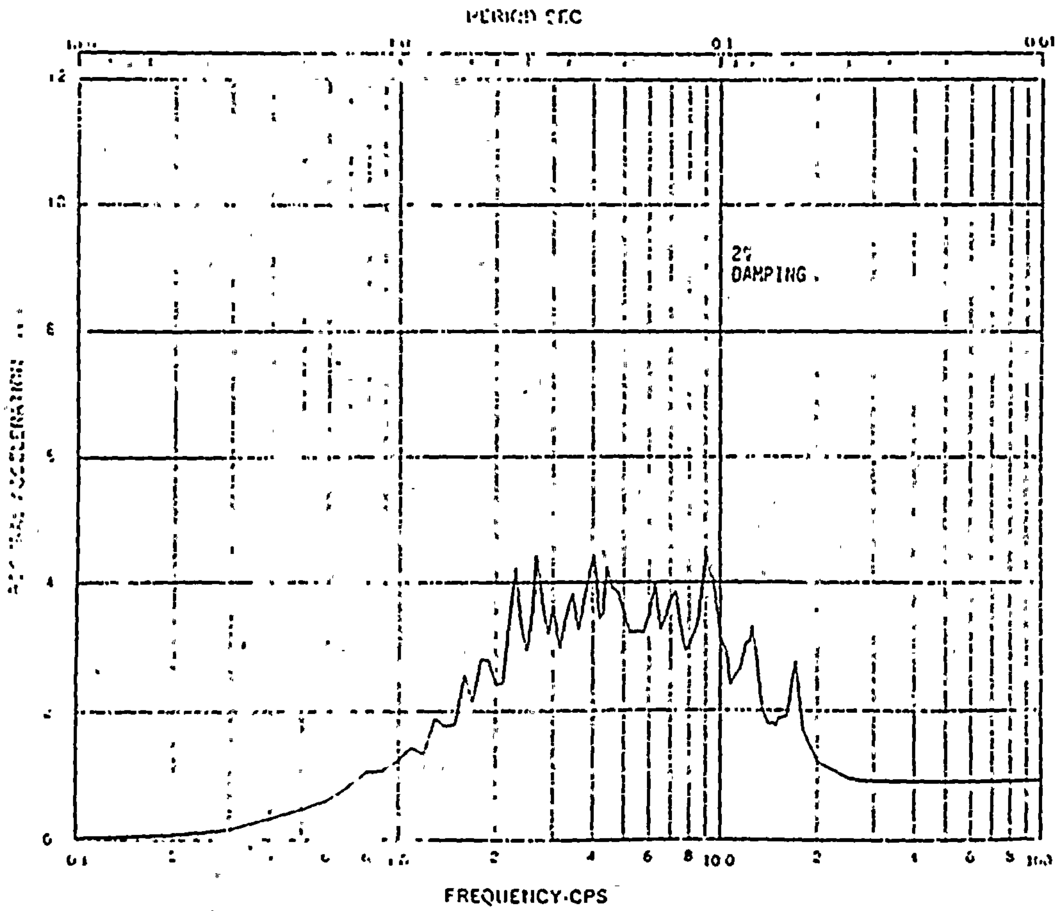

AUX. + CONT. (ELEV. 140 OF AUX.) - SURFACE FOUND. - 30 DEGREE SV
(SASSI CASE ACS2)

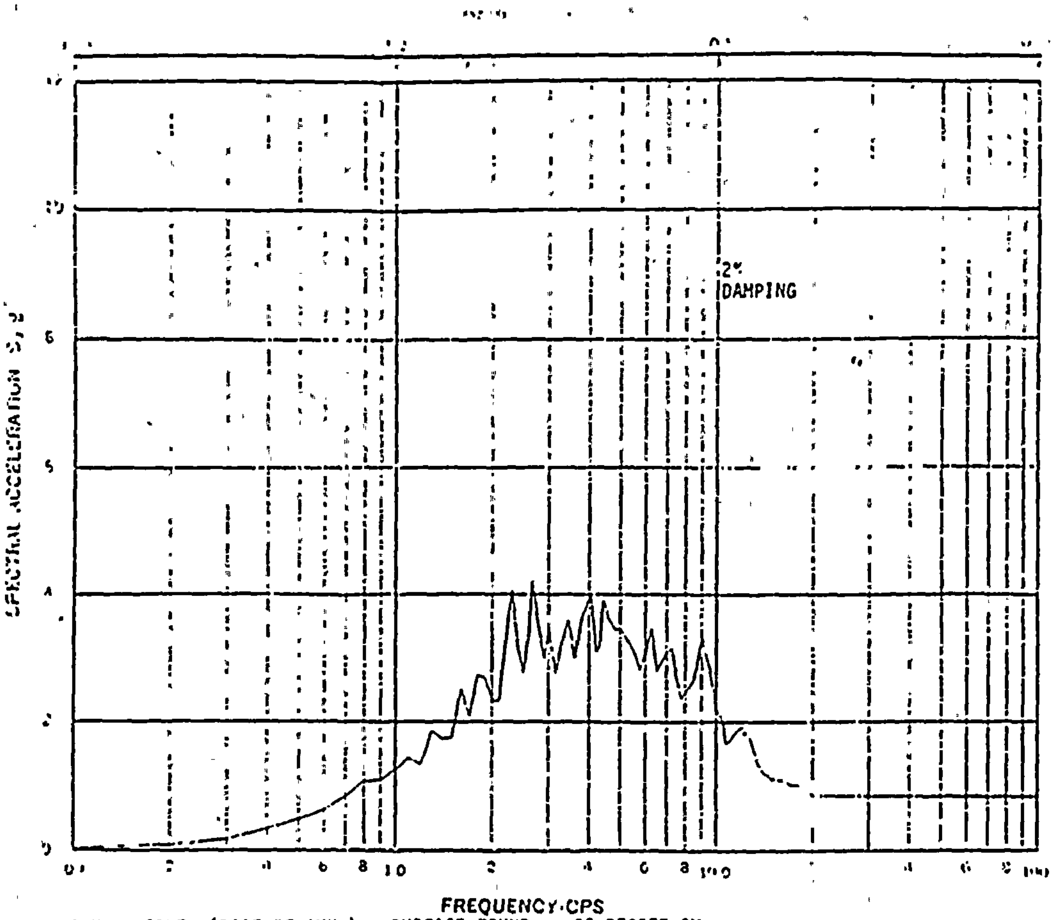

AUX. + CONT. (BASE OF AUX.) - SURFACE FOUND. - 30 DEGREE SV
(CLASSI)

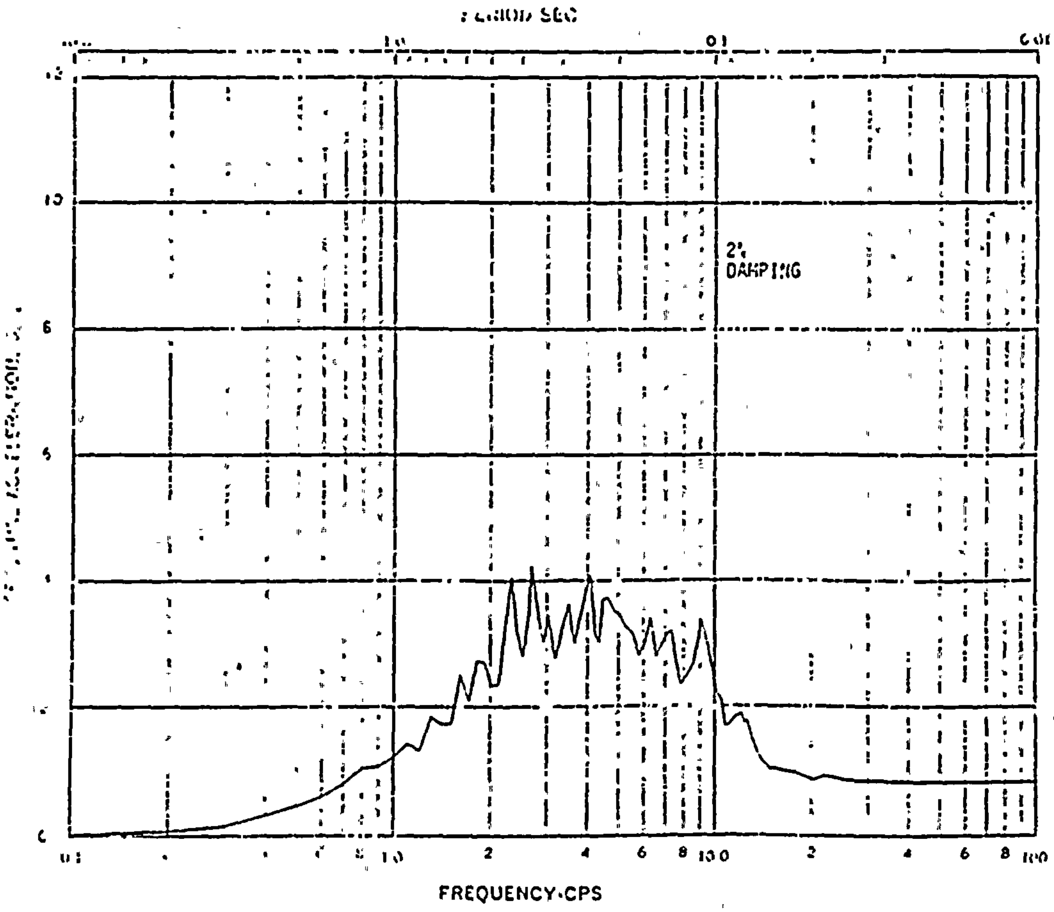

AUX. + CONT. (BASE OF AUX.) - SURFACE FOUND. - 30 DEGREE SV
(SASSI CASE ACS2)

ANALYSES OF RECORDED EARTHQUAKE DATA AND CORRELATION WITH ANALYTICAL MODELS

1. Introduction

The available earthquake data recorded at the DCPP site have been analyzed for the purpose of identify the dynamics characteristics of the DCPP power block structures for correlation with the analytical models. The dynamic characteristics planned to be identified from the data are: (1) the SSI frequencies; (2) the amplitudes of the SSI response amplification functions; and (3) the SSI effect on the structures. However, due to low intensity levels of recorded earthquake motions and wide variations in the site geology and topology of the free-field recording stations and, thus, the recorded free-field ground motions, the amplitudes of the SSI response amplification functions as well as the SSI effects on the structures cannot be reliably assessed. Consequently, the analyses of recorded data in this study are only used to assess the SSI frequencies of the DCPP power block structures.

2. Instrumentations

The specification of the recording sensors are provided in Table 1. The locations and orientations of these sensors in Unit 1 and Unit 2 containment buildings, auxiliary building, and turbine building, and those in the free-field are shown in Figures 1 through 4, respectively.

3. Available Recorded Motions

The earthquake ground motions recorded at DCPP site used in this study are shown in Table 2. As can be seen from this table, the peak free-field horizontal accelerations of the five earthquake listed - Pt. Sal, Coalinga, Pt. San Luis, Santa Maria, and St. Martin earthquakes, are all of low level amplitude with none exceeding 0.02 g.

The specific components of recorded earthquake motions available for this study are summarized in Table 3. Those components that have been used in the analysis are also identified in this table.

4. Data Analysis Techniques

In processing the recording data, two data analysis techniques have been used to identify the SSI frequencies of DCPP power block structures. These two analysis techniques are referred to as the "transfer function (TF) technique" and the "response spectrum ratio (RSR) technique." The schematic diagram of the TF and RSR techniques are shown in Figure 5.

As shown in Figure 5, a selected pair of recorded motions are first preprocessed to remove the non-zero mean (i.e., zero-meaned) and then smoothed at the beginning and the tail end of the time history using a cosine-tapered function. These zero-meaned and smoothed (DS) motions are then augmented with zeroes to make 2^N data points to suit the FFT algorithm used for the data analysis.

In applying the transfer function technique, the pair of DS motions are analyzed using the Bechtel DATAN code (Ref. 2). The smoothed transfer function is computed using this code as the ratio of the amplitude of the smoothed cross-power spectral density (CPSD) between the two selected DS motions, to the smoothed power spectral density (PSD) of the DS motion designated to be the input motion.

In applying the response spectral ratio technique, the 2% damping response spectra of the two selected DS motions are generated, and their response spectrum ratios are computed using the Bechtel MSPEC code (Ref. 1).

5. Analysis Results

The results of analyses of the recorded data obtained from using the TF and RSR techniques are presented in Figures 6 through 19. In each of these figures, the smoothed transfer function and the coherence function computed from using DATAN, and the 2% damping response spectra and the response spectrum ratio computed from using MSPEC are plotted for a selected pair of recorded motions. The empirical SSI frequencies can be identified from these figures as the frequencies corresponding to the peaks of the transfer function and the response spectrum ratios.

The analysis results for the containment building are shown in Figures 6 through 10. In Figure 6, the transfer function of the motion at the free-field (FF) to the motion of the containment at springline (CS) obtained from the analytical model used in the Phase II study, and from recorded motions are compared. The EW SSI frequency of the containment shell can be clearly identified from the transfer functions show in Fig. 6 to be about 4 Hz. The NS and vertical SSI frequencies can similarly be identified from Figures 7 and 8, respectively, to be about 4 Hz and 13 Hz. The analysis results for the internal structure using the recorded motions at top of internal (TI) and containment base (CB) are shown in Figures 9 through 10. The EW and NS SSI frequencies for the internal structures can be estimated from Figures 9 and 10, respectively, to be in the range of 9 to 10 Hz.

The analysis results for the auxiliary building are shown in Figures 11 through 18. The analysis results in Figures 11 through 14 are based on the recorded motions for the Pt. San Luis earthquake; and Figures 15 through 18 are based on recorded motions for the St. Martin earthquake. Since all three recording sensors in the auxiliary building are located

at low elevation of the building (El. 100'), the recorded motions do not provide as good a data base for analysis using the transfer function technique as those for the containment building. However, the analysis results shown in Figures 11 through 18 using the recorded free-field ground motions and the three recorded motions at El. 100' of the auxiliary building appear to give some indications that the horizontal (EW and NS) SSI frequencies of the auxiliary building are in the range of about 7 to 9 Hz where the response spectral ratios show amplifications.

Due to the lack of available recorded data in the turbine building, the identification of SSI frequencies is not feasible. The analysis results for the NS component of recorded motions at El. 140' of turbine building and the free-field ground motion near warehouse are shown in Figure 19. As shown, the identification of any SSI frequency from the results cannot be made. Efforts are being pursued to obtain additional recorded data in the turbine building from the Pt. San Luis earthquake and the St. Martin earthquake.

6. Empirical SSI Frequencies

Based on the results obtained to date from the analysis of the recorded data of the low level earthquakes, preliminary conclusions on empirical SSI frequencies that can be inferred from the low level earthquakes are as follows:

(1) the EW and NS fundamental SSI frequencies of the containment shell are both about 4 Hz;

(2) the vertical SSI frequency of the containment shell is about 13 Hz;

(3) the EW and NS SSI frequencies of the containment internal structure are about 9 to 10 Hz;

(4) the EW and NS SSI frequencies of the auxiliary building appear to be in the range of 7 to 9 Hz, but these frequencies are not as conclusive as those for the containment structure;

(5) due to limited recorded data available to date for the turbine building, the SSI frequencies of the turbine building cannot yet be identified.

7. Correlation with Analytical Models

The empirical SSI frequencies that can reliably be inferred from the analysis of recorded data are being used for correlation with the frequencies obtained from 3-D analytical SSI models currently under development. The fundamental SSI frequency of the SSI model of the containment shell structure has been shown to be in excellent agreement with the empirical frequency. The correlation of the analytical and the empirical results for the internal structure is currently being performed. Due to the lack of a clear indication of the empirical frequencies for the auxiliary building, the correlation with the analytical model for the building is expected to be more difficult. A correlation of analytical and empirical frequencies of the turbine building is currently not feasible. Whether a correlation can ever be made for the turbine building will depend on the reliability of additional recorded data that are being pursued for this building.

8. References

(1) Bechtel Power Corporation," CE789 (MSPEC) - Computing and Plotting Response Spectra," Computer Program User/Theoretical/Verification Manual, Revision 1, July 1984.

(2) Bechtel Power Corporation," CE928 (DATAN) - Probabilistic Data Analysis," User Manual, Revision 1, June 1984.

TABLE 1

SENSOR SPECIFICATION CHART*

DCS-Deck Nos.	Sensor Type (See Note 1)	Channel No. (See Note 2)	Max G	Location: Elev. (ft)	Location: Unit	Location: Description	Orientation (See Notes 3 and 4): Ch 1	Ch 2	Ch 3
	TR		1	89	1	Outside Containment - Base, Basic (SMA 3) System & Trigger (See Note 5)	180	270	Vert
	TR		3	303.5	1	Top of Containment, Basic (SMA 3) System (See Note 5)	180	270	Vert
	TR		1	64	1, 2	Aux. Building (U) - (18), Basic (SMA 3) System (See Note 5)	180	270	Vert
1-1	TR		1	89	1	Outside Containment - Base, NW Sector	Vert	118	28
1-2	TR		1	89	1	Outside Containment - Base - NE Sector	Vert	240	150
2-4	Single	3	1	91	1	Containment - Near Reactor, Between SG 1-3 and SG 1-4	--	--	Vert
1-3	TR		2	140	1	Containment - Operating Deck, Near Steam Generator No. 1-1	Vert	180	90
1-4	TR		2	140	1	Containment - Operating Deck, Near Steam Generator No. 1-3	Vert	0	270
2-4	B	1 & 2	2	140	1	Containment - Operating Deck, Annulus-South (See Note 6)	90	180	See Deck 2-4
3-1	B	1 & 2	2	140	1	Containment - Operating Deck, Annulus-West	180	90	Blank
2-2	TR		3	231	1	Containment Liner, Dome Springline - NE Sector	Vert	60	330
2-3	TR		3	231	1	Containment Liner, Dome Springline - S Sector	Vert	180	90
3-2	TR		3	231	1	Containment Liner, Dome Springline - NW Sector	Vert	300	210
4-3	B	1 & 2	1	89	2	Outside Containment - Base, N Sector	Vert	90	See Deck 4-3 and 4-4
4-4	B	1 & 2	1	89	2	Outside Containment - Base, SE Sector	Vert	200	See Deck 4-3 and 4-4
5-1	B	1 & 2	1	89	2	Outside Containment - Base, SW Sector - Trigger "A"	Vert	320	Blank
3-3	TR		1	100	1	Aux. Bldg. - (Fuel Handling), Between SPT Fuel Pool & HVAC Filter Room	Vert	0	270
3-4	TR		1	100	1, 2	Aux. Bldg. (H) - (18), Wall Next to Stairs - W End	Vert.	270	180
4-1	TR		1	100	1, 2	Aux. Bldg. (U) - (18), E end next to liquid holdup tanks - Trigger "B"	Vert	90	0
5-3	TR		1	--	--	Free Field, Near Reservoir	Vert	1	271
5-2	TR		1	85	1	Turbine Building, N End, Switch Gear Room	Vert	0	270
4-3 4-4	B	3	1	140	1	Turbine Building, N End, Turbine Deck	--	--	0, Deck 4-3 270, Deck 4-4
4-2	TR		1	85	2	Turbine Building, S End, Stairs	Vert	180	90
2-1	TR		1	89	1	Outside Containment Base, S Sector	Vert	0	270
6-1	TR		1	--	--	Free Field, Near Warehouse (See Note 7)	Vert	176	86
5-4	TR		1	--	--	Free Field, Near Meteorological Tower	Vert	84	354

*See following page for table notes.

TABLE 2

EARTHQUAKE GROUND MOTIONS RECORDED AT DCPP SITE

Earthquake	Date	Local Magnitude (M_L)	Epicenter Distance (KM)	Focal Depth (KM)	Peak Free-Field Horizontal Ground Acceleration (g)
Point Sal	5/28/80	4.6	30	6.0	.012
Coalinga	5/02/83	6.7	110	8.4	.014
Saint Martin	6/29/83	5.4	85	-	.023
Santa Maria	6/20/84	4.3	30	9.4	.011
Pt. San Luis	11/12/84	2.4	5	4.9	.027

TABLE 3

RECORDED MOTIONS

DESCRIPTION	DECK	CHANNEL	DIRECTION	EARTHQUAKE				
				PT. SAL	SANTA MARIA	COALINGA	PT. SAN LUIS	ST. MARTIN
<u>CONTAINMENT</u>	1-1	1	VERT	✓	✓	N/A	N/A	N/A
		2	N60W	N/A	✓	N/A	N/A	N/A
		3	N30E	✓	✓	N/A	N/A	N/A
	1-2	1	VERT	✓	✓	N/A	N/A	N/A
Containment		2	N60E	✓	✓	N/A	N/A	N/A
Base		3	N30W	✓	✓	N/A	N/A	N/A
	2-1	1	VERT	✓	*✓	N/A	N/A	N/A
		2	N-S	N/A	*✓	N/A	N/A	N/A
		3	E-W	N/A	*✓	N/A	N/A	N/A
	2-4	3	VERT	✓	✓	✓	N/A	N/A
		1	E-W	✓	✓	✓	N/A	N/A
		2	N-S	✓	✓	✓	N/A	N/A
	1-3	1	VERT	✓	✓	✓	N/A	N/A
		2	N-S	✓	✓	✓	N/A	N/A
Top of		3	E-W	✓	✓	✓	N/A	N/A
Internal	1-4	1	VERT	✓	*✓	✓	N/A	N/A
		2	N-S	✓	*✓	✓	N/A	N/A
		3	E-W	✓	*✓	✓	N/A	N/A
	3-1	1	N-S	✓	✓	✓	N/A	N/A
		2	E-W	✓	✓	✓	N/A	N/A
		3	VERT	N/A	N/A	N/A	N/A	N/A
	2-2	1	VERT	✓	✓	✓	N/A	N/A
		2	N60E	✓	✓	✓	N/A	N/A
		3	N30W	✓	✓	✓	N/A	N/A
Containment	2-3	1	VERT	✓	*✓	✓	N/A	N/A
@ Springline		2	N-S	✓	*✓	✓	N/A	N/A
		3	E-W	*✓	*✓	*✓	N/A	N/A
	3-2	1	VERT	✓	✓	✓	N/A	N/A
		2	N60W	✓	✓	✓	N/A	N/A
		3	N30E	✓	✓	✓	N/A	N/A

<u>Notes</u>: ✓ = Available, N/A = Not Available, * = Used in the analysis.

TABLE 3

RECORDED MOTIONS (Cont'd)

DESCRIPTION	DECK	CHANNEL	DIRECTION	EARTHQUAKE: PT. SAL	EARTHQUAKE: SANTA MARIA	EARTHQUAKE: COALINGA	EARTHQUAKE: PT. SAN LUIS	EARTHQUAKE: ST. MARTIN
AUX. BLDG.								
	3-3	1	VERT	N/A	√	√	√	√
North Wing		2	N-S	N/A	√	√	*√	*√
@ El. 100		3	E-W	N/A	√	√	*√	*√
	3-4	1	VERT	N/A	√	√	√	√
Core West		2	E-W	N/A	√	√	*√	*√
@ El. 100		3	N-S	N/A	√	√	*√	*√
	4-1	1	VERT	√	√	√	N/A	N/A
		2	E-W	√	√	√	N/A	N/A
		3	N-S	√	√	√	N/A	N/A
TURBINE BLDG.								
	5-2	1	VERT	N/A	√	N/A	N/A	N/A
Turbine		2	N-S	N/A	√	N/A	N/A	N/A
Base		3	E-W	N/A	√	N/A	N/A	N/A
	4-2	1	VERT	N/A	√	√	N/A	N/A
		2	N-S	N/A	√	√	N/A	N/A
		3	E-W	N/A	√	√	N/A	N/A
Turbine	4-3	3A	N-S	*√	N/A	N/A	N/A	N/A
Deck, N End	4-4	3B	E-W	N/A	√	N/A	N/A	N/A
FREE-FIELD GROUND MOTION								
	5-3	1	VERT	N/A	N/A	√	√	√
Near		2	N-S	N/A	N/A	√	*√	*√
Reservoir		3	E-W	N/A	N/A	√	*√	*√
Near	5-4	1	VERT	N/A	√	N/A	√	N/A
Meteorolo-		2	E-W	N/A	*√	N/A	√	N/A
gical Tower		3	N-S	N/A	√	N/A	√	N/A
Near	6-1	1	VERT	√	N/A	√	√	N/A
Warehouse		2	N-S	*√	N/A	√	√	N/A
		3	E-W	*√	N/A	*√	√	N/A

Notes: √ = Available, N/A = Not Available, * = Used in the analysis.

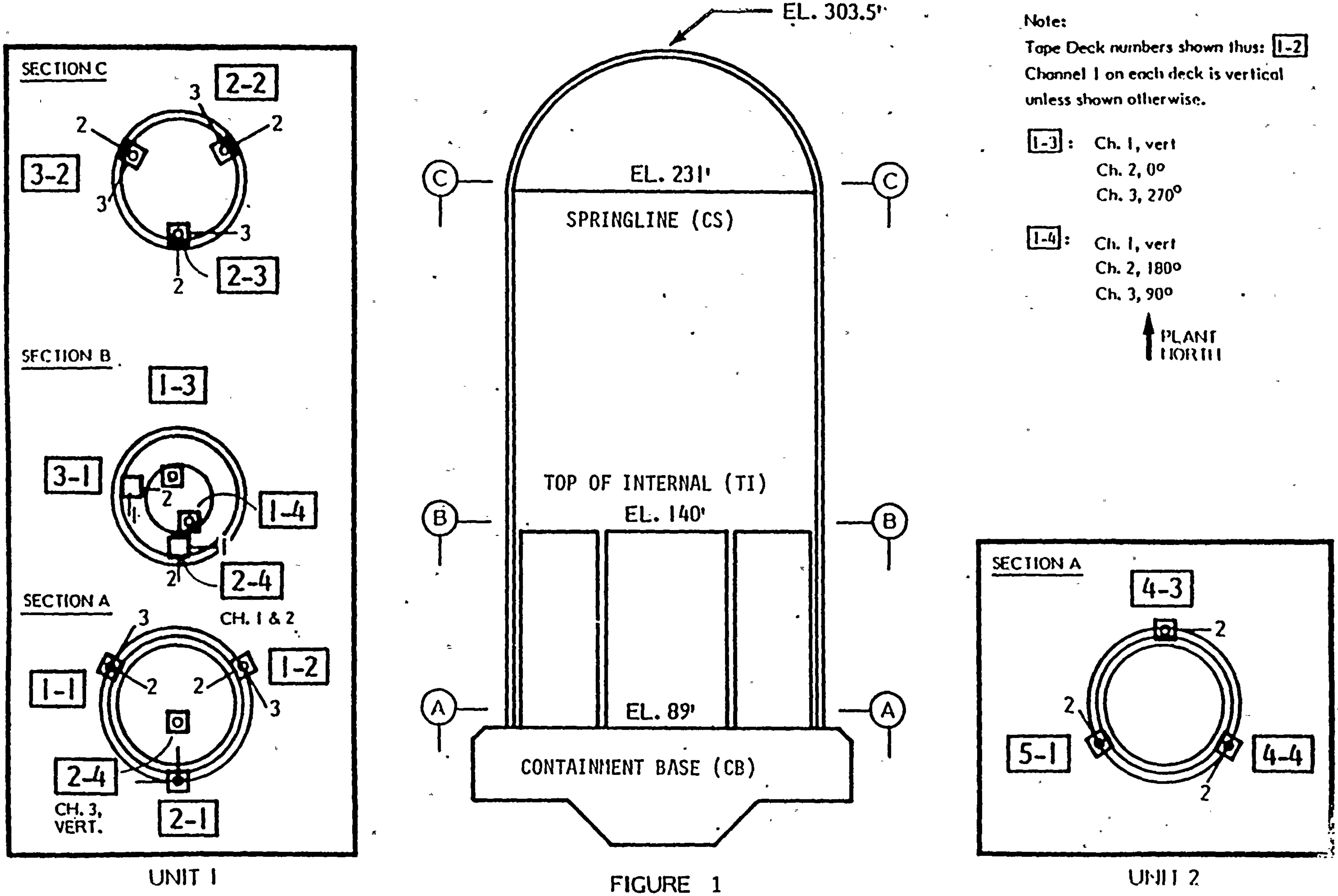

FIGURE 1

SUPPLEMENTAL SEISMIC INSTRUMENTATION
CONTAINMENT STRUCTURES
DIABLO CANYON UNITS 1 & 2

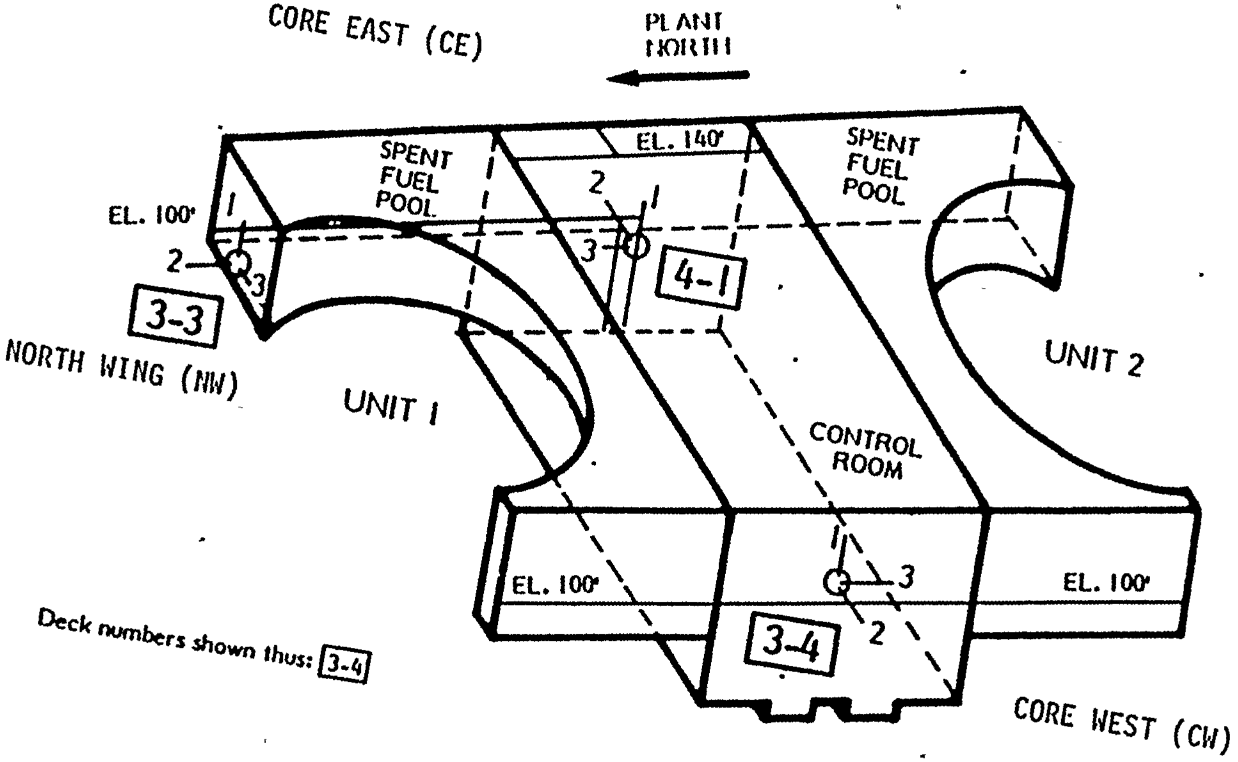

FIGURE 2
SUPPLEMENTAL SEISMIC INSTRUMENTATION
AUXILIARY BUILDING
DIABLO CANYON UNITS 1 & 2

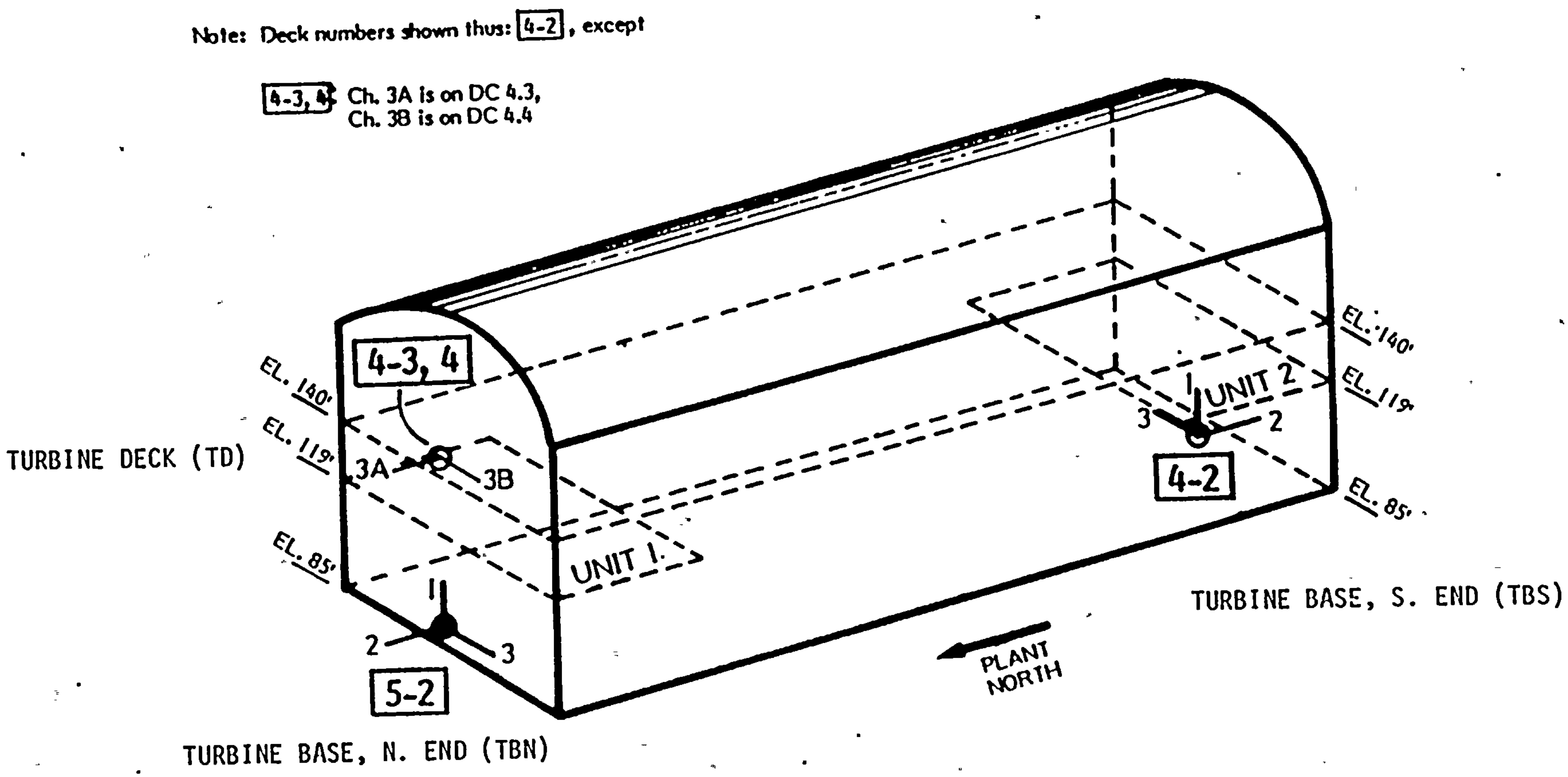

FIGURE 3
SUPPLEMENTAL SEISMIC INSTRUMENTATION
TURBINE BUILDING
DIABLO CANYON UNITS 1 & 2

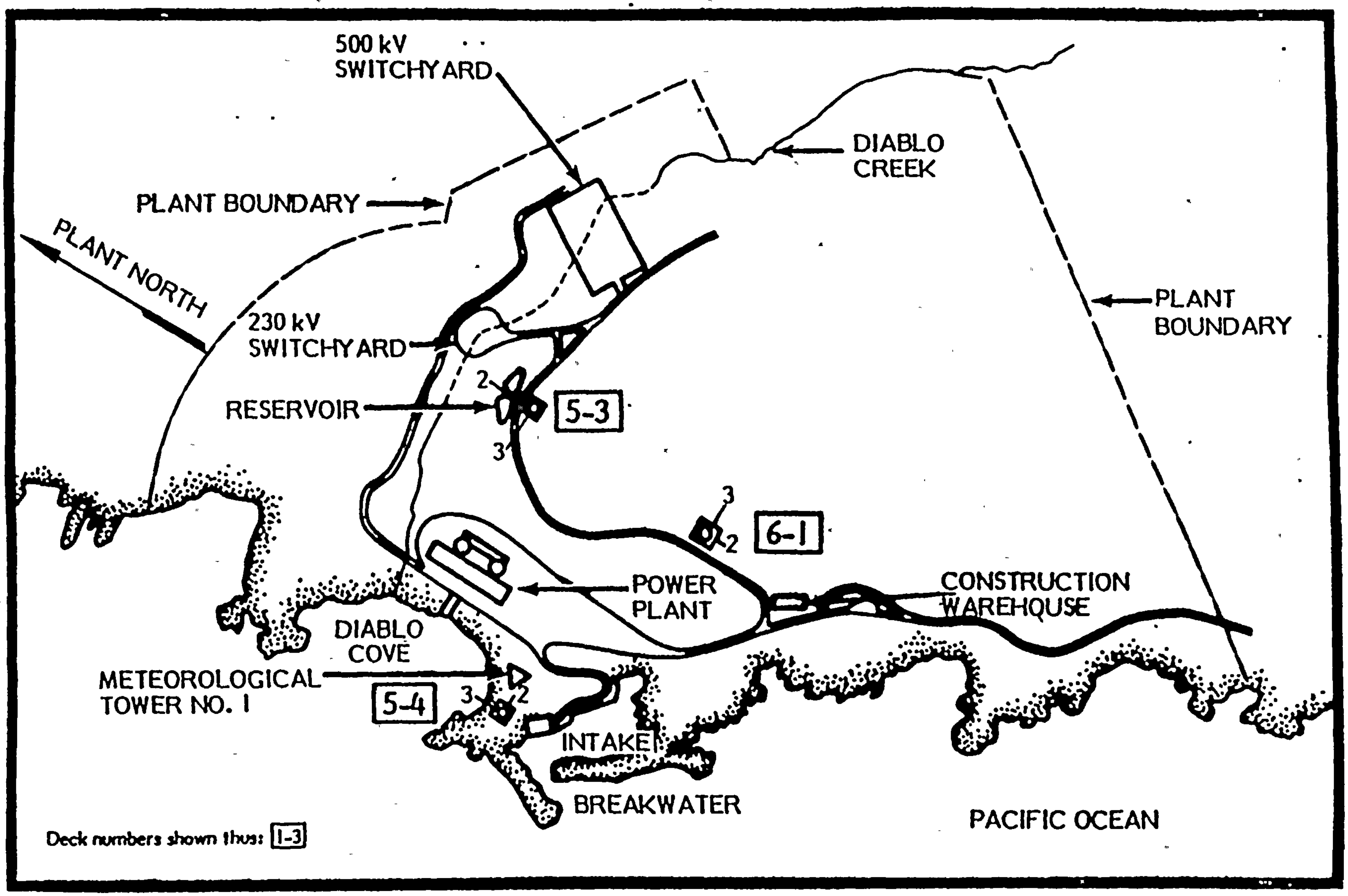

FIGURE 4

SUPPLEMENTAL SEISMIC INSTRUMENTATION
IN FREE FIELD
DIABLO CANYON POWER PLANT

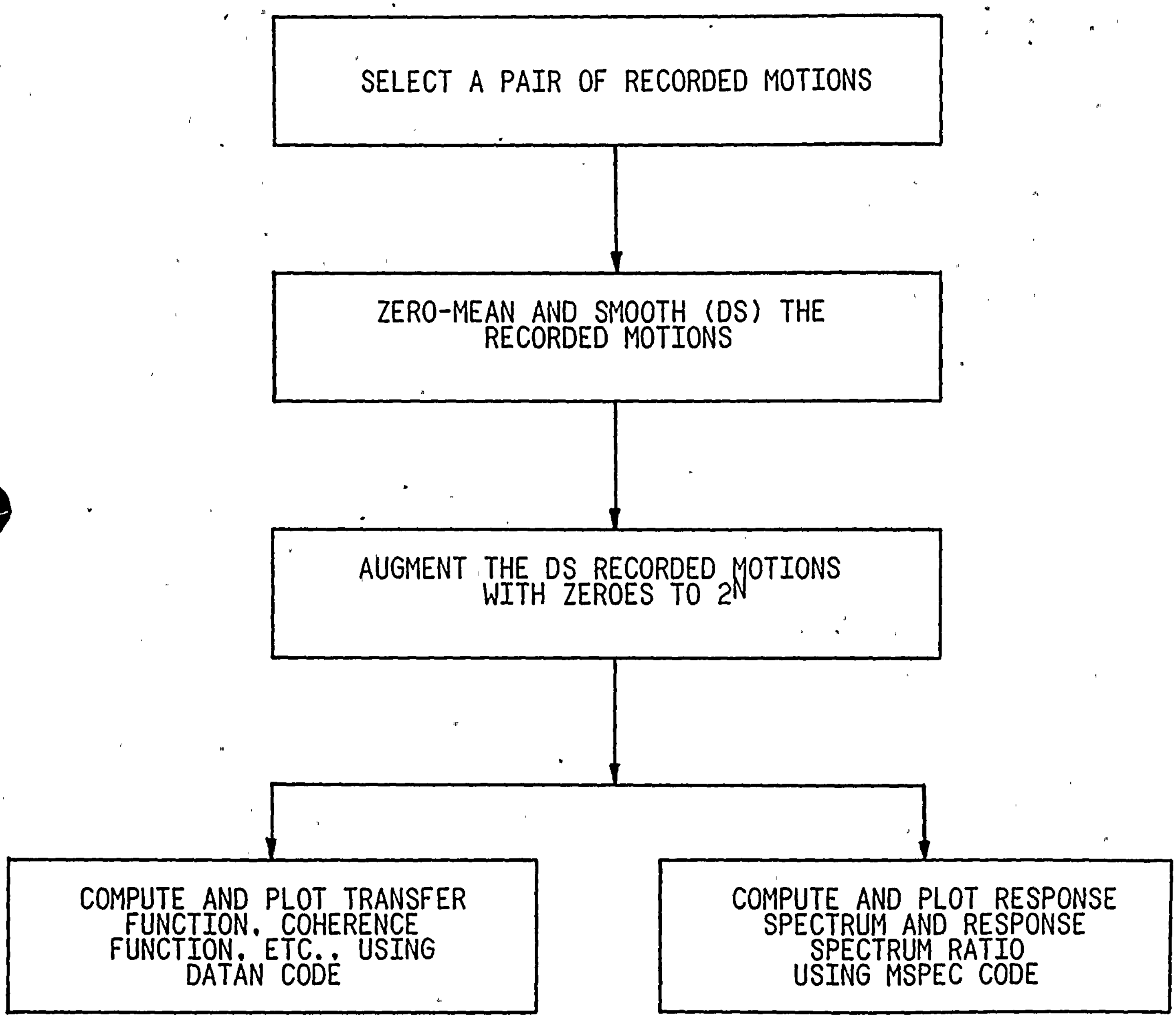

FIGURE 5 SCHEMATIC DIAGRAM OF DATA ANALYSIS TECHNIQUES

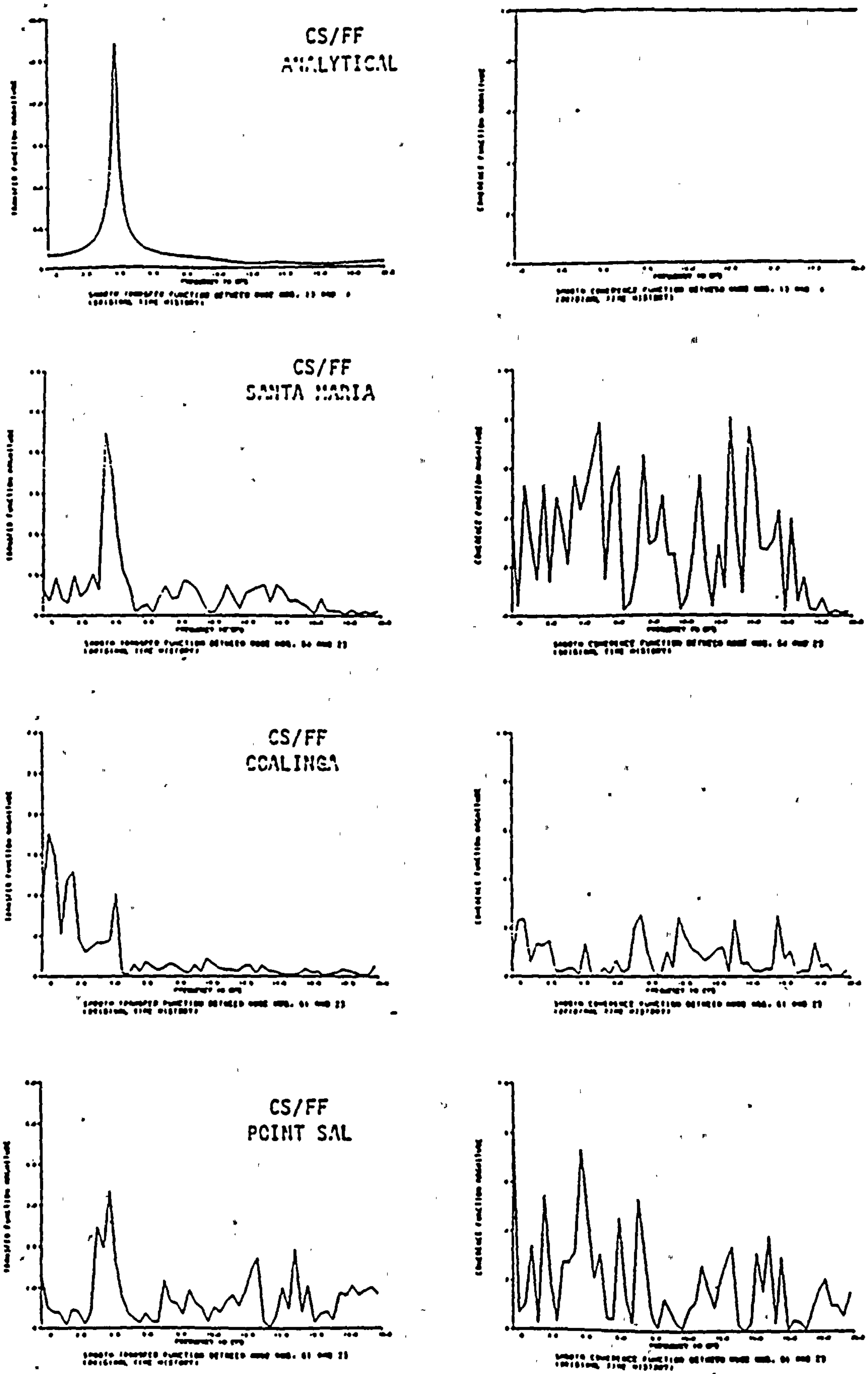

FIGURE 6 EAST-WEST COMPONENT AT CONTAINMENT SPRINGLINE (CS) AND FREE-FIELD (FF) - ANALYTICAL AND EARTHQUAKE RECORDS

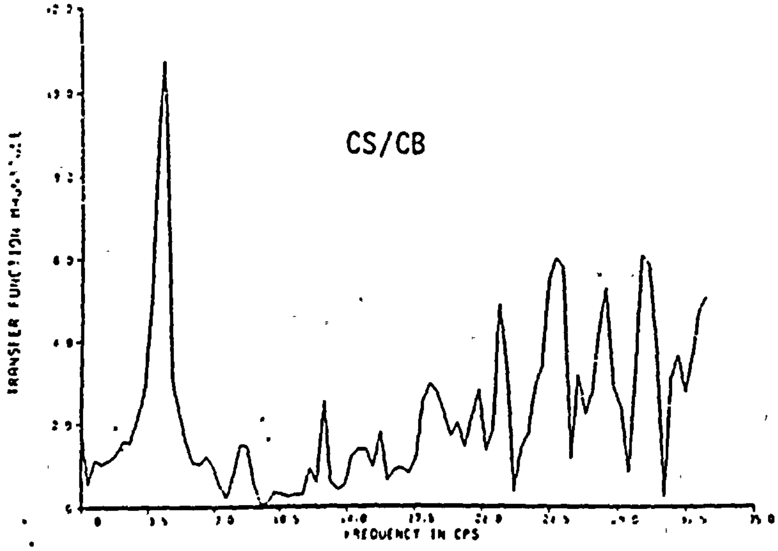

TRANSFER FUNCTION

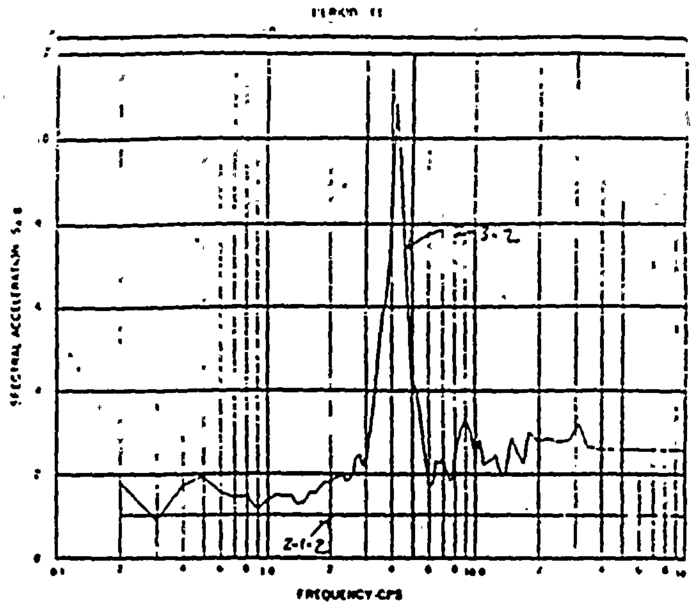

RESPONSE SPECTRUM RATIO

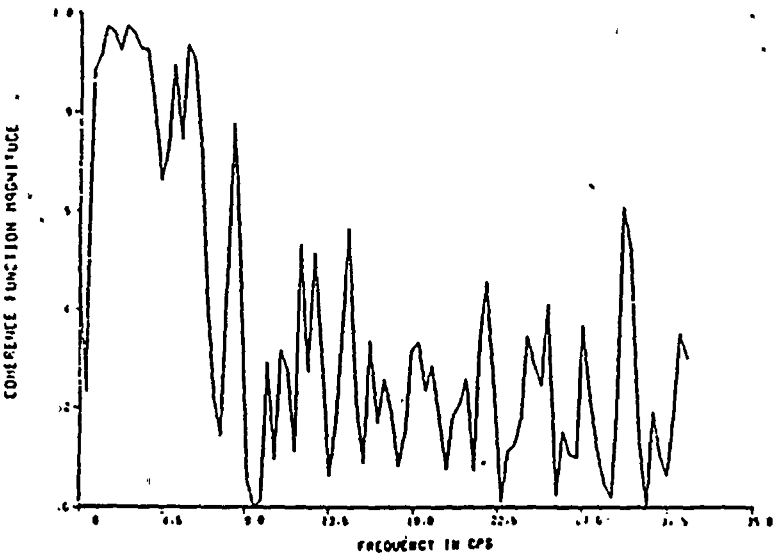

COHERENCE FUNCTION

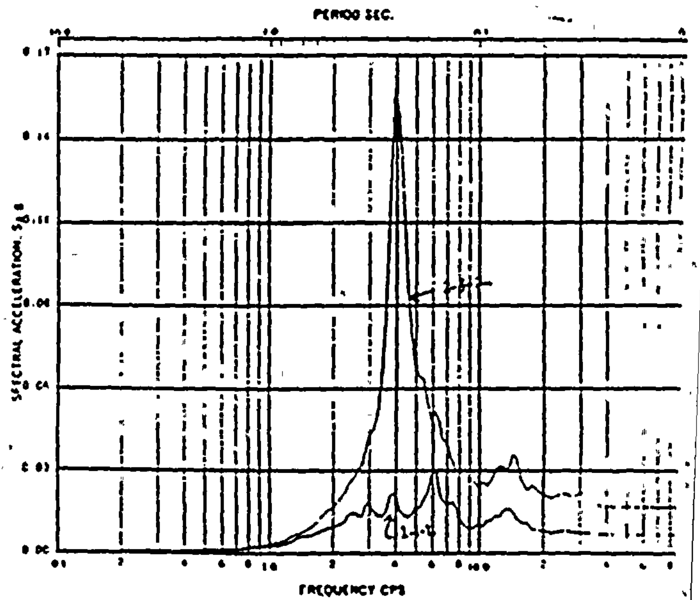

RESPONSE SPECTRUM

FIGURE 7 NORTH-SOUTH COMPONENT AT CONTAINMENT SPRING LINE (CS) AND CONTAINMENT BASE (CB) - SANTA MARIA EARTHQUAKE

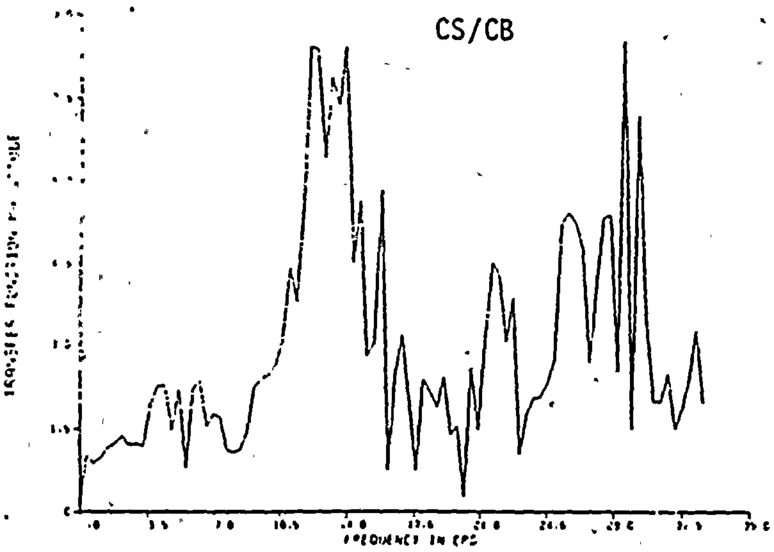

TRANSFER FUNCTION

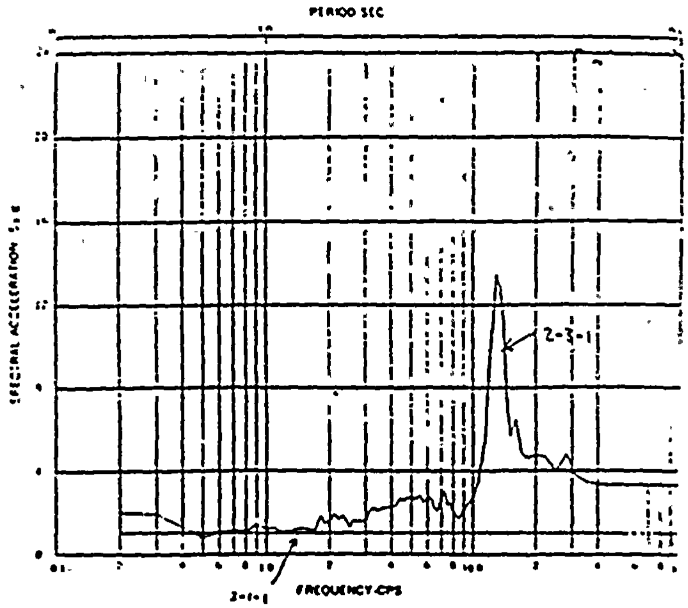

RESPONSE SPECTRUM RATIO

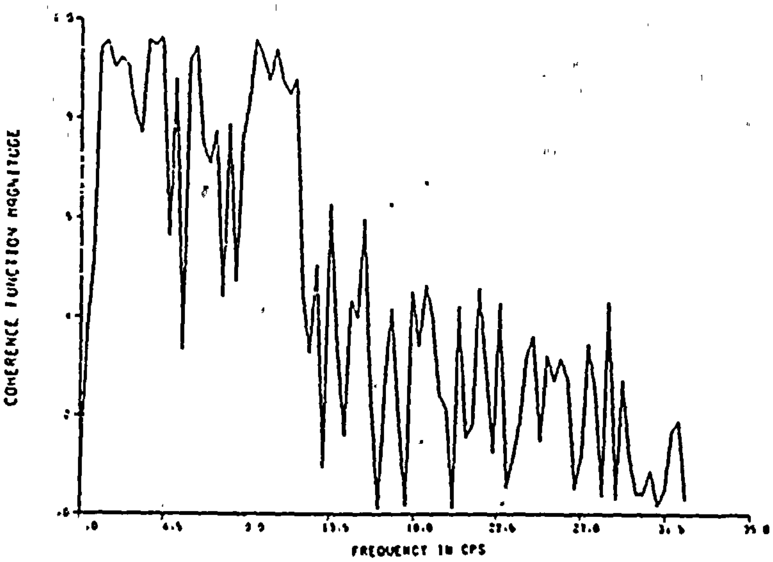

COHERENCE FUNCTION

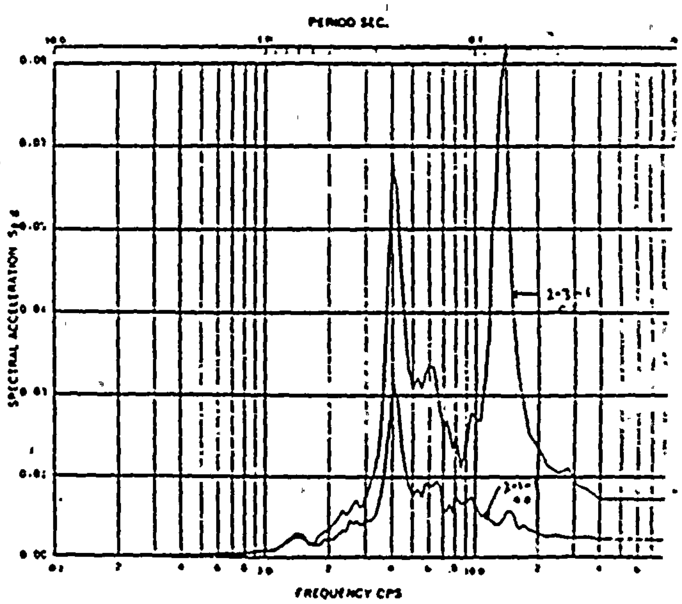

RESPONSE SPECTRUM

FIGURE 8 VERTICAL COMPONENT AT CONTAINMENT SPRINGLINE (CS) AND CONTAINMENT BASE (CB) - SANTA MARIA EARTHQUAKE

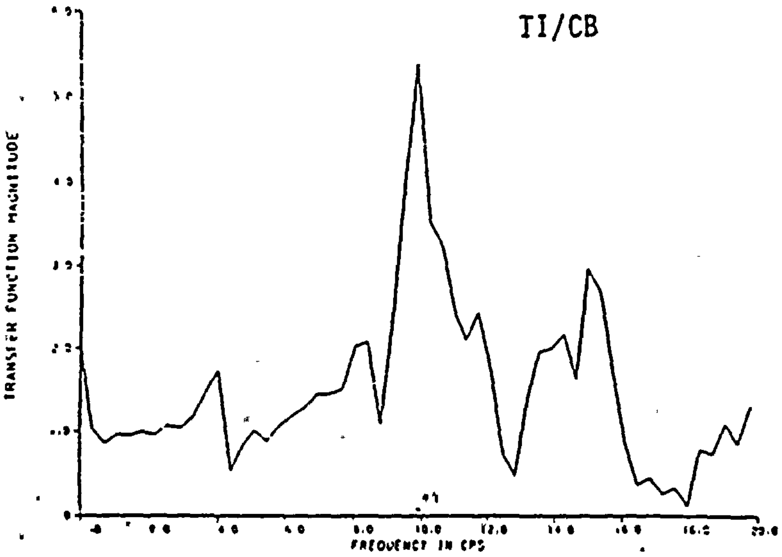

TRANSFER FUNCTION

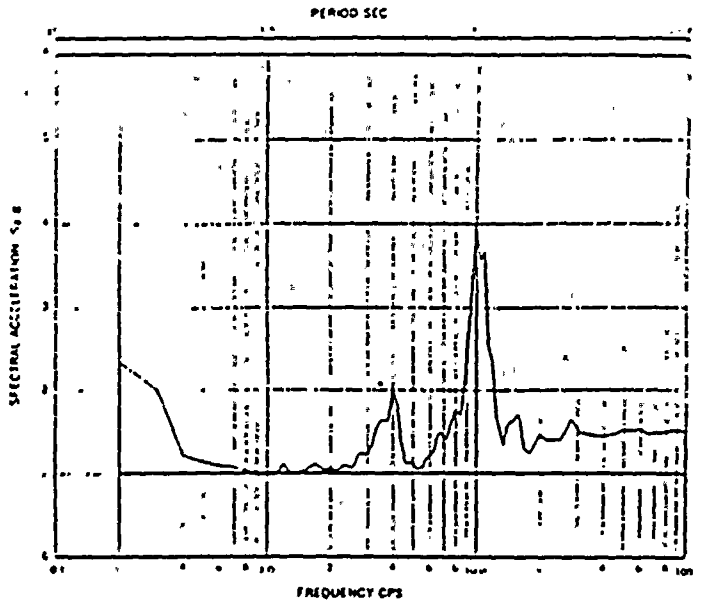

RESPONSE SPECTRUM RATIO

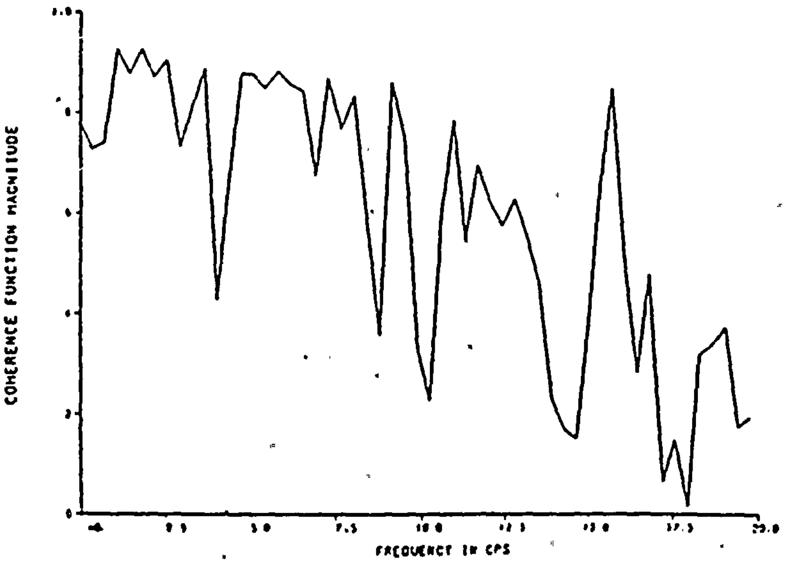

COHERENCE FUNCTION

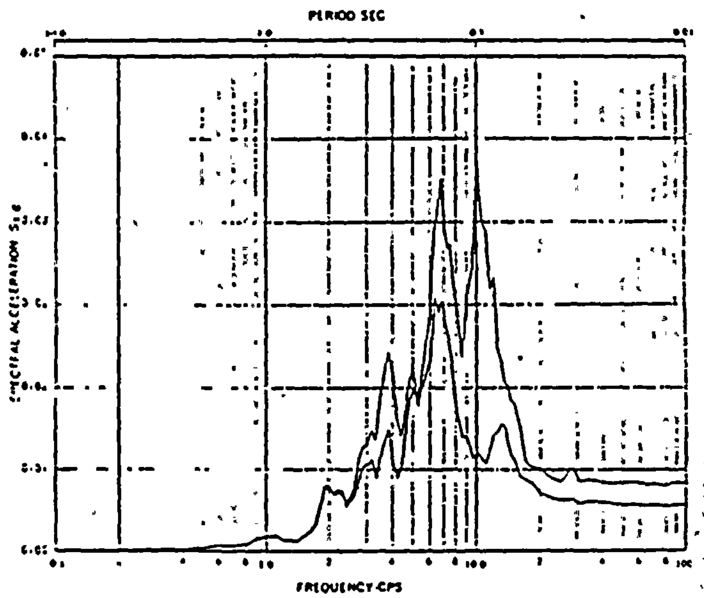

RESPONSE SPECTRUM

FIGURE 9 EAST-WEST COMPONENT AT TOP OF INTERNAL STRUCTURE (TI) AND CONTAINMENT BASE (CB) - SANTA MARIA EARTHQUAKE

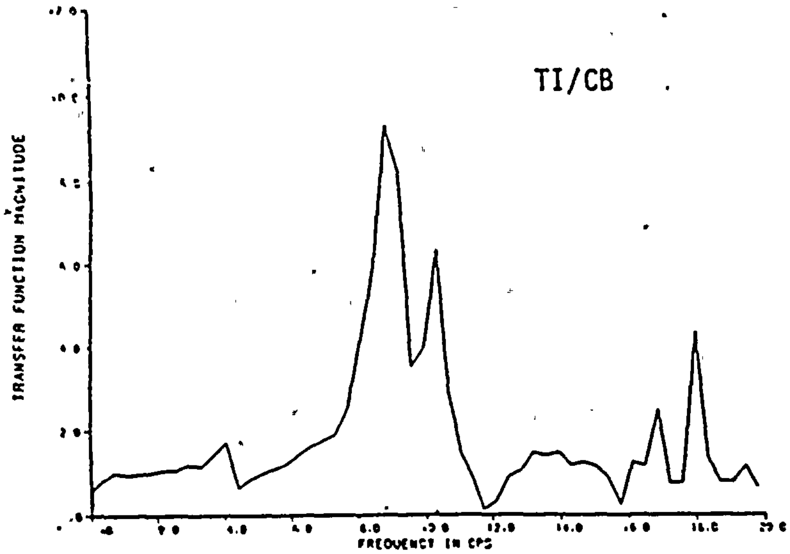

TRANSFER FUNCTION

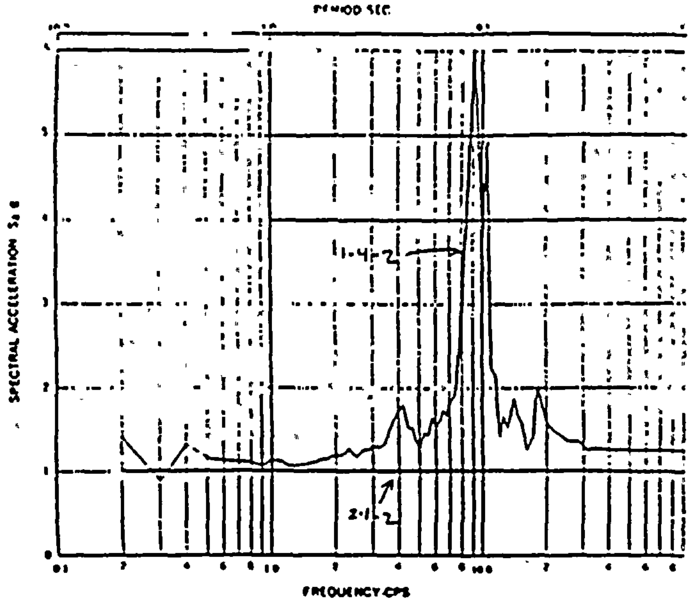

RESPONSE SPECTRUM RATIO

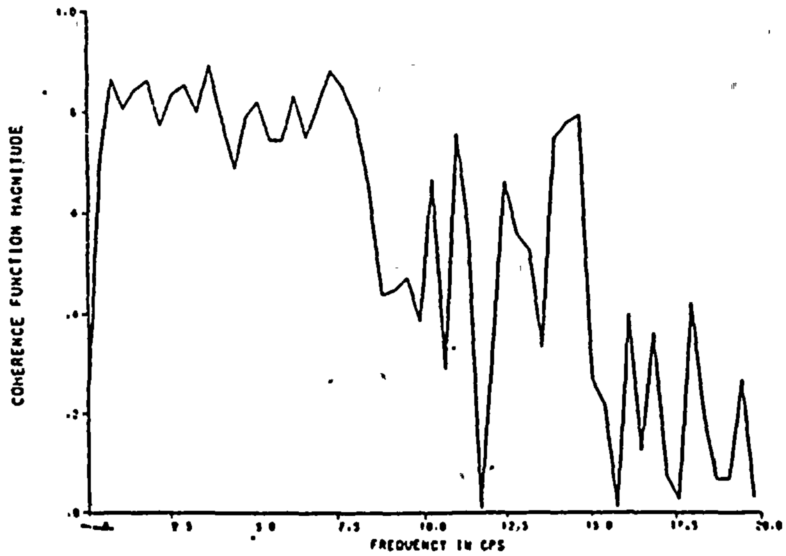

COHERENCE FUNCTION

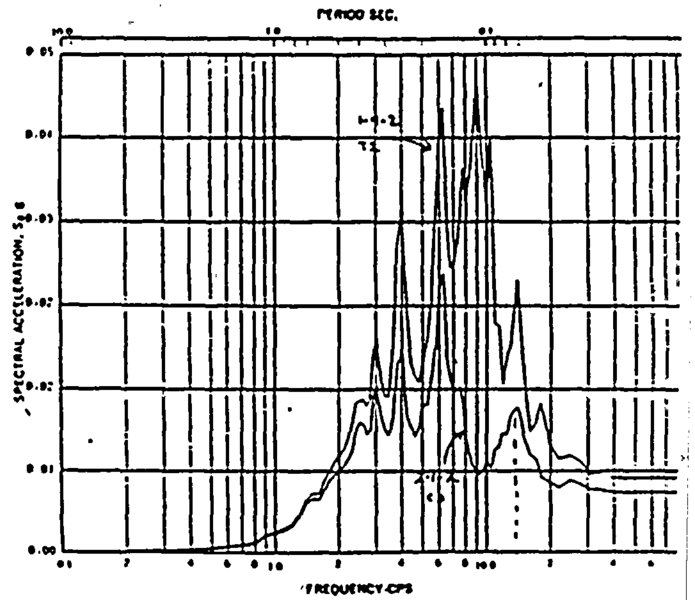

RESPONSE SPECTRUM

FIGURE 10 NORTH-SOUTH COMPONENT AT TOP OF INTERNAL STRUCTURE (TI) AND CONTAINMENT BASE (CB) - SANTA MARIA EARTHQUAKE

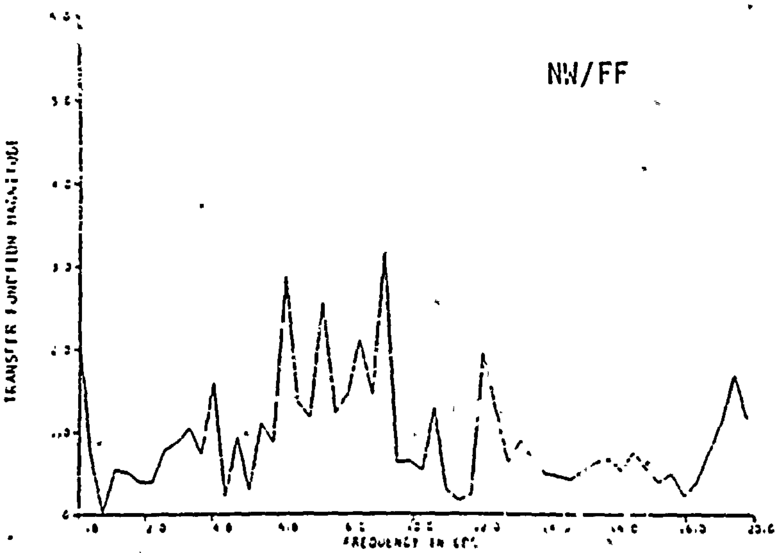

TRANSFER FUNCTION

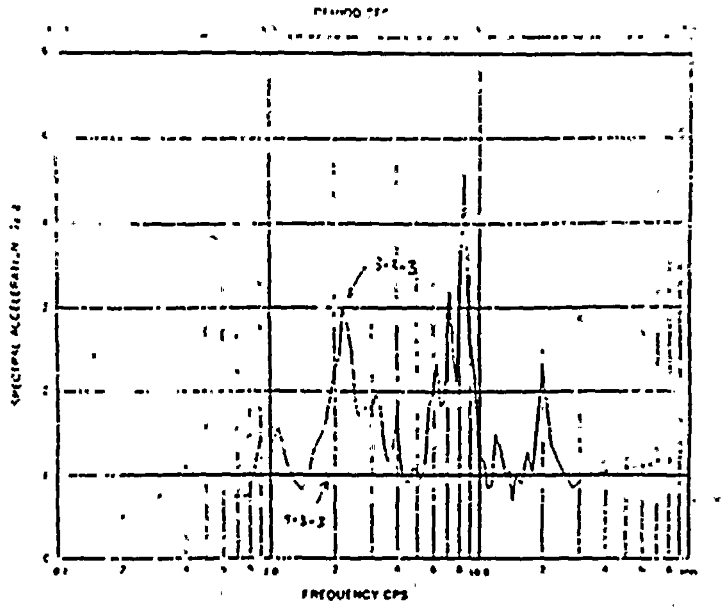

RESPONSE SPECTRUM RATIO

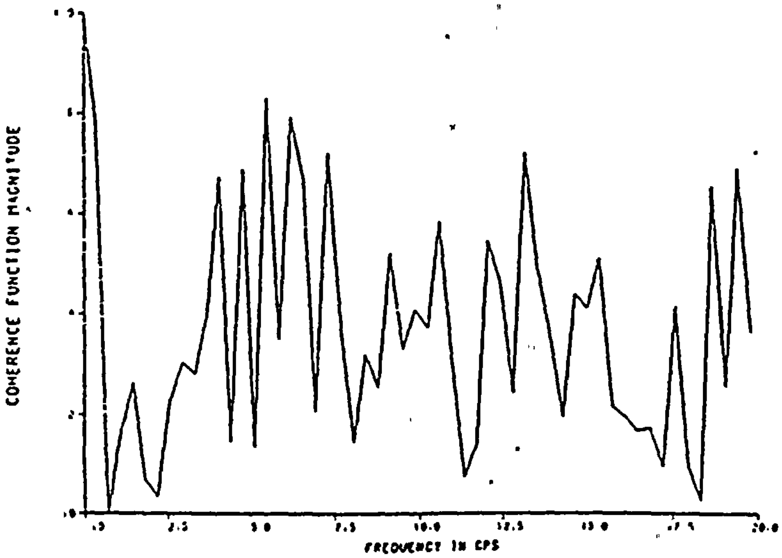

COHERENCE FUNCTION

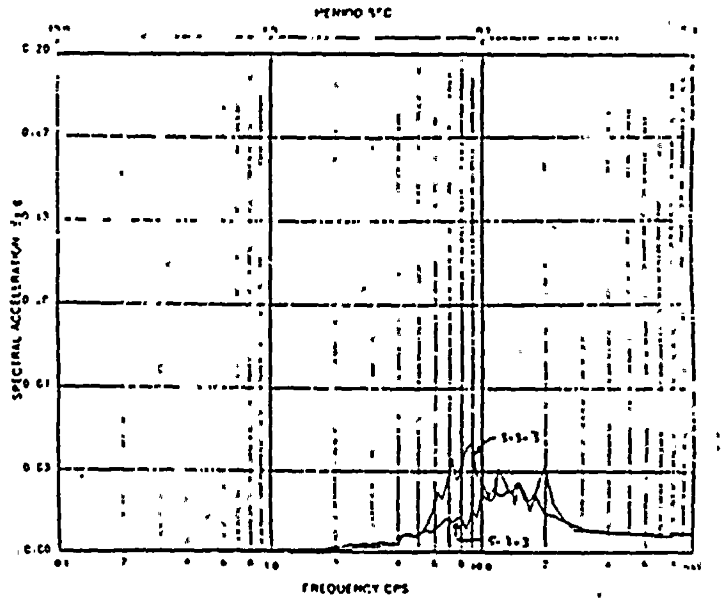

RESPONSE SPECTRUM

FIGURE 11   EAST-WEST COMPONENT AT NORTH WING OF AUXILIARY BUILDING (NW) AND FREE-FIELD (FF) - SAN LUIS EARTHQUAKE

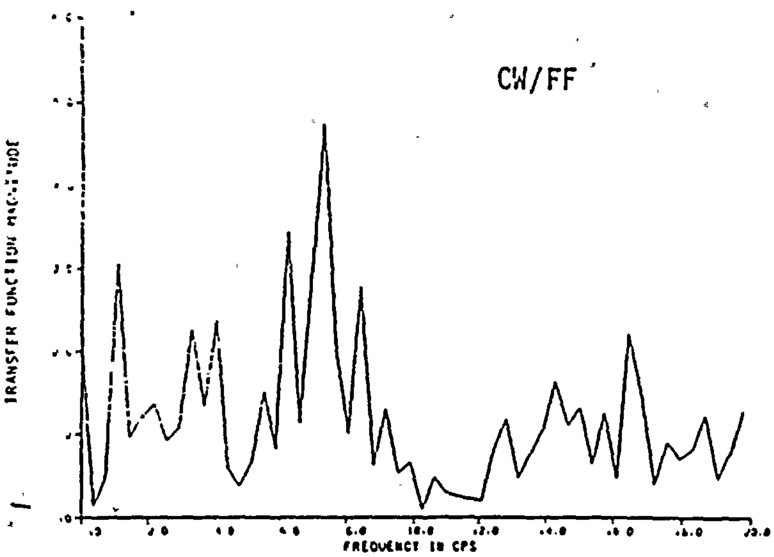

TRANSFER FUNCTION

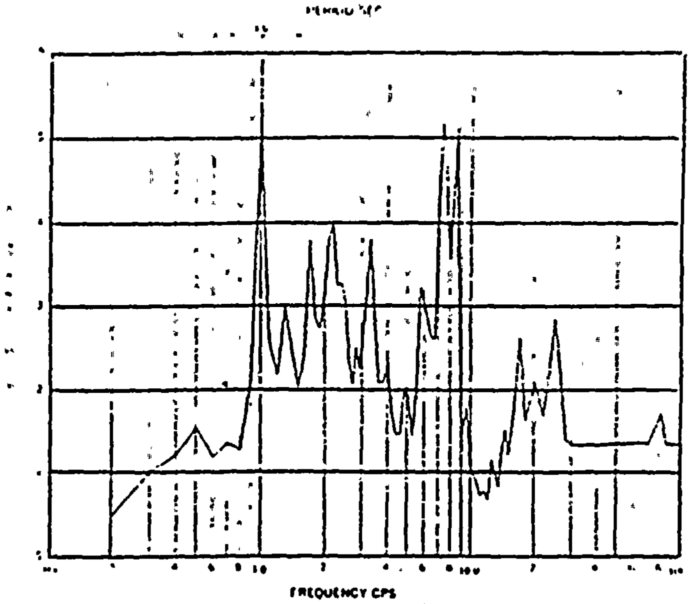

RESPONSE SPECTRUM RATIO

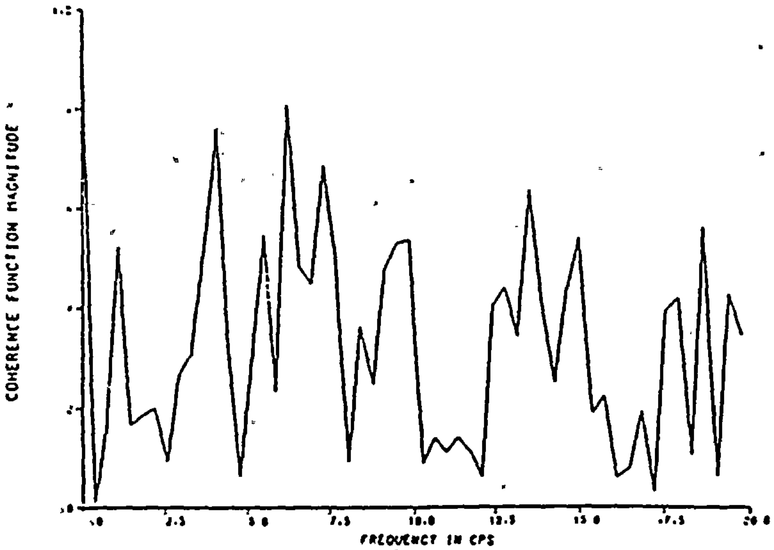

COHERENCE FUNCTION

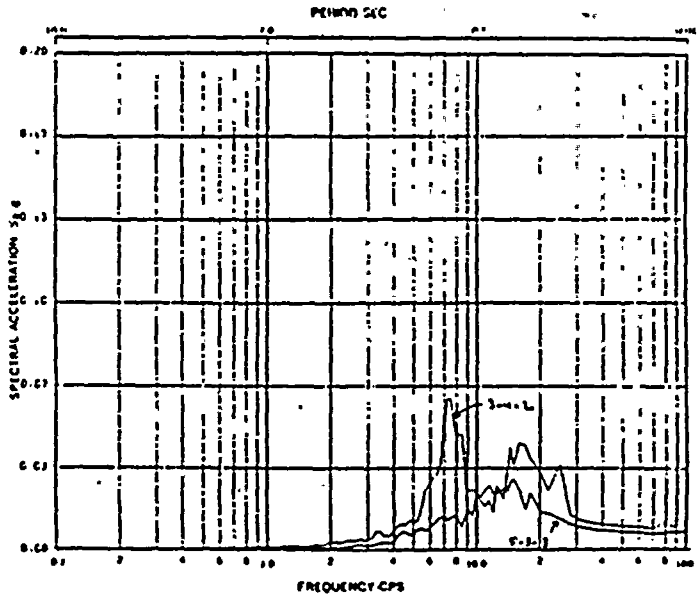

RESPONSE SPECTRUM

FIGURE 12 EAST-WEST COMPONENT AT CORE WEST OF AUXILIARY BUILDING (CW) AND FREE-FIELD (FF) - SAN LUIS EARTHQUAKE

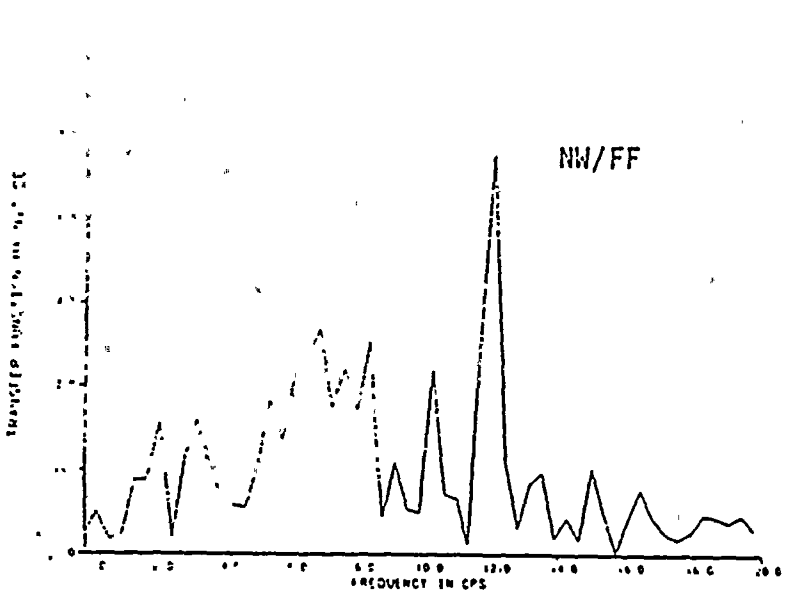

TRANSFER FUNCTION

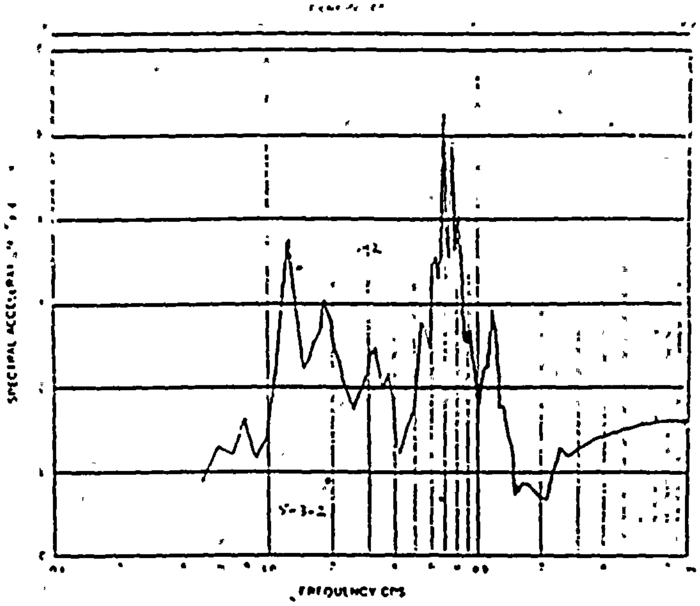

RESPONSE SPECTRUM RATIO

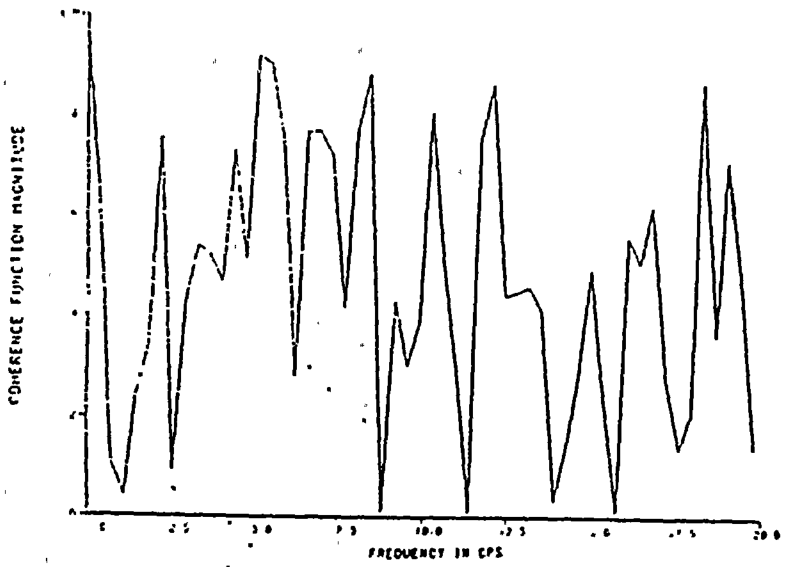

COHERENCE FUNCTION

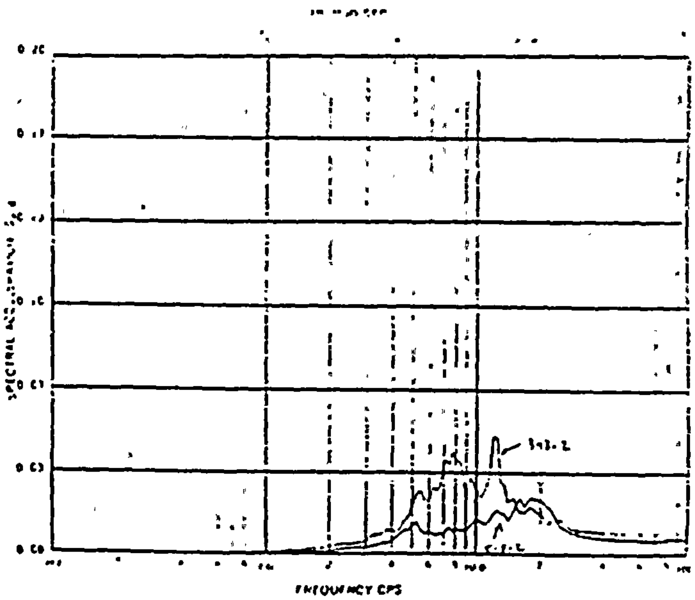

RESPONSE SPECTRUM

FIGURE 13 NORTH-SOUTH COMPONENT AT NORTH WING (NW) OF AUXILIARY BUILDING AND FREE-FIELD (FF) - SAN LUIS EARTHQUAKE

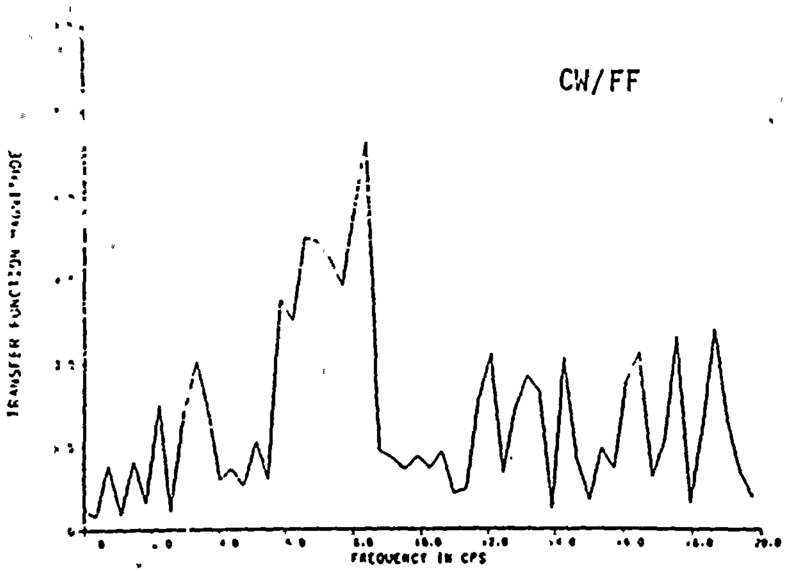

TRANSFER FUNCTION

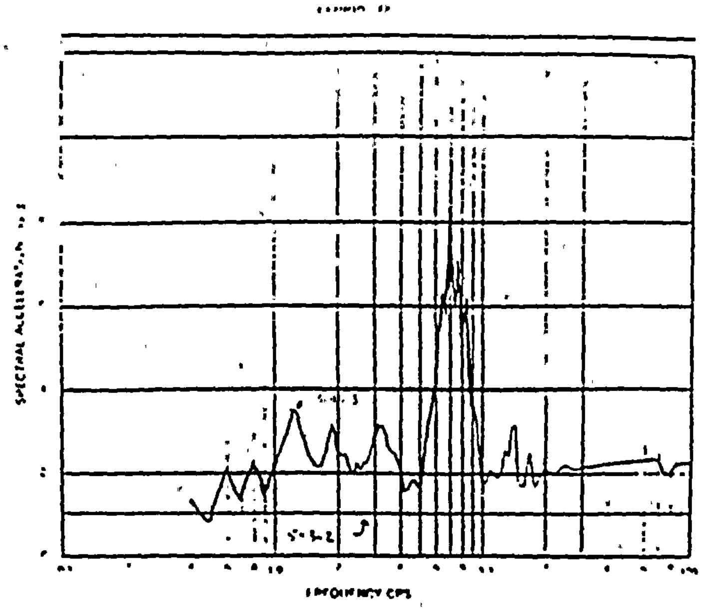

RESPONSE SPECTRUM RATIO

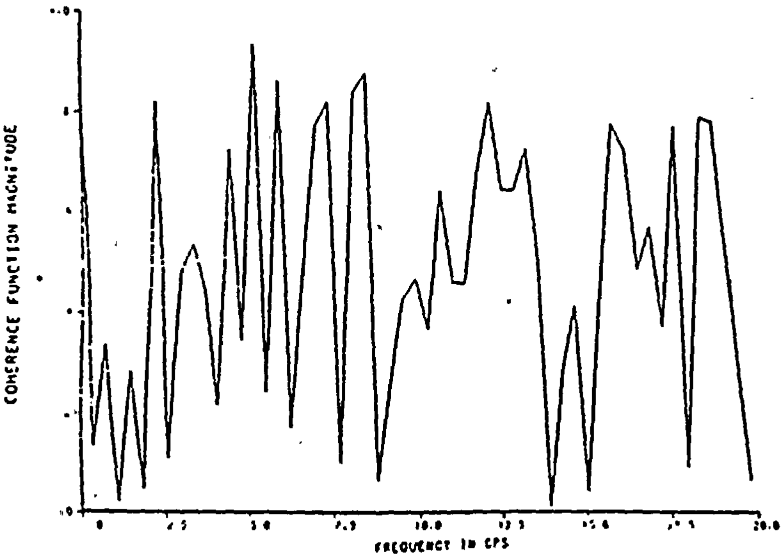

COHERENCE FUNCTION

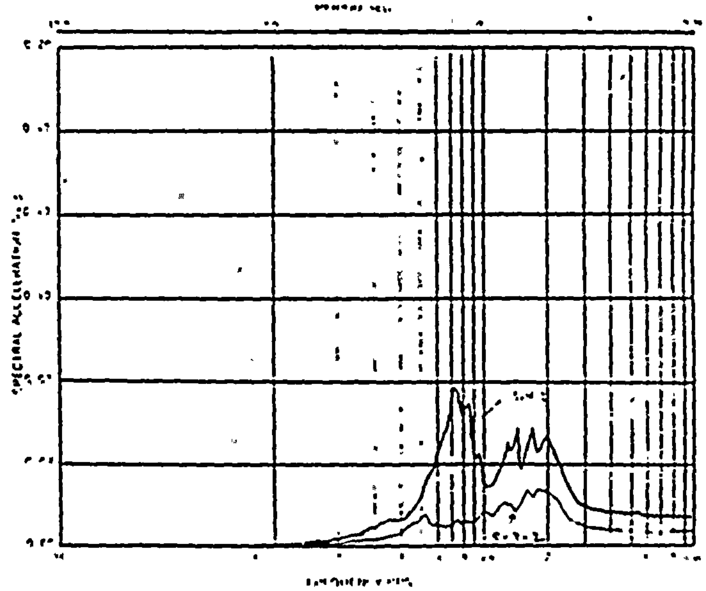

RESPONSE SPECTRUM

FIGURE 14 NORTH-SOUTH COMPONENT AT CORE WEST (CW) OF AUXILIARY BUILDING AND FREE-FIELD (FF) - SAN LUIS EARTHQUAKE

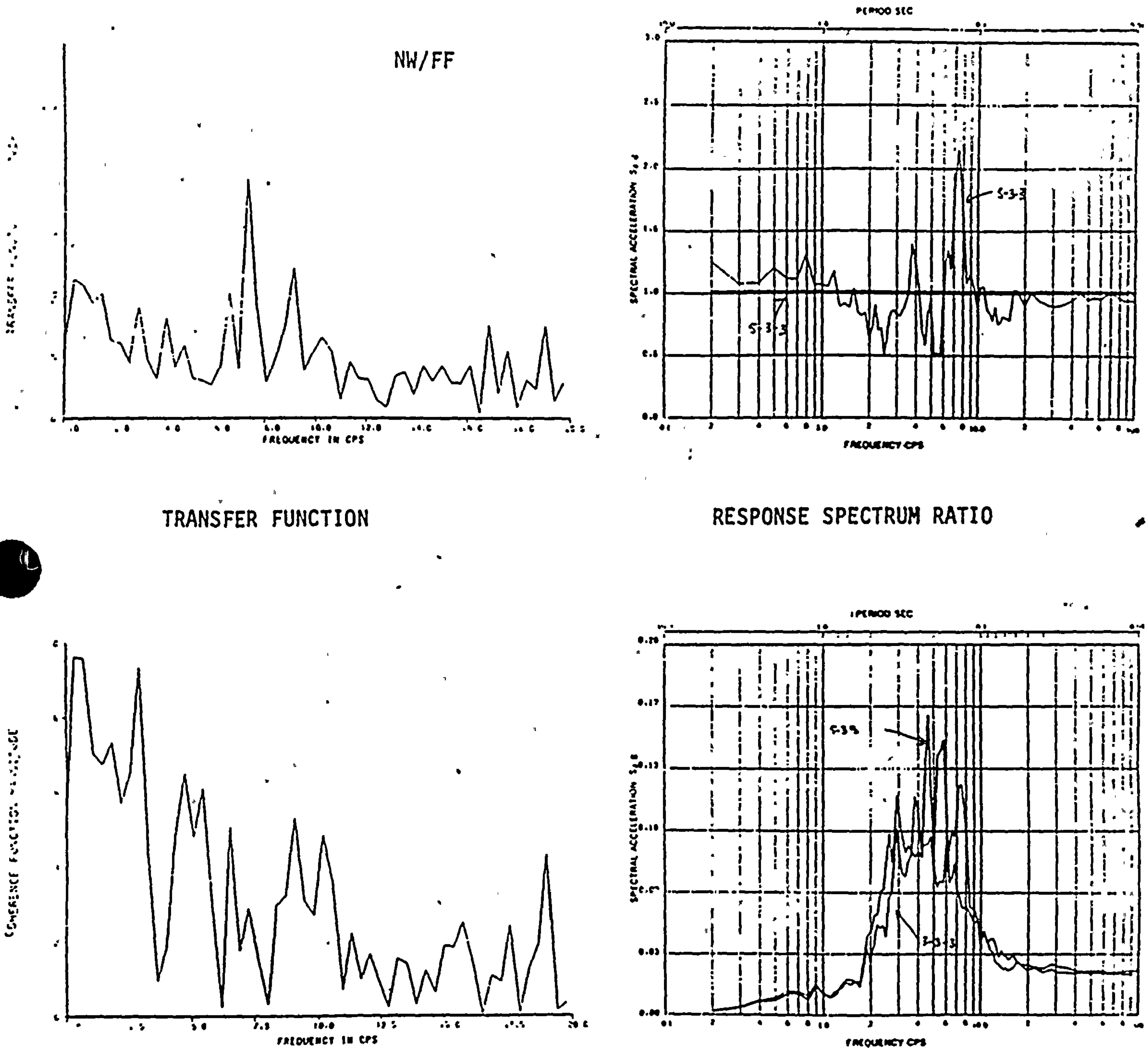

TRANSFER FUNCTION

RESPONSE SPECTRUM RATIO

COHERENCE FUNCTION

RESPONSE SPECTRUM

FIGURE 15 EAST-WEST COMPONENT AT NORTH WING (NW) OF AUXILIARY BUILDING AND FREE-FIELD (FF) - ST. MARTIN EARTHQUAKE

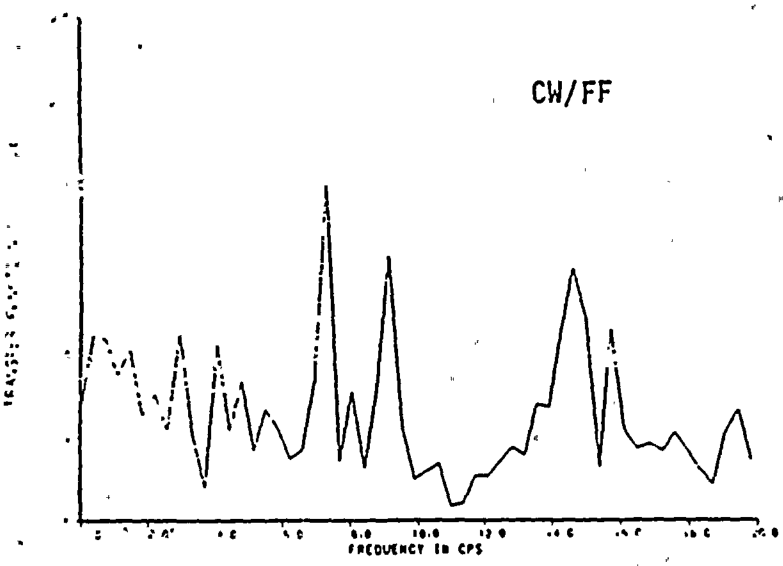

TRANSFER FUNCTION

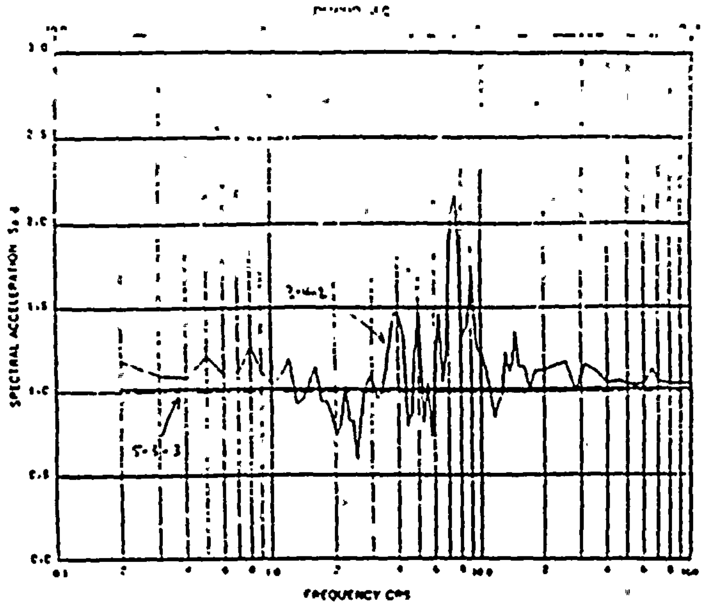

RESPONSE SPECTRUM RATIO

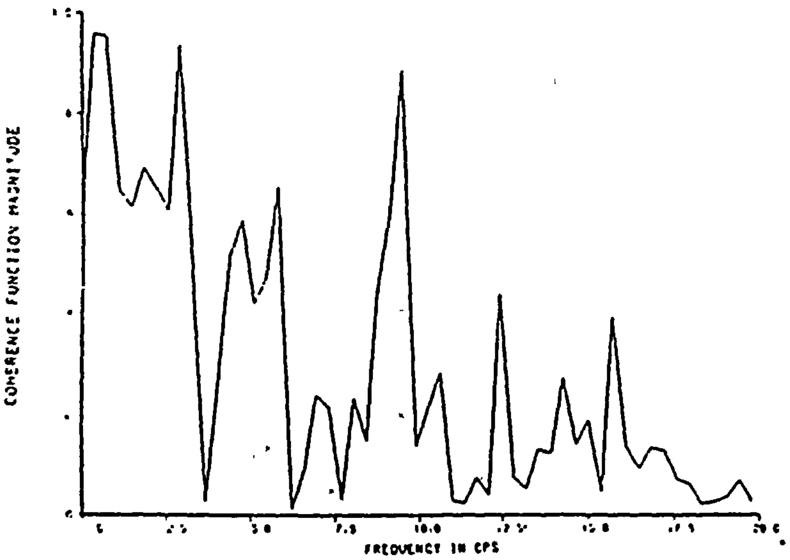

COHERENCE FUNCTION

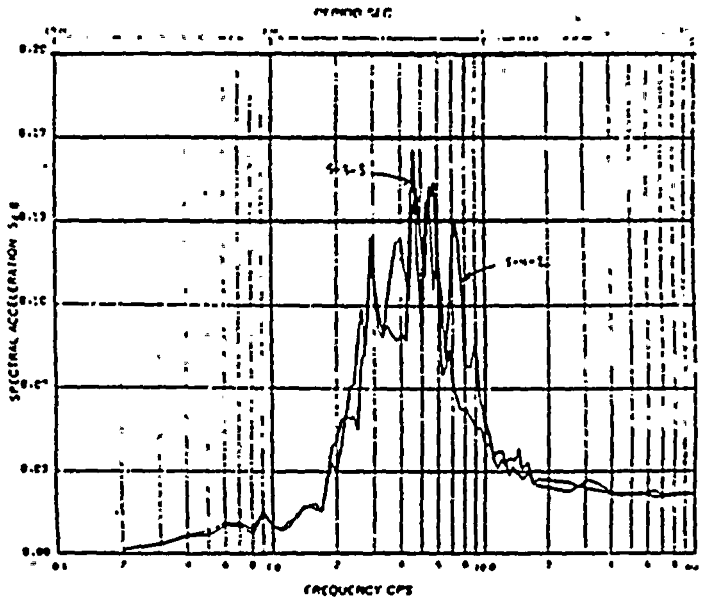

RESPONSE SPECTRUM

FIGURE 16   EAST-WEST COMPONENT AT CORE WEST (CW) OF AUXILIARY BUILDING AND FREE-FIELD (FF) - ST. MARTIN EARTHQUAKE

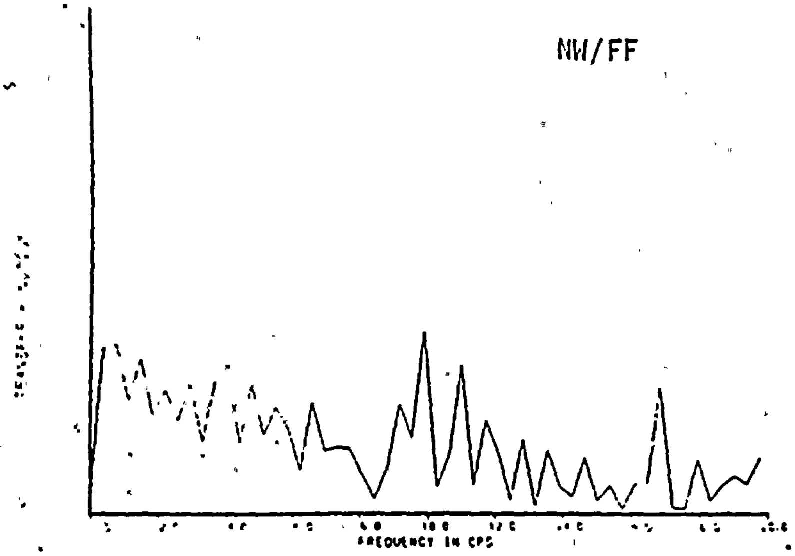

TRANSFER FUNCTION

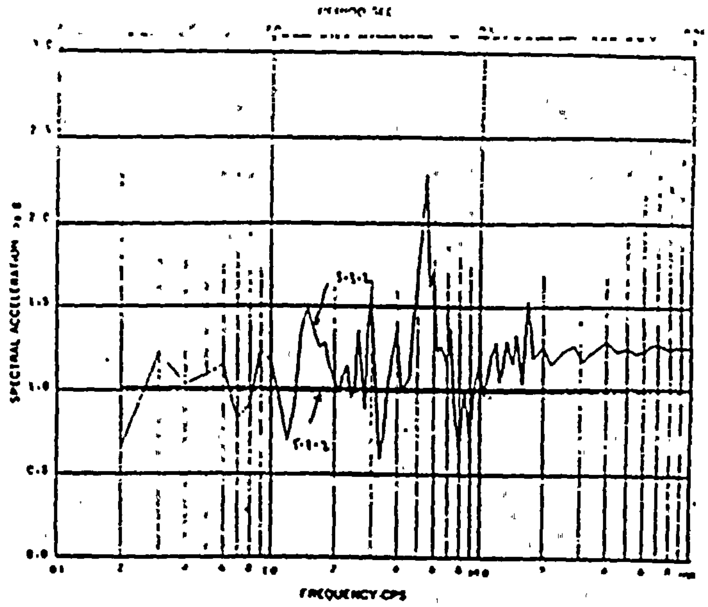

RESPONSE SPECTRUM RATIO

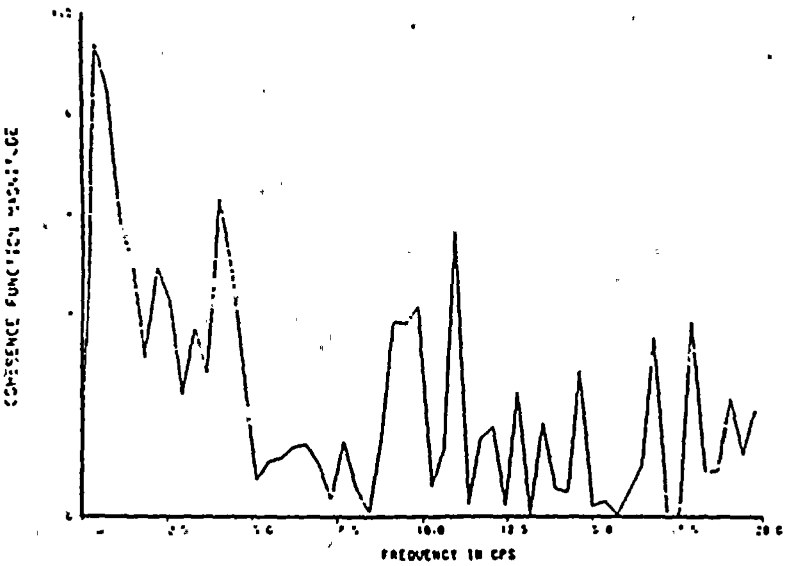

COHERENCE FUNCTION

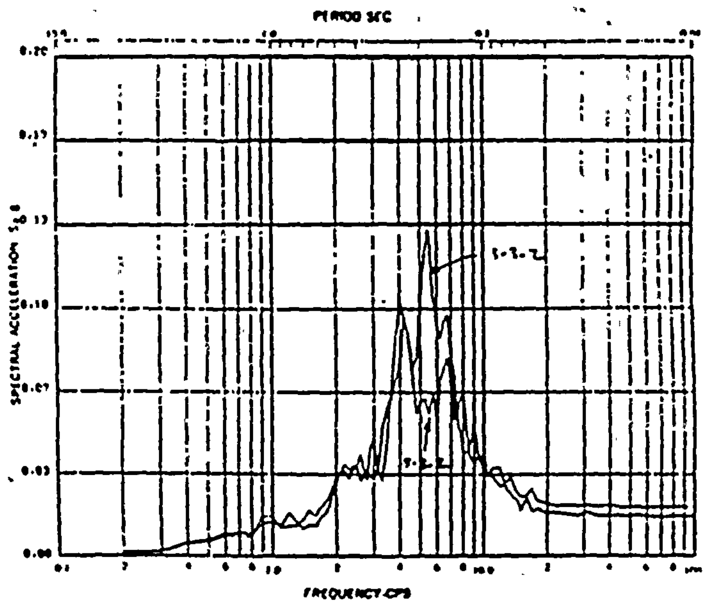

RESPONSE SPECTRUM

FIGURE 17 NORTH-SOUTH COMPONENT AT NORTH WING (NW) OF AUXILIARY BUILDING AND FREE-FIELD (FF) - ST. MARTIN EARTHQUAKE

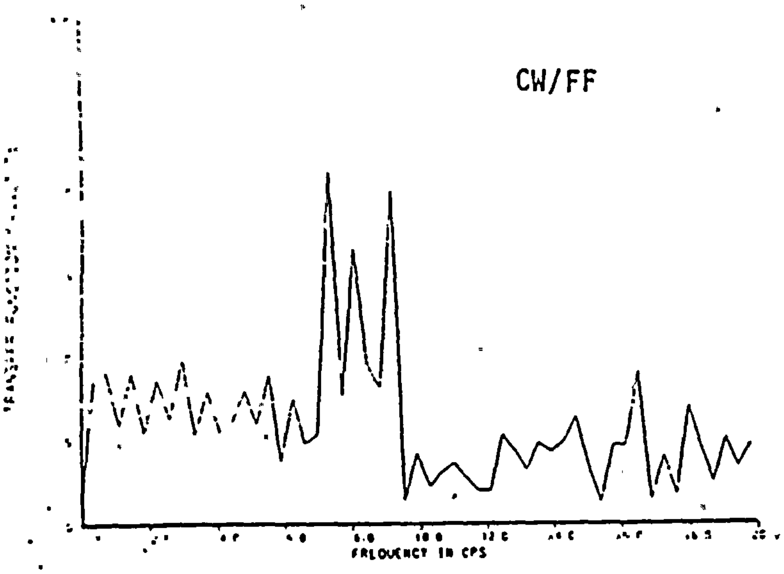

TRANSFER FUNCTION

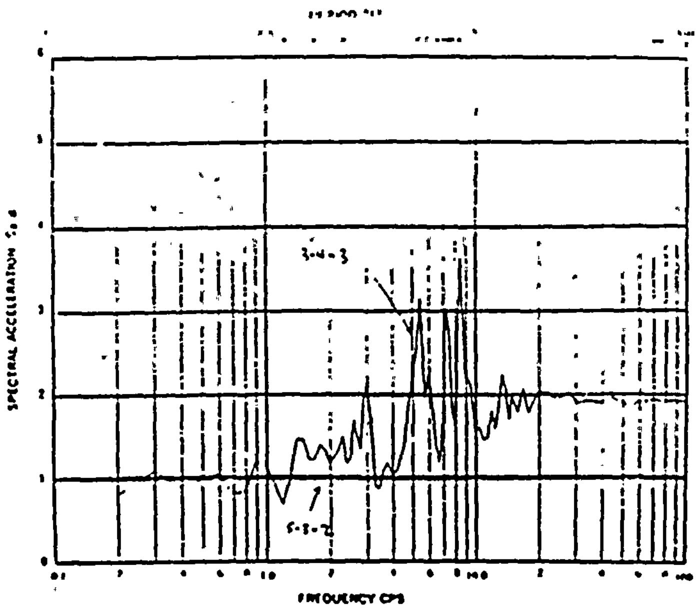

RESPONSE SPECTRUM RATIO

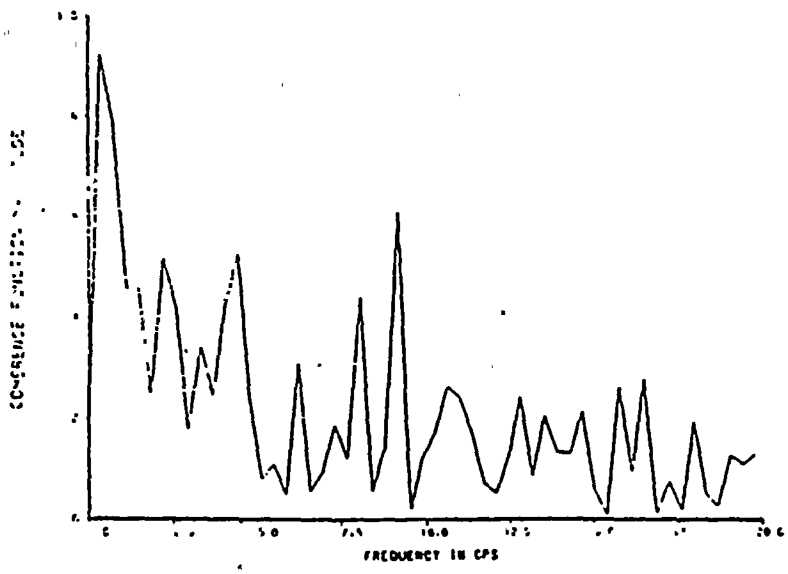

COHERENCE FUNCTION

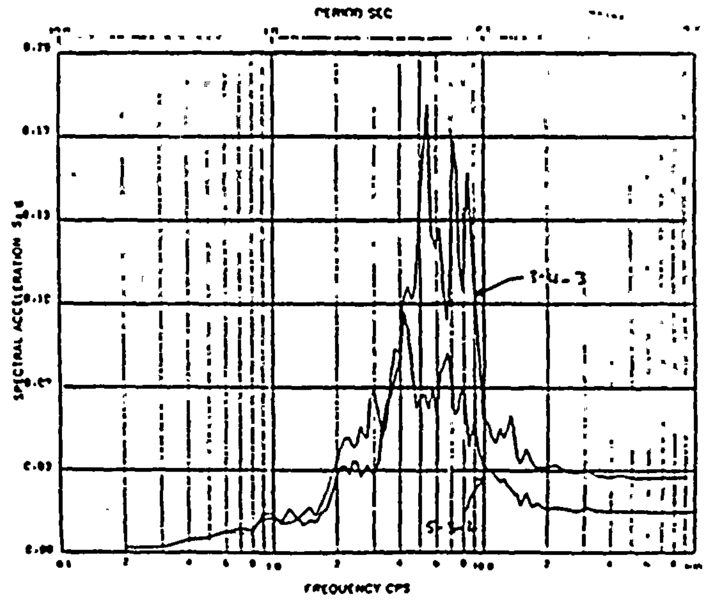

RESPONSE SPECTRUM

FIGURE 18 NORTH-SOUTH COMPONENT AT CORE WEST (CW) OF AUXILIARY BUILDING AND FREE-FIELD (FF) - ST. MARTIN EARTHQUAKE

TD/FF

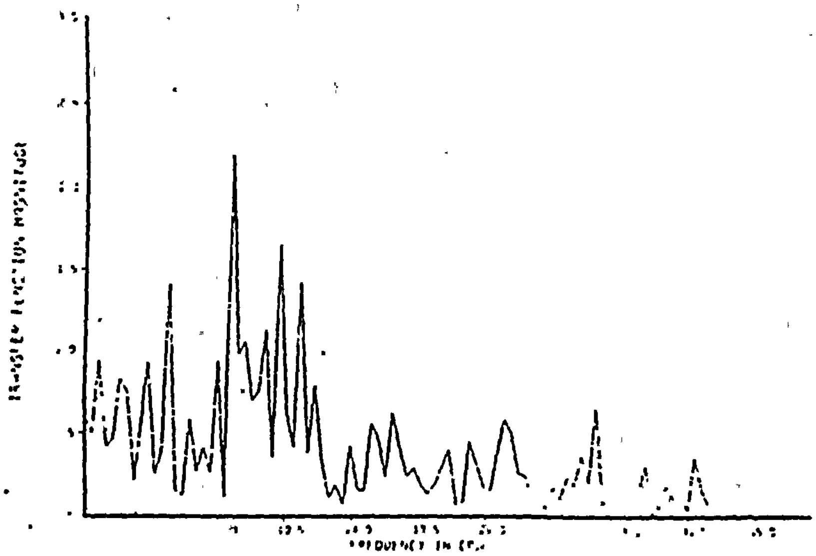

TRANSFER FUNCTION

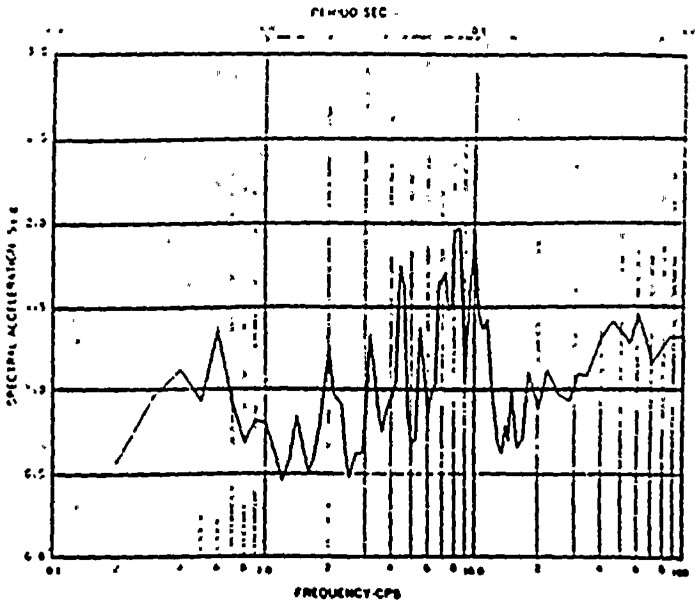

RESPONSE SPECTRUM RATIO

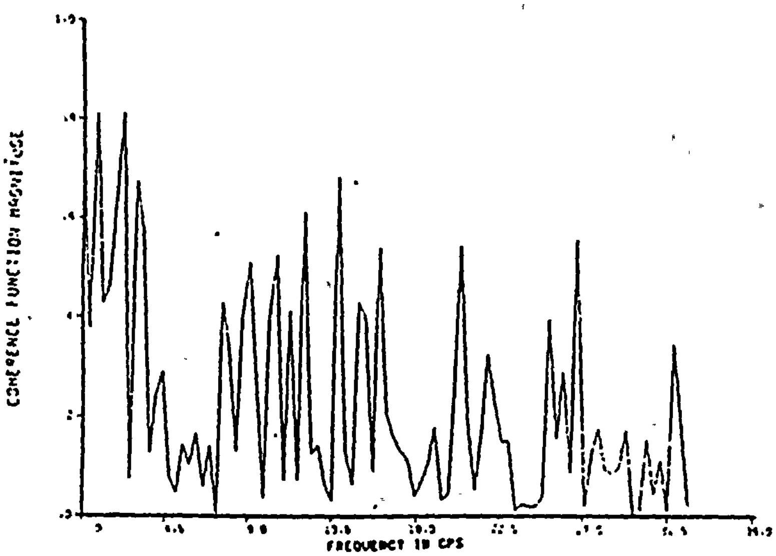

COHERENCE FUNCTION

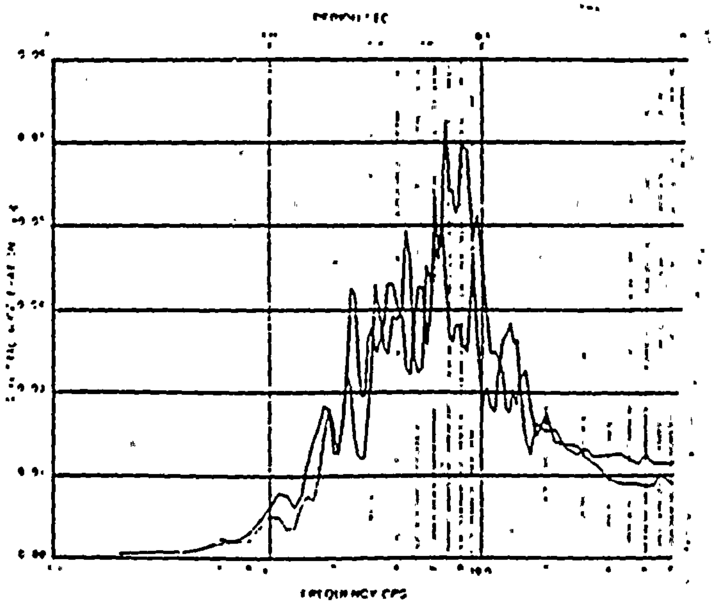

RESPONSE SPECTRUM

FIGURE 19 NORTH-SOUTH COMPONENT AT TURBINE DECK (TD) AND FREE-FIELD - PT. SAL EARTHQUAKE

MODELS FOR GENERAL CHARACTERIZATION OF SPATIAL INCOHERENCY

1. COVARIANCE MODELS

   o LOH (ONE- AND TWO-PARAMETER MODELS)

   o HARADA (ONE-PARAMETER MODEL)

2. COHERENCY MODELS

   o LOH (ONE- AND TWO-PARAMETER MODELS)

   o HARICHANDRAN AND VANMARCKE (FIVE-PARAMETER MODEL)

   o LUCO AND WONG (ONE-PARAMETER MODEL)

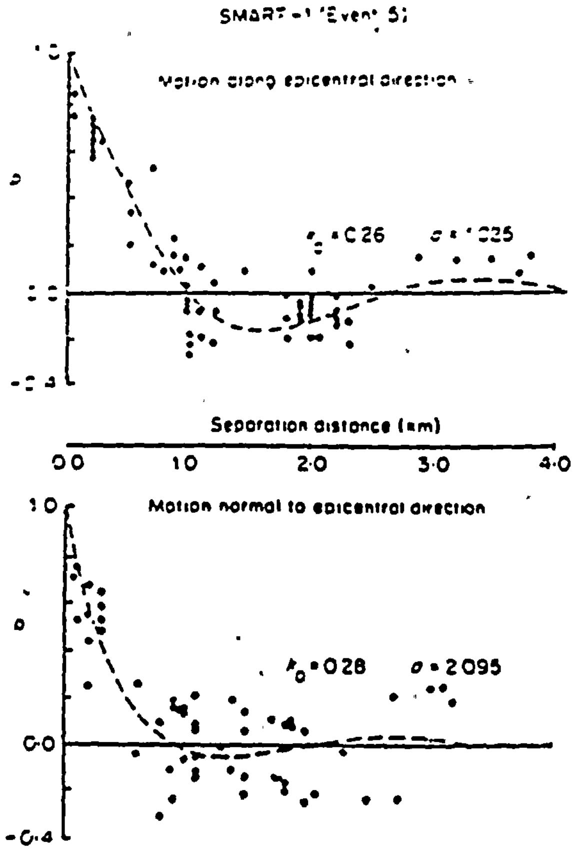

Estimated Parameters for Covariance Model Proposed by Loh
(From Ref. 11)

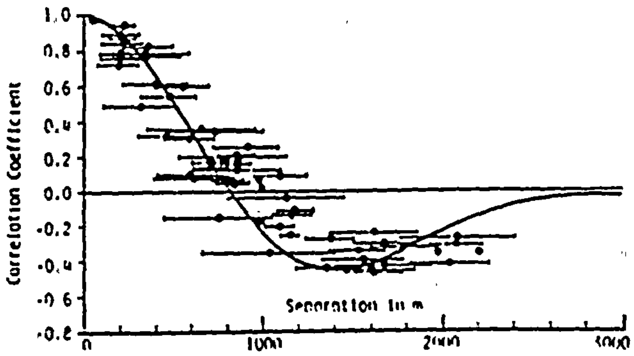

Estimated Parameters for Covariance Model Proposed by Harada
(From Ref. 6)

COHERENCY MODELS

$$S_{gmn}(\overline{x}, \omega)=S_{gmn}(\overline{o}, \omega)\gamma(\overline{x}, \omega)\exp(-i\omega\overline{x}_1/V_n)$$
$$m,n = 1, 2, 3$$

<u>LOH MODEL</u> (REF. 11)

$$\gamma(\overline{x}, \omega) = \begin{cases} \exp(-\alpha_1 |\overline{x}|) \\ (1+\alpha_1 |\overline{x}|+\alpha_1 |\overline{x}|^2)\exp(-\alpha_1 |\overline{x}|) \\ \exp\left[-(\alpha_1\overline{x})^2\right] \\ \exp\left[-(\alpha_1+\alpha_2\omega)|\overline{x}|\right] \end{cases}$$

Coefficients: α_1 and α_2

<u>HARICHANDRAN AND VANMARCKE</u> (REF. 5)

$$\gamma(\overline{x},\omega) = A\exp\left[-\frac{2\overline{x}}{\alpha\theta(\omega)}(1-A+\alpha A)\right] + (1-A)\exp\left[-\frac{2\overline{x}}{\theta(\omega)}(1-A+\alpha A)\right]$$

where

$$\theta(\omega) = k\left[1+\left(\frac{\omega}{\omega_0}\right)^b\right]^{-\frac{1}{2}}$$

Coefficients: A, α, k, ω_0 and b

<u>LUCO AND WONG</u> (REF. 12)

$$\gamma(\overline{x},\omega)=\exp\left[-(\gamma\omega|\overline{x}|)^2\right]$$

Coefficient: γ

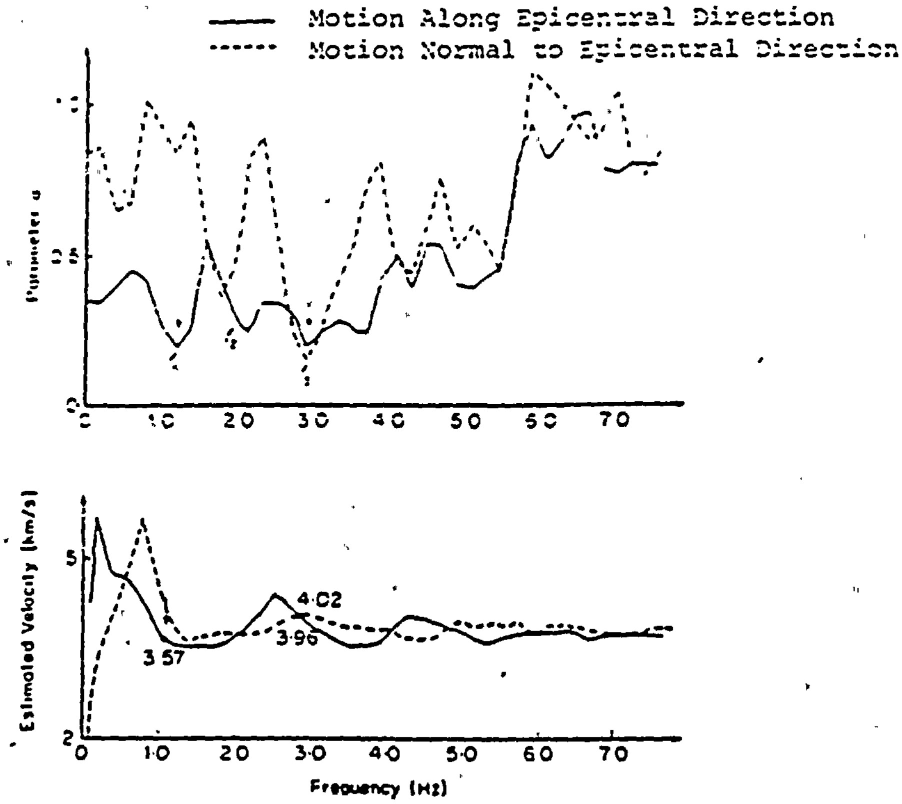

Estimated Parameters for Coherency Model Proposed by Loh
(Ref. 11)

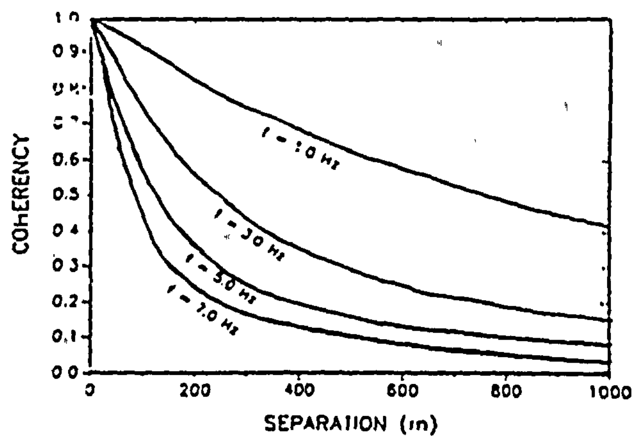

Coherency Model Proposed by Harichandran and Vanmarcke
(Ref. 5)

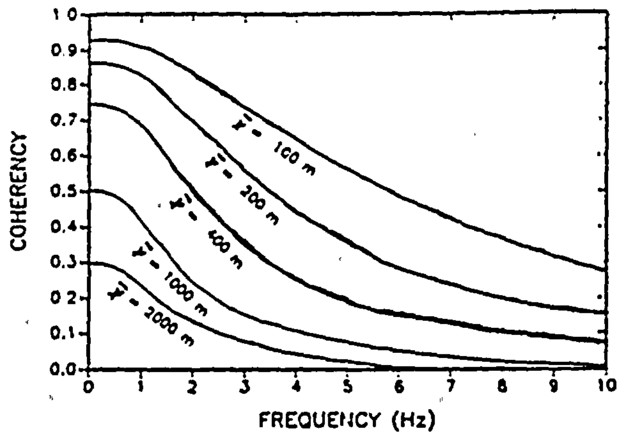

Coherency Model Proposed by Harichandran and Vanmarcke
(Ref. 5)

IMPLEMENTATION OF SPATIAL INCOHERENCY
OF GROUND MOTIONS FOR SSI ANALYSIS

1. DETERMINISTIC APPROACH - USING CLASSI CODE

2. PROBABILISTIC APPROACH - USING PROSPEC AND CLASSI CODES

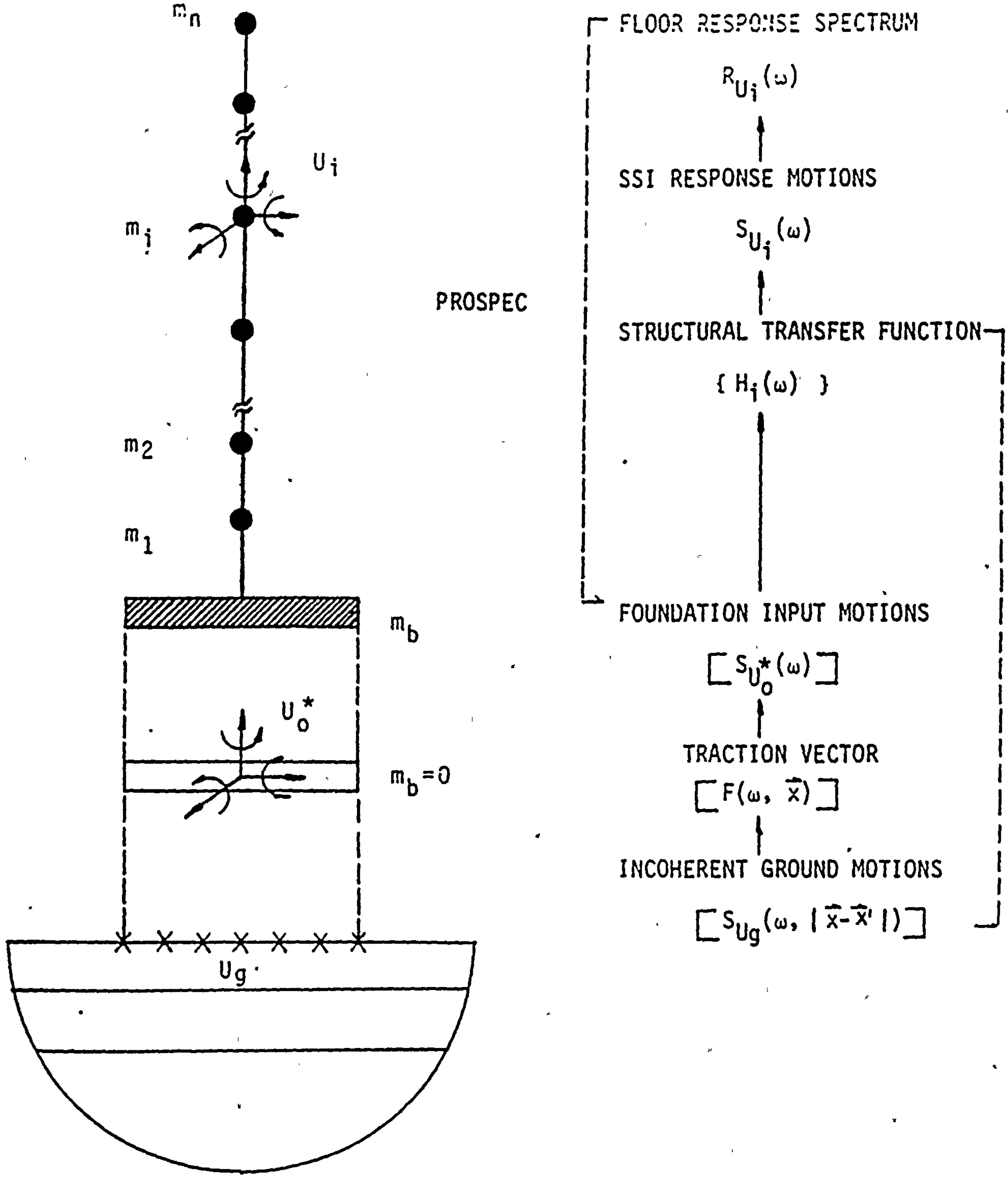

FIGURE 1 SCHEMATIC DIAGRAM OF PROBABILISTIC APPROACH FOR INCORPORATING INCOHERENT GROUND MOTIONS

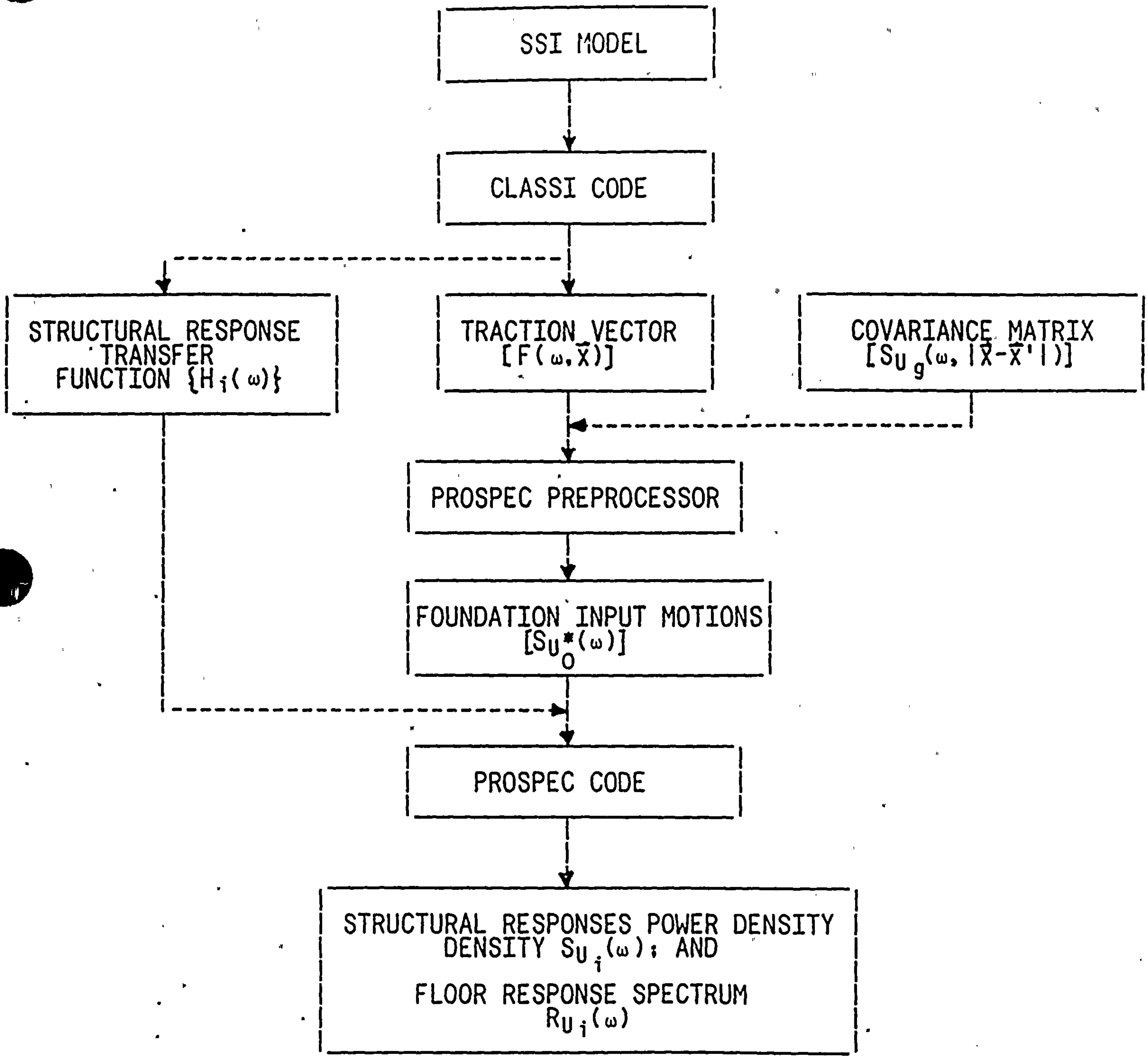

FLOW DIAGRAM OF PROBABILISTIC APPROACH
USING PROSPEC AND CLASSI CODES FOR
INCORPORATING INCOHERENT GROUND MOTIONS

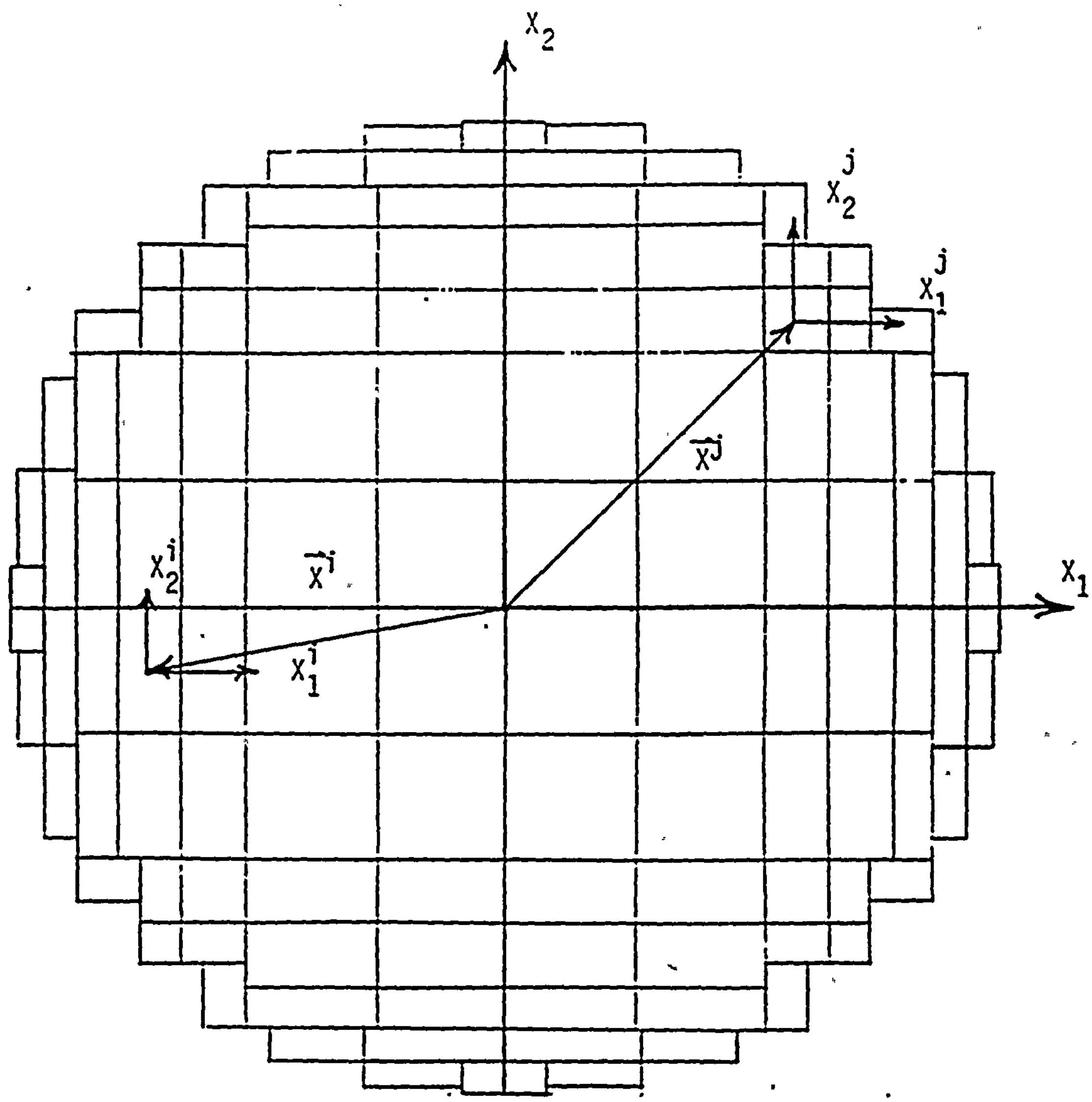

CLASSI MODEL OF DISCRETIZED
FOUNDATION SUBREGIONS

COVARIANCE MATRIX

$$
\underset{(3N\times 3N)}{\left[S_g(|\vec{x}^i-\vec{x}^j|,\omega)\right]} =
\left[\begin{array}{ccccccc}
\left[S^{11}_{gmn}\right] & \cdots & \left[S^{1i}_{gmn}\right] & \cdots & \left[S^{1j}_{gmn}\right] & \cdots & \left[S^{1N}_{gmn}\right] \\
 & \ddots & \vdots & & \vdots & & \vdots \\
 & & \underset{(3x3)}{\left[S^{ii}_{gmn}\right]} & \cdots & \underset{(3x3)}{\left[S^{ij}_{gmn}\right]} & \cdots & \left[S^{iN}_{gmn}\right] \\
 & \text{SYMMETRICAL} & & \ddots & \vdots & & \vdots \\
 & & & & \underset{(3x3)}{\left[S^{jj}_{gmn}\right]} & \cdots & \left[S^{jN}_{gmn}\right] \\
 & & & & & \ddots & \vdots \\
 & & & & & & \left[S^{NN}_{gmn}\right]
\end{array}\right]
$$

Luco and Mita assumed the following form of covariance function $\bar{S}^{ij}_{gmn}$ between subregions i and j:

$$S^{ij}_{gmn} = S^{ij}_{gmn}\,(|\vec{x}^i-\vec{x}^j|,\omega) = S_{gmn}\,(\vec{o},\omega)\,\exp\left[-(\gamma\omega\,|\vec{x}^i-\vec{x}^j|)^2\right];$$

$$m,\ n = 1,\ 2,\ 3;\ i,\ j = 1,\ 2 \ldots.,\ N$$

where, $S_{gmn}\,(\vec{o},\omega)$ = PSD (m=n) or CPSD (m≠n) of the free-field ground motion at a reference point

γ = dimensionless spatial incoherence parameter

N = number of foundation subregions

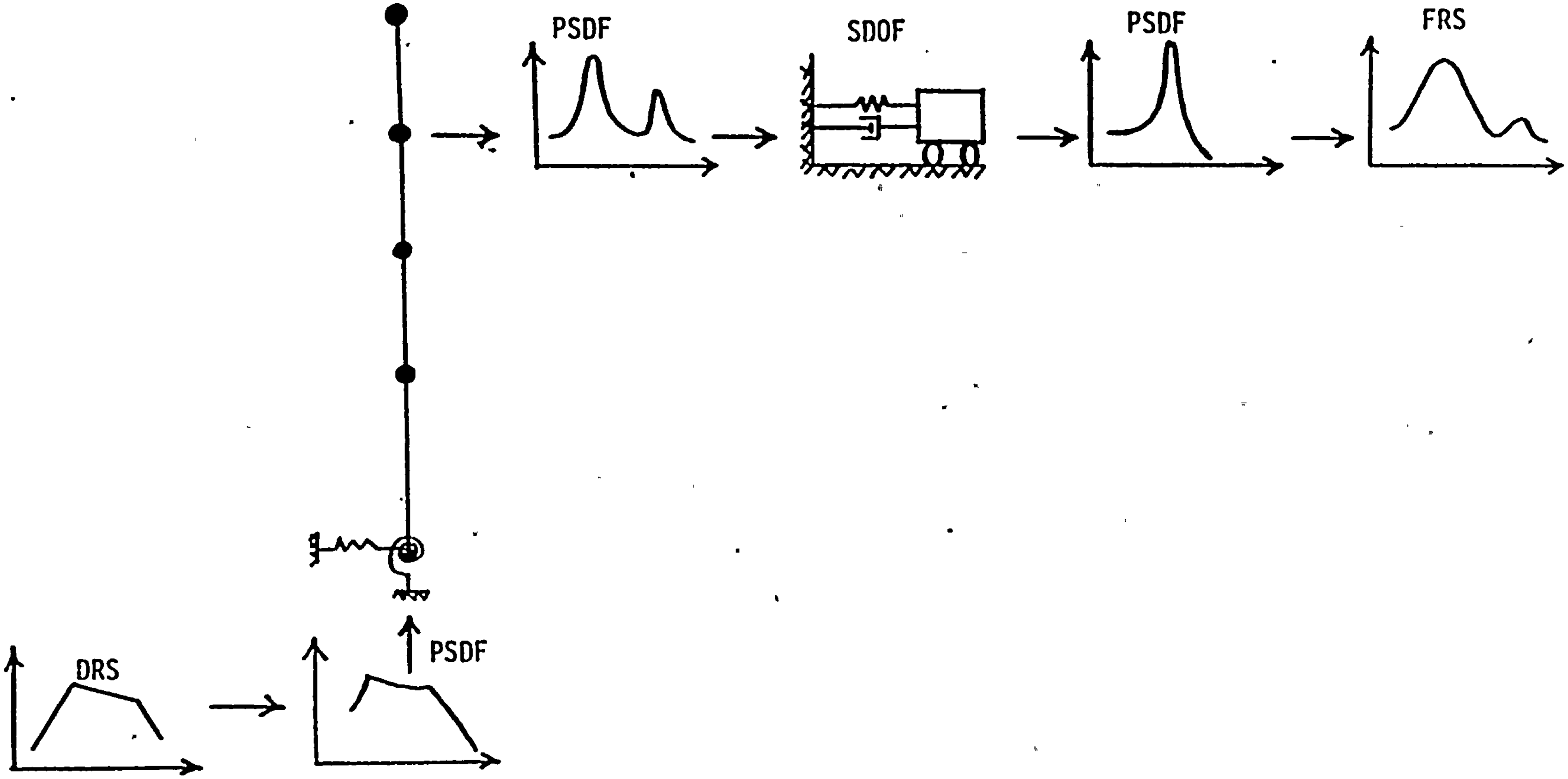

Schematic Diagram of the Approach Adopted in the Computer Program PROSPEC

VALIDATION OF ANALYSIS METHODOLOGY

- PROBABILISTIC APPROACH FOR SSI ANALYSIS DUE TO INCOHERENCY WILL BE BENCHMARKING AGAINST ANALYTICAL SOLUTIONS BY LUCO AND MITA (REF. 13)

- VALIDITY OF PROSPEC COMPUTATIONAL PROCEDURE FOR GENERATING PROBABILISTIC FLOOR RESPONSE SPECTRUM HAS BEEN DEMONSTRATED IN REF. 8

ASSESSMENT OF SSI RESPONSES DUE TO SPATIAL INCOHERENCY

- COMPUTE THE "RESPONSE SPECTRUM RATIO" AS THE RATIO OF THE SPECTRAL VALUE OF THE SSI RESPONSE DUE TO INCOHERENT GROUND MOTIONS TO THE SPECTRAL VALUE OF THE CORRESPONDING RESPONSE DUE TO COHERENT GROUND MOTIONS

- USE THE RESPONSE SPECTRUM RATIO, IN CONJUNCTION WITH ENGINEERING JUDGMENT, TO ASSESS THE EFFECTS OF THE INCOHERENT GROUND MOTION INPUT ON THE VARIABILITY OF SSI RESPONSE

NONLINEAR SSI ANALYSIS

FOR

BASE.UPLIFTING

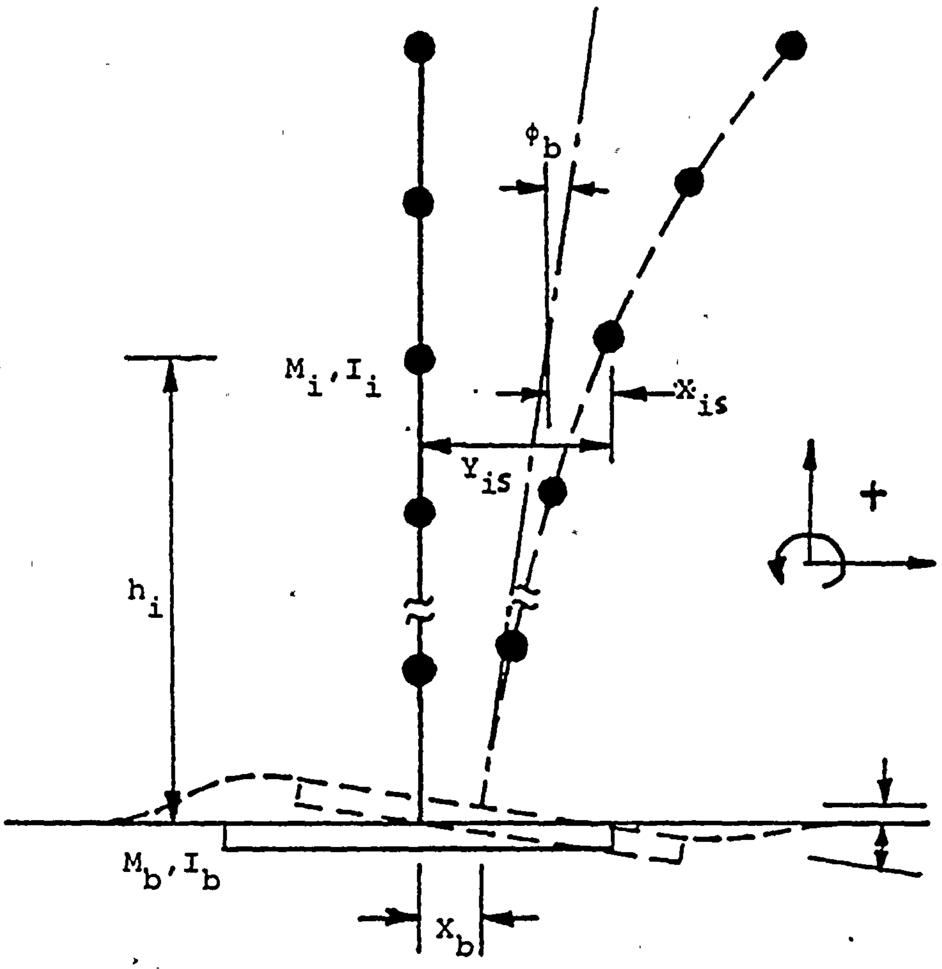

The coordinate system for a soil-structure interaction system

LINEAR CONSTITUTIVE EQUATIONS FOR THE FOUNDATION

$$\begin{Bmatrix} H \\ P \\ M \end{Bmatrix} = \begin{bmatrix} C_x & & \\ & C_y & \\ & & C_\phi \end{bmatrix} \begin{Bmatrix} \dot{X}_b \\ \dot{Y}_b \\ \dot{\phi}_b \end{Bmatrix} + \begin{bmatrix} K_x & & \\ & K_y & \\ & & K_\phi \end{bmatrix} \begin{Bmatrix} X_b \\ Y_b \\ \phi_b \end{Bmatrix}$$

$$\begin{Bmatrix} H \\ P \\ M \end{Bmatrix} = \begin{Bmatrix} H^D \\ P^D \\ M^D \end{Bmatrix} + \begin{Bmatrix} H^S \\ P^S \\ M^S \end{Bmatrix}$$

where

$$\begin{Bmatrix} H^D \\ P^D \\ M^D \end{Bmatrix} = \begin{bmatrix} C_x & & \\ & C_y & \\ & & C_\phi \end{bmatrix} \begin{Bmatrix} \dot{X}_b \\ \dot{Y}_b \\ \dot{\phi}_b \end{Bmatrix}$$

$$\begin{Bmatrix} H^S \\ P^S \\ M^S \end{Bmatrix} = \begin{bmatrix} K_x & & \\ & K_y & \\ & & K_\phi \end{bmatrix} \begin{Bmatrix} X_b \\ Y_b \\ \phi_b \end{Bmatrix}$$

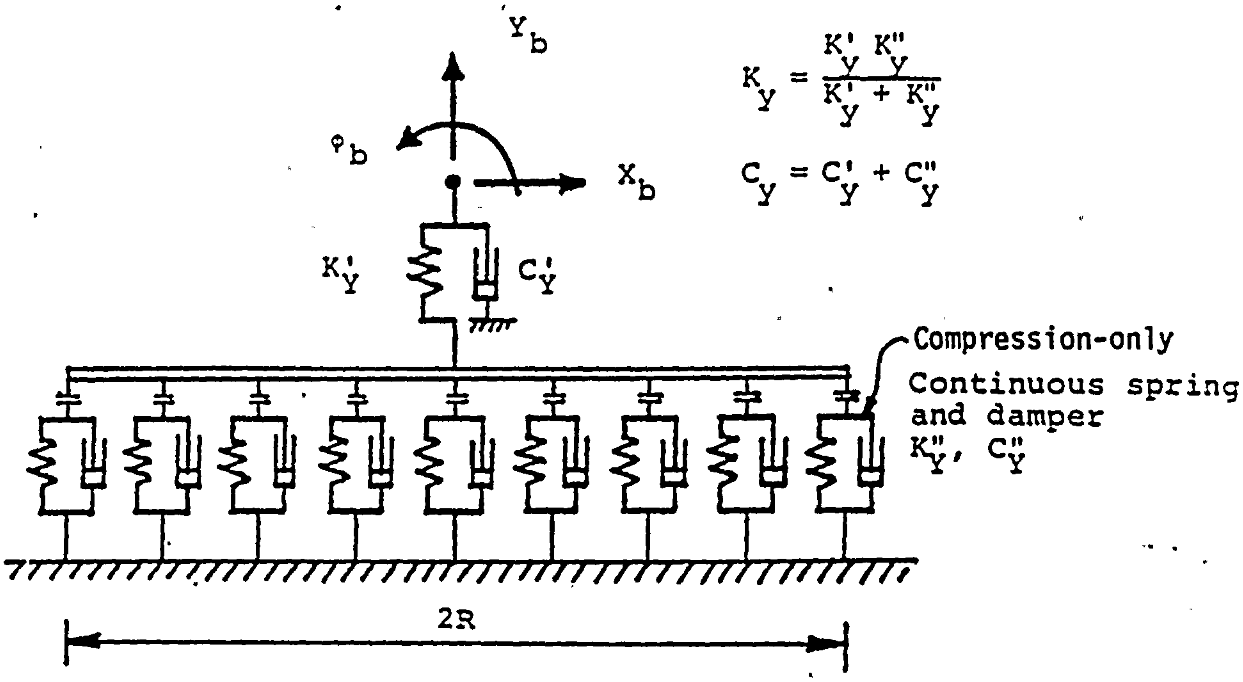

Vertical spring and damper mechanism

for circular basemat

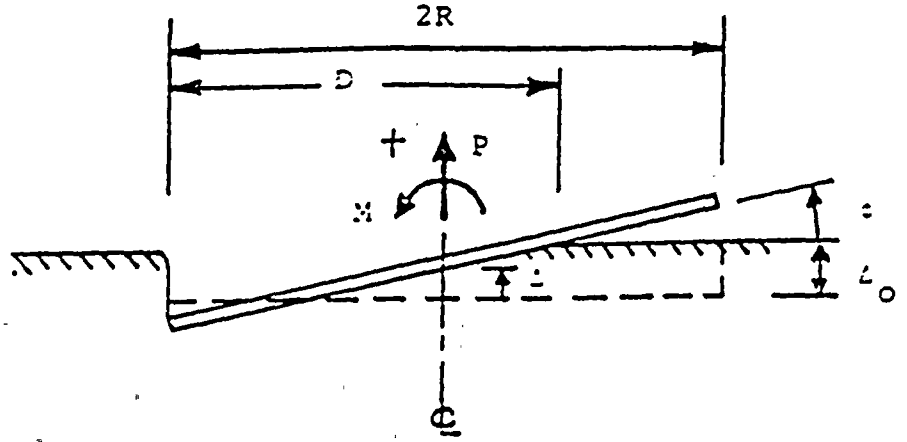

Configuration of circular basemat at uplifted position

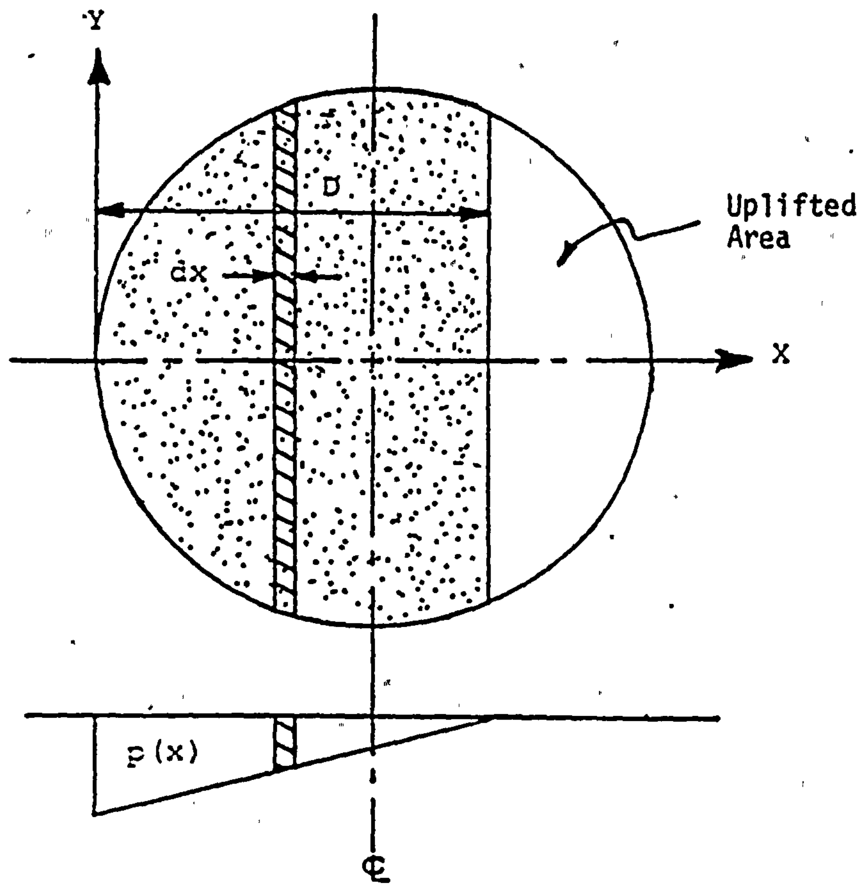

Pressure diagram for circular basemat at uplifted position

WINKLER DISTRIBUTED SPRING

$$k_\phi = \frac{K_\phi}{I_B} \quad ; \quad I_B = \frac{\pi R^4}{4}$$

VERTICAL RESISTANCE FORCE

$$P^S = \int_0^D p(x)(2y)dx - W$$

$$= \quad 2k_\phi R \int_0^D D\phi_b(1 - x/D)\sqrt{1-(x/R - 1)^2}dx - W$$

OVERTURNING RESISTANCE MOMENT

$$M^S = \int_0^D p(x)(R-x)(2y)dx$$

$$= 2k_\phi R \int_0^D D\phi_b(1-x/D)(R-x)\sqrt{1-(x/R - 1)^2}\, dx$$

INTEGRATION

$$P^S = \frac{2K_\phi \phi_b}{R} \left[f_1(r) - 2rf_o(r)\right] - W$$

$$M^S = K_\phi \phi_b \left[f_2(r) - 2rf_1(r)\right]$$

where

$$f_o(r) = \frac{2}{\Pi} \int_{-1}^{r} \sqrt{1-s^2}\, ds$$

$$f_1(r) = \frac{4}{\Pi} \int_{-1}^{r} s\sqrt{1-s^2}\, ds$$

$$f_2(r) = \frac{8}{\Pi} \int_{-1}^{r} s^2\sqrt{1-s^2}\, ds$$

$$f_o(r) = \frac{1}{2} + \frac{r}{\Pi}\sqrt{1-r^2} + \frac{1}{\Pi} \sin^{-1} r$$

$$f_1(r) = \frac{-4}{3\Pi}\sqrt{(1-r^2)^3}$$

$$f_2(r) = f_o(r) + \frac{3}{2}\, r\, f_1(r)$$

$$s = X/R - 1 \qquad -1 \le s \le 1$$

$$r = D/R - 1 \qquad -1 \le r \le 1$$

TANGENT STIFFNESSES

$$\begin{Bmatrix} dP^s \\ dM^s \end{Bmatrix} = \begin{bmatrix} \frac{4K_\phi}{R^2} f_o(r) & \frac{2K_\phi}{R} f_1(r) \\ \frac{2K_\phi}{R} f_1(r) & K_\phi \; f_2(r) \end{bmatrix} \begin{Bmatrix} dy_b \\ d\phi_b \end{Bmatrix}$$

WHICH REDUCES TO

$$\begin{Bmatrix} dP^s \\ dM^s \end{Bmatrix} = \begin{bmatrix} \frac{4K_\phi}{R^2} & \\ & K_\phi \end{bmatrix} \begin{Bmatrix} dy_b \\ d\phi_b \end{Bmatrix}$$

when $r = \pm 1$.
NO UPLIFT

MODIFICATION TO THE TANGENT STIFFNESS

$$\begin{Bmatrix} dP^s \\ dM^s \end{Bmatrix} = \begin{bmatrix} K_{yy} & K_{y\phi} \\ K_{y\phi} & K_{\phi\phi} \end{bmatrix} \begin{Bmatrix} dy_b \\ d\phi_b \end{Bmatrix}$$

where

$$K_{yy} = \left(\frac{K_y'}{K_y' + K_y''}\right) \frac{4K_\phi}{R^2} f_o(r)$$

$$K_{y\phi} = \frac{K'}{K_y' + K_y''} \quad \frac{2K_\phi}{R} f_1(r)$$

$$K_{\phi\phi} = K_\phi f_2(r) - \left(\frac{1}{K_y' + K_y''}\right) \left[\frac{2K_\phi}{R} f_1(r)\right]^2$$

$$K_y'' = \frac{4K_\phi}{R^2} f_o\,(r), \quad -1 \le r \le 1$$

DAMPING FORCE AND MOMENT AT UPLIFTED POSITION

$$\begin{Bmatrix} P^D \\ M^D \end{Bmatrix} = \begin{bmatrix} \frac{4C_\phi}{R^2} f_o(r) & \frac{2C_\phi}{R} f_1(r) \\ \frac{2C_\phi}{R} f_1(r) & C_\phi f_2(r) \end{bmatrix} \begin{Bmatrix} \dot{y}_b \\ \dot{\phi}_b \end{Bmatrix}$$

MODIFICATION TO THE DAMPING MATRIX

$$\begin{Bmatrix} P^D \\ M^D \end{Bmatrix} = \begin{bmatrix} C_{yy} & C_{y\phi} \\ C_{y\phi} & C_{\phi\phi} \end{bmatrix} \begin{Bmatrix} \dot{y}_b \\ \dot{\phi}_b \end{Bmatrix}$$

where

$$C_{yy} = C_y f_o(r)$$

$$C_{y\phi} = \frac{2C_\phi}{R} f_1(r)$$

$$C_{\phi\phi} = C_\phi f_2(r)$$

TANGENT DAMPING MATRIX

$$\begin{Bmatrix} dP^D \\ dM^D \end{Bmatrix} = \begin{bmatrix} C_{yy} & C_{y\phi} \\ C_{y\phi} & C_{\phi\phi} \end{bmatrix} \begin{Bmatrix} d\dot{y}_b \\ d\dot{\phi}_b \end{Bmatrix}$$

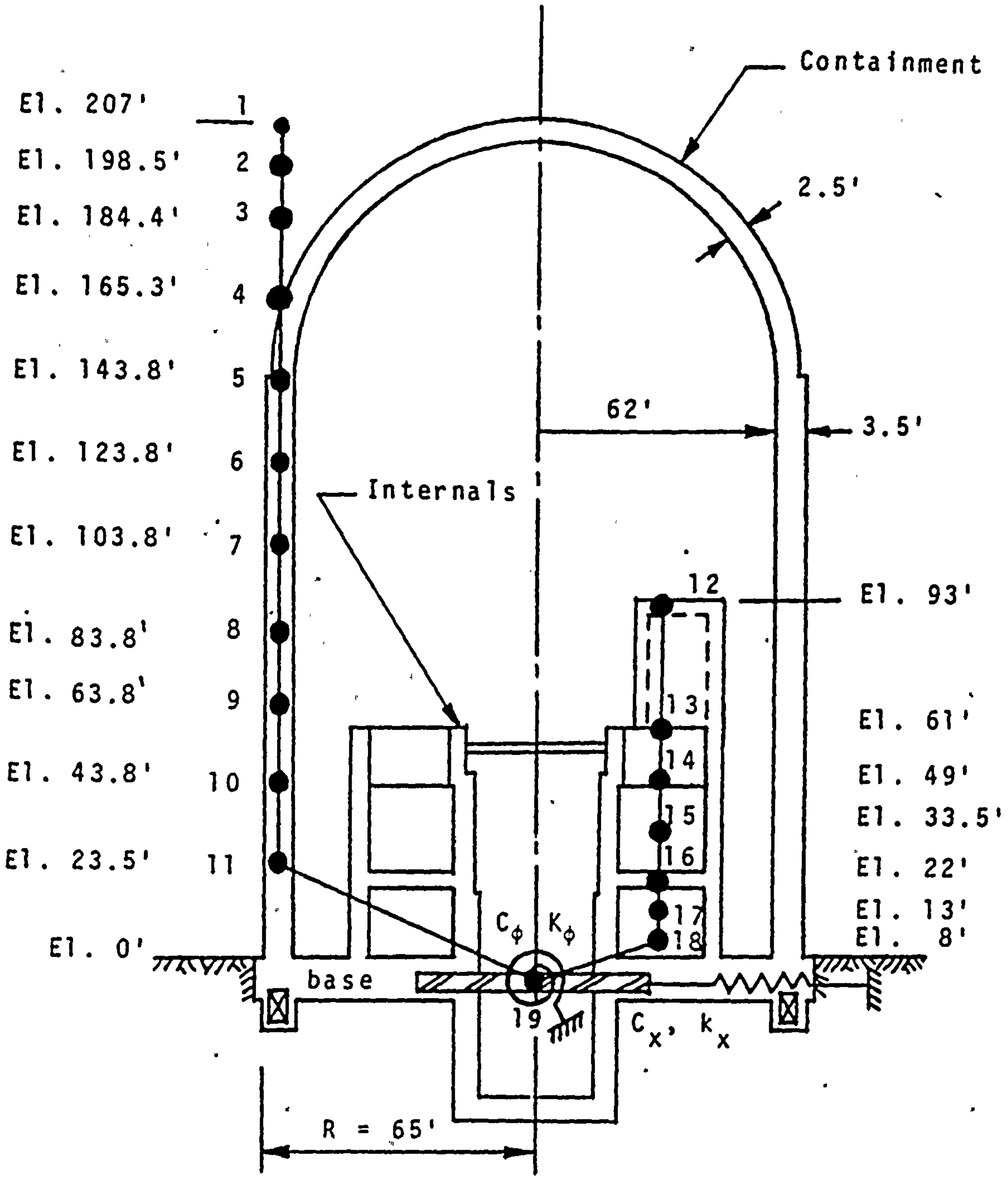

Lumped mass model of the P.W.R. containment and internal structures

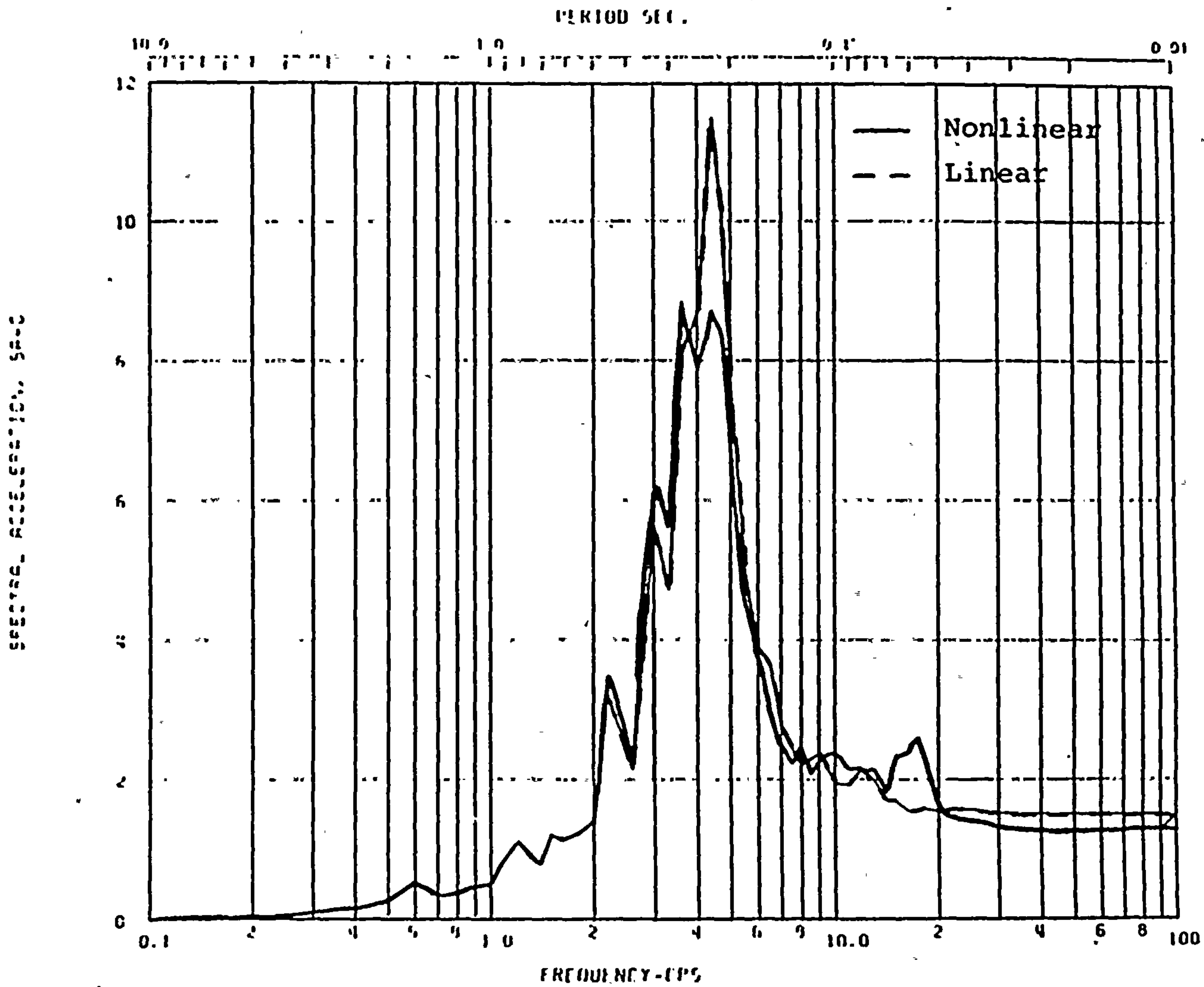

Comparison of nonlinear and linear horizontal response spectra at Node 1 (V_s = 3,000 fps, 2% damping 0.4g Taft motion)

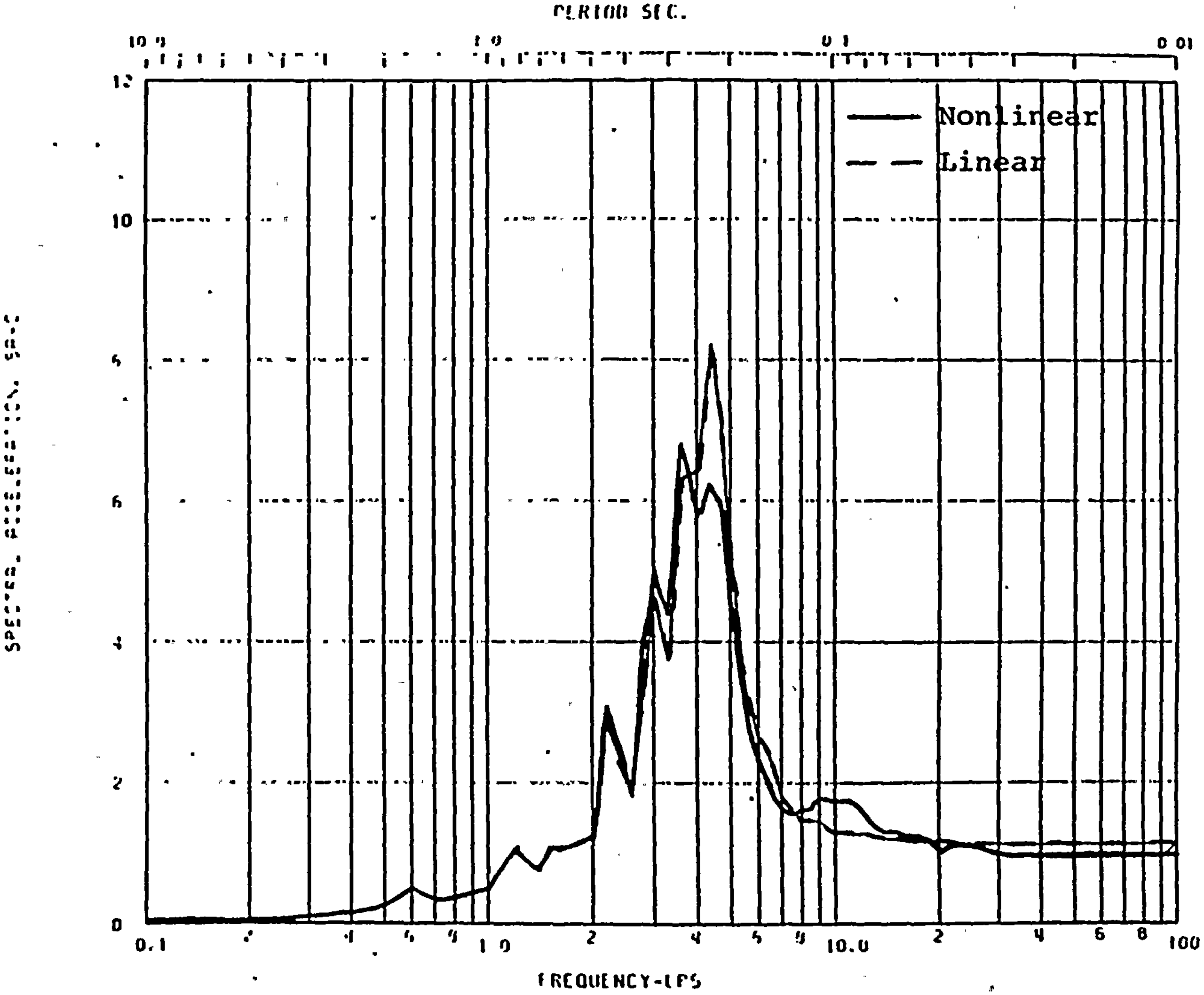

Comparison of nonlinear and linear horizontal response spectra at Node 5 (V_s = 3,000 fps, 2% damping, 0.4g Taft motion)

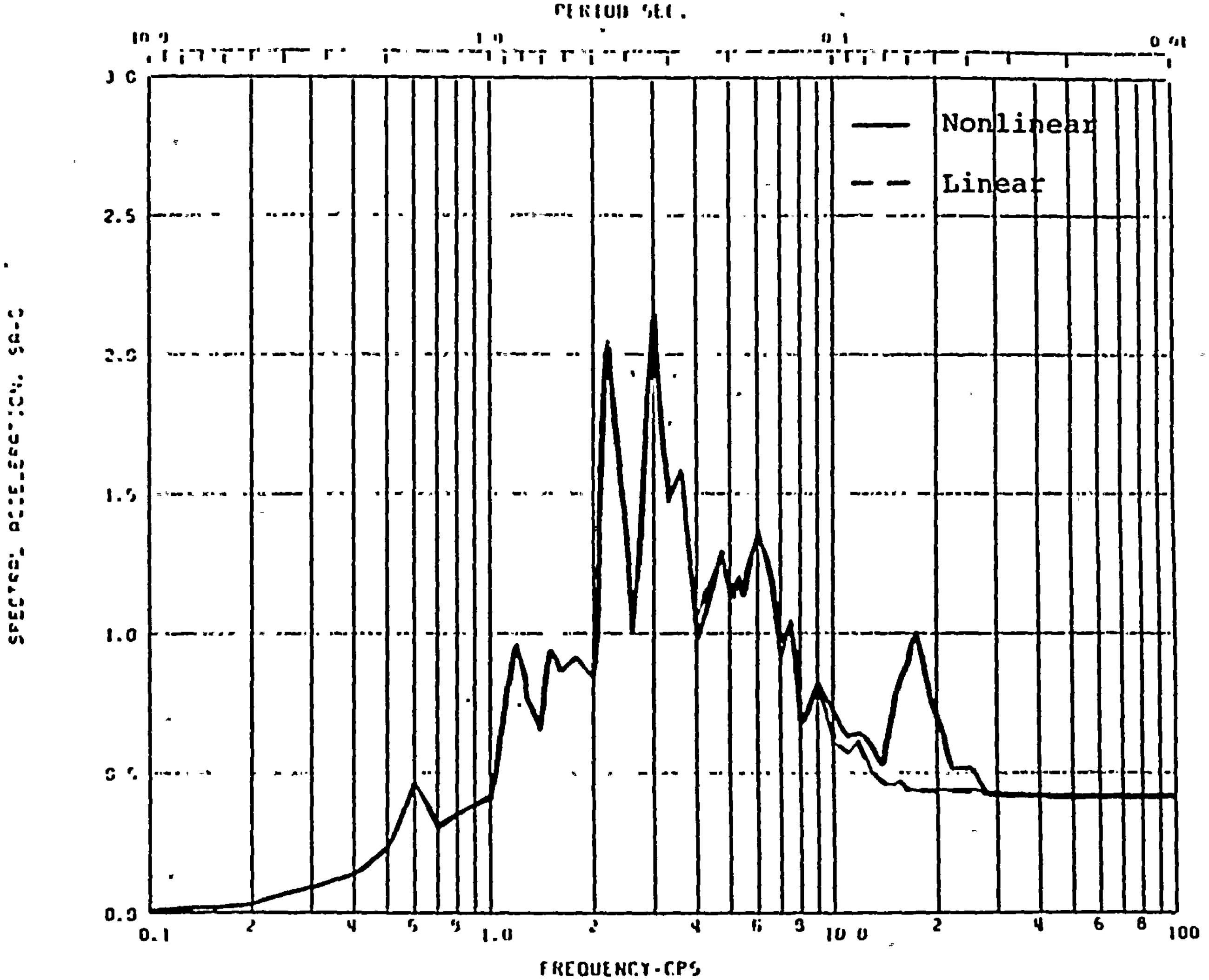

Comparison of nonlinear and linear horizontal response spectra at basemat (V_S = 3,000 fps, 2% damping, 0.4g Taft motion)

MODIFICATIONS TO UPLIFT ANALYSIS METHOD FOR SURFACE STRUCTURES FOR DCPP-LTSP APPLICATION:

1. MODIFY THE NONLINEAR CONSTITUTIVE EQUATIONS TO INCLUDE THE EFFECT OF EMBEDMENT

2. MODIFY THE DAMPING MATRIX TO INCLUDE THE ADDED ENERGY DISSIPATION DUE TO IMPACT RESULTING FROM CLOSING OF GAP AFTER UPLIFT

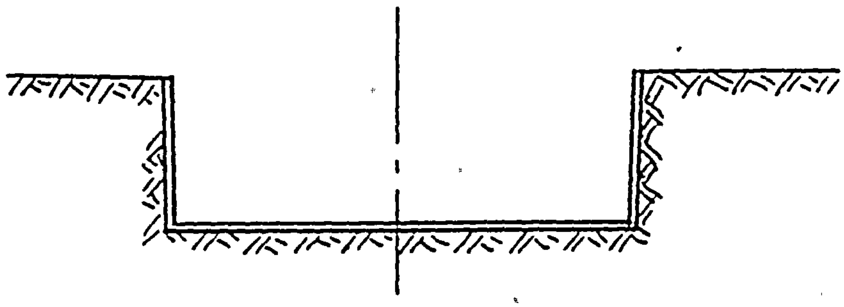

Configuration of An Embedded Foundation

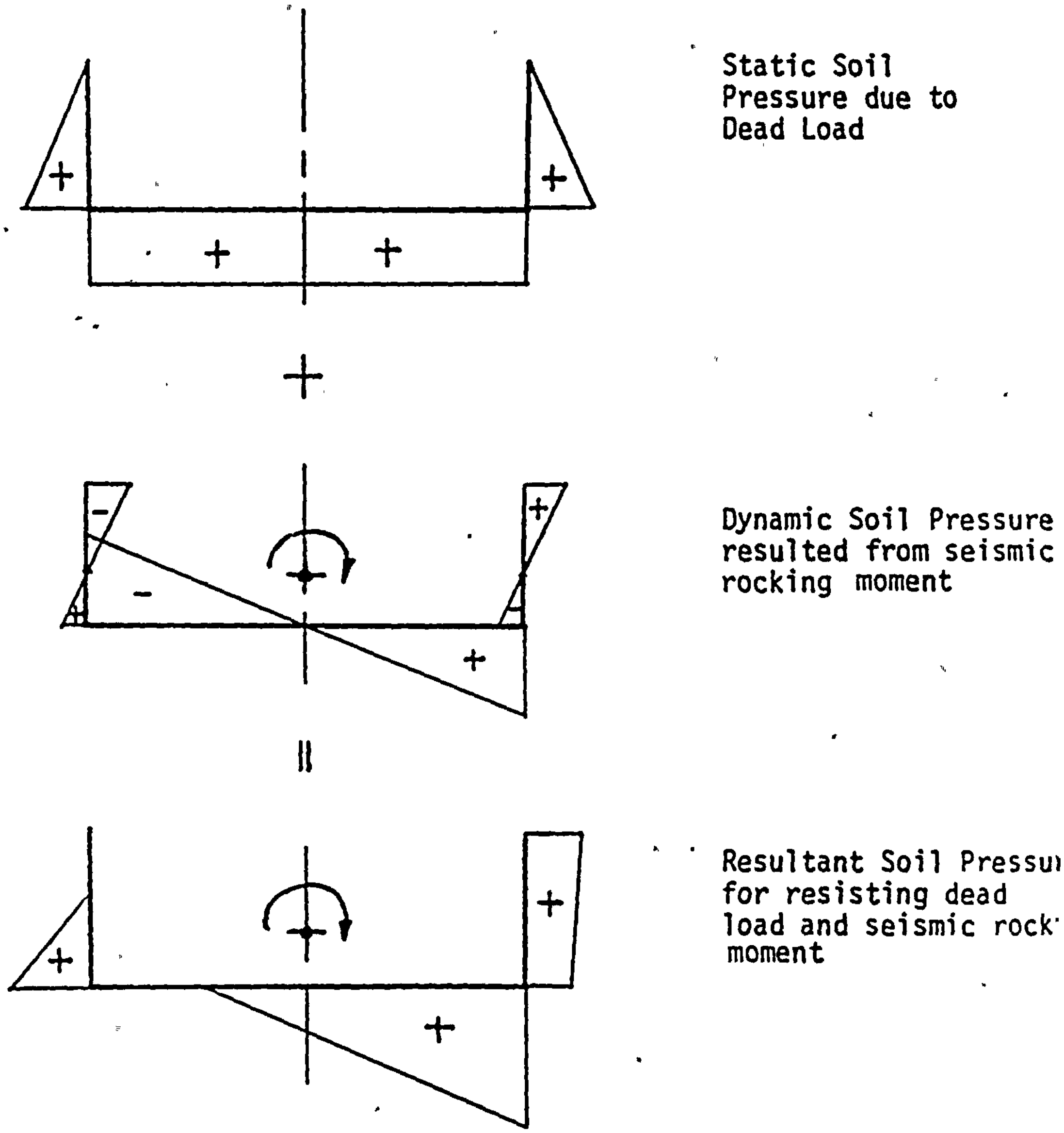

Schematic Soil Pressure Diagram for an Uplifted Embedded Foundation

ASSESSMENT OF EFFECT OF UPLIFT ON SSI RESPONSE

1. LINEAR (WITHOUT UPLIFT) AND NONLINEAR (WITH UPLIFT) ANALYSES WILL BOTH BE PERFORMED

2. RESPONSE RATIOS OF THE NONLINEAR RESPONSES TO THE LINEAR RESPONSES WILL BE DEVELOPED

3. RESPONSE RATIOS WILL BE APPLIED TO THE CLASSI/SASSI LINEAR RESPONSES TO ASSES THE EFFECT OF UPLIFT ON SSI RESPONSES IN CONJUNCTION WITH ENGINEERING JUDGMENT

[redacted]

FIXED-BASE CONTAINMENT STRUCTURAL MODEL AND MODAL PROPERTIES

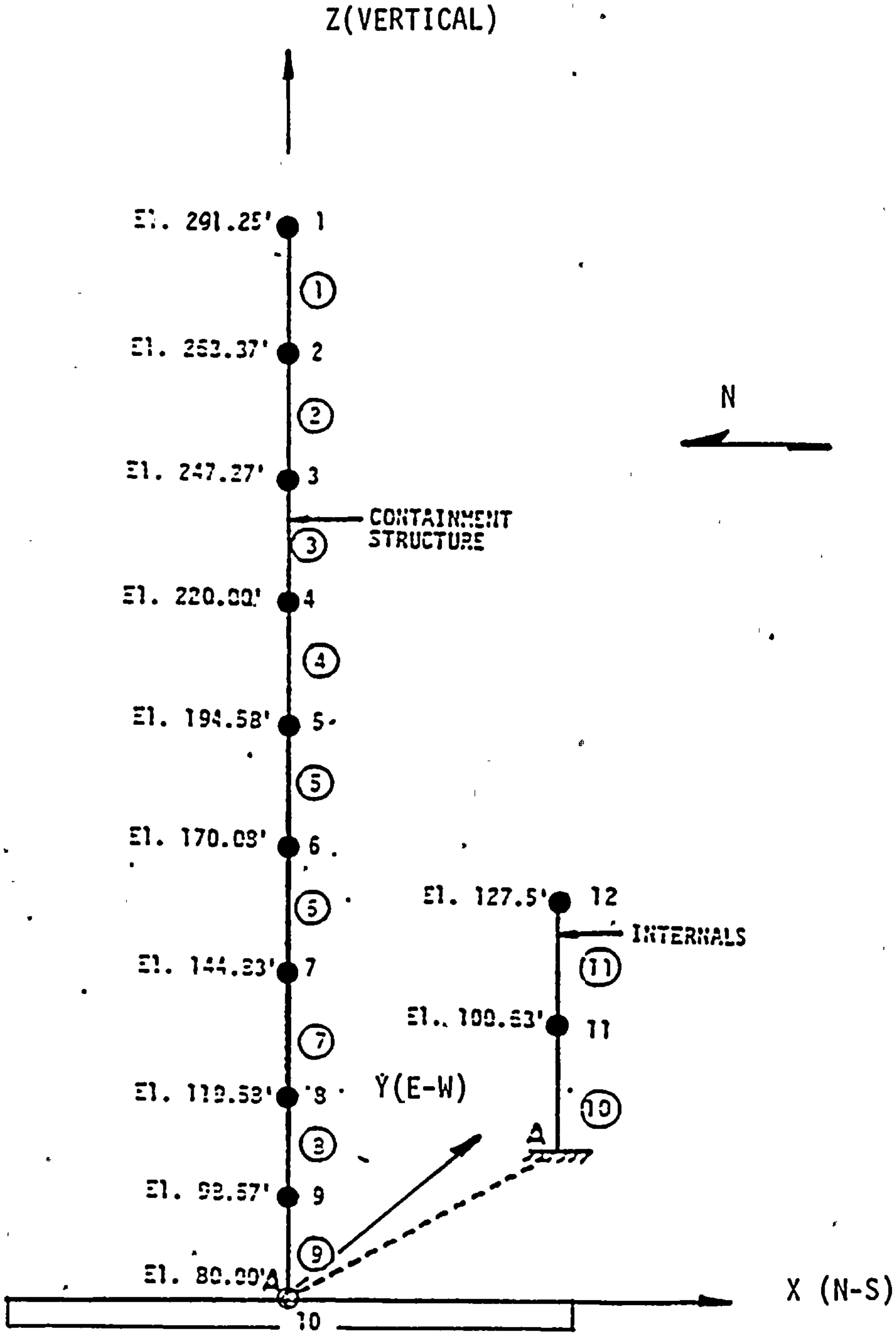

Containment and Internal Structure Model

PROPERTIES OF THE STRUCTURAL MODELS OF THE CONTAINMENT BUILDING AND INTERNALS

Joint Properties: Mass No.	Joint Properties: Weight (kips)		Member Properties: Location between Joint No.	Area (ft^2)	Shear Area (ft^2)	Moment of Inertia $\times 10^{-6}$ (ft^4)
1	2421.44	CONTAINMENT				
			1 to 2	1119	560	0.494
2	3815.70					
			2 to 3	1119	560	1.604
3	4169.90					
			3 to 4	1412	706	3.260
4	6417.46					
			4 to 5	1656	828	4.280
5	6407.80					
			5 to 6			
6	6388.48					
			6 to 7			
7	6481.86					
			7 to 8			
8	5924.80					
			8 to 9			
9	5393.50					
			9 to 10			
10	-			(BASE)		
		INTERNAL	10 to 11	2013	1172	1.720 (E-W)
					1192	1.913 (N-S)
11	13647.0					
			11 to 12	1991	816	1.785 (E-W)
					1372	2.036 (N-S)
12	16903.0					

Note:

Modulus of Elasticity: Containment $E_c = 5.1 \times 10^5$ ksf, $G_c = 2.04 \times 10^5$ ksf
Internal $E_i = 6.5 \times 10^5$ ksf, $G_i = 2.61 \times 10^5$ ksf

FIXED-BASE MODAL PROPERTIES

A. CONTAINMENT STRUCTURE

MODE NO	FREQUENCY (cps)	MODAL MASS X OR Y	MODAL MASS Z
1	4.7	1116	-
2	13.2	-	1233
3	13.9	235	-
4	24.9	64	-
5	34.4	28	-

B. INTERNAL STRUCTURE

MODE NO	FREQUENCY (cps)	MODAL MASS X	MODAL MASS Y	MODAL MASS Z
1	13.9	886	-	-
2	15.6	-	857	-
3	33.5	-	-	864

"CLASSI" SURFACE-SUPPORTED FOUNDATION MODEL AND IMPEDANCES FOR THE CONTAINMENT

PLEASE REPLACE DATA PACKAGE B, ITEMS #2 AND #3 WITH THE ATTACHED PAGES.

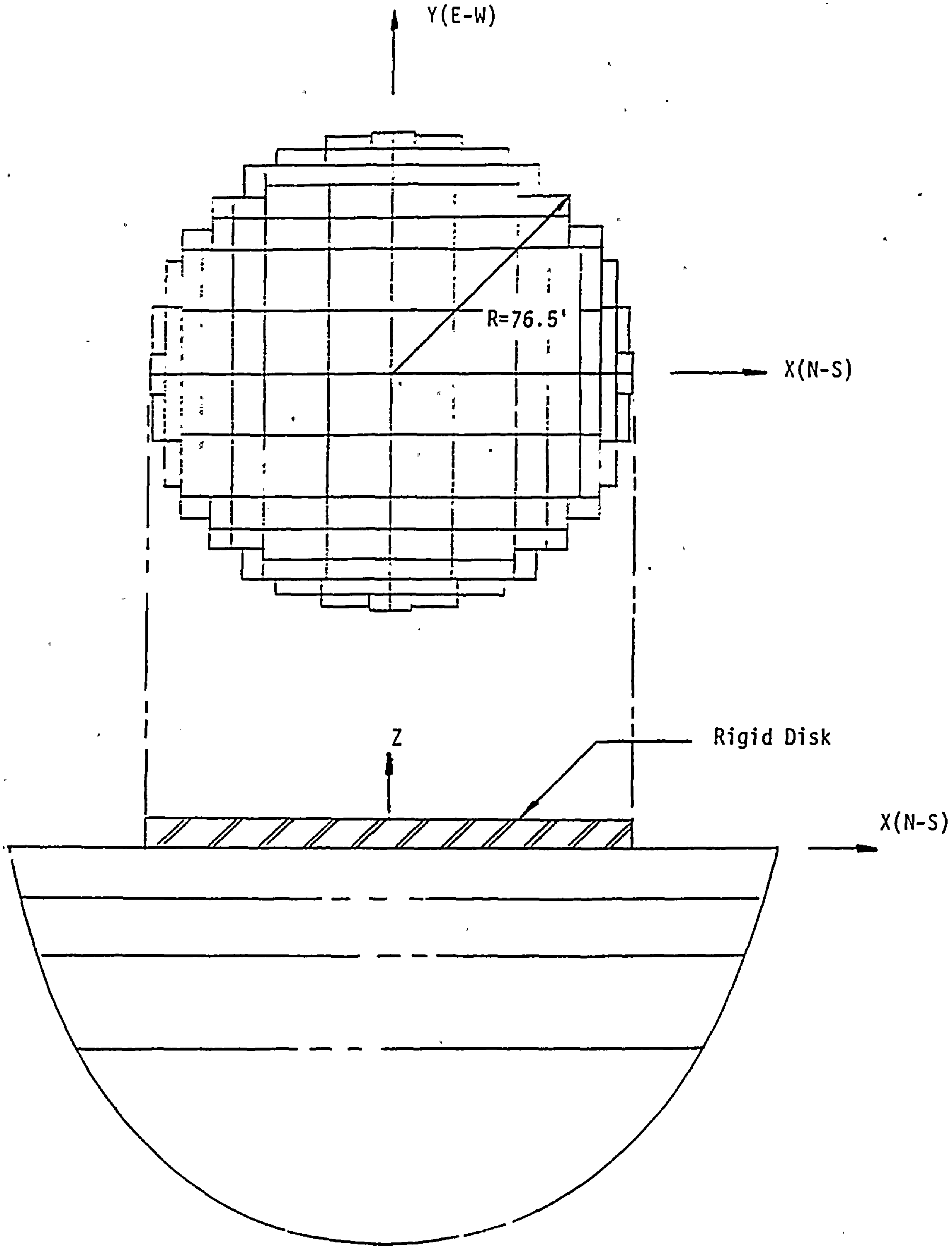

CLASSI Surface Foundation Model

CLASSI SURFACE FOUNDATION

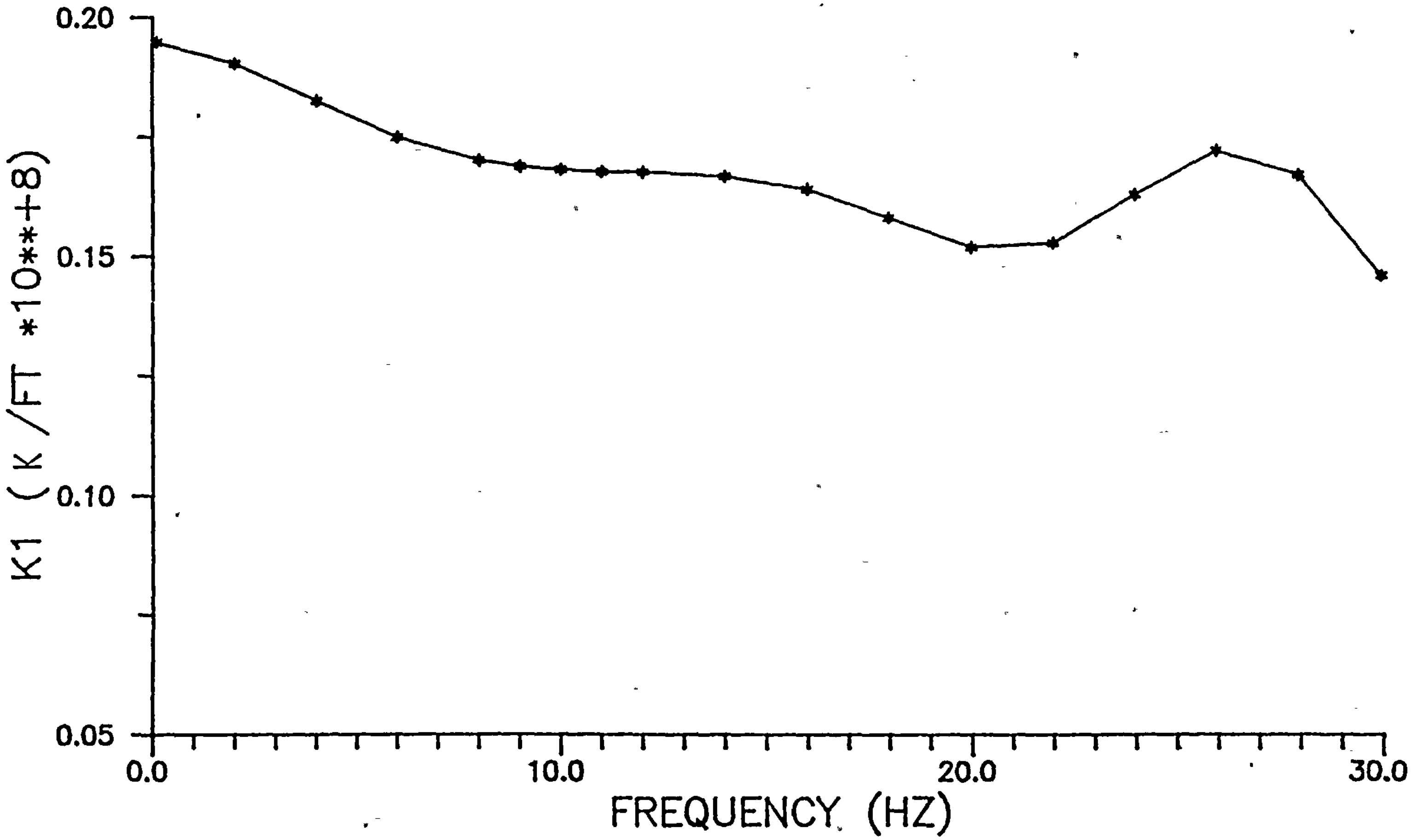

Horizontal Stiffness Impedance for Translation in X Direction
(Same as for Translation in Y Direction)

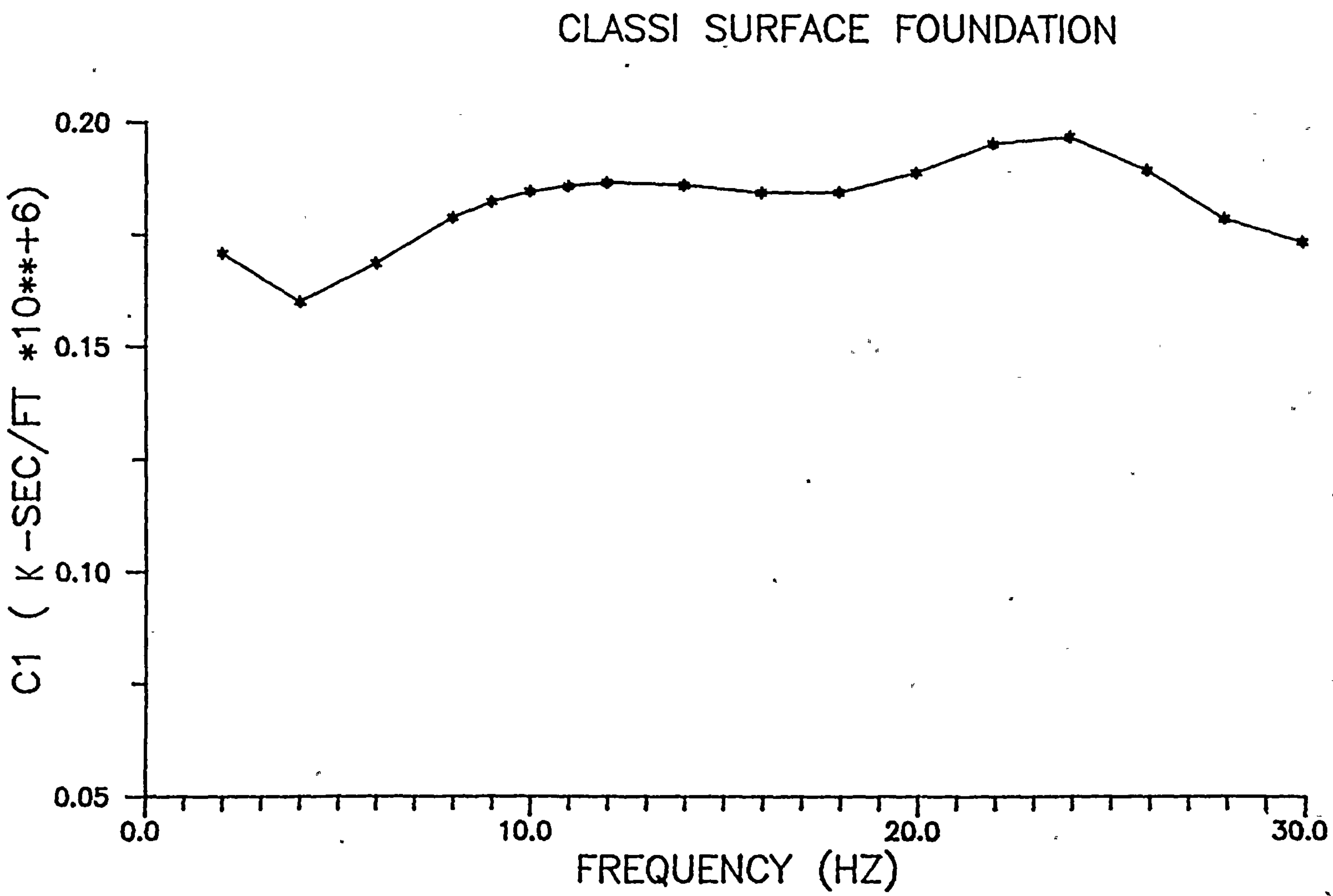

Horizontal Damping Impedance for Translation in X Direction
(same for Translation Y Direction)

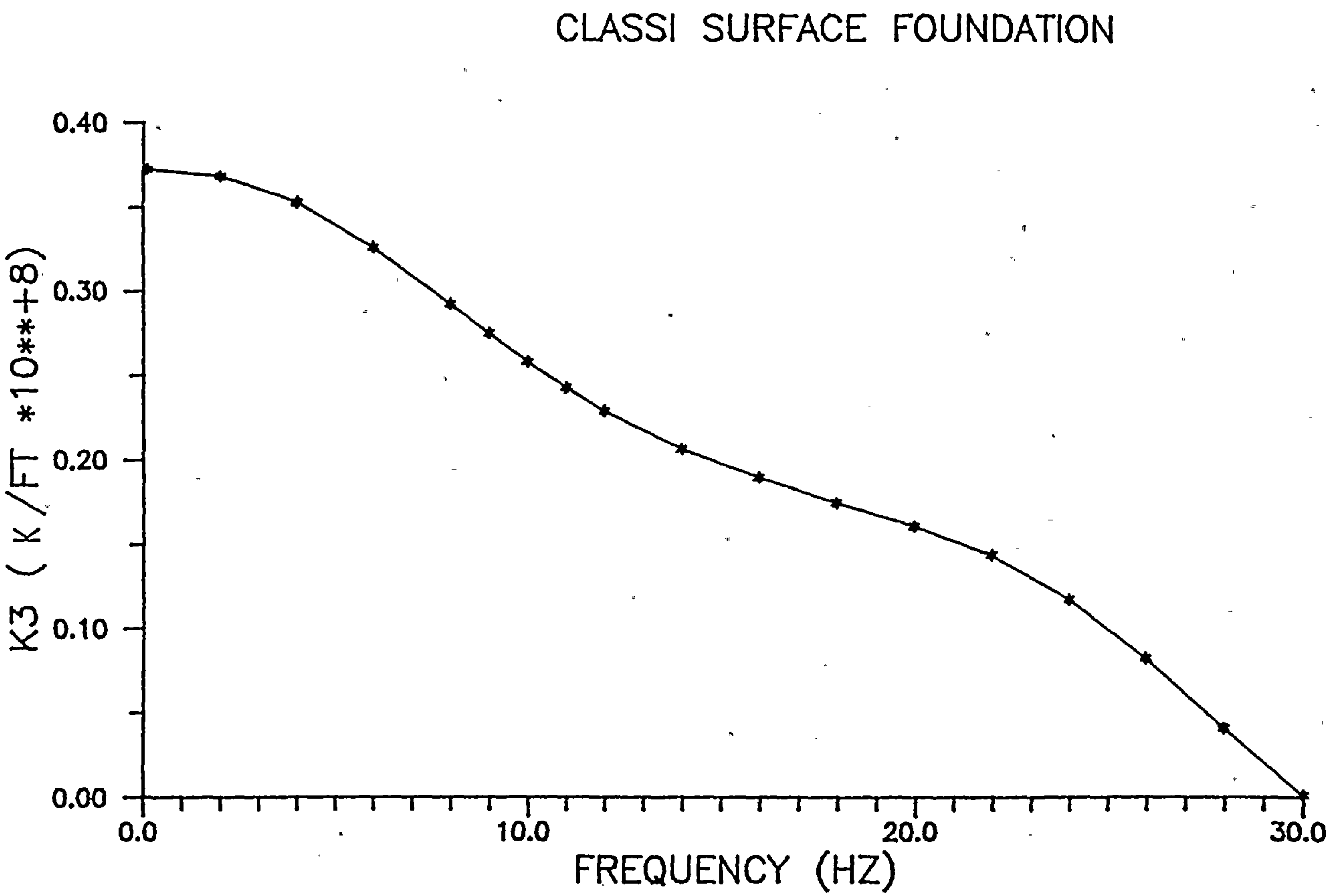

Vertical Stiffness Impedance for Translation in Z Direction

CLASSI SURFACE FOUNDATION

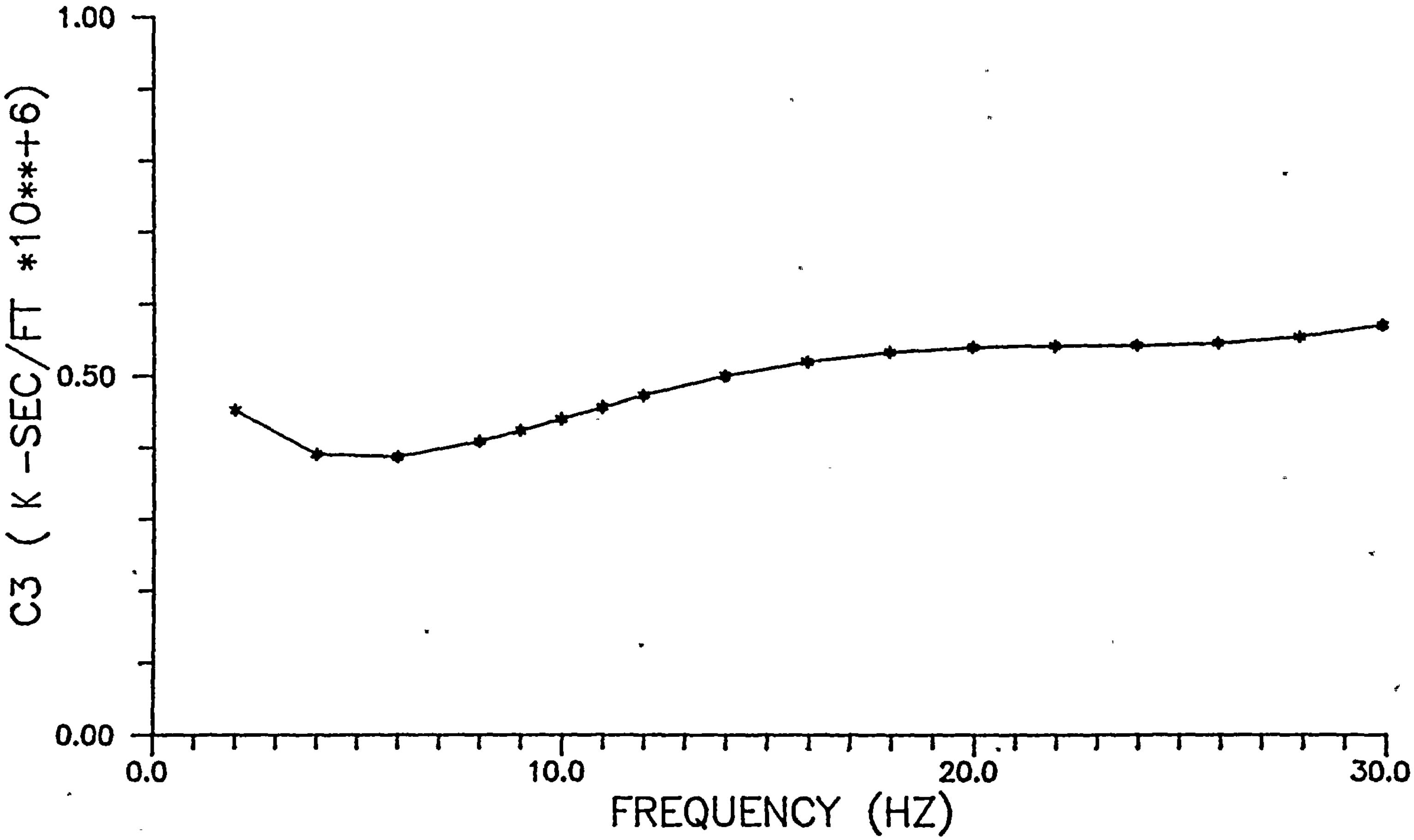

Vertical Damping Impedance for Translation in Z Direction

CLASSI SURFACE FOUNDATION

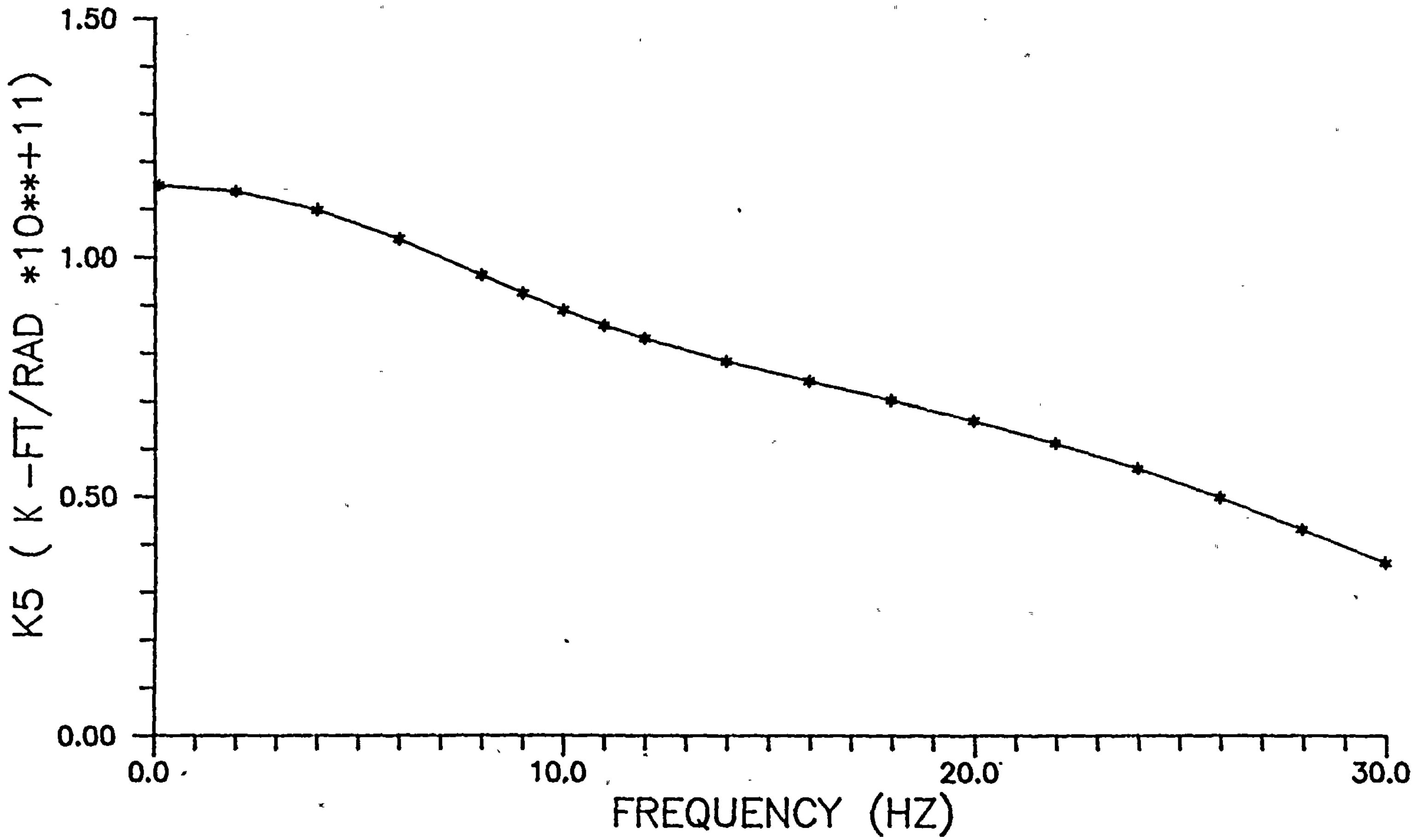

Rocking Stiffness Impedance About Y Axis (Same for Rocking About X Axis)

CLASSI SURFACE FOUNDATION

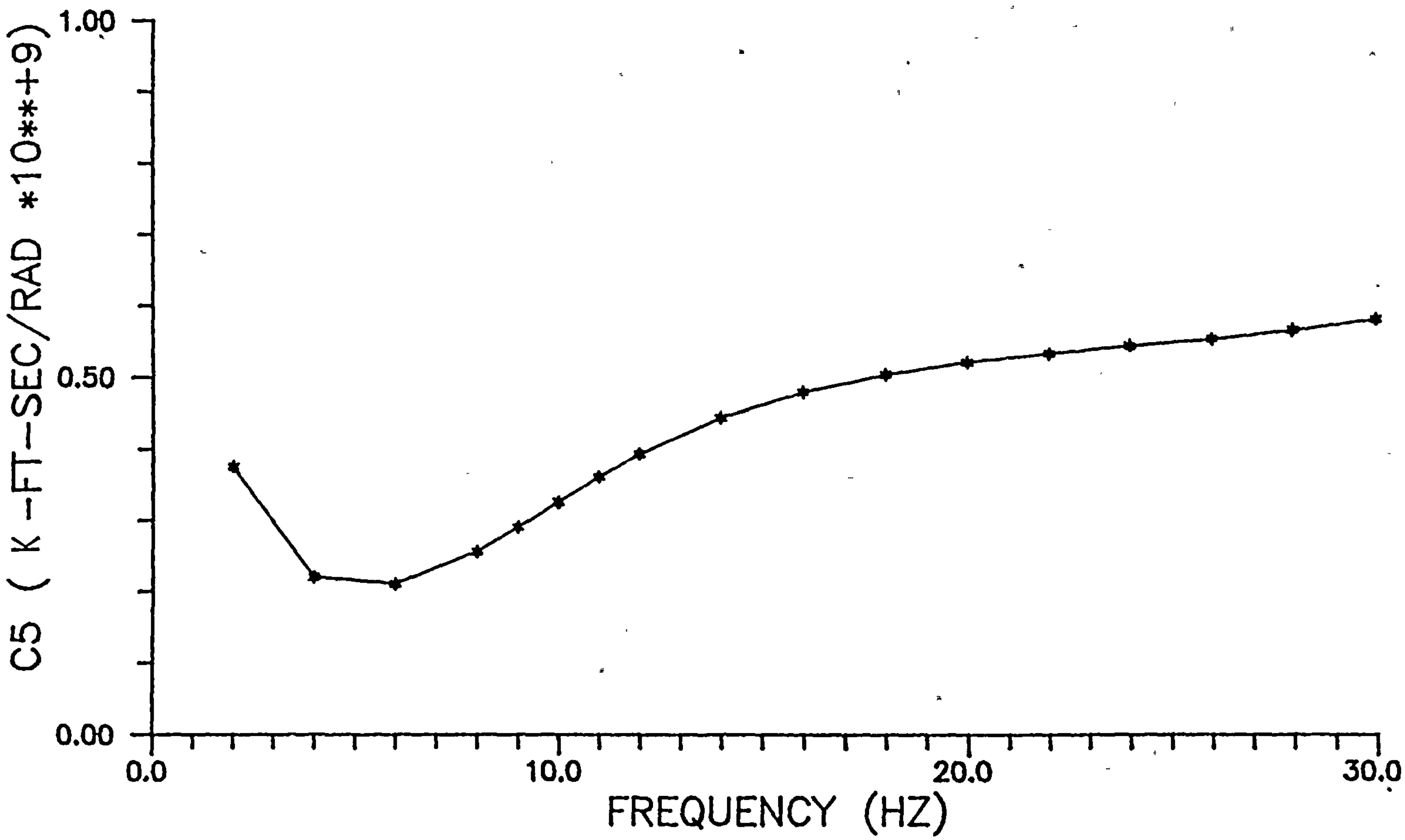

Rocking Damping Impedance About Y Axis (Same for Rocking About X Axis)

CLASSI SURFACE FOUNDATION

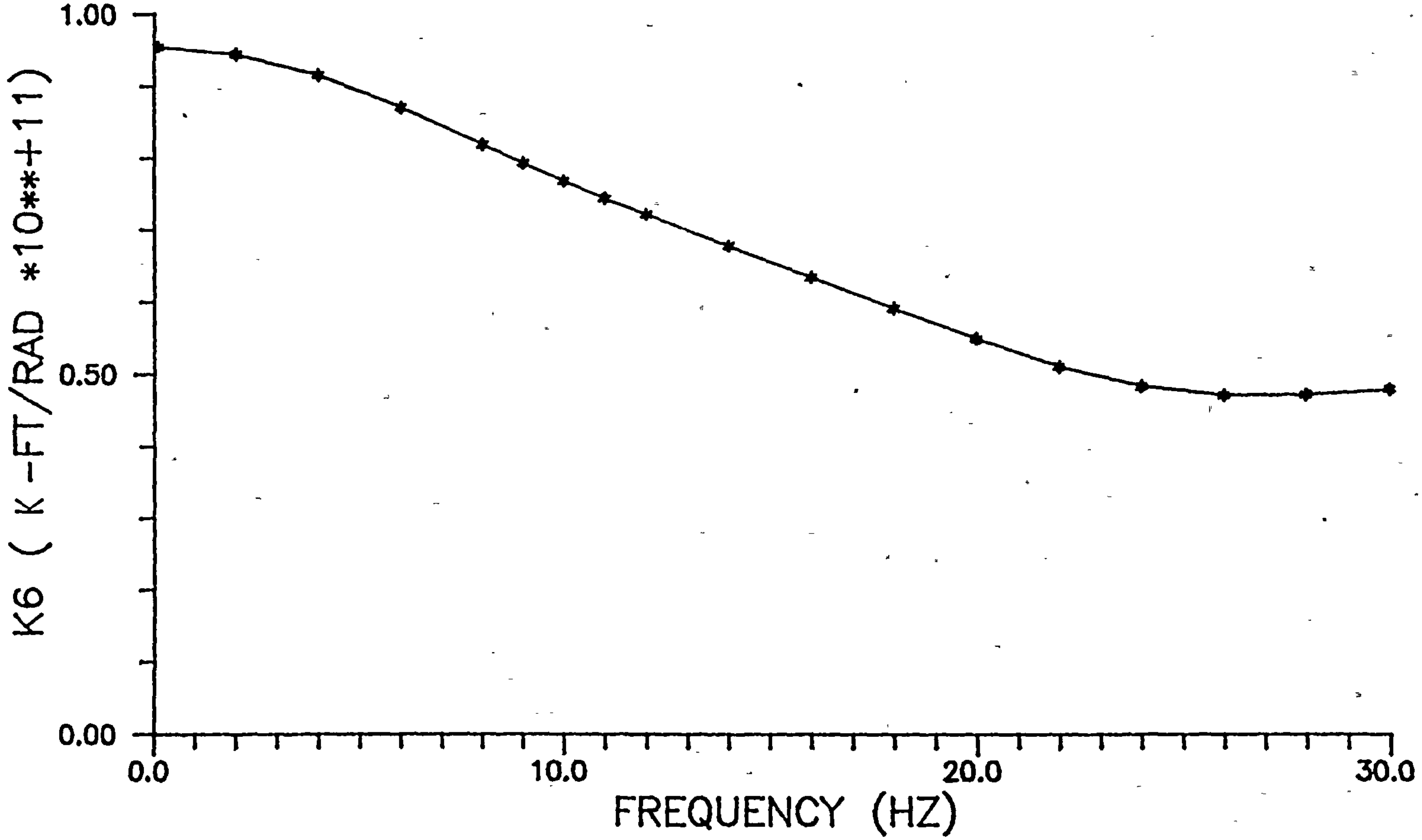

Torsional Stiffness Impedance About Z Axis

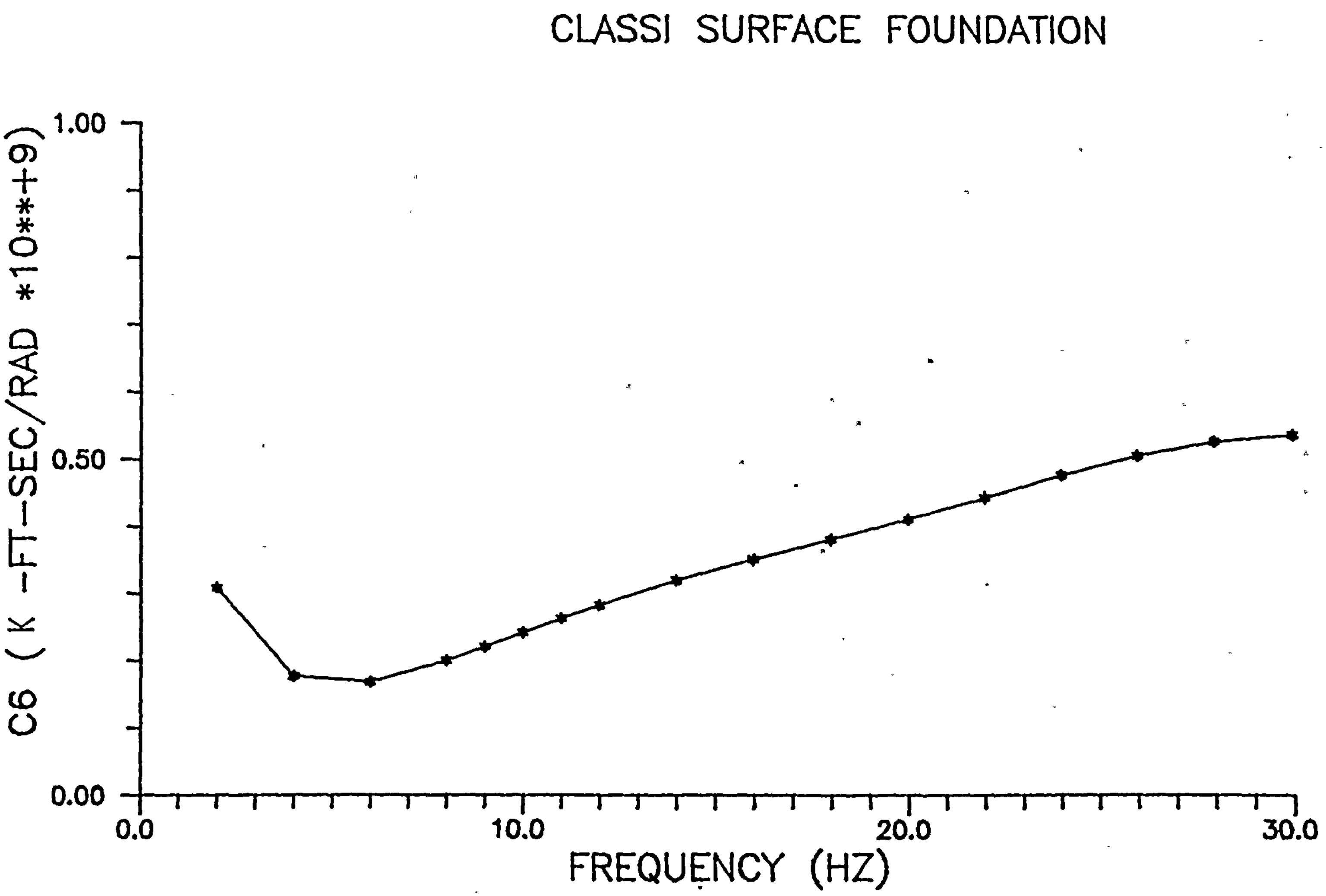

Torsional Damping Impedance About Z Axis

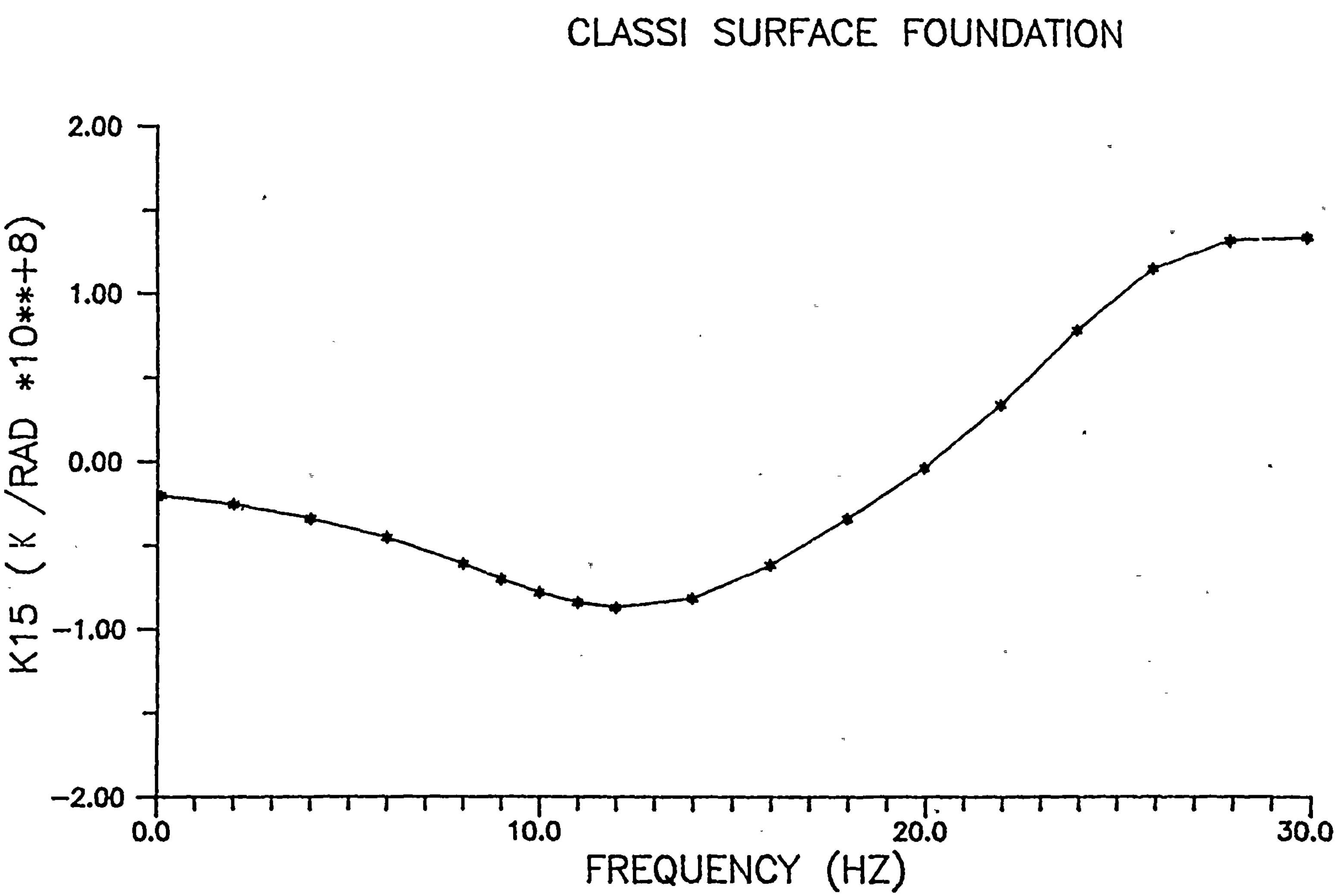

Coupling Stiffness Impedance Between Translation in X Direction and Rocking About Y Axis (Same for Coupling Between Translation in Y Direction and Rocking About X Axis)

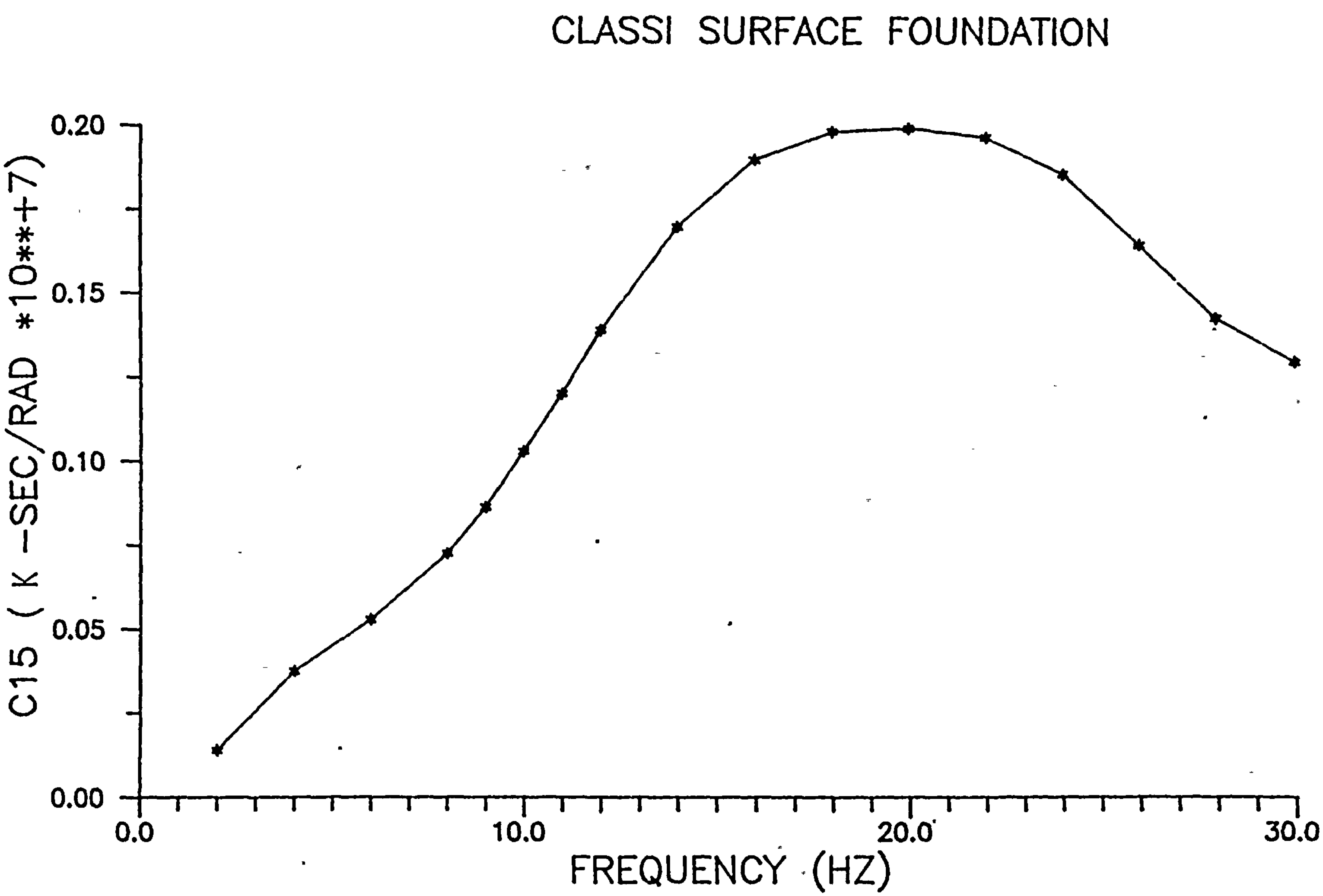

Coupling Damping Impedance Between Translation in X Direction and Rocking About Y Axis (Same for Coupling Between Translation in Y Direction and Rocking About X Axis)

"SASSI" SURFACE-SUPPORTED AND EMBEDDED FOUNDATION MODEL AND IMPEDANCES FOR THE CONTAINMENT

"SASSI" SURFACE-SUPPORTED AND
EMBEDDED FOUNDATION MODEL AND
IMPEDANCES FOR THE CONTAINMENT

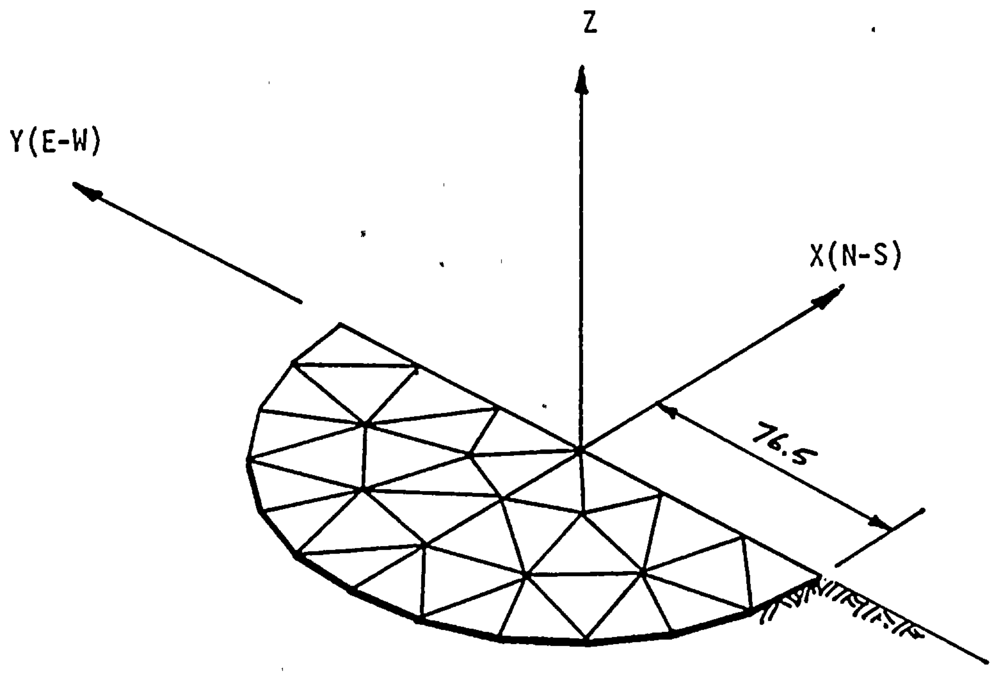

SASSI Surface Foundation Half-Model

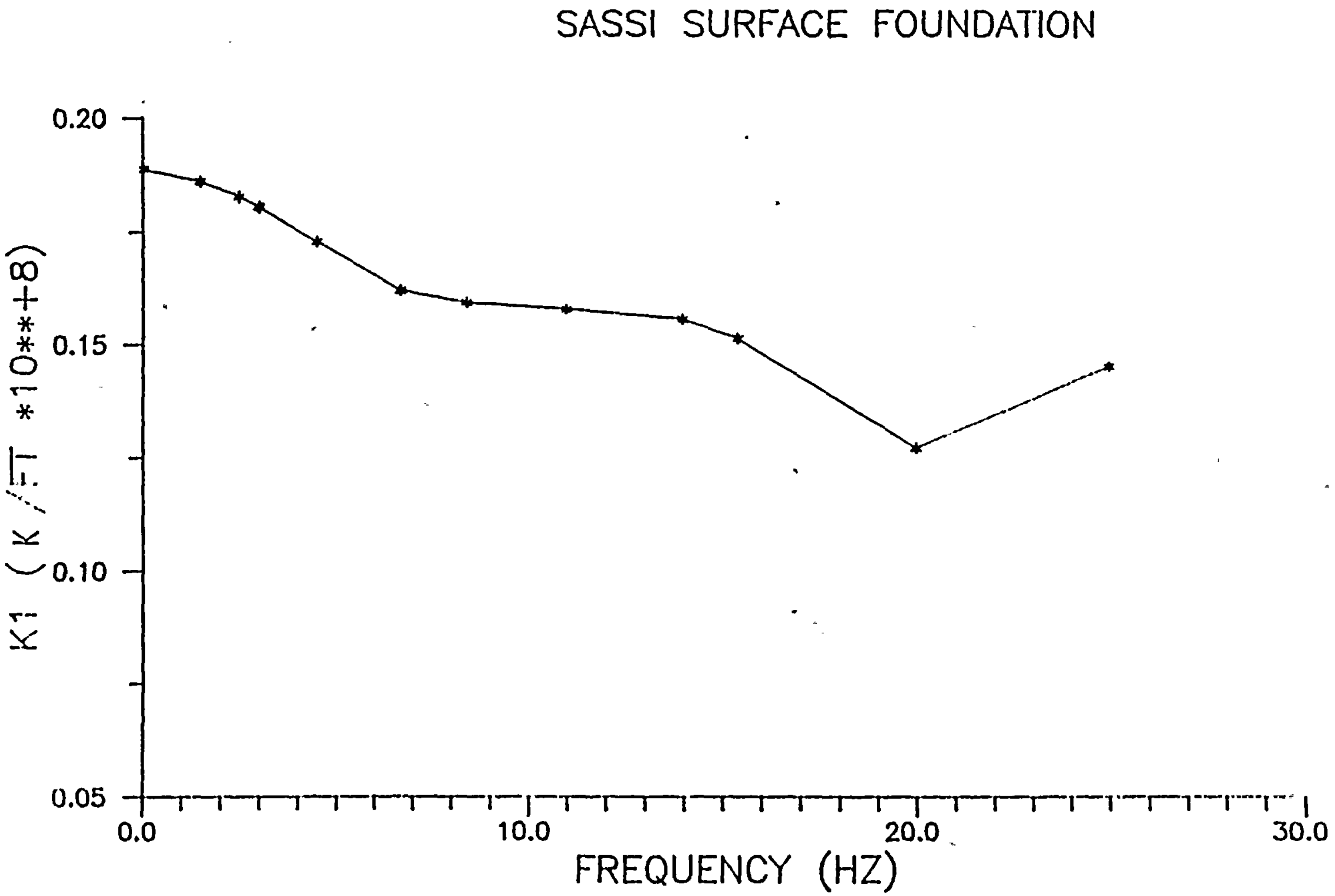

Horizontal Stiffness Impedance for Translation in X Direction (Same as for Translation in Y Direction)

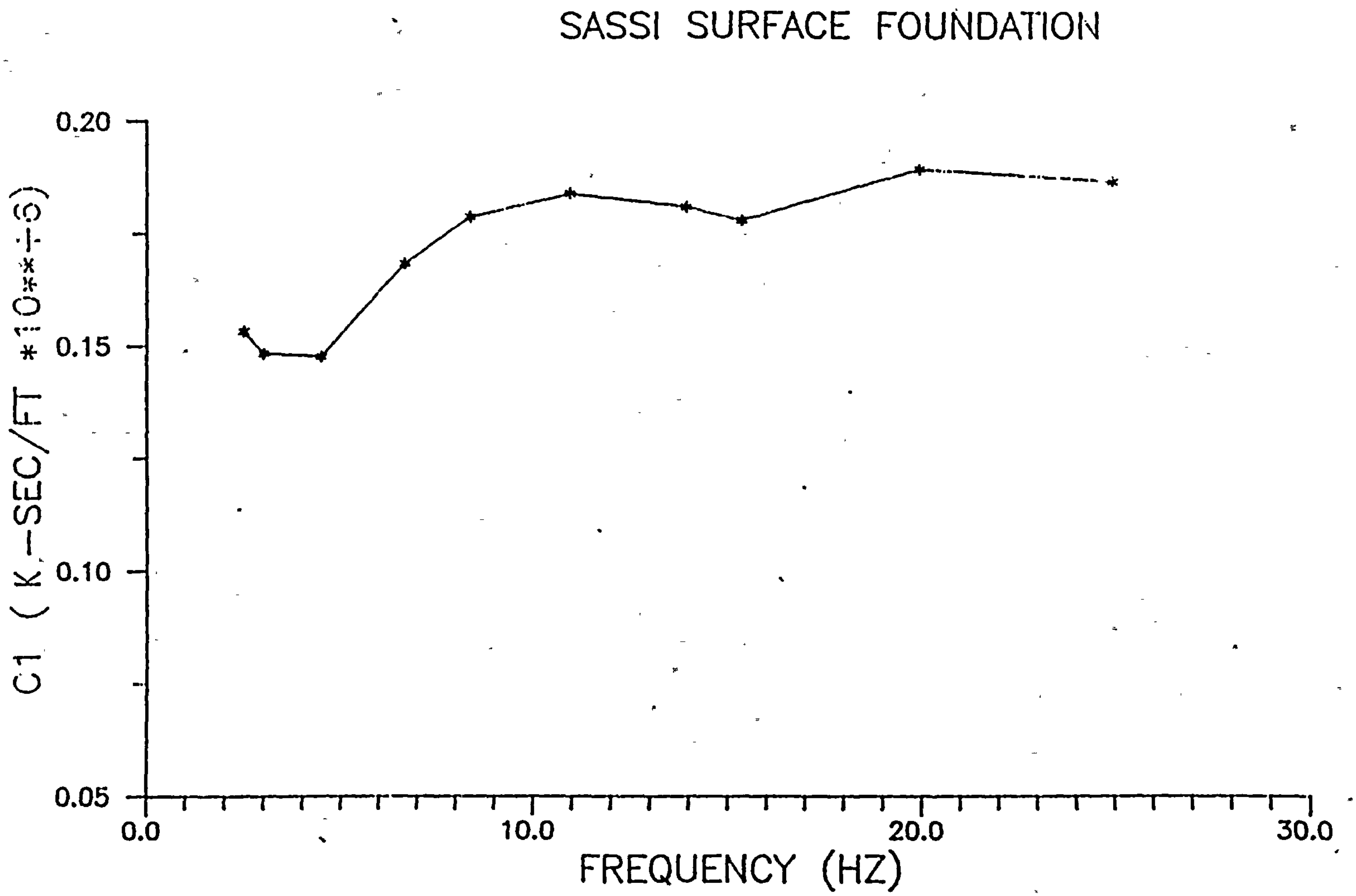

Horizontal Damping Impedance for Translation in X Direction
(Same for Translation in Y Direction)

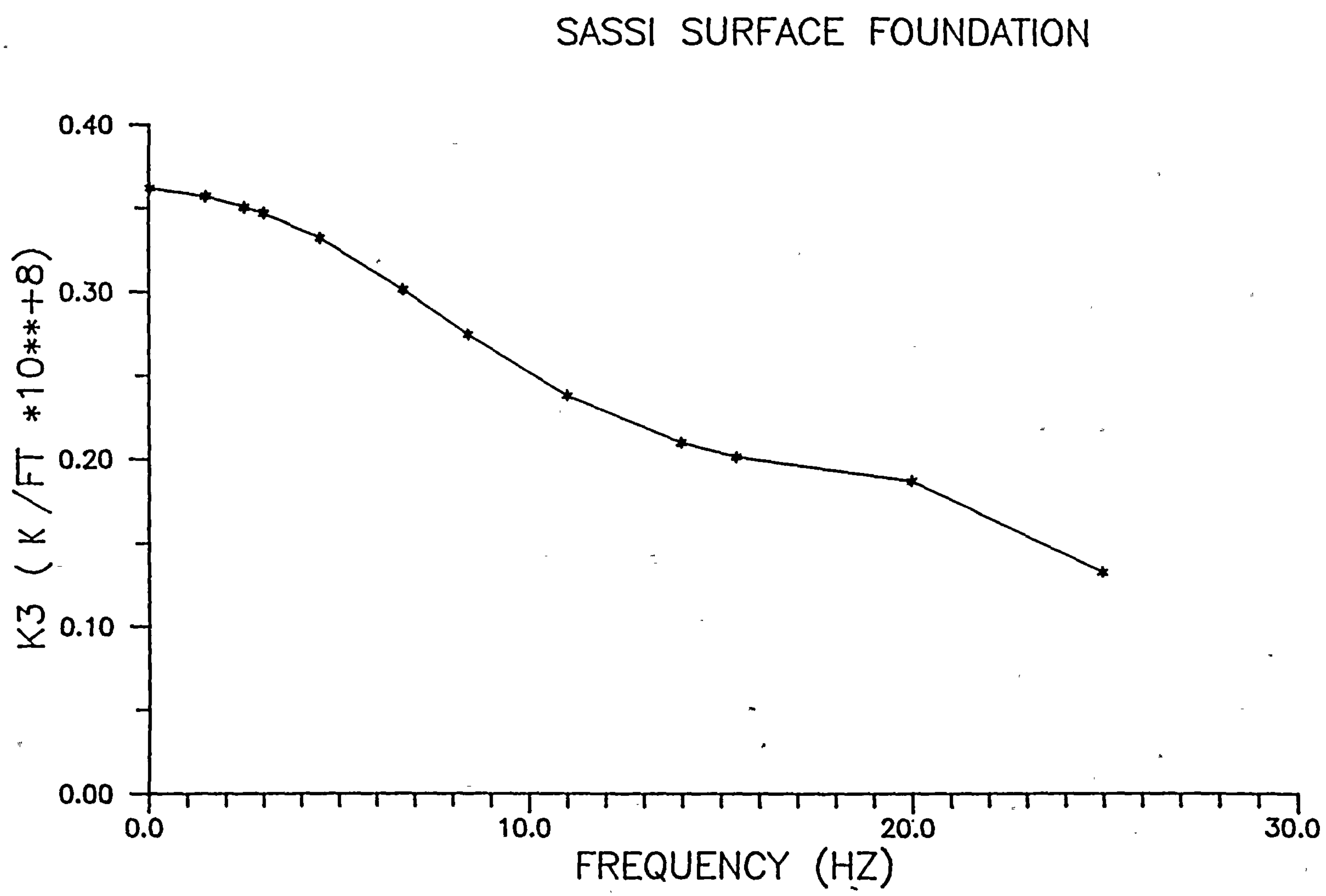

Vertical Stiffness Impedance for Translation in Z Direction

SASSI SURFACE FOUNDATION

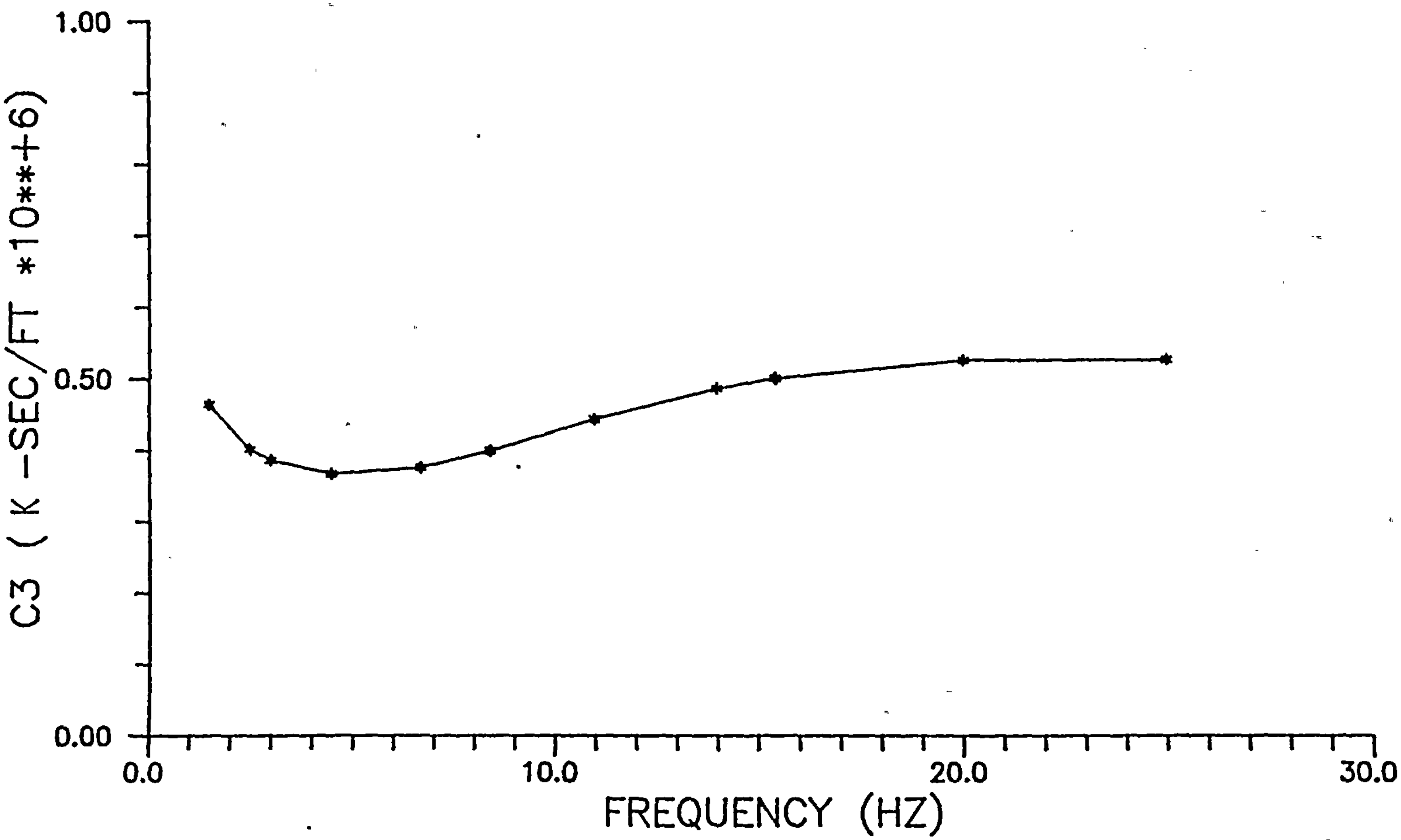

Vertical Damping Impedance for Translation in Z Direction

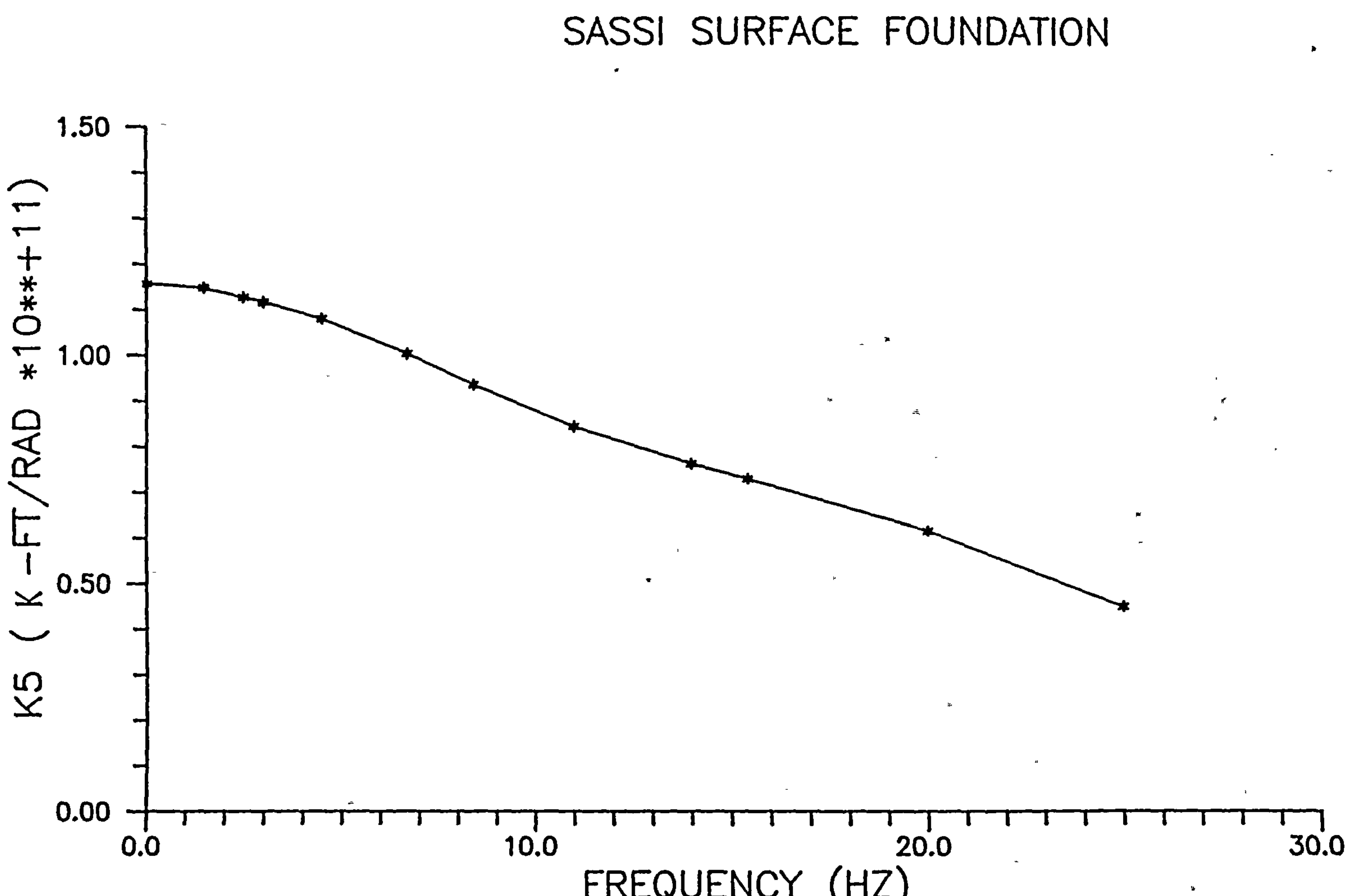

Rocking Stiffness Impedance About Y Axis (Same for Rocking About X Axis)

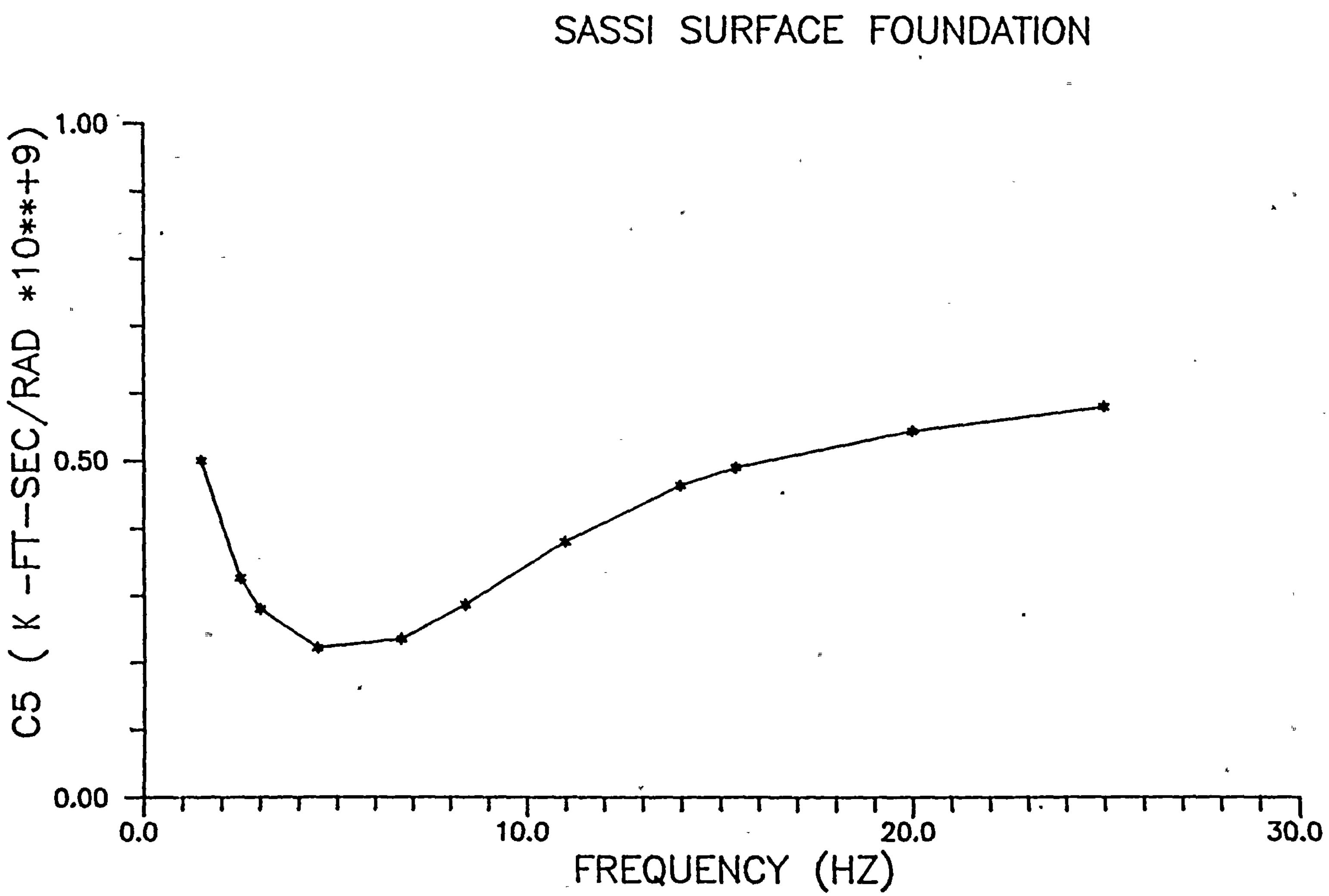

Rocking Damping Impedance about Y Axis (Same for Rocking About X Axis)

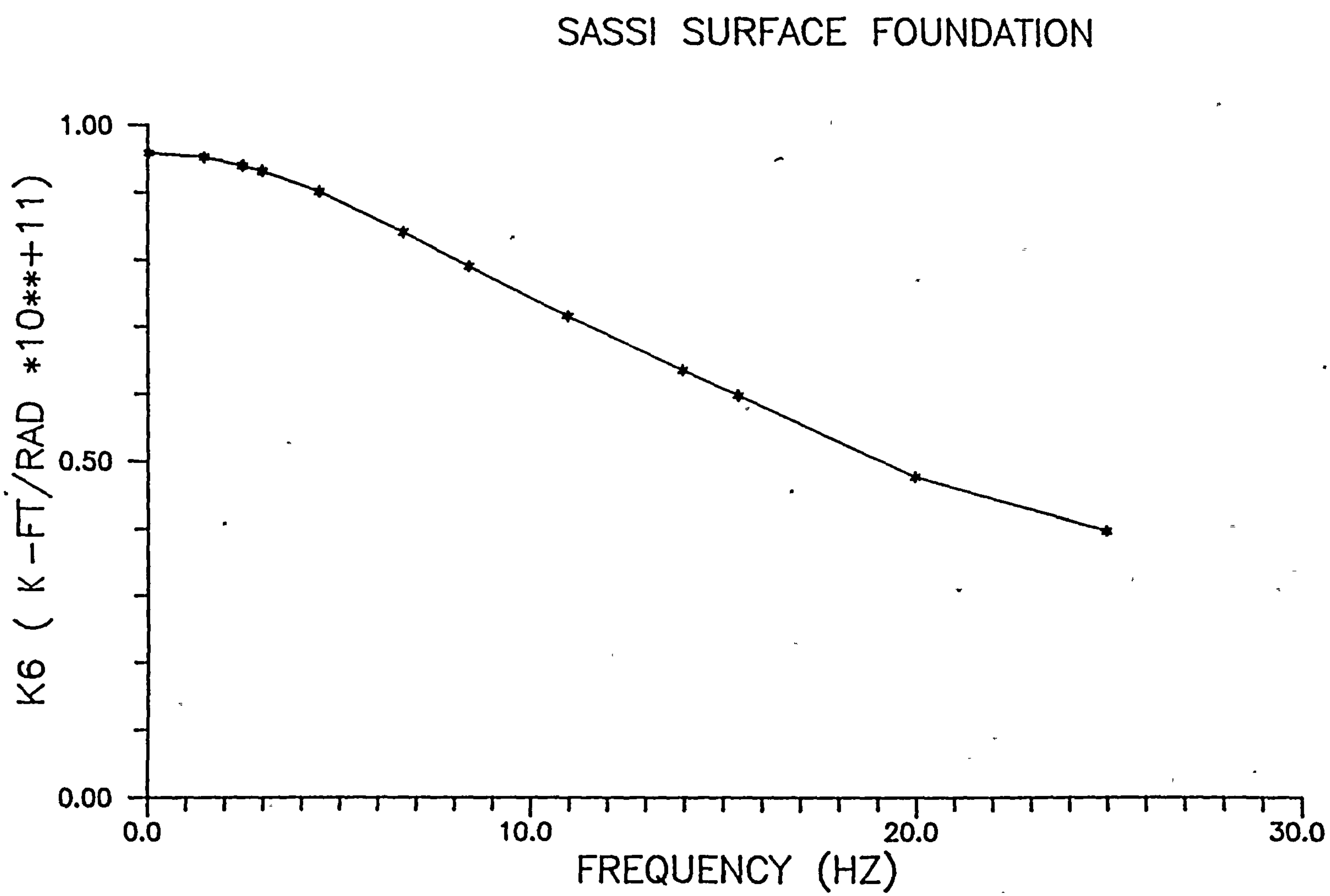

Torsional Stiffness Impedance About Z Axis

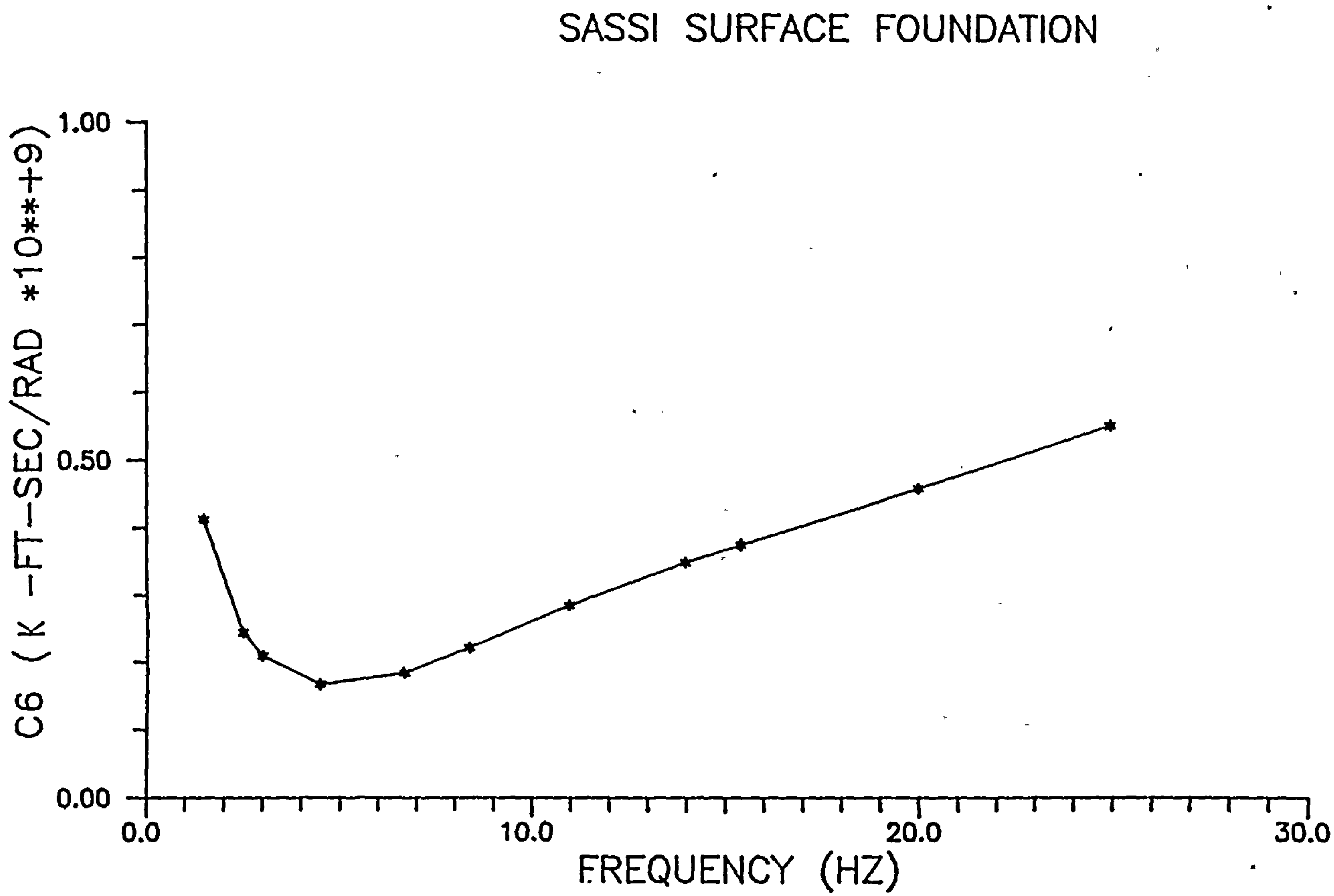

Torsional Damping Impedance About Z Axis

SASSI SURFACE FOUNDATION

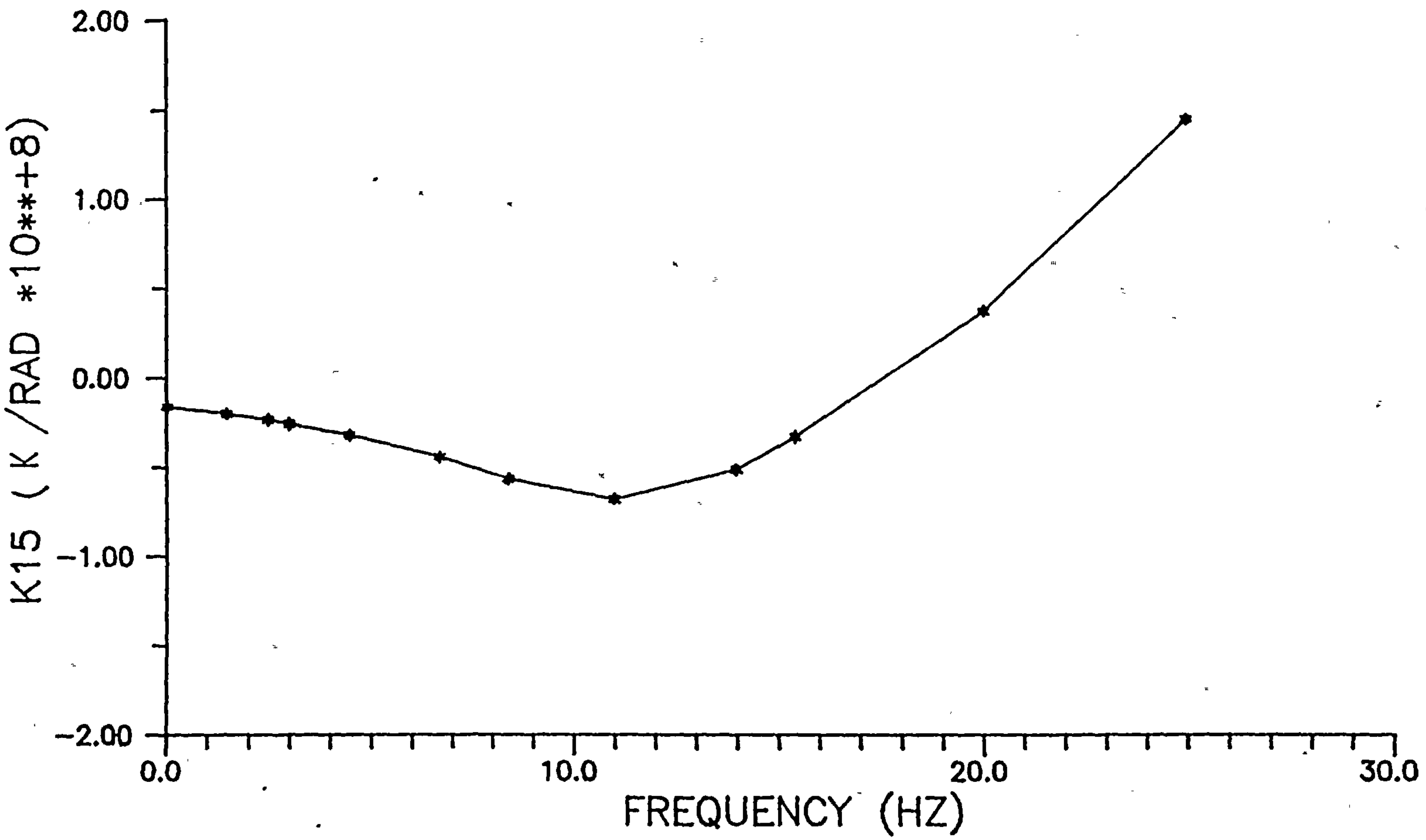

Coupling Stiffness Impedance Between Translation in X Direction and Rocking About Y Axis (Same for Coupling Between Translation in Y Direction and Rocking About X Axis)

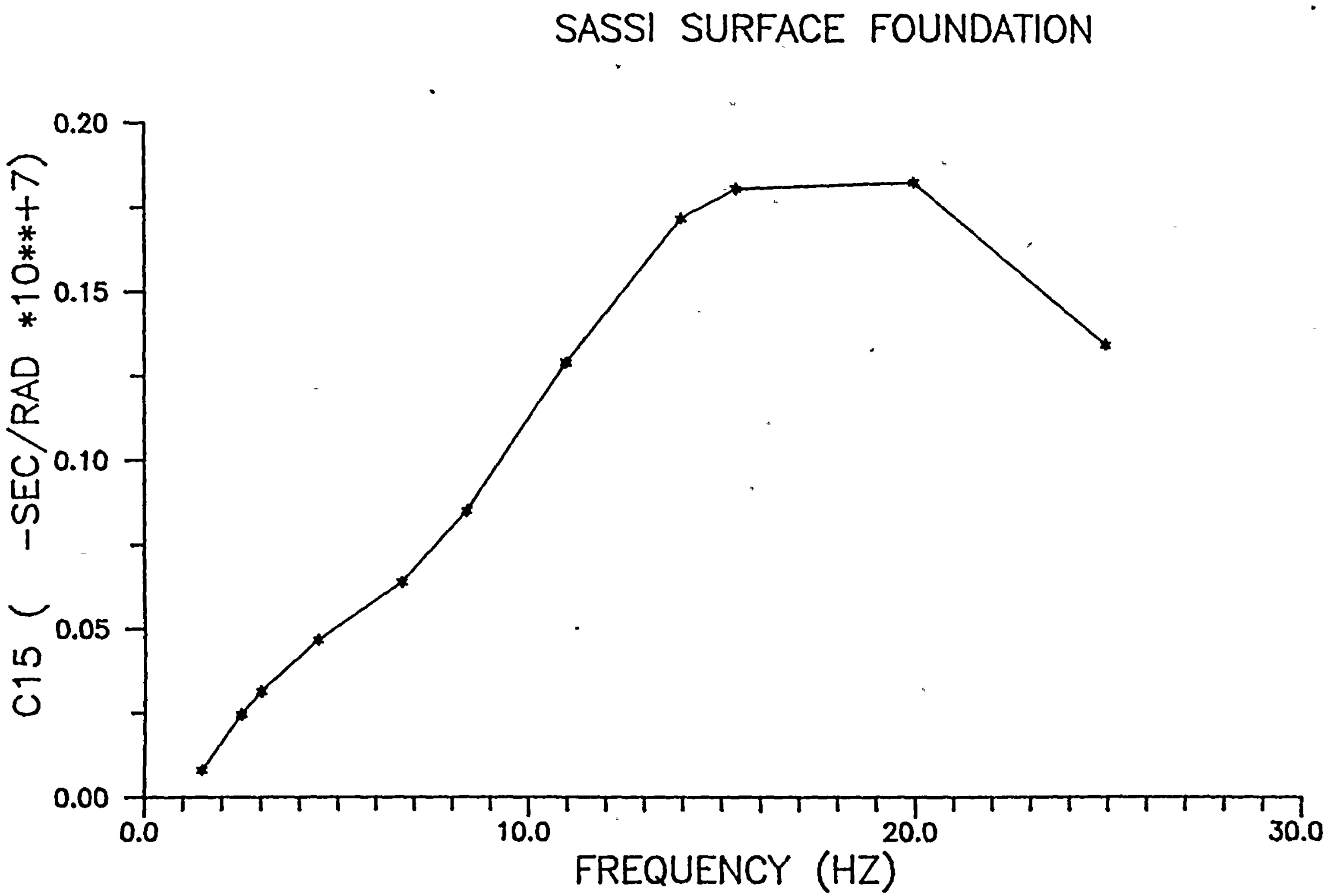

Coupling Damping Impedance Between Translation in X Direction and Rocking About Y Axis (Same for Coupling Between Translation in Y Direction and Rocking About X Axis)

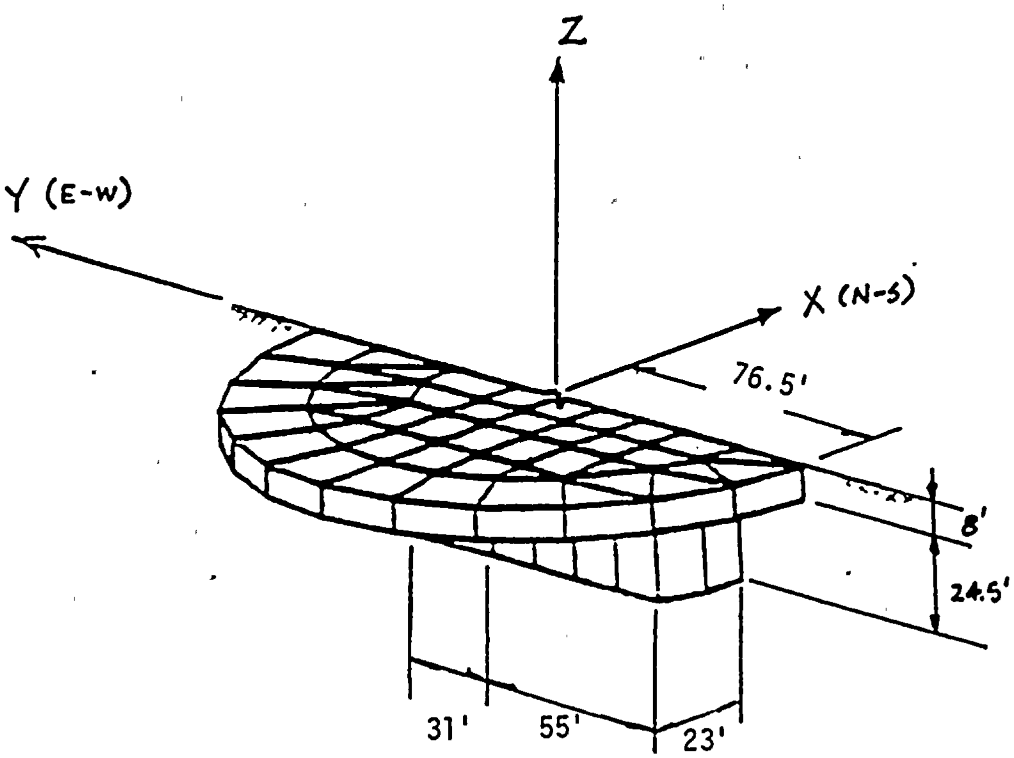

SASSI Embedded Foundation Model

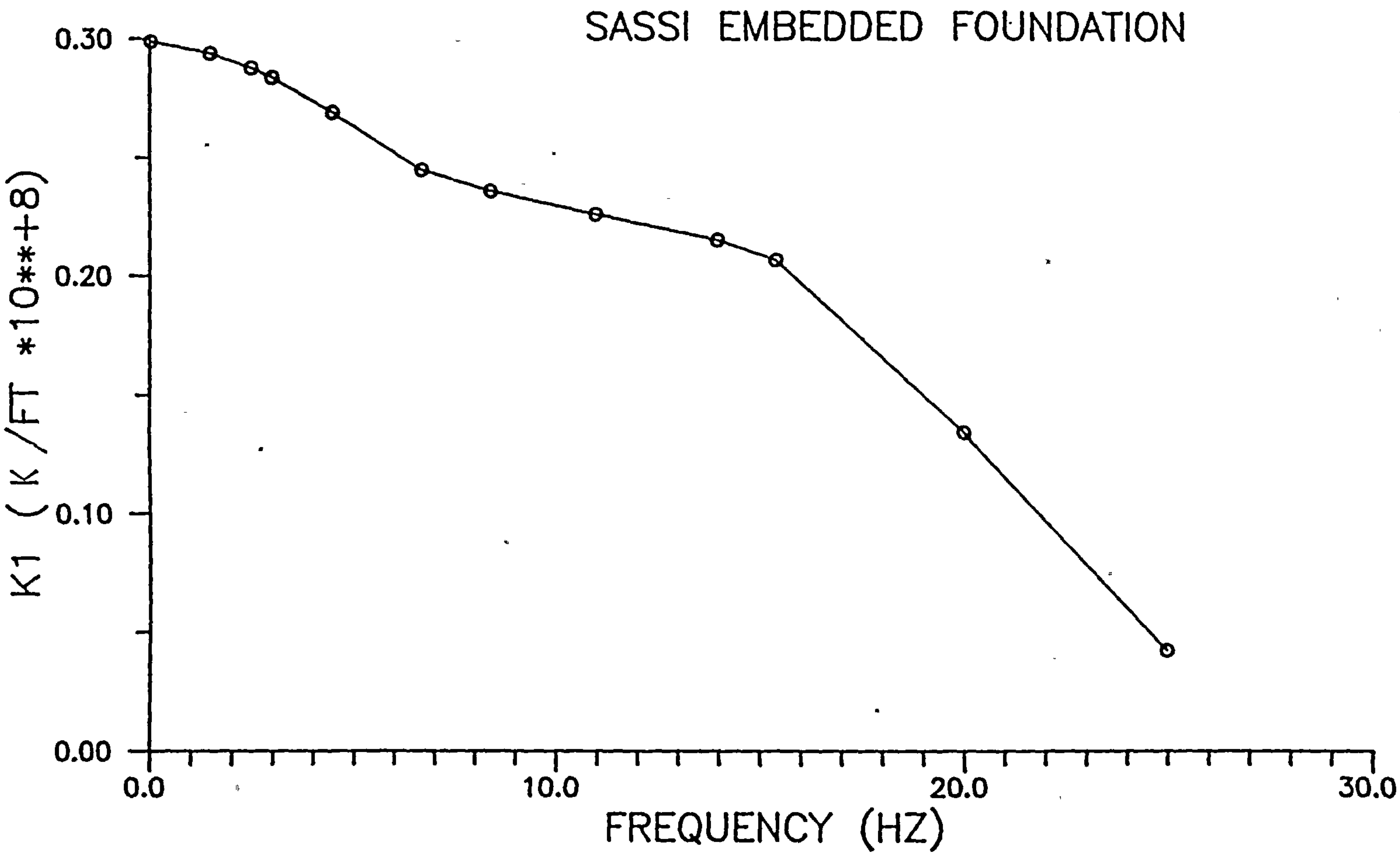

Horizontal Stiffness Impedance for Translation in X Direction

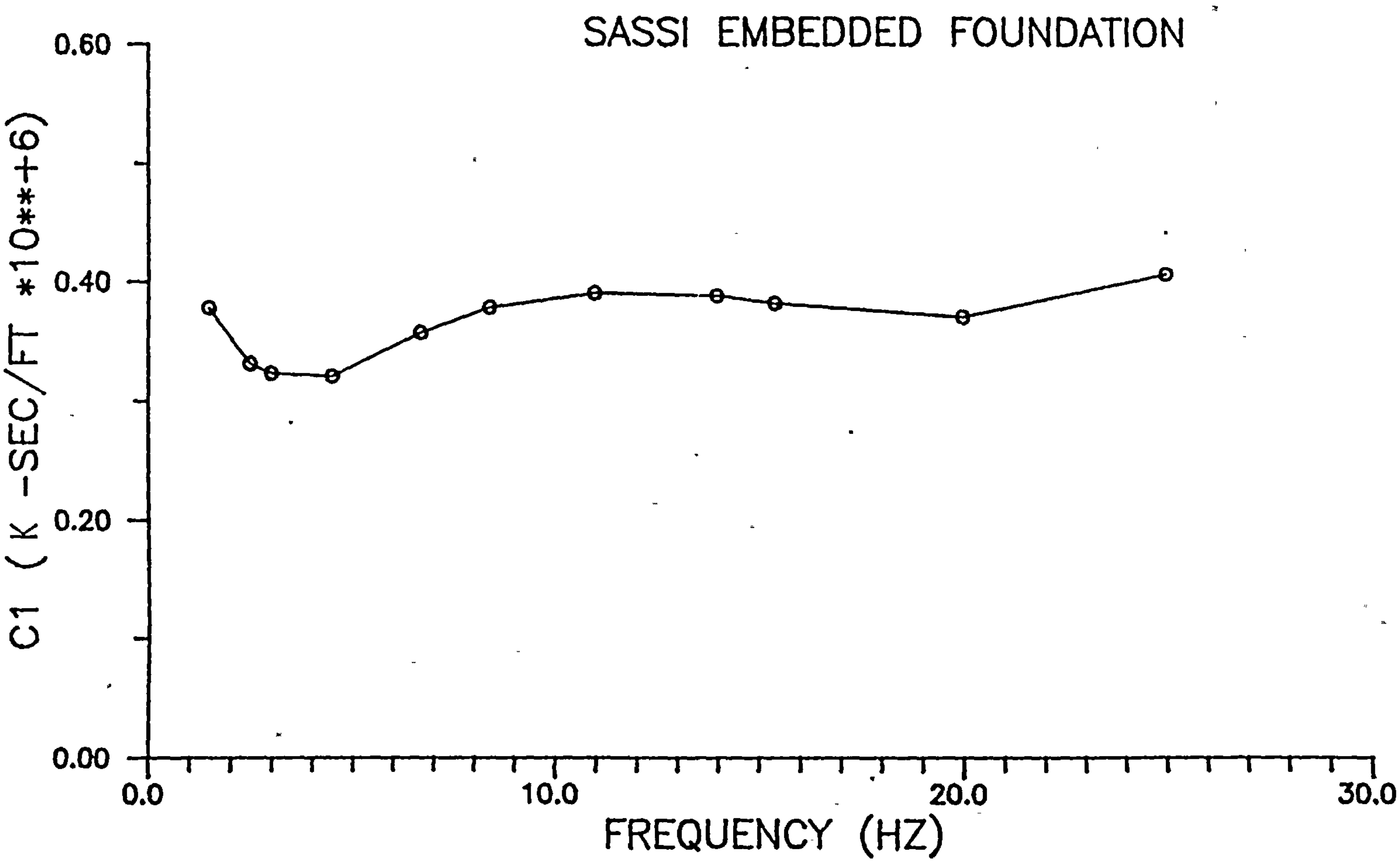

Horizontal Damping Impeance for Translation in X Direction

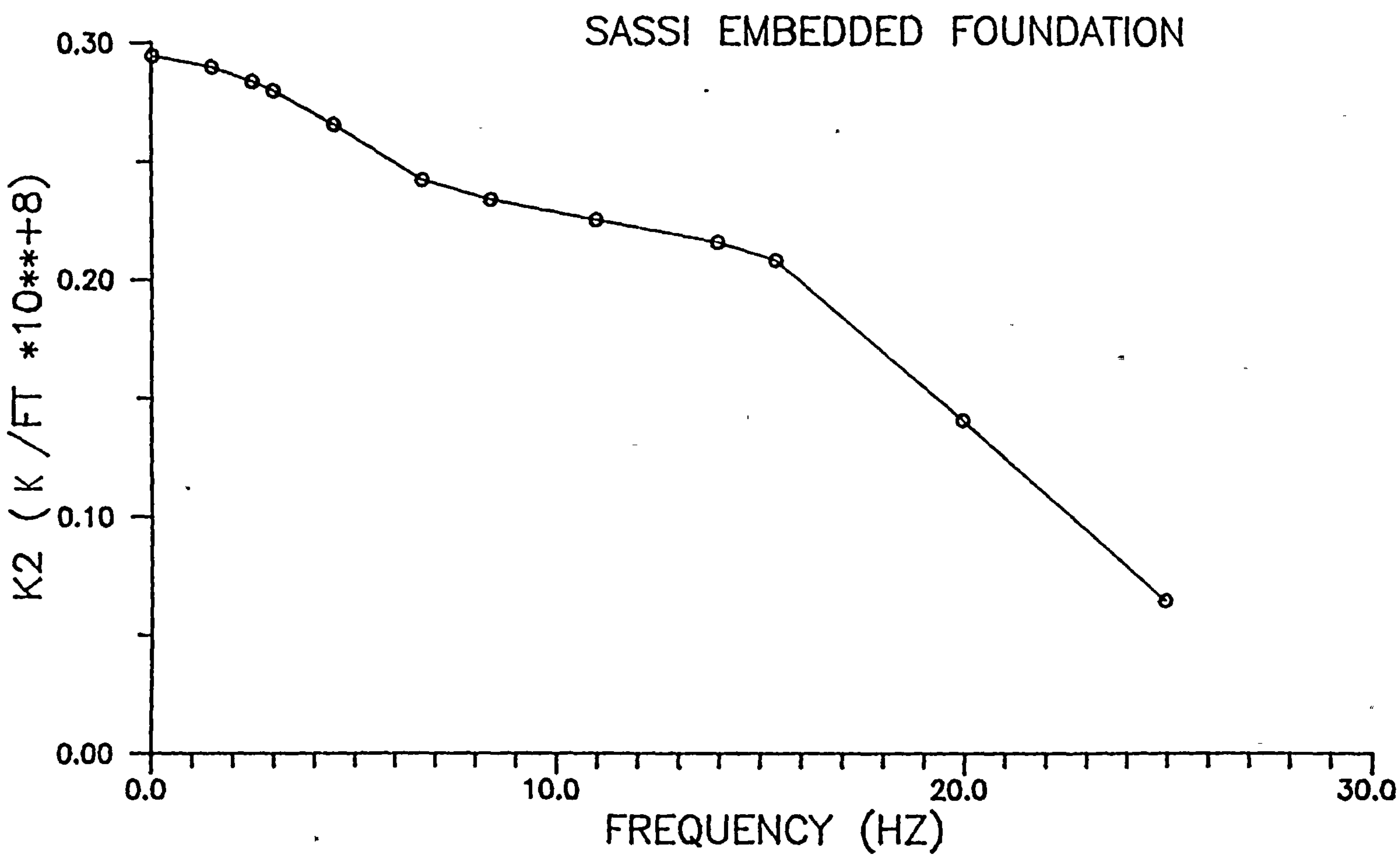

Horizontal Stiffness Impedance for Translation in Y Direction

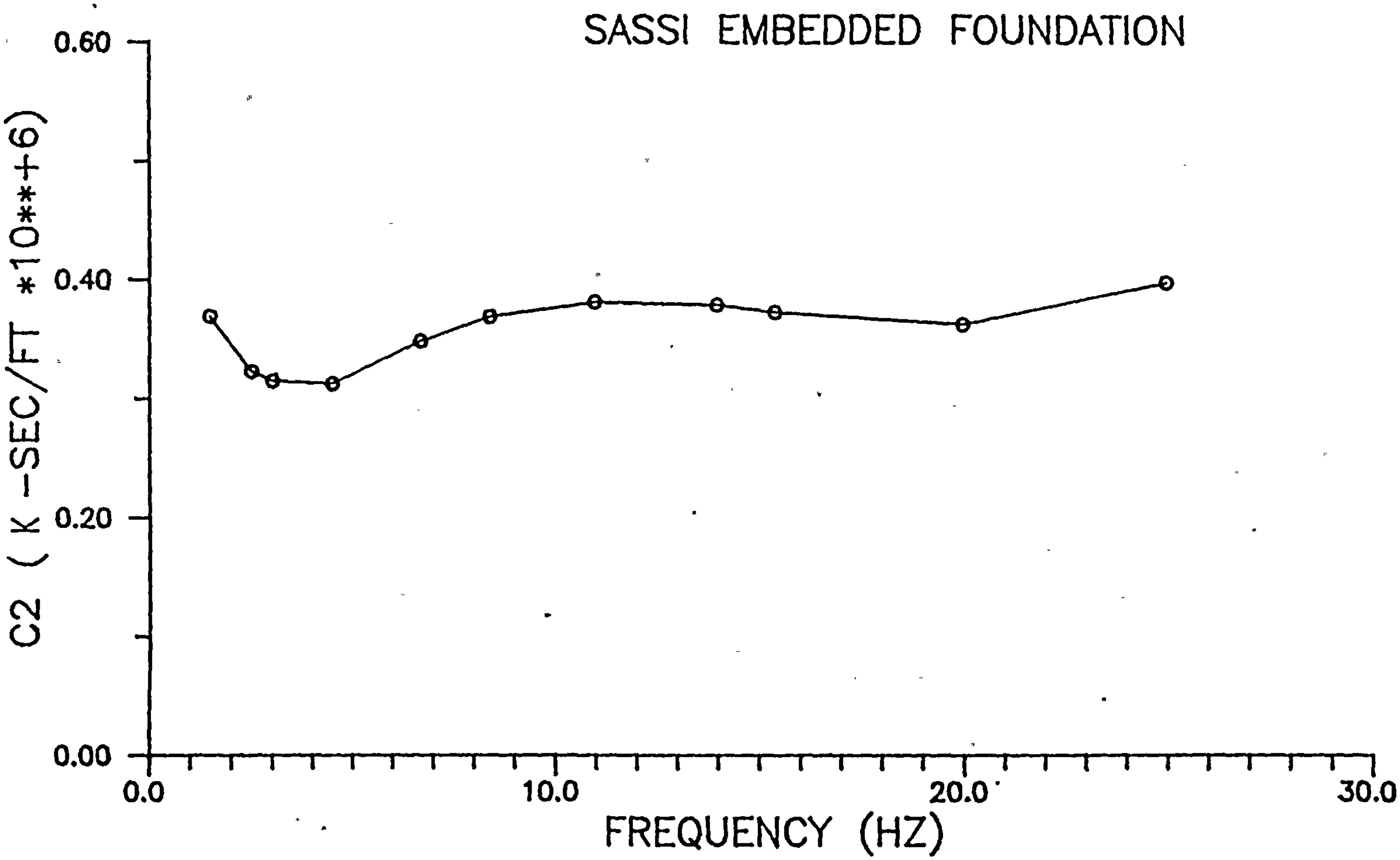

Horizontal Damping Impedance for Translation in Y Direction

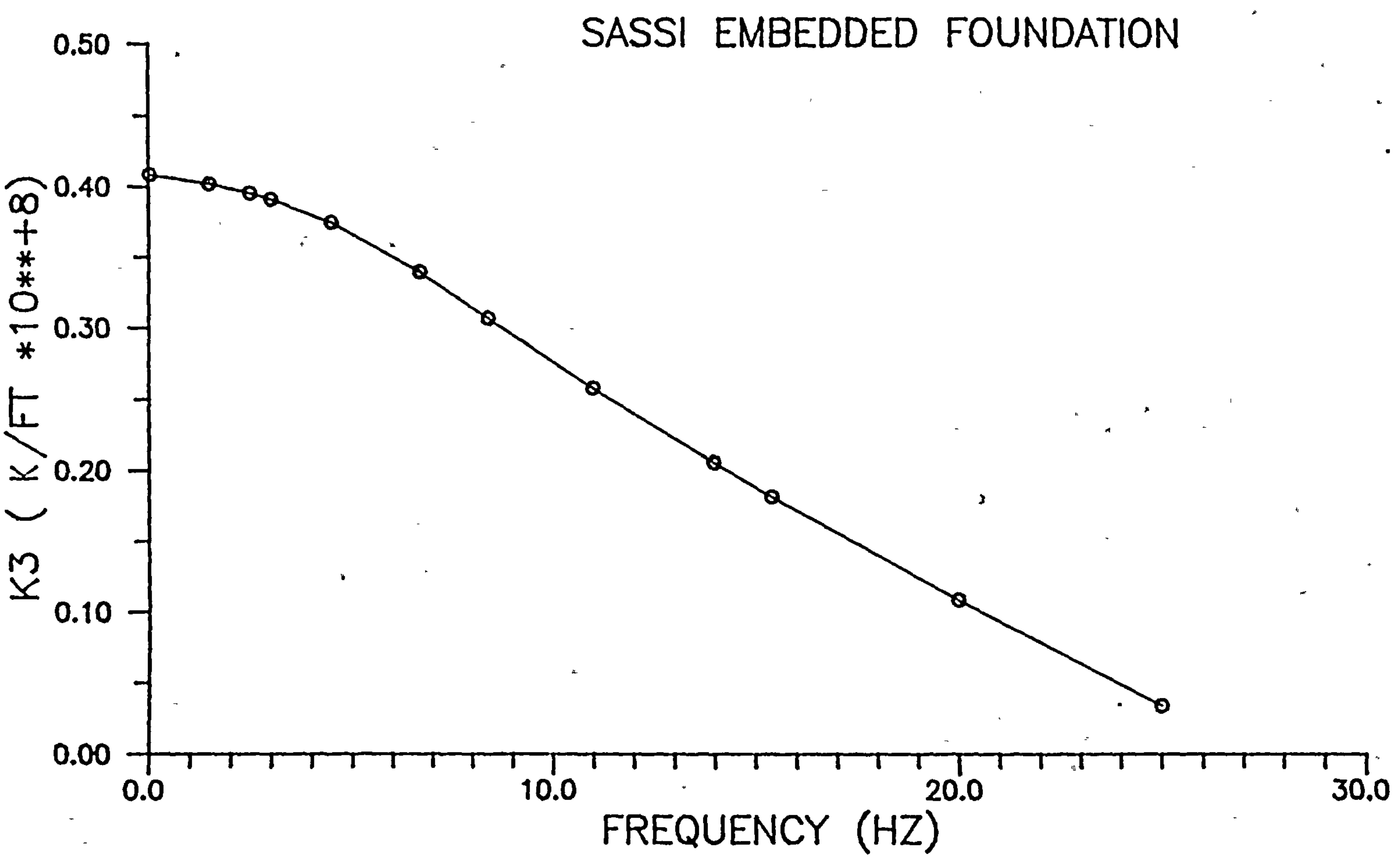

Vertical Stiffness Impedance for Translation in Z Direction

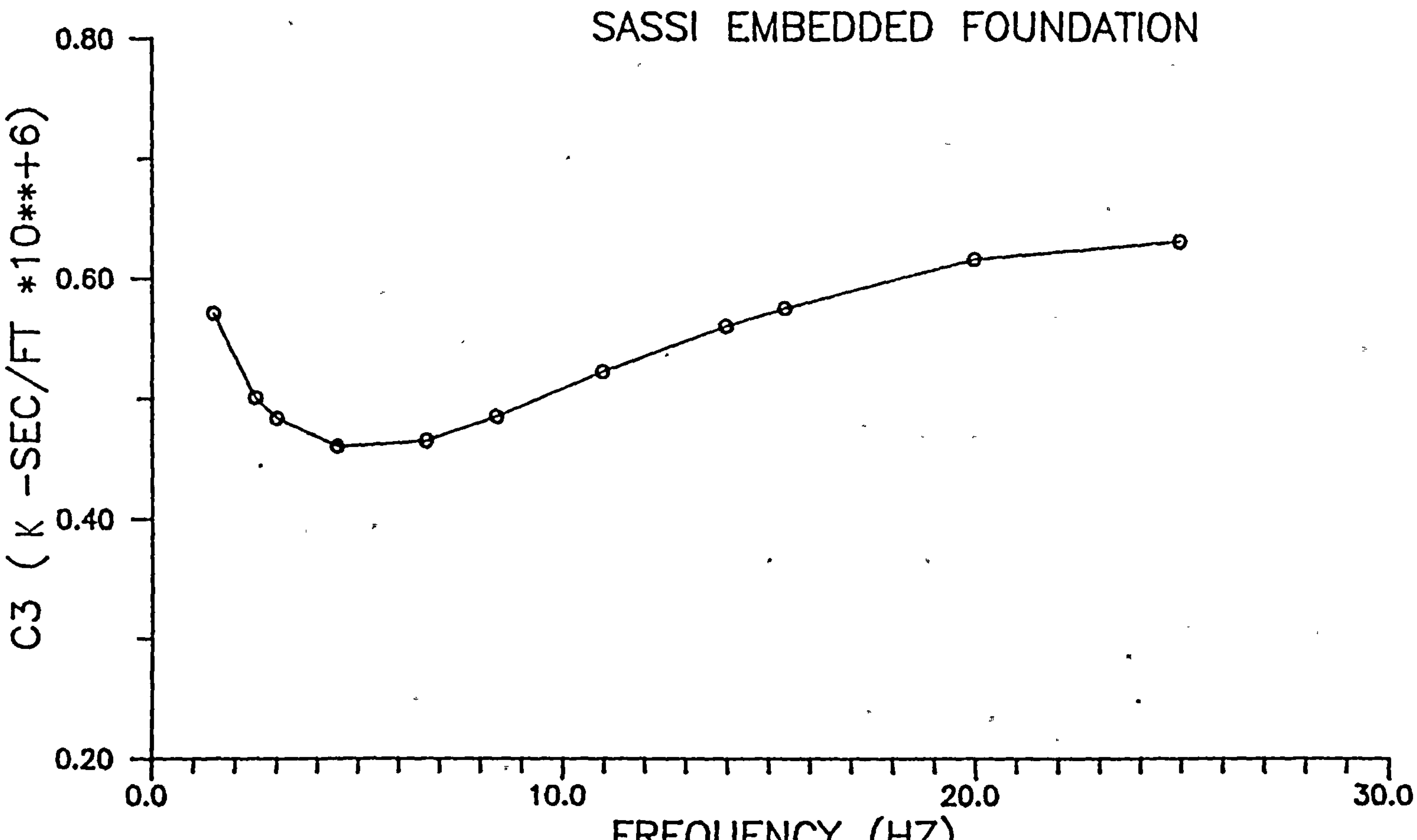

Vertical Damping Impedance for Translation in Z Direction

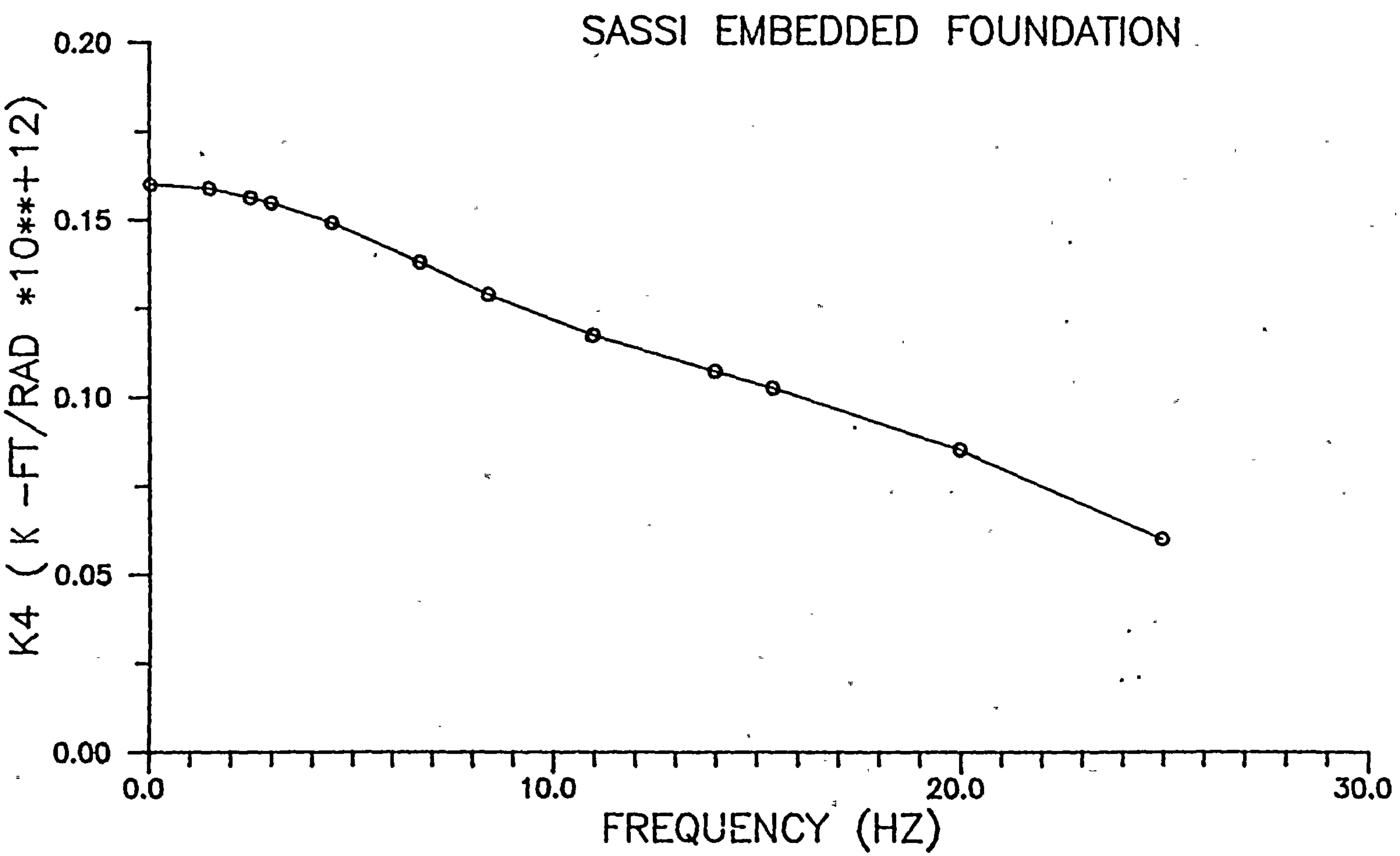

Rocking Stiffness Impedance About X Axis

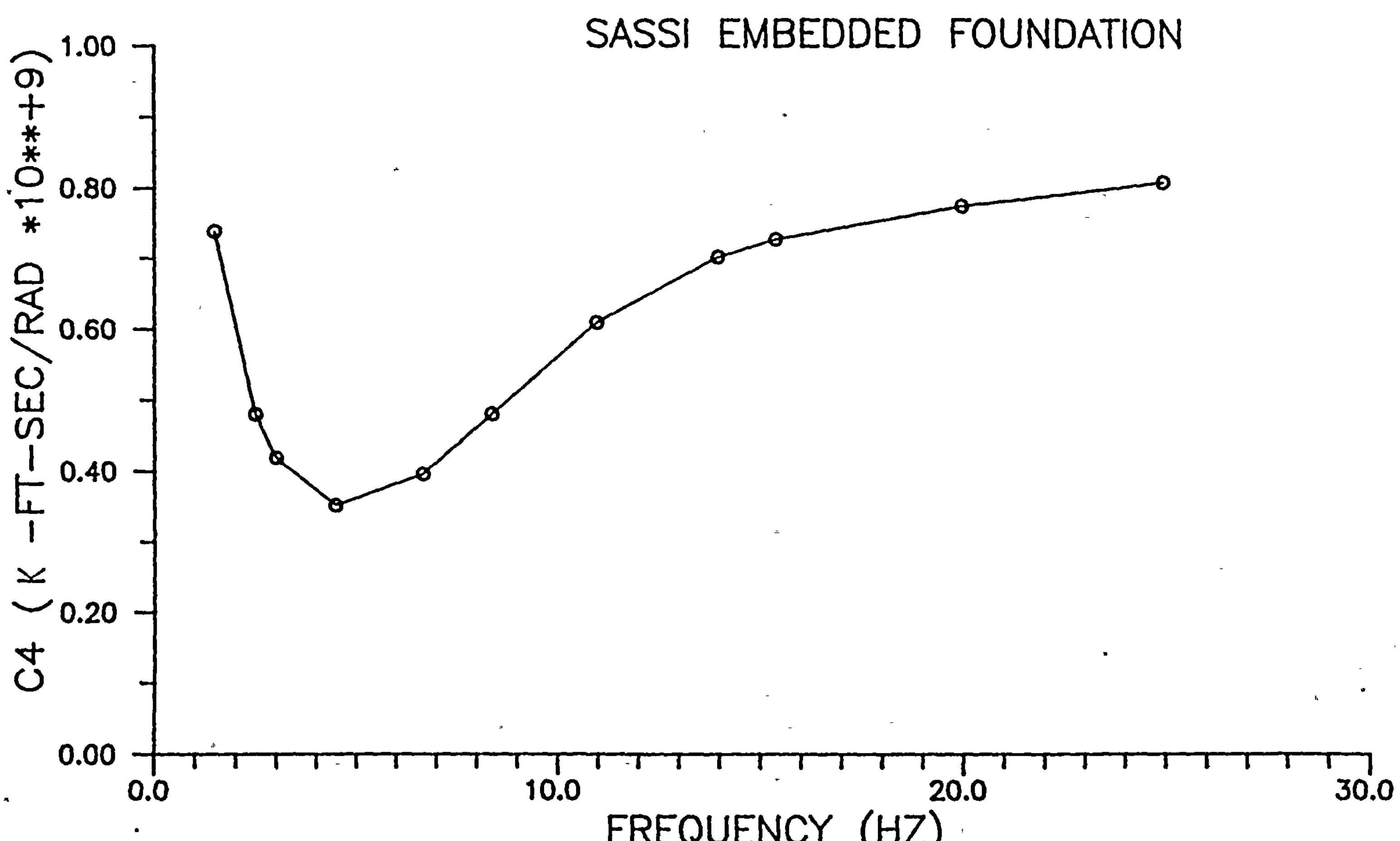

Rocking Damping Impedance About X Axis

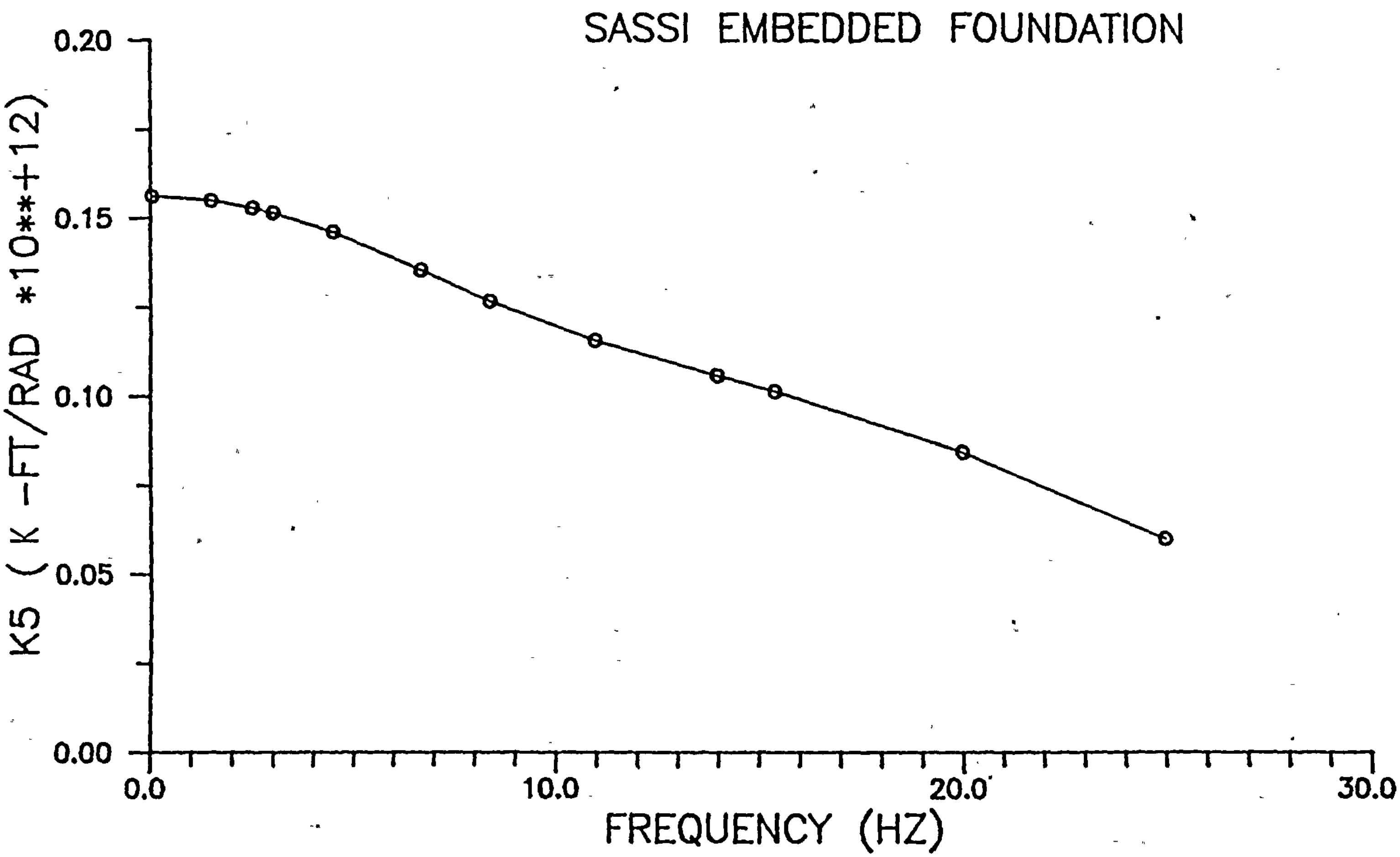

Rocking Stiffness Impedance About Y Axis

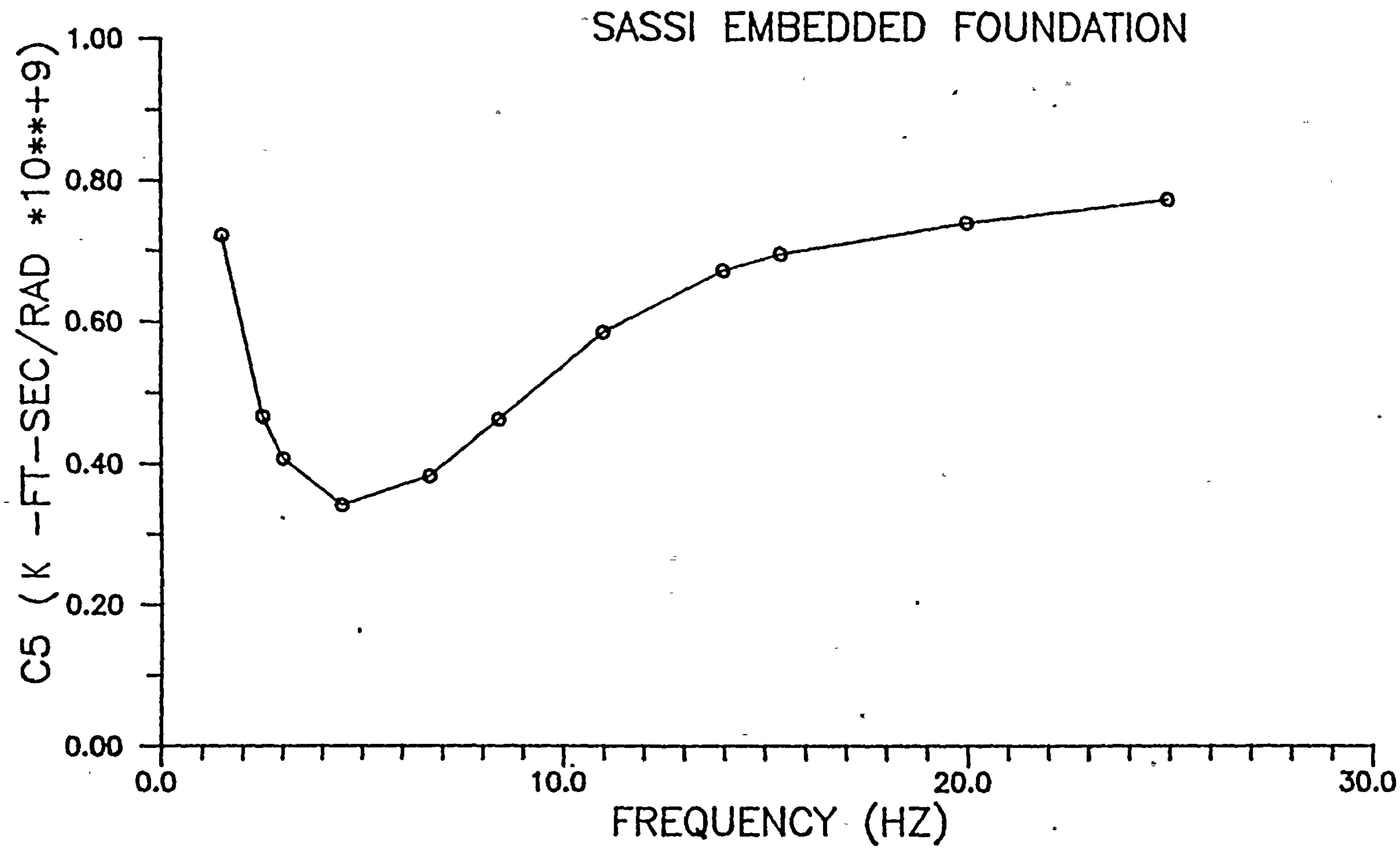

Rocking Damping Impedance About Y Axis

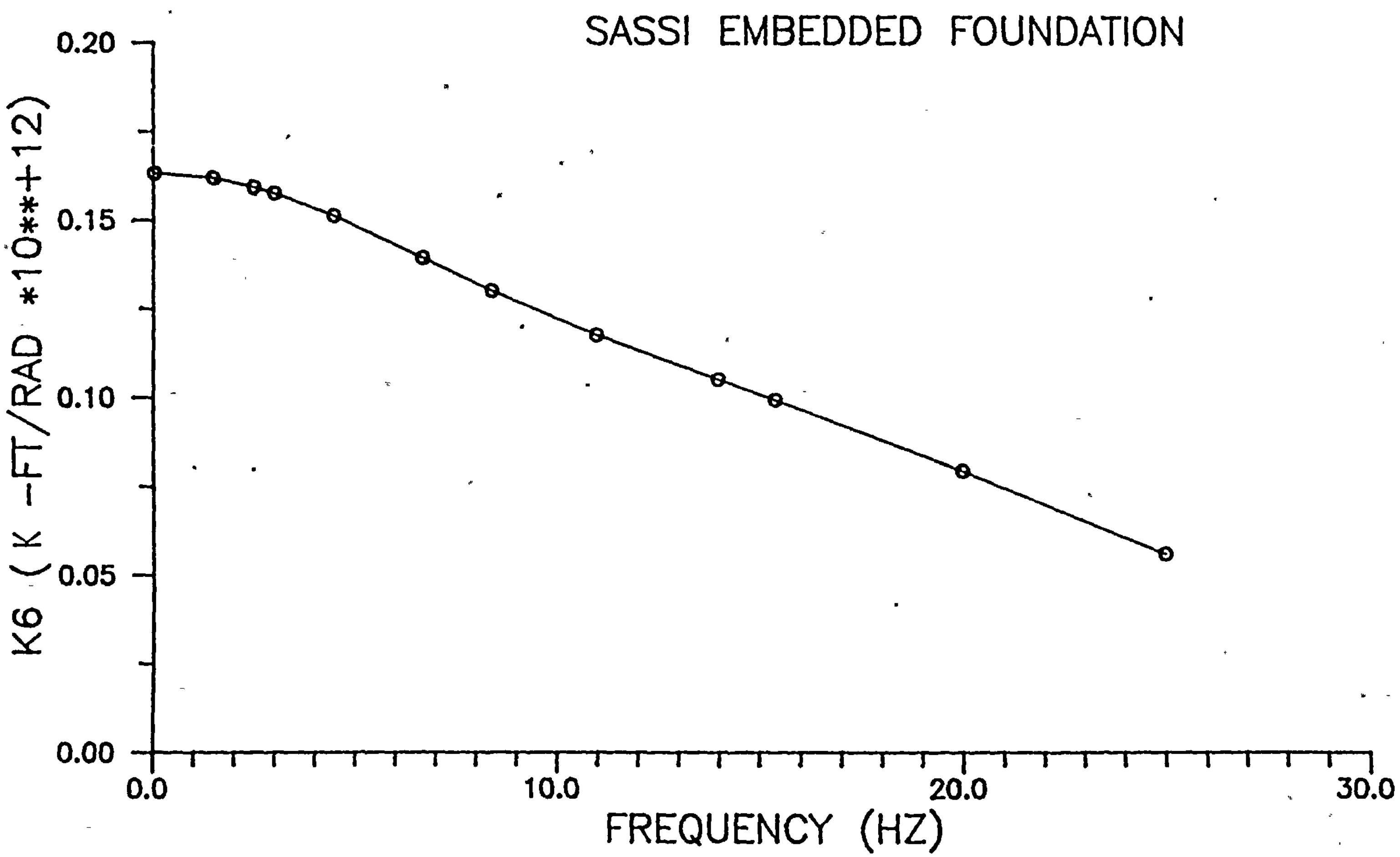

Torsional Stiffness Impedance About Z Axis

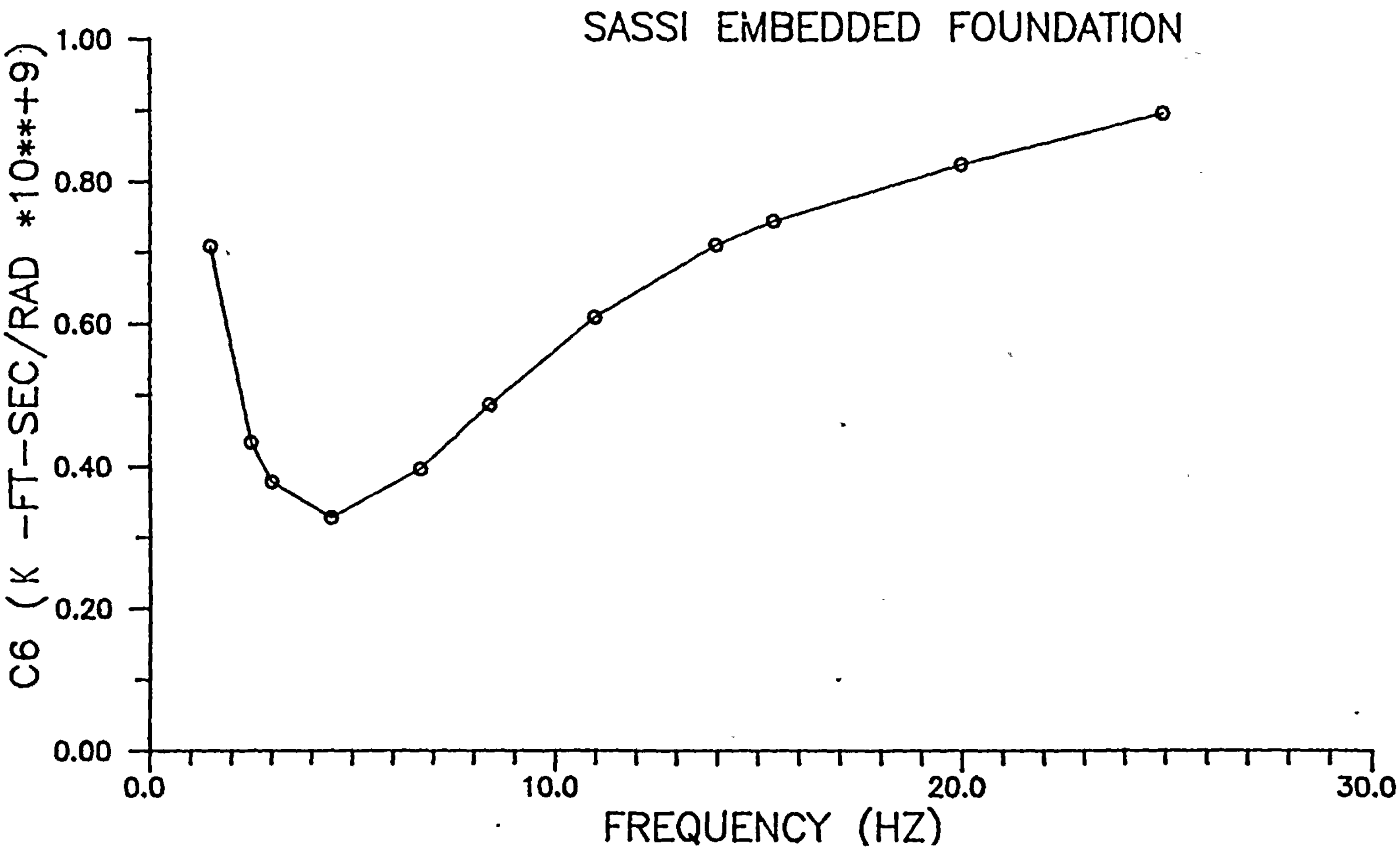

Torsional Damping Impedance About Z Axis

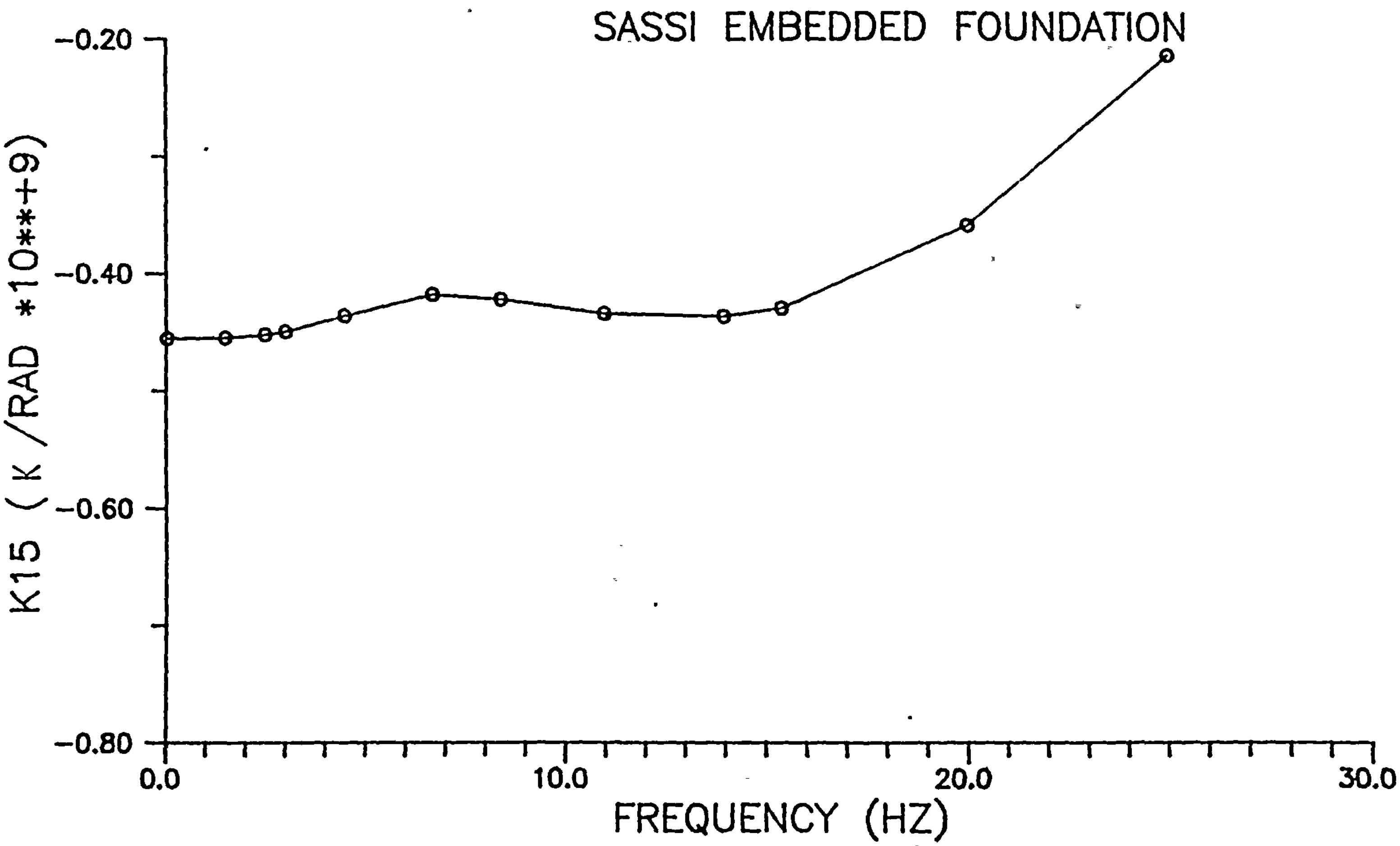

Coupling Stiffness Impdance Between Translation in X Direction and
Rocking About Y Axis

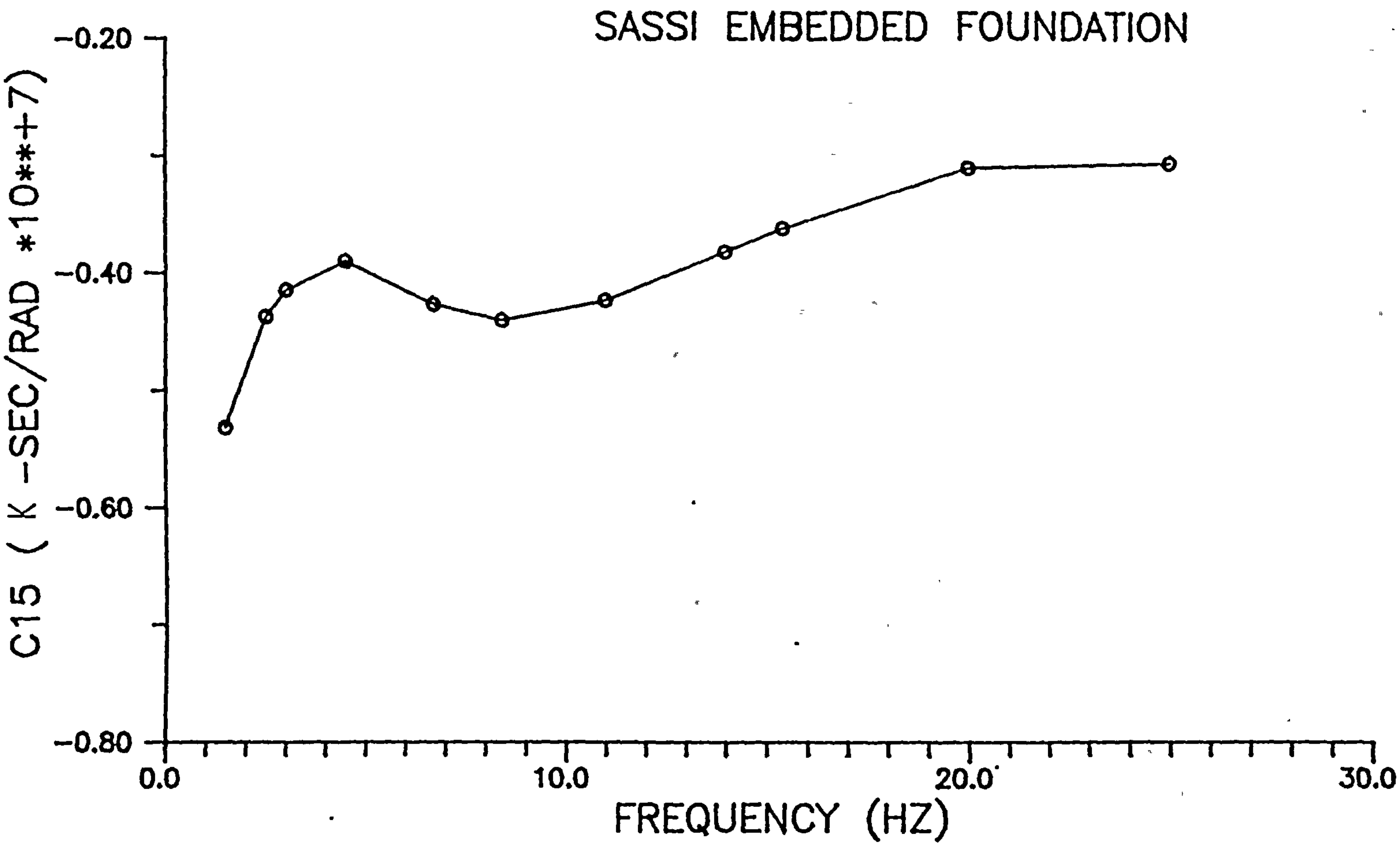

Coupling Damping Impedance Between Translation in X Direction and Rocking About Y Axis

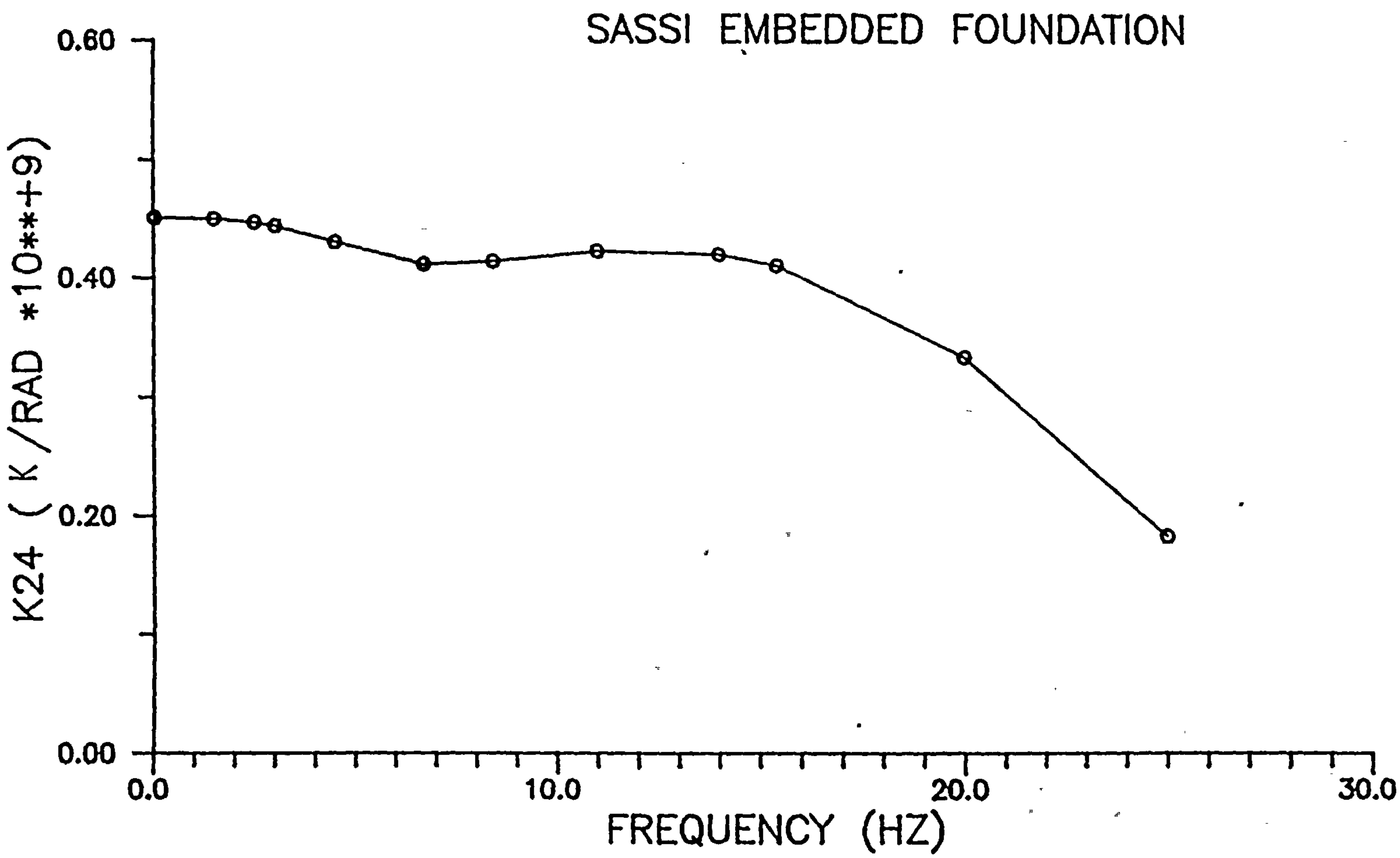

Coupling Stiffness Impedance Between Translation in Y Direction and Rocking About X Axis

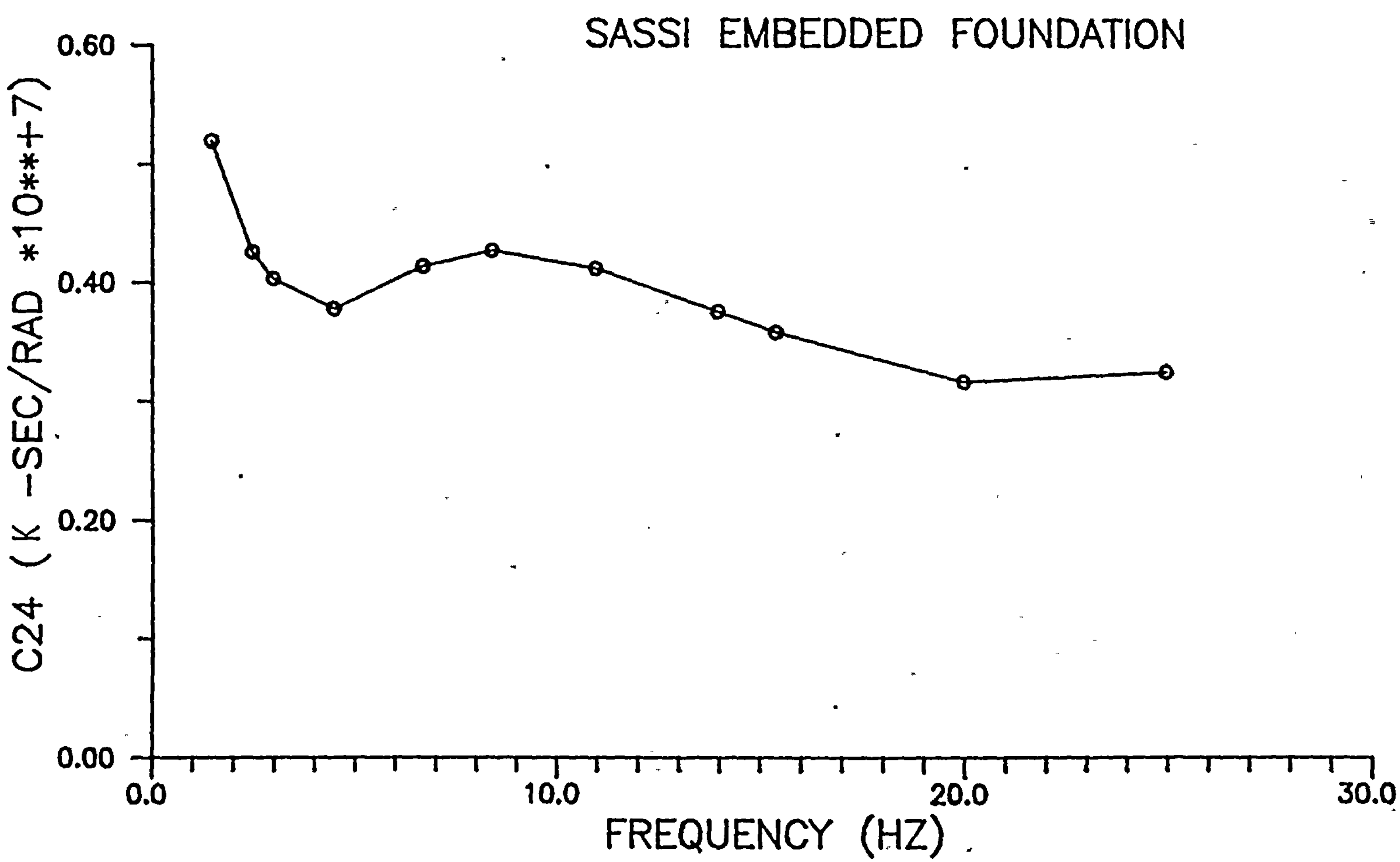

Coupling Damping Impedance Between Translation in Y Direction and Rocking About X Axis

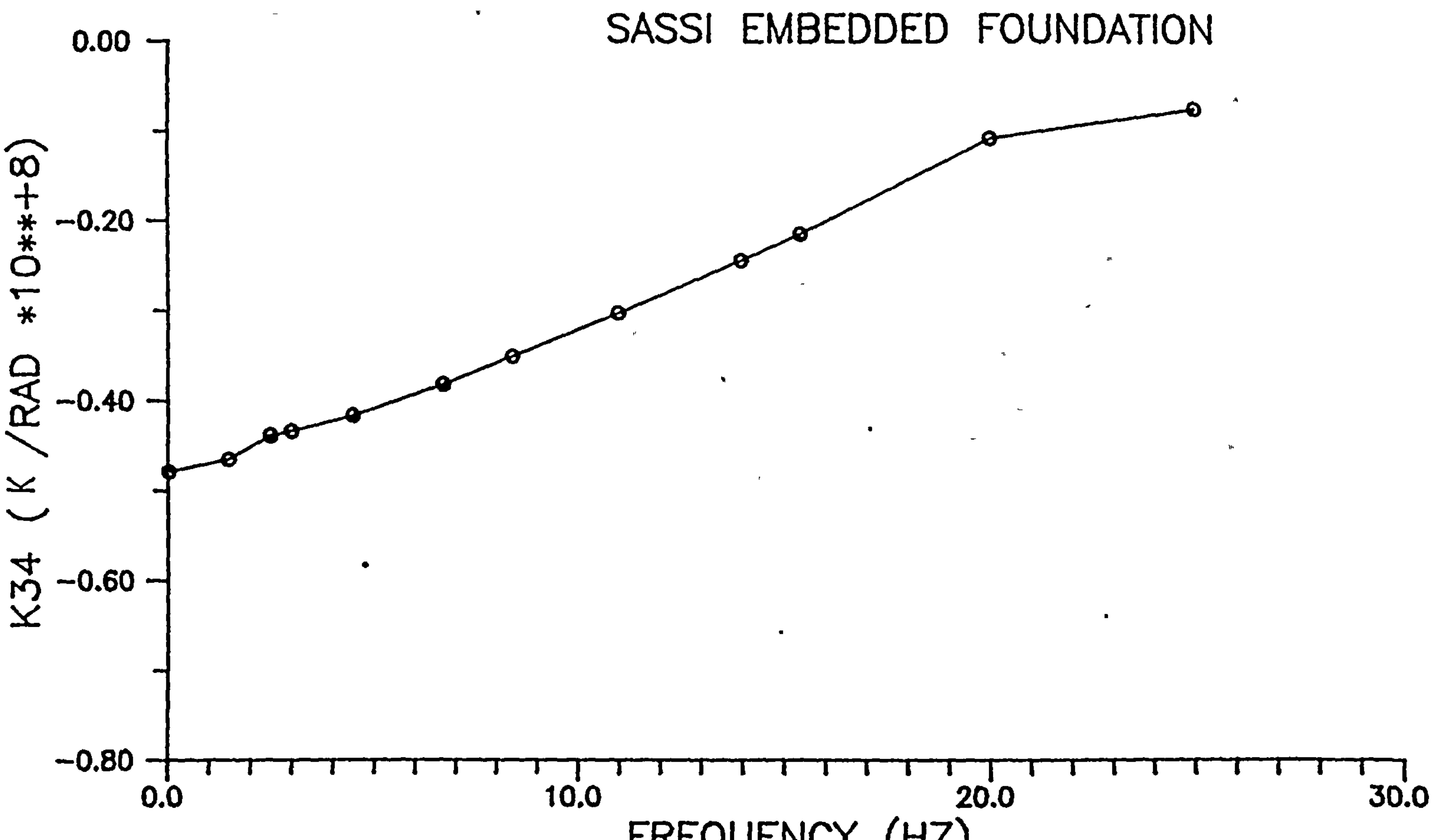

Coupling Stiffness Impedance Between Translation in Z Direction and Rocking About X Axis

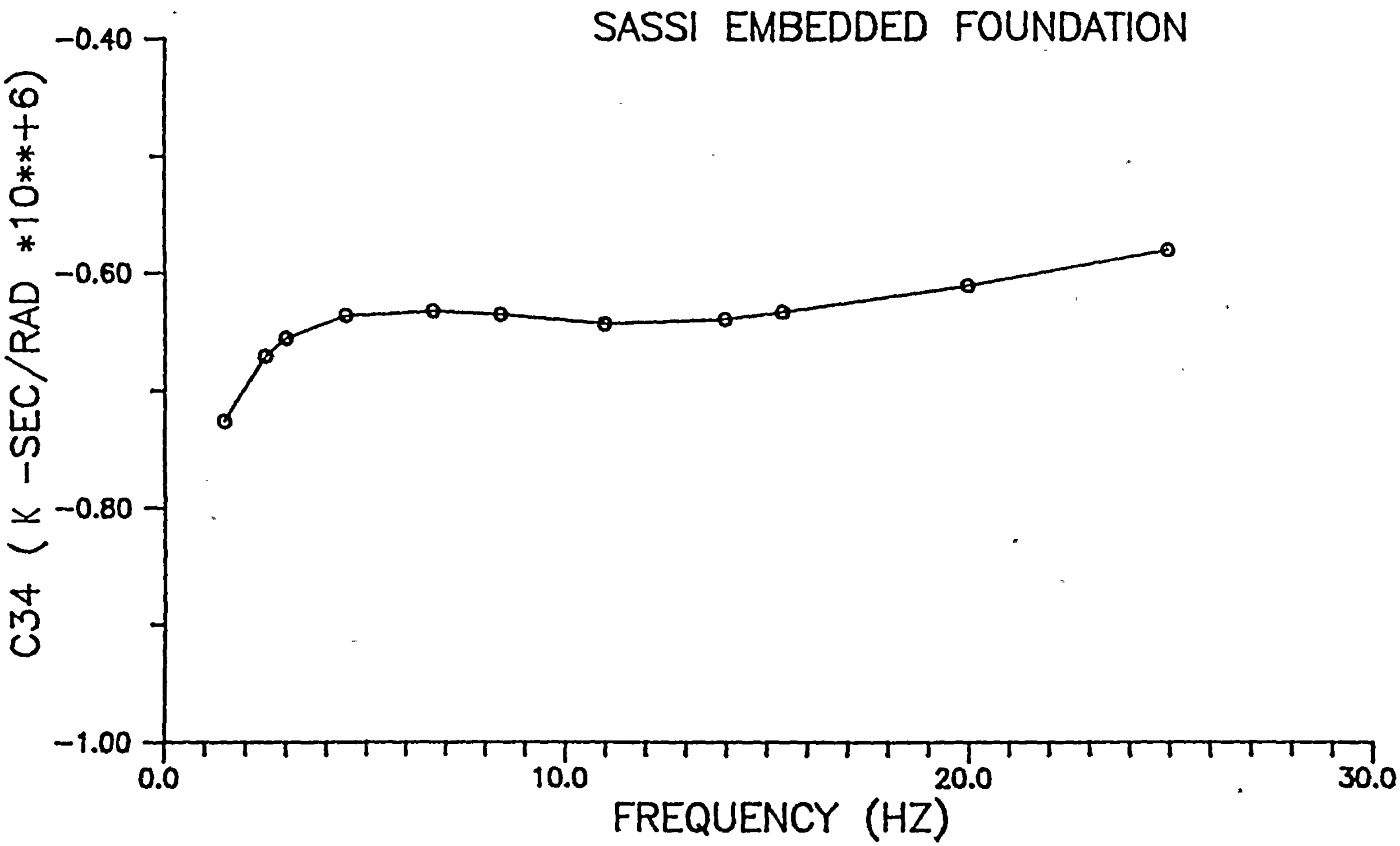

Coupling Damping Impedance Between Translation in Z Direction and
Rocking About X Axis

Data Package B Item #4

LISTING OF THE HOSGRI TIME HISTORY USED
IN LTSP-SSI PARAMETRIC STUDIES
FOR THE CONTAINMENT STRUCTURE

.006284	.065468	.044507	-.017043	-.038916	-.015208	.055784	.140970	1
.164340	.087535	-.003680	-.055911	-.042699	.008817	.044194	.047979	2
.032876	.012915	-.030960	-.044813	-.034736	-.039956	-.080438	-.075985	3
[illegible]18887	.108270	.120110	.028271	-.083847	-.131590	-.061270	.015202	4
[illegible]06949	-.079754	-.121400	-.095582	-.018897	.050443	.032647	-.035487	5
-.074452	-.001676	.098288	.114420	.000019	-.131640	-.134970	-.011903	6
.125740	.135090	.034980	-.034410	.043790	.193120	.254920	.168210	7
.022840	-.036574	.021546	.083242	.039641	-.056096	-.097125	-.048589	8
.014351	.028920	-.013255	-.093788	-.138760	-.114050	-.026203	.057881	9
.120070	.122400	.097742	.106590	.121150	.115590	.123480	.169970	10
.196790	.172110	.139160	.131010	.077853	-.044894	-.153370	-.203610	11
-.221480	-.202400	-.239700	-.376950	-.468050	-.388460	-.236960	-.166960	12
-.198500	-.219650	-.221730	-.198300	-.137470	-.064233	-.062053	-.094556	13
-.023223	.030029	.083595	.103830	.083829	.000777	-.054795	-.054178	14
.003698	.045529	.042238	.049156	.053891	.108150	.161530	.271160	15
.328350	.310630	.208520	.097143	.113870	.177040	.221680	.197290	16
.145830	.074515	.059777	.033645	-.088185	-.215730	-.223820	-.223560	17
-.185850	-.094959	-.089457	-.190180	-.240510	-.165260	-.044492	.006209	18
-.054362	-.157420	-.190820	-.109840	.001936	.007599	-.068870	-.099862	19
-.019554	.073841	.053746	-.090578	-.208540	-.142970	.048531	.257510	20
.343690	.282910	.175490	.154840	.142110	.139970	.212560	.296220	21
.355890	.407570	.436350	.365850	.252800	.129590	.022814	.011126	22
.060406	.078030	.023010	-.047808	-.124740	-.203590	-.229640	-.109450	23
-.019043	-.031720	-.104630	-.138050	-.152520	-.130150	-.086704	-.175980	24
-.219140	-.152860	-.068778	-.135840	-.285090	-.407960	-.449470	-.344730	25
-.173160	-.068688	.000420	.020110	-.002738	.011727	.113670	.274020	26
.311760	.264050	.163900	.093172	.040948	.029999	.031984	.009567	27
.024335	.048869	.004833	-.021717	-.035714	-.072848	-.027264	.024343	28
[illegible]079707	.157810	.191910	.076398	-.036390	-.027637	.027799	.104430	29
[illegible]7960	.089132	.054400	.107970	.168930	.199720	.147330	.013820	30
[illegible]68408	-.014509	.057192	-.022444	-.186530	-.376270	-.375760	-.240460	31
-.108390	-.097726	-.194900	-.288910	-.204850	-.045725	-.009376	-.060134	32
-.173900	-.215250	-.198610	-.164430	-.211450	-.265120	-.257430	-.162420	33
-.035743	.007575	-.019607	-.027590	-.040541	-.025512	.072994	.151130	34
.161080	.133030	.069604	.019311	.010487	-.009631	-.013721	.151170	35
.224780	.236850	.222200	.216760	.154250	.055458	-.021702	-.092900	36
-.069628	-.040598	-.042502	-.103230	-.156380	-.040235	.140670	.201490	37
.174850	.141320	.111120	.144970	.206880	.227220	.246410	.217290	38
.197520	.216550	.228780	.182410	.128600	.043497	-.017560	-.004542	39
.051886	.093208	.087280	-.003056	-.060509	-.074282	-.148420	-.173200	40
-.133190	-.187380	-.342630	-.387090	-.368740	-.287350	-.164070	-.148000	41
-.158430	-.131130	-.072803	-.052446	-.032414	-.103830	-.124270	.012108	42
.121900	.113580	.016243	-.128780	-.290650	-.236130	-.062073	-.039206	43
-.117940	-.179860	-.153370	-.039232	.098250	.108120	.023303	-.015565	44
.015826	.107150	.125610	-.017820	-.172210	-.131320	.048557	.212970	45
.263910	.176740	.019916	-.054846	-.118730	-.134490	-.091746	-.066846	46
-.043759	.005690	-.006517	-.089964	-.161070	-.245890	-.276250	-.153640	47
-.024578	.063780	.085700	.077072	.033073	.008217	.019646	.117590	48
.224450	.204320	.128770	.109790	.075529	.079768	.117400	.035003	49
-.100590	-.055067	-.026621	-.202220	-.362590	-.490810	-.561100	-.418830	50
-.248800	-.139270	-.127160	-.179080	-.262120	-.229270	-.128820	-.066582	51
-.018784	-.057969	-.169030	-.229980	-.128820	-.048136	.008132	.152910	52
.250850	.268380	.258320	.276150	.202340	.180180	.145900	.164280	53
.241390	.329020	.327610	.218740	.086503	.019283	.095227	.173920	54
[illegible]34660	.047394	.014728	-.075970	-.086279	-.005844	.008408	-.071425	55
[illegible]6732	.080847	.171880	.171060	.082996	-.050517	-.049637	.123400	56
.290430	.321660	.251700	.210220	.300080	.470670	.553520	.499600	57
.385340	.310430	.290630	.284170	.181210	.073115	.043360	.083550	58
.120470	.158200	.141250	.034421	-.006536	.002494	.072481	.190670	59
.262420	.214810	.061227	-.049365	-.001733	-.011492	-.043487	.136900	60

.247560	.218760	.227500	.289760	.184320	.094408	.071025	.061623	61
.118100	.123430	.002822	-.167870	-.303280	-.239800	-.085475	.016668	62
-.027707	-.037745	-.024863	.002393	.063143	.092038	.046420	.086876	63
[illegible]7990	.158750	.242820	.192610	.119930	.050997	-.000975	-.032859	64
[illegible]2240	-.024988	-.109380	-.219880	-.325610	-.349440	-.303500	-.247410	65
-.214780	-.251370	-.402240	-.480660	-.394780	-.315110	-.267040	-.212390	66
-.198850	-.137830	-.017544	.020257	-.028881	-.058650	-.026123	.081634	67
.206540	.208600	.110610	.004972	-.128960	-.115020	-.017795	-.065358	68
-.192600	-.284870	-.287520	-.202720	-.113990	-.111200	-.177350	-.221460	69
-.167780	-.094356	-.162440	-.328890	-.424410	-.388010	-.198220	.095300	70
.134130	.096166	.163620	.187900	.056586	.095915	.145910	-.135660	71
-.229590	-.161320	-.152200	-.190810	-.143550	-.219440	-.334690	-.145850	72
.171980	.265180	.214340	.067890	-.057527	-.223160	-.267520	-.101550	73
-.317190	-.365460	-.418180	-.237630	-.099354	.087406	.192510	.147720	74
.169030	.308260	.434410	.387630	.190290	.056700	.009850	.027605	75
.246140	.391030	.391620	.299960	.312040	.333890	.412110	.532240	76
.411650	.263070	.079809	-.027159	-.075966	-.098823	-.135940	-.116880	77
-.087995	-.015214	.087533	.107000	.159690	.142080	.094750	-.068693	78
-.006479	-.004301	-.163990	-.273580	-.293500	-.313930	-.169440	.003428	79
-.091840	-.104400	.056767	.106750	.006664	-.025147	-.226800	-.357340	80
-.385410	-.310250	-.256130	-.255820	-.294940	-.349690	-.298260	-.129380	81
.058957	.122000	.067177	-.003367	.037010	.132310	.126860	-.067208	82
-.093404	-.097270	.011997	.063480	.145390	.042870	-.104460	-.079879	83
.067365	.041495	.014748	.041711	-.002023	-.054108	.028743	.150110	84
.154940	.159820	.202950	.181120	.150360	.167790	.205880	.324660	85
.526270	.601680	.629280	.750000	.718060	.588540	.512030	.421440	86
.366440	.341770	.257420	.045289	-.131520	-.170280	-.172690	-.328570	87
-.431660	-.476070	-.509910	-.548070	-.557740	-.569200	-.631090	-.561490	88
-[illegible]76630	-.447750	-.390510	-.325960	-.318940	-.285480	-.221870	-.168450	89
[illegible]2134	.093516	.117140	.246990	.386190	.372480	.283140	.291090	90
[illegible]57250	.164560	.041347	-.022761	-.084675	-.037328	.099618	.147300	91
.116530	.132070	.187200	.083678	-.013571	-.069157	-.080402	-.022376	92
.145900	.216410	.227810	.215690	.223500	.249650	.259060	.244160	93
.203350	.063452	-.015616	.072287	.121100	.115910	.159840	.161220	94
.064106	.066647	-.014247	-.184210	-.247550	-.171900	.030494	.247870	95
.386610	.317960	.185540	.055711	.080449	.038762	-.011737	.097000	96
.239560	.162240	.032544	-.056162	-.300120	-.510950	-.587990	-.616570	97
-.611950	-.575770	-.579530	-.559660	-.534670	-.473310	-.304390	-.133300	98
-.055947	-.031960	-.080357	-.133900	.064236	.113340	.149300	.211430	99
.159980	.146800	.281150	-.122670	-.532150	-.527120	-.403810	-.311400	100
.099831	.309190	.193190	.401130	.493990	.424610	.512220	.603120	101
.162220	-.069485	-.299030	-.548270	-.590400	-.455130	-.319340	-.204780	102
-.082720	-.016376	-.047858	-.135690	-.115410	.020089	.032460	.016554	103
.273060	.335590	.421100	.396540	.222260	.101040	.147840	.066243	104
.120840	.096249	-.091869	-.159380	.008615	.025900	.088465	.127190	105
.024213	-.004403	.051816	.071436	.174730	.182900	.133570	.342740	106
.494400	.383890	.314010	.341380	.057229	.068685	.102830	.090262	107
.078993	.186770	.236840	.238330	.434830	.462940	.529770	.553280	108
.454080	.346020	.253040	.099690	.018095	-.022150	-.025698	-.019801	109
-.081453	-.180610	-.284060	-.345450	-.478280	-.624180	-.720880	-.745650	110
-.750000	-.749700	-.749160	-.750000	-.750000	-.718290	-.634640	-.494310	111
-.276430	-.168650	-.067666	.066428	.157630	.200940	.227700	.190650	112
.162770	.199020	.177450	.055001	.134550	.072989	-.011417	.038959	113
.178040	-.003812	-.263410	-.417390	-.144780	-.065476	.067089	.199270	114
[illegible]7600	.053542	.163250	.261920	.154550	.041864	-.059012	-.202940	115
[illegible]3450	-.295330	-.441970	-.581480	-.540120	-.485510	-.352720	-.183940	116
-.082147	-.011268	.078665	.190770	.343570	.392410	.387140	.389610	117
.348990	.316990	.283890	.232630	.143250	.128430	.193130	.227190	118
.206730	.168170	.147680	.140090	.196070	.191690	.111020	.041485	119
.031316	.047435	.083723	.065264	.042351	.038199	.048408	.031764	120

.110880	.030041	-.035974	-.063139	-.044625	-.054553	-.047938	-.043281	121
-.091242	-.047616	.036164	.061722	.082182	.101270	.132260	.199760	122
.245820	.217970	.142440	.073084	.066290	.041803	-.005472	-.068436	123
-.[illegible]5840	-.068925	.026823	.066360	.047702	-.023272	-.068497	-.100980	124
-.[illegible]5266	-.072127	-.098388	-.097119	-.065192	-.058481	-.070371	-.160920	125
-.275540	-.334590	-.364990	-.392400	-.402960	-.437410	-.456720	-.436420	126
-.410320	-.382530	-.366950	-.372430	-.324000	-.232640	-.122870	.075217	127
.223940	.324430	.472180	.576890	.626220	.672390	.680960	.602380	128
.639290	.624990	.560460	.479630	.353270	.173570	.080997	.013928	129
-.102280	-.202660	-.281850	-.405910	-.364180	-.367150	-.459390	-.480590	130
-.375800	-.295470	-.161070	-.063432	-.078507	-.139510	-.161540	-.129680	131
-.103780	-.101540	-.064679	-.034810	-.006025	.027021	.050373	-.015559	132
-.012474	-.006141	-.014668	.029908	.055463	.041842	.085527	.116410	133
.117880	.180460	.195210	.097262	.168700	.119350	-.033472	-.010279	134
.179370	.168910	.349300	.179150	.034643	-.007887	-.018011	-.051735	135
.027298	.057737	.043897	.042555	.091843	-.001587	-.078953	-.073728	136
-.060138	-.105600	-.132610	-.113910	-.118120	-.176910	-.227090	-.254190	137
-.366810	-.359010	-.299770	-.348920	-.428550	-.400390	-.353160	-.325840	138
-.215960	-.192820	-.188240	-.006680	.198450	.219930	.133690	.094608	139
-.063788	-.030202	.069602	.165690	.163800	.173720	.206630	.243910	140
.329030	.368160	.358090	.317950	.404650	.436290	.497410	.416760	141
.386730	.392740	.433050	.448890	.365020	.235650	.122340	-.001377	142
-.131640	-.205740	-.246610	-.371880	-.459430	-.515470	-.604350	-.640130	143
-.633220	-.639050	-.597390	-.477260	-.350390	-.236580	-.156780	-.080896	144
.046090	.173520	.273480	.343600	.363260	.409250	.499570	.434750	145
.466310	.449240	.381050	.250480	.335930	.164200	-.175260	-.296760	146
-.382910	-.451540	-.355190	-.195660	-.175290	-.090046	.048146	.141940	147
.299130	.327420	.279250	.329520	.304890	.181540	.076483	-.018236	148
-.[illegible]59630	-.211430	-.199430	-.183440	-.216140	-.264730	-.245250	-.272200	149
[illegible]7940	-.172870	.017536	.093970	.055786	.098724	.085514	.034149	150
-.[illegible]23654	-.005037	.043642	.082211	.210040	.242190	.228440	.231430	151
.280800	.244860	.139390	.037203	-.170660	-.212650	-.268680	-.236640	152
-.256590	-.247470	-.194700	.027835	.058942	.029570	.038558	-.017959	153
-.074741	.000362	.103060	-.168280	-.236720	-.200970	-.087912	-.022796	154
-.038167	-.078086	-.137490	-.151270	-.107510	-.024978	-.069107	-.155250	155
.152330	.249350	.304920	.450500	.401660	.206420	.095091	.141190	156
-.114190	-.114710	-.160660	-.129070	-.072253	.029788	.049919	.031052	157
.047016	-.014144	.012632	.143250	.070399	.035985	.027883	-.122840	158
-.041126	.022025	-.092013	-.042237	.032405	.129190	.257030	.418630	159
.445710	.354180	.314230	.302790	.216230	.105460	-.012257	-.088164	160
-.063153	-.023199	.003401	-.004570	-.020981	.061555	.188050	.231930	161
.207170	.174140	.146030	.162580	.126990	-.022588	-.246700	-.387210	162
-.482840	-.492740	-.451920	-.405660	-.320770	-.193150	-.094796	-.074796	163
.208550	.294410	.407950	.395550	.364260	.252980	.173700	.163530	164
.122940	.063837	.011149	-.049397	-.095313	-.143870	-.222310	-.251290	165
-.353120	-.418600	-.470040	-.303970	-.338920	-.362240	-.244860	-.167910	166
-.253120	-.156730	-.086957	-.226260	-.168430	-.067272	-.063303	-.011944	167
.042804	.058429	.081712	.094005	.036116	-.021832	-.060182	-.239150	168
-.317950	-.298740	-.290310	-.261700	-.158920	-.077281	-.031182	.089948	169
.204610	.276690	.363120	.520680	.468240	.422290	.404170	.244050	170
.103490	.099706	.104030	.039587	.066943	.096184	.033163	-.012090	171
-.016326	-.030332	-.046453	.079035	.150120	.179280	.102360	.073425	172
.148940	.154970	.203000	.284270	.311320	.316970	.360930	.330660	173
.247610	.238980	.176950	.086723	-.007084	-.155410	-.265640	-.311660	174
[illegible]54320	-.508890	-.503070	-.506670	-.457140	-.347520	-.348760	-.335010	175
[illegible]0640	-.108230	-.095028	.186880	.118460	.083541	.147370	-.030218	176
-.156180	-.181480	-.226160	-.264120	-.250700	-.261590	-.263370	-.268180	177
-.324940	-.292840	-.197860	-.193440	-.140200	-.046136	.000244	.061649	178
.160770	.201060	.220360	.233040	.380190	.428780	.488330	.428930	179
.425760	.380920	.286790	.270530	.252310	.143770	.032677	-.002504	180

-.083159	-.154710	-.090875	-.262180	-.380680	-.341000	-.237850	-.161050	181
-.097290	-.055559	-.093211	-.033412	.061754	.103250	.106870	.119700	182
.040342	.031000	.062199	.080865	.086012	.104590	.102210	.081273	183
[illegible]0040	.223480	.221900	.133170	.102840	.078666	.065800	.072653	184
[illegible]9593	.005630	-.001330	.045996	.080837	.085112	.101590	.136780	185
.126960	.124490	.125360	.083619	.125720	.151730	.164370	.135430	186
.143700	.107590	.064825	.061539	-.016167	-.044371	-.047527	-.036793	187
-.041373	-.022168	-.026131	-.074219	-.030956	-.055589	-.090460	-.151910	188
-.195150	-.237930	-.244010	-.218340	-.201340	-.182920	-.162900	-.194050	189
-.238990	-.248630	-.264210	-.234010	-.206750	-.177390	-.148550	-.106460	190
-.058493	-.025584	.012735	.052920	.056847	.090861	.152890	.181290	191
.199170	.240220	.269170	.252690	.265720	.259210	.207700	.154090	192
.134570	.087653	.044281	.034967	.004466	-.025005	-.032168	-.046024	193
-.080745	-.093108	-.105390	-.123110	-.121370	-.107700	-.097954	-.080061	194
-.070732	-.076540	-.071081	-.067129	-.090902	-.095263	-.090347	-.130130	195
-.118540	-.088229	-.069395	-.057906	-.032945	-.030205	-.033226	-.028030	196
-.058839	-.050542	.003601	.041668	.035252	.051607	.038910	.025671	197
.039254	.037568	.005848	-.019674	-.023562	-.021664	-.022110	-.021961	198
-.020665	-.027612	-.045725	-.047851	-.046240	-.062997	-.090033	-.109910	199
-.106350	-.096554	-.093293	-.050025	-.006223	-.025463	-.064651	-.061843	200
-.069529	-.063826	-.014959	.040960	.061640	.101130	.150330	.173200	201
.206530	.224560	.239910	.230370	.213120	.201630	.202090	.188540	202
.168240	.157230	.131660	.097618	.105020	.070639	.018423	.021207	203
.002522	-.040780	-.075725	-.090829	-.141070	-.142440	-.131360	-.099171	204
-.082083	-.043795	-.010213	.004753	.043400	.050742	.033596	.054827	205
.049257	.006050	-.041040	-.063155	-.101910	-.111200	-.085858	-.083718	206
-.086002	-.057907	-.022222	-.006283	.014049	.037340	.051902	.063194	207
.078517	.087555	.077945	.086456	.084482	.060480	.034175	.022492	208
.010796	-.007762	-.020493	-.038660	-.055675	-.064514	-.068449	-.069244	209
[illegible]3054	-.054141	-.030576	-.006554	.011437	.051230	.099074	.122040	210
[illegible]4980	.157720	.146460	.115610	.090103	.051679	.012711	-.017511	211
-.059469	-.082350	-.098316	-.119480	-.127190	-.123200	-.123230	-.107200	212
-.089216	-.075528	-.060509	-.039381	-.020480	-.007054	.005894	.025289	213
.038437	.055390	.070357	.071019	.054375	.036821	.013057	-.018483	214
-.048406	-.076306	-.102430	-.118940	-.147900	-.156370	-.157310	-.141220	215
-.121980	-.099039	-.086866	-.085639	-.063491	-.048510	-.034862	-.023194	216
-.019752	-.023397	-.026478	-.033858	-.045054	-.056838	-.067211	-.075648	217
-.081754	-.086313	-.086958	-.100750	-.101870	-.086514	-.063317	-.038885	218
-.007849	.019079	.041501	.068114	.090526	.106670	.121220	.129450	219
.139770	.141420	.138910	.125820	.116280	.104160	.091941	.082723	220
.069194	.052985	.032287	.009200	-.012602	-.035296	-.058157	-.066837	221
-.081260	-.091163	-.088934	-.089835	-.104570	-.108990	-.115520	-.123060	222
-.119370	-.119830	-.125180	-.114000	-.111610	-.093221	-.065535	-.034344	223
-.009597	.025574	.054399	.075202	.103680	.129480	.144640	.176430	224
.190580	.184580	.171910	.151010	.119340	.093457	.070521	.049650	225
.033646	.021829	.017415	-.001404	-.020388	-.024262	-.023691	-.030141	226
-.029479	-.022892	-.022431	-.006268	.011073	.019040	.026848	.034014	227
.032219	.030676	.027996	.021677	.021135	.019341	.012259	.006900	228
.000665	-.010766	-.021885	-.034301	-.042706	-.038091	-.024071	-.004220	229
.016992	.035987	.051502	.058945	.059924	.052232	.037888	.018991	230
-.001760	-.021427	-.041142	-.059305	-.070522	-.081923	-.088063	-.099843	231
-.106070	-.109230	-.110260	-.100630	-.078824	-.057431	-.033484	-.004835	232
.016359	.034028	.050386	.056957	.059635	.061331	.058755	.052975	233
.046544	.034531	.022522	.011597	-.003499	-.015949	-.025083	-.032330	234
-.[illegible]1645	-.024270	-.013081	.005001	.024811	.043079	.060359	.073708	235
[illegible]471	.082615	.083961	.084916	.076301	.073431	.073795	.062580	236
.027932	-.001097	-.035777	-.078549	-.107470	-.120600	-.132230	-.137330	237
-.122660	-.110170	-.095996	-.080553	-.064327	-.049283	-.036709	-.023833	238
-.008251	.008830	.021767	.035836	.047099	.051431	.050431	.048006	239
.040549	.029596	.018070	.011804	.009384	.008000	.009991	.008616	240

.001463	-.006361	-.013857	-.022137	-.023703	-.019043	-.011616	.000875	241
.010228	.020373	.034699	.042199	.036725	.035348	.031222	.024755	242
.024295	.023317	.017478	.016315	.017427	.015522	.015257	.014492	243
[illegible]3371	.017833	.024453	.020639	.019154	.017982	.012641	.002263	244
[illegible]3943	-.033008	-.052705	-.067845	-.075807	-.077889	-.078082	-.072654	245
-.059476	-.048062	-.034162	-.017541	-.003450	.007721	.018068	.029122	246
.044385	.057713	.068357	.076755	.080829	.081293	.081615	.077521	247
.068765	.060507	.052013	.042866	.035249	.026513	.017005	.007738	248
-.000608	-.008845	-.013422	-.015808	-.011719	-.002228	.009358	.022095	249
.035674	.041428	.041548	.041933	.036647	.024188	.017859	.010181	250
-.024147	-.026934	-.020986	-.018851	-.008621	.005276	.012958	.021291	251
.032818	.041177	.048529	.057612	.057514	.053897	.047916	.029460	252
.005755	-.017725	-.047496	-.068055	-.080116	-.099927	-.116350	-.126560	253
-.141210	-.153980	-.158560	-.169270	-.178470	-.175410	-.170700	-.161380	254
-.137660	-.113470	-.092492	-.067972	-.047151	-.033290	-.021814	-.008769	255
-.002103	.006562	.022319	.042642	.061404	.076433	.091099	.098637	256
.104770	.114110	.123410	.135660	.152970	.171780	.191230	.208570	257
.219180	.223720	.221890	.210790	.190330	.163440	.129620	.089408	258
.046957	.005523	-.034268	-.073467	-.105140	-.129820	-.149690	-.160470	259
-.162690	-.160620	-.154420	-.144600	-.137460	-.133360	-.130880	-.130290	260
-.124310	-.116090	-.110620	-.098380	-.080170	-.063399	-.045383	-.028945	261
-.021748	-.019644	-.020356	-.018292	-.014614	-.017024	-.018703	-.011764	262
-.005297	.005230	.027535	.047864	.061962	.081652	.101720	.110960	263
.117940	.120340	.110940	.096398	.079866	.057053	.031944	.010937	264
-.010846	-.024557	-.027245	-.020693	-.006250	.011209	.031150	.048738	265
.065777	.079178	.086269	.088067	.084866	.079829	.073792	.064640	266
.051696	.039589	.028079	.011293	-.004538	-.019793	-.038240	-.055406	267
-.067487	-.077939	-.087100	-.089694	-.088074	-.082811	-.071072	-.051688	268
-.025104	.008034	.046578	.087786	.118690	.142000	.157540	.157360	269
[illegible]5070	.124110	.093574	.057423	.025327	-.005244	-.034549	-.055954	270
[illegible]74392	-.093947	-.109070	-.124070	-.136680	-.141450	-.142020	-.136810	271
-.125660	-.111710	-.094495	-.080216	-.069572	-.056636	-.044915	-.035154	272
-.020954	-.007480	.001371	.012185	.020557	.022507	.023748	.023453	273
.021285	.022766	.026844	.033732	.044983	.055408	.064997	.074344	274
.077656	.080007	.081025	.074816	.071595	.071531	.066663	.064459	275
.064200	.053646	.038394	.024222	.001769	-.018536	-.030533	-.040320	276
-.043568	-.039963	-.033644	-.024053	-.013799	-.006194	.002436	.008060	277
.009397	.012811	.013655	.009677	.012601	.011960	.005312	.001610	278
-.005363	-.013615	-.015653	-.014103	-.014580	-.008127	.001634	.009876	279
.021427	.029652	.032543	.033448	.029776	.023960	.019667	.015871	280
.015640	.018408	.020374	.025527	.029504	.026517	.020957	.011337	281
-.003953	-.018757	-.033089	-.049383	-.063709	-.075930	-.087037	-.096184	282
-.103630	-.109670	-.113300	-.114580	-.109850	-.101930	-.095784	-.085997	283
-.073228	-.064452	-.056222	-.047591	-.042501	-.035268	-.021980	-.001478	284
.023917	.051682	.082534	.111820	.128820	.140430	.149220	.143690	285
.134450	.129470	.119380	.107260	.099041	.085431	.066772	.048948	286
.027571	.005982	-.011910	-.028594	-.038812	-.043027	-.048475	-.044204	287
-.037094	-.039282	-.038421	-.035338	-.036963	-.030594	-.014324	-.000754	288
.016454	.038475	.052639	.062963	.067716	.061374	.051408	.038383	289
.023909	.013695	.005144	-.002032	-.006519	-.013065	-.019451	-.021402	290
-.023133	-.022501	-.016647	-.011624	-.005075	.004122	.008388	.008919	291
.007218	-.001317	-.012688	-.024563	-.037916	-.046857	-.050570	-.051343	292
-.047010	-.042882	-.043195	-.043277	-.045357	-.050217	-.051571	-.051925	293
-.053190	-.048747	-.041514	-.036512	-.026857	-.018066	-.011932	-.006466	294
[illegible]2821	-.000359	.000421	.003142	.010358	.018121	.023778	.031000	295
[illegible]3984	.031755	.032036	.029899	.022728	.021261	.023504	.027142	296
.040674	.057475	.071730	.089207	.098645	.100910	.105630	.105060	297
.101410	.099712	.090345	.077464	.072575	.065325	.055030	.046163	298
.035391	.020899	.014291	.003050	-.012170	-.017520	-.039683	-.070537	299
-.030419	-.035408	-.056811	-.059381	-.059646	-.075352	-.069124	-.000097	300

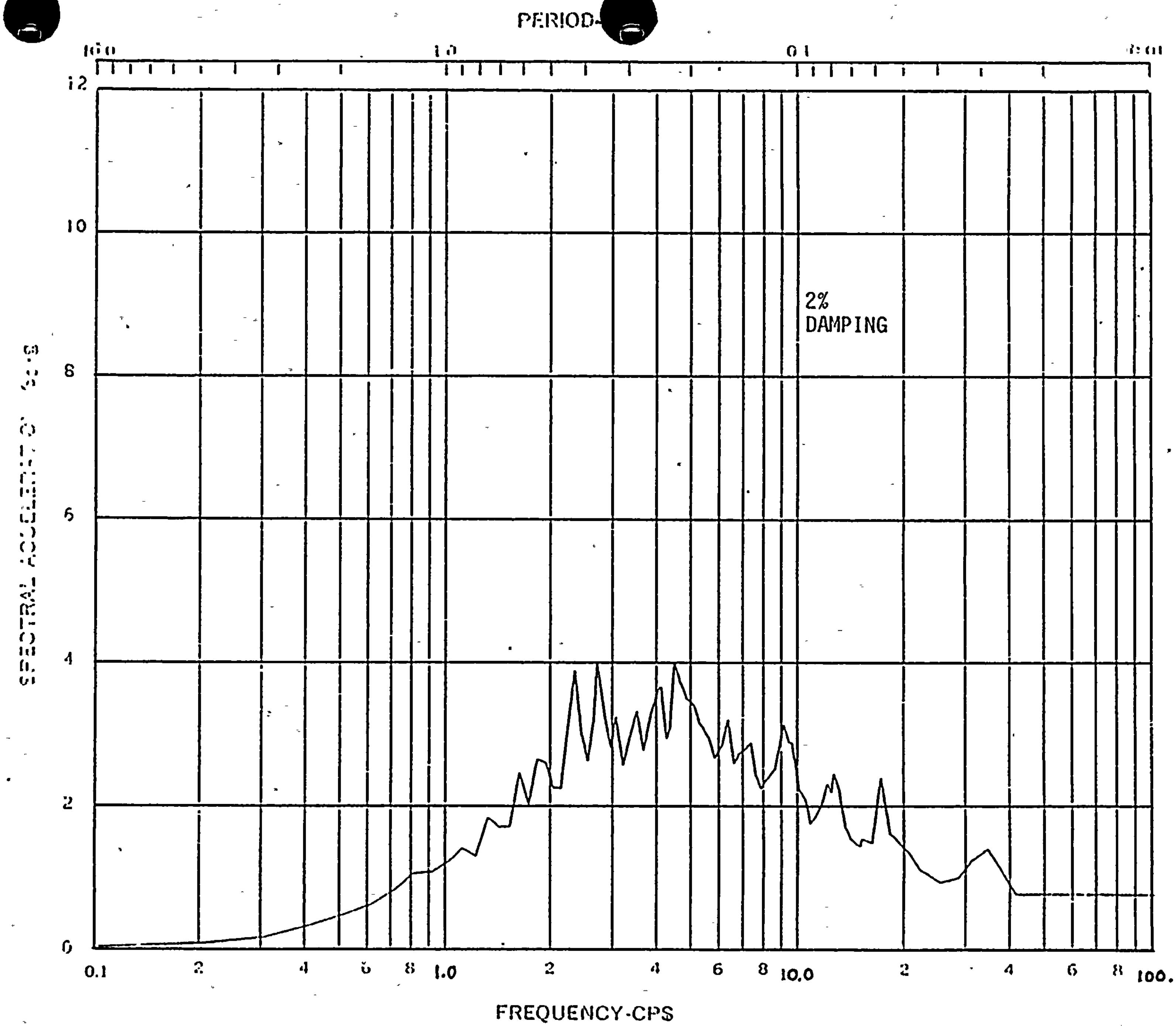

2% Damping Response Spectrum of the Hosgri Time History

NO. OF SPECTRA= 1
NO. OF FREQ.= 89 (READ FROM CARDS)
NO. OF DAMPINGS= 1

DAMPING . . .
.02000

FREQUENCIES . . .

.10000	.20000	.30000	.40000	.50000	.60000	.70000
.80000	.90000	1.00000	1.10000	1.20000	1.30000	1.40000
1.50000	1.60000	1.70000	1.80000	1.90000	2.00000	2.10000
2.20000	2.30000	2.40000	2.50000	2.60000	2.66000	2.70000
2.80000	2.90000	3.00000	3.15000	3.30000	3.45000	3.60000
3.80000	4.00000	4.04000	4.17000	4.20000	4.29000	4.33000
4.40000	4.42000	4.60000	4.80000	5.00000	5.21000	5.50000
5.75000	6.00000	6.25000	6.50000	6.75000	7.00000	7.25000
7.50000	7.75000	8.00000	8.50000	9.00000	9.33000	9.50000
10.00000	10.35000	10.50000	10.70000	11.00000	11.50000	12.00000
12.30000	12.50000	12.95000	13.00000	13.08000	13.50000	14.00000
14.50000	14.82000	15.00000	16.00000	17.00000	18.00000	20.00000
[illegible]2.00000	25.00000	28.00000	31.00000	34.00000		

PEAK ACCELERATION= .75000

SPECTRUM-DAMPING= .020

.01485	.06155	.14866	.30914	.45287	.59403	.79556
1.03216	1.05061	1.19718	1.37986	1.28269	1.79706	1.67470
1.68725	2.41930	2.00829	2.61040	2.56872	2.22233	2.22158
3.09543	3.23703	2.97960	2.60364	3.15620	3.94240	3.72607
3.19139	2.78965	3.19686	2.54597	2.95008	3.28053	2.74953
3.28339	3.62279	3.63480	3.01581	2.92005	3.06530	3.37399
3.86886	3.93997	3.68022	3.45152	3.37758	3.11714	2.93708
2.64432	2.80210	3.16745	2.57119	2.70528	2.76729	2.84426
2.39991	2.22229	2.33462	2.48450	3.09912	2.85533	2.84980
2.18425	2.07822	1.97831	1.73780	1.80226	1.97056	2.27532
2.17488	2.41644	2.21096	2.15618	2.04602	1.67348	1.51557
1.45267	1.42840	1.51918	1.47327	2.35773	1.59316	1.37395
1.08408	.92156	.98011	1.24370	1.38241		

Data Package C Item #1

IDENTIFICATION OF WAVE TYPES, DIRECTIONS, AND VELOCITIES USING SMART-1 STRONG MOTION ARRAY DATA

C. H. Loh (I)
J. Penzien (II)
Presenting Author: C. H. Loh

SUMMARY

Presented in this paper is a method for identifying wave types, directions, and velocities contained in strong earthquake ground motions. After transforming the motions into components along their principal axes, use is made of a principal variance ratio R(f), defined as the ratio of the minor principal variance to the major principal variance for those components of motion within frequency band Δf centered on frequency f_0. At those frequencies where R(f) has very low values, single wave types dominate the motions. Using directions of principal axes and phase lag information, wave types, directions, and velocities are identified.

INTRODUCTION

At a meeting in Hawaii during May 1978, the need for strong earthquake ground motion arrays was discussed and plans were developed for promoting such arrays in many locations on a world-wide basis (Ref. 1). One site selected at the workshop as having high potential for frequently experiencing future strong motions was north-eastern Taiwan. Responding to the great need, a strong motion array was installed in this area in the town of Lotung in the fall of 1980 under the joint effort of the Academia Sinica in Taiwan and the University of California, Berkeley, with financial support provided by the National Science Council and the National Science Foundation (Ref. 2).

The strong-motion array in Lotung, called SMART-1, is a two-dimensional surface array consisting of a center station C00 and three concentric circles (inner I, middle M, and outer O) each having 12 stations with radii of 200 meters, 1 km, and 2 km, respectively, as shown in Fig. 1. This arrangement of 37 stations was selected to optimize the expected information to be obtained from both the engineering and seismological points of view. The instruments in this array record digitally with a common time base accurate to 1 millisecond over a duration which includes 2.5 seconds of pre-trigger memory. Fortunately, many earthquakes have triggered the array since the installation providing a wealth of strong ground motion data.

It is the purpose of this paper to present selected results of a single study carried out using SMART-1 data in which a promising method for identifying wave types, directions, and velocities was developed. Due to space limitations, application of the method herein is restricted to a limited number of motions recorded during the earthquake of January 29, 1981 (Event 5);

(I) Associate Professor of Civil Engineering, National Central Universtiy, Taipei, Taiwan, China

(II) Professor of Structural Engineering, University of California, Berkeley, California, U.S.A.

see Ref. 2. This earthquake was centered 30 km S26°E of the center of the array. Its focal depth was 11 km and its Richter magnitude calculated locally by the Institute of Earth Sciences in Taipei was 6.9.

CROSS CORRELATIONS AND PRINCIPAL DIRECTIONS

In an attempt to identify wave types, directions, and velocities produced by the earthquake of January 29, 1981 (Event 5), let us first examine the cross correlation coefficient given by

$$\rho_{ij}(\tau) \equiv \frac{R_{ij}(\tau)}{\sqrt{R_{ii}(0)\ R_{jj}(0)}} \tag{1}$$

where

$$R_{ij}(\tau) \equiv \int_{t_o - \frac{\Delta T}{2}}^{t_o + \frac{\Delta T}{2}} x_i(t)\ x_j(t+\tau)\ dt \tag{2}$$

and where $x_i(t)$ and $x_j(t)$ are the recorded acceleration time-histories in the x-direction (East-West) at stations i and j, respectively; see Fig. 2. In Eq. (2), ΔT is a time window centered on time t_o, and τ is a time lag. If the ground motions at these stations were produced primarily by a single travelling wave, then the above cross correlation coefficient, which can range from +1 to -1, would show high correlation for τ equal to the time required for the wave to travel between the two stations. This value of τ would, of course, depend upon the direction of wave propagation as well as wave velocity.

Using t_o = 50.3 sec and ΔT = 7.0 sec so as to include the significant high intensity portions of the motions recorded at all stations in the time window of Eq. (2), cross correlation coefficients were generated over the range $0<\tau<3$ sec for many station pairs. It is pertinent to point out that the plots of these coefficients against time lag τ are not characteristic of those produced by pairs of motions dominated by a single travelling wave. Their shapes and low values of cross correlation suggest the simultaneous presence of multiple waves travelling in different directions with different velocities. Selecting the maximum cross correlation coefficient on each plot, one can examine the relationship between maximum cross correlation and distance (true distance; not projected distance) as shown in Fig. 3. In this figure, the exponential curve was derived by a least squares fitting of the data points shown. The rapid loss of maximum cross correlation with distance supports the above suggestion that multiple waves having different wave velocities and directions are simultaneously present at all stations. As a consequence of this observation, it was concluded that resolution of the motions into their frequency components and into their principal directions was required before identification of wave types, directions, and velocities could be made possible.

Following along these lines, let us transform the x and y recorded components of horizontal ground motion at a point into their $\tilde{x}$ and $\tilde{y}$ components in accordance with Fig. 2; thus,

$$\begin{aligned} \tilde{x}(t) &= x(t)\ \cos\phi + y(t)\ \sin\phi \\ \tilde{y}(t) &= -x(t)\ \sin\phi + y(t)\ \cos\phi \end{aligned} \tag{3}$$

Next, using time and frequency domain windows, the Fourier transforms of these new components are calculated using relations of the type

$$A_{\tilde{x}}(f) \equiv \int_{t_o - \frac{\Delta T}{2}}^{t_o + \frac{\Delta T}{2}} \tilde{x}(t) \exp(-i2\pi ft)dt \tag{4}$$

$$\tilde{x}(t) = \int_{-f_o - \frac{\Delta f}{2}}^{-f_o + \frac{\Delta f}{2}} A_{\tilde{x}}(f) \exp(i2\pi ft)\, df + \int_{f_o - \frac{\Delta f}{2}}^{f_o + \frac{\Delta f}{2}} A_{\tilde{x}}(f) \exp(i2\pi ft)\, df \tag{5}$$

where window lengths ΔT and Δf are centered on time t_o and frequency f_o, respectively.

The direction of maximum intensity as a function of frequency f_o can be obtained by maximizing the variance function

$$R_{\tilde{x}_i\tilde{x}_i}(\tau=0,\phi) = R_{x_ix_i}(0)\cos^2\phi + R_{y_iy_i}(0)\sin^2\phi + 2\,R_{x_iy_i}(0)\cos\phi\sin\phi \tag{6}$$

with respect to ϕ giving (Refs. 3,4,5)

$$\phi_o(f_o) = \frac{1}{2}\tan^{-1}\frac{2\,R_{x_iy_i}(0)}{R_{x_ix_i}(0) - R_{y_iy_i}(0)} \tag{7}$$

Angle $\phi_o(f_o)$ in Eq. (7) denotes two principal directions which are 90° apart; one being the major principal direction, the other the minor principal direction. The corresponding principal variances will be denoted by $R_{\tilde{x}_i\tilde{x}_i}(f_o)$ and $R_{\tilde{y}_i\tilde{y}_i}(f_o)$, respectively.

PRINCIPAL VARIANCE RATIO

Let us now define a principal variance ratio as given by

$$R(f_o) \equiv \frac{R_{\tilde{y}_i\tilde{y}_i}(f_o)}{R_{\tilde{x}_i\tilde{x}_i}(f_o)} \tag{8}$$

which varies over the range $0<R<1$. If we examine the motion at station i for discrete values of f_o, consistent with the discrete frequencies of the Fast Fourier Transform (FFT) method used in evaluating Eqs. (4) and (5), we find the following results: (1) When $R(f_o)=1$, there are no principal directions because the harmonic motion at frequency f_o moves along a circular path at constant angular velocity $2\pi f_o$ as shown in Fig. 4; i.e., the motion is equivalent to two resultant harmonics in orthogonal directions having equal amplitudes but being 90° out-of-phase, (2) When $0<R(f_o)<1$, principal directions do exist with the motion being along an ellipse; i.e., the motion is equivalent to two resultant harmonics in orthogonal directions with different amplitudes and they are 90° out-of-phase, and (3) When $R(f_o)=0$, principal directions exist but the motion is along a straight line; i.e., a pure harmonic exists. For $R(f_o)>0$, the two orthogonal waves could be made up of the superposition of multiple waves moving in different directions. Thus, in the interest of identifying wave types,

directions, and velocities, attention should be concentrated on those discrete frequencies having low values of $R(f_o)$. Fortunately for the SMART-1 data analyzed, these frequencies represent frequencies of high energy transmission as will be shown subsequently.

Figure 5 shows plots of the major principal variance $R_{\tilde{x}_1\tilde{x}_1}(f_o)$, the principal variance ratio $R(f_o)$, and the dominant (or major principal) direction $\phi_o(f_o)$ for the horizontal ground motions recorded at stations C00, I03, and I06. It is significant to note that at frequencies f_1, f_2, f_3, and f_4, representing high intensity motions, i.e., high major principal variances, the corresponding principal variance ratios are low indicating dominant wave transmissions in the neighborhood of these frequencies. Note that the dominant directions are nearly toward the epicenter for frequencies f_1 and f_2 but are much closer to the normal direction for frequencies f_3 and f_4. If the dominant waves are propagating in the general direction away from the epicenter, this observation suggests that Rayleigh waves are the primary source of energy transmission for frequencies less than about 2.5 Hz and that shear waves (SH waves; perhaps in part Love waves) are the primary source of energy transmission for frequencies from 2.5 Hz to about 6 Hz. Above these frequencies, the directions of propagation are quite variable.

Let us now examine in further detail the dominant directions of motions at frequencies $f_1 = 1.17$ Hz and $f_3 = 2.85$ Hz for many stations in addition to stations C00, I03, and I06 represented in Fig. 5. As suggested above, the dominant ground motions at these frequencies seem to be caused primarily by Rayleigh and shear (SH) waves, respectively. Figures 6 and 7 show the dominant direction at frequencies 1.17 Hz and 2.85 Hz, respectively, at many stations as given by Eq. (7). The average dominant direction ϕ_o over the array is also shown in these figures. Note that the average dominant direction in Fig. 6 is reasonable close to the epicentral direction while the average dominant direction in Fig. 7 is close to the normal direction.

We may now use these two average dominant directions to generate corresponding functions

$$R_{\tilde{x}_i\tilde{x}_j}(\tau) \equiv \int_{t_0 - \frac{\Delta T}{2}}^{t_o + \frac{\Delta T}{2}} \tilde{x}_i(t)\, \tilde{x}_j(t+\tau)\, dt \qquad (9)$$

for ground motions recorded at many station pairs across the array. Noting the maximum cross correlation for each station pair over the entire range of τ and the corresponding relative distance between stations as projected on the average dominant axis, valuable plots can be obtained as shown in Fig. 8. Each data point represents a station pair. The upper plot in Fig. 8 is for f_o equal to 1.17 Hz while the lower plot is for f_o equal to 2.85 Hz. Straight lines fitted by least squares yield wave velocities (inverse values of the line slopes) equal to 2.4 km/sec and 5.3 km/sec for the Rayleigh and shear wave velocities, respectively.

Because a uniform elastic half space transmits Rayleigh waves at a velocity equal to 0.9 times the shear wave velocity, an explanation is needed of the mixture in the same time window of SH waves with local velocity of 5.3 km/sec and Rayleigh waves with velocities of 2.4 km/sec. The usual seismological interpretation of this large difference in local apparent velocities is that

the SH waves are associated with longer travel paths from the earthquake source to the array in the vicinity of which the SH wave fronts move steeply upwards through the soil. Thus, the apparent shear wave velocity is largely controlled by the more rigid, deeper rocks in the crust. On the other hand, the Rayleigh waves develop near the surface between the source and the array so that their wave velocities are largely controlled by the shallower less stiff materials.

According to this explanation the vertical components of ground motion in the time window studied should be significant in the frequency range of the Rayleigh waves but relatively insignificant in the frequency range of the transverse shear waves described above. This prediction was tested by computing the three-dimensional particle motions as a function of frequency f_0. The results show that the particle orbits agree well with the above prediction; i.e., significant vertical displacements are present in the frequency band 0.25 to 1.5 Hz, but relatively small vertical displacements are present in the frequency band 2.5 - 3.1 Hz.

CONCLUDING STATEMENT

Although further verification is needed, the method presented herein for identifying wave types, directions, and velocities making use of major principal variances and directions and a principal variance ratio shows considerable promise. Since generating the above results, the authors have generalized the method to a consistent three-dimensional form which permits further improvement of the results.

ACKNOWLEDGMENTS

The authors express their sincere thanks and appreciation to the National Science Council and the National Science Foundation for their financial support of the SMART-1 array project through grants Nos. CEE-7908982 and 70-0202-M0001-03, respectively.

REFERENCES

1. Iwan, W. D. (Editor), Proc. Int. Workshop Strong Motion Earthquake Instrument Arrays, Hawaii, 103 (1978).

2. Bolt, B. A., Loh, C. H., Penzien, J., Tsai, Y. B., and Yeh, Y. T., "Preliminary Report On The SMART-1 Strong Motion Array In Taiwan," Earthquake Engineering Research Center Report UCB/EERC-82/13, University of California, Berkeley, (1982).

3. Penzien, J. and Watabe, M., "Characteristics of 3-Dimensional Earthquake Ground Motion," Earthquake Eng. Struct. Dynamics, 3, 365-373, (1975).

4. Kubo, T. and Penzien, J., "Analysis of Three-Dimensional Strong Earthquake Ground Motions Along Principal Axes, San Fernando Earthquake," Earthquake Eng. Struct. Dynamics, 7, 265-278, (1979).

5. Kubo, T. and Penzien, J., "Simulation of Three-Dimensional Strong Ground Motions Along Principal Axes, San Fernando Earthquake," Earthquake Eng. Struct. Dynamics, 7, 279-294, (1979).

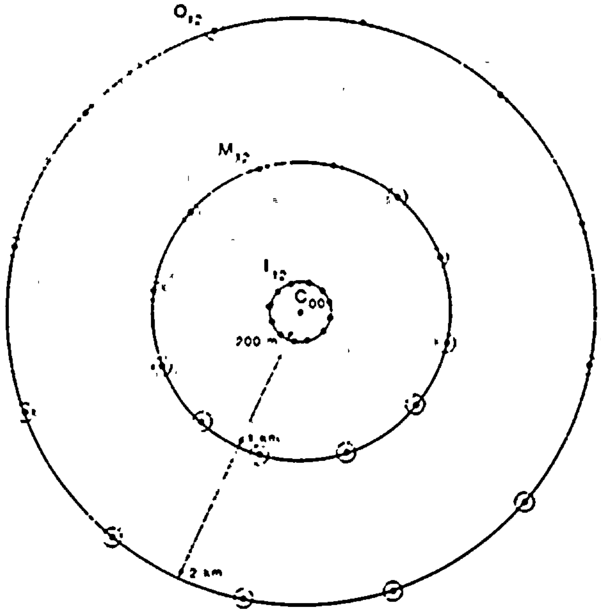

Fig. 1 The SMART 1 array

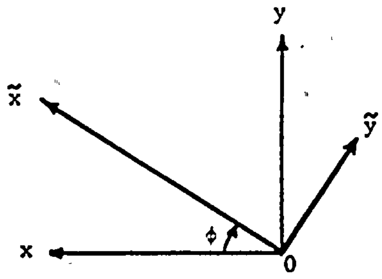

Fig. 2 Coordinate transformation of two horizontal components

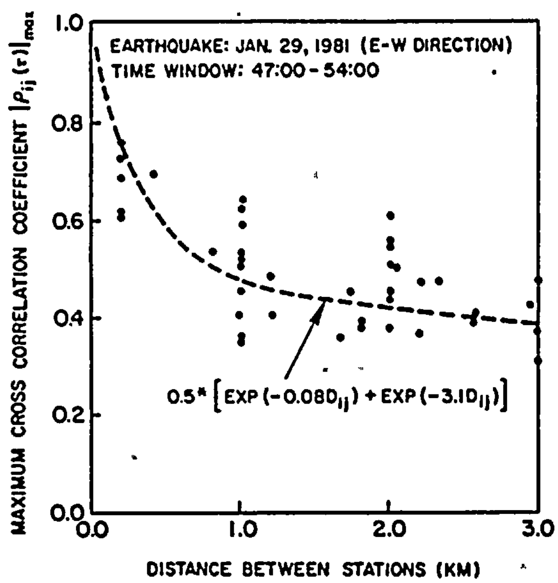

Fig. 3 Attenuation of correlation coefficient ρ

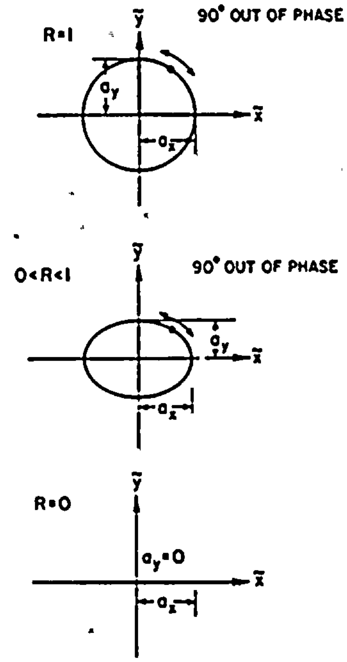

Fig. 4 Physical meaning of principal variance ratio

Earthquake; January 29, 1981

t_o=50:30   ΔT=7.0 sec

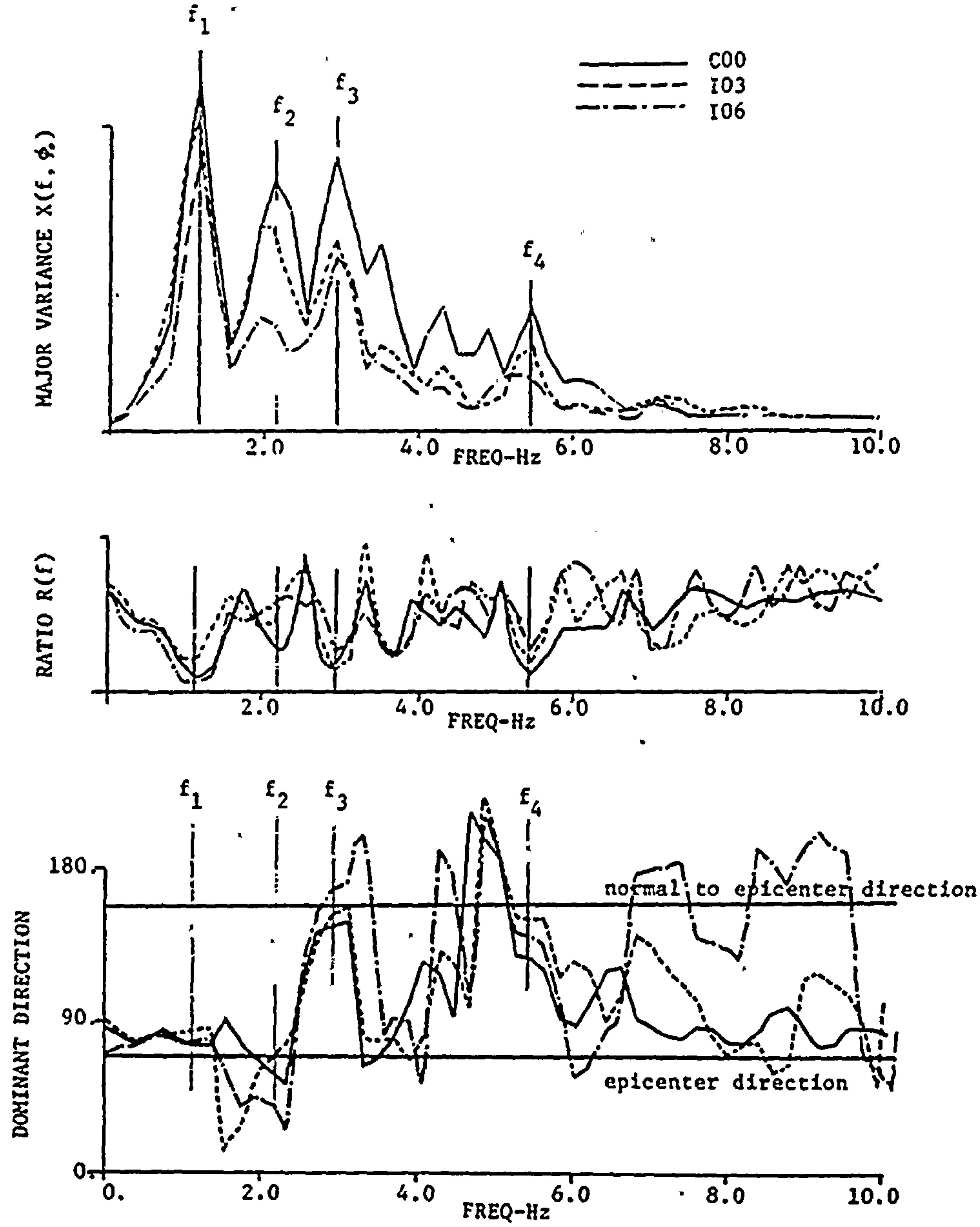

Fig. 5 Major principal variance, variance ratio and dominant direction for Event 5

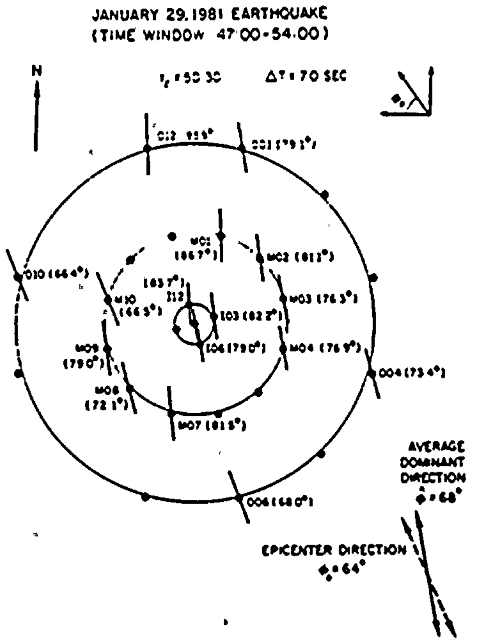

Fig. 6 Dominant directions at 1.17 Hz for Event 5

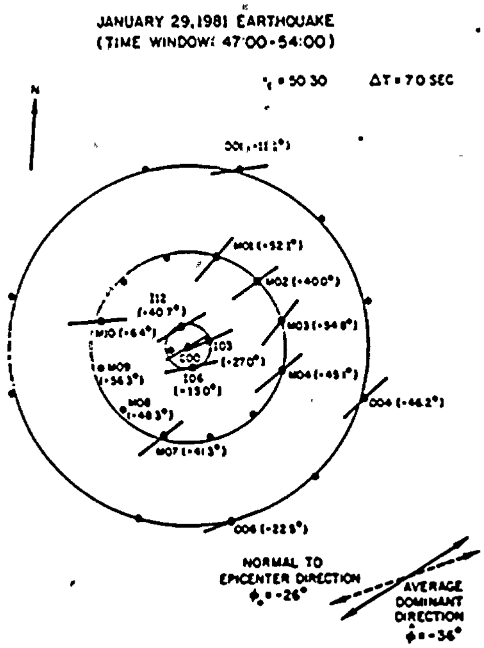

Fig. 7 Dominant directions at 2.85 Hz for Event 5

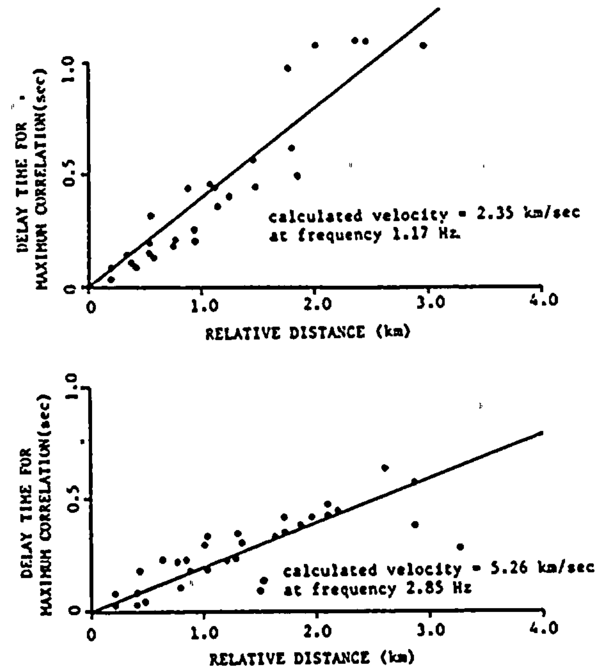

Fig. 8 Identification of wave velocity at frequencies 1.17 Hz and 2.85 Hz

Data Package C Item #2

EARTHQUAKE ENGINEERING AND STRUCTURAL DYNAMICS, VOL. 10, 575-591 (1982)

ENGINEERING ANALYSES OF SMART 1 ARRAY ACCELEROGRAMS

C. H. LOH, J. PENZIEN AND Y. B. TSAI

Earthquake Engineering Research Center, University of California, Richmond, California, U.S.A.
and
Institute of Earth Sciences, Academia Sinica, Taipei, Taiwan, R.O.C.

SUMMARY

Presented are the results of engineering analyses of selected accelerograms recorded by the SMART 1 strong motion array in Taiwan which is described in a companion paper by B. A. Bolt, Y. B. Tsai, K. Yeh and M. K. Hsu, entitled *Earthquake Strong Motions Recorded by a Large Near-source Array of Digital Seismographs.* These analyses include (1) transformations to principal axes, (2) generation of Fourier amplitude spectra, (3) development of generalized response spectrum ratios for characterizing multi-support excitations and (4) moving window analyses in the time and frequency domains for studying the spatial variations of recorded ground motions.

INTRODUCTION

As described in a companion paper,[1] the SMART 1 strong motion array in Taiwan consists of a central station and 36 stations located on three concentric rings (12 stations each) as shown in Figure 1. This arrangement is designed to provide basic ground motion data for both seismological and engineering studies. The seismological studies include source mechanism and energy transmission phenomena while the engineering studies concentrate on the influence of spatial variations of ground motions on the dynamic response of large structural systems such as industrial buildings, bridges and dams. This paper is restricted to

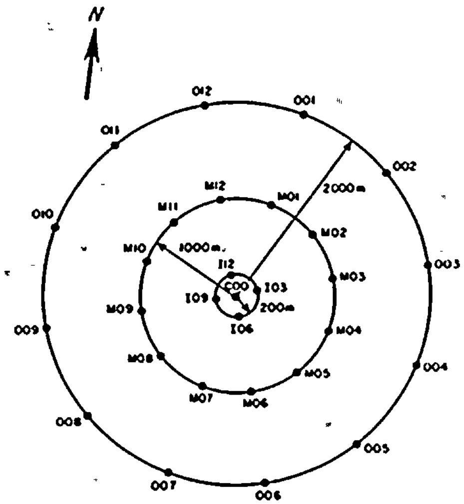

Figure 1. SMART 1 strong motion array

0098-8847/82/040575-17 $01.70

Received 26 August 1981
Revised 10 November 1981

the engineering studies using selected accelerograms recorded during the earthquakes of 14 November 1980 and 29 January 1981. The results presented focus on the correlations of multi-support excitations and their influence on the dynamic response of linear structural systems.

RESPONSE OF LINEAR SYSTEMS TO MULTI-SUPPORT EXCITATIONS

A. *General system*

The equations of motion for a discrete parameter linear structural system subjected to multi-support excitations can be written in the form

$$m\ddot{r}^t + c\dot{r}^t + kr^t = p(t) \tag{1}$$

where r^t is the total displacement vector from a fixed reference containing n components, i.e. $n = n_s + n_b$ where n_s is the number of degrees of freedom in the system exclusive of support displacements and n_b is the number of degrees of freedom associated with the support displacements, $p(t)$ is the load vector containing non-zero components only for the support interaction forces, and m, c and k are the $n \times n$ mass, damping and stiffness matrices, respectively. This equation can be partitioned and written in the form

$$\begin{bmatrix} m_{ss} & m_{sb} \\ m_{bs} & m_{bb} \end{bmatrix}\begin{Bmatrix} \ddot{r}_s^t \\ \ddot{r}_b^t \end{Bmatrix} + \begin{bmatrix} c_{ss} & c_{sb} \\ c_{bs} & c_{bb} \end{bmatrix}\begin{Bmatrix} \dot{r}_s^t \\ \dot{r}_b^t \end{Bmatrix} + \begin{bmatrix} k_{ss} & k_{sb} \\ k_{bs} & k_{bb} \end{bmatrix}\begin{Bmatrix} r_s^t \\ r_b^t \end{Bmatrix} = \begin{Bmatrix} 0 \\ p_b \end{Bmatrix} \tag{2}$$

where r_s^t and r_b^t represent the n_s and n_b degrees of freedom, respectively.

The total response can be separated into quasi-static and dynamic response of the form

$$r^t = \begin{Bmatrix} r_s^{qs} \\ r_b^{qs} \end{Bmatrix} + \begin{Bmatrix} r_s^d \\ 0 \end{Bmatrix} \tag{3}$$

where components in vector r_b^{qs} are identical to the corresponding prescribed support displacements in vector r_b^t, components in r_s^{qs} are the quasi-static displacements in the n_s degrees of freedom caused by the support displacements in r_b^t, and components in r_s^d are dynamic displacements in the n_s degrees of freedom.

The quasi-static response is obtained from the first of equations (2) upon letting $\ddot{r}^t$ and $\dot{r}^t$ equal zero vectors; thus, giving

$$r_s^{qs} = -k_{ss}^{-1}k_{sb}r_b^t \tag{4}$$

The dynamic response is obtained from the first of equations (2) upon substitution of equations (3) and (4), giving

$$m_{ss}\ddot{r}_s^d + c_{ss}\dot{r}_s^d + k_{ss}r_s^d = [m_{ss}k_{ss}^{-1}k_{sb} - m_{sb}]\ddot{r}_b^t + [c_{ss}k_{ss}^{-1}k_{sb} - c_{sb}]\dot{r}_b^t \tag{5}$$

The second term on the right-hand side of equation (5) equals zero for stiffness proportional damping and is small for other forms of damping when the damping ratios are low, say less than 10 per cent of critical; therefore, it can be dropped from the equation without introducing significant error. The dynamic response can then be obtained from the approximate relation

$$m_{ss}\ddot{r}_s^d + c_{ss}\dot{r}_s^d + k_{ss}r_s^d \doteq [m_{ss}k_{ss}^{-1}k_{sb} - m_{sb}]\ddot{r}_b^t \tag{6}$$

Solving for fixed base structural mode shapes and frequencies using

$$m_{ss}\ddot{r}_s^d + k_{ss}r_s^d = 0 \tag{7}$$

the vector r_s^d can be expressed in terms of the resulting $n_s \times n_s$ modal matrix Φ_s and the n_s fixed base modal coordinates Y_s as given by

$$r_s^d = \Phi_s Y_s \tag{8}$$

Introducing equation (8) into (6) and using the orthogonality properties of the fixed base modes, uncoupled normal mode equations of motion for the fixed base structure are obtained as given by

$$M_s\ddot{Y}_s + C_s\dot{Y}_s + K_sY_s = \Phi_s^T[m_{ss}k_{ss}^{-1}k_{sb} - m_{sb}]\ddot{r}_b^t \tag{9}$$

where M_s, C_s and K_s are $n_s \times n_s$ diagonal matrices defined by

$$\begin{aligned} M_s &\equiv \Phi_s^T m_{ss}\Phi_s \\ C_s &\equiv \Phi_s^T c_{ss}\Phi_s = 2M_s\omega_s\xi_s \\ K_s &\equiv \Phi_s^T k_{ss}\Phi_s = \omega_s^2 M_s \end{aligned} \tag{10}$$

where ω_s is a diagonal matrix containing the fixed base normal mode frequencies and ξ_s is a vector containing the n_s normal mode damping ratios. It is assumed here that damping matrix c_{ss} is of the Caughey form so that uncoupled damped normal modes exist.

It should be recognized that generalized shape functions and corresponding amplitudes could also be used in formulating the original discrete parameter equations of motion. Normally, however, the standard finite element approach would be used.

B. *Special case of the general system*

Consider a special case of the general system formulated above where $n_s = 1$, $n_b = 2$ and $n = 3$. Let the two prescribed single-component support displacements at supports A and B in this case be denoted by $v_{gA}(t)$ and $v_{gB}(t)$, respectively. Equation (3) can now be written as

$$r^t = \begin{Bmatrix} r_1^t(t) \\ v_{gA}(t) \\ v_{gB}(t) \end{Bmatrix} = \begin{Bmatrix} r_1^{qs}(t) \\ v_{gA}(t) \\ v_{gB}(t) \end{Bmatrix} + \begin{Bmatrix} r_1^d(t) \\ 0 \\ 0 \end{Bmatrix} \tag{11}$$

Note that the single degree of freedom in the fixed base system as represented by $r_1^d(t)$ could be any single normal mode of the multi-degree fixed base system or any other single generalized shape function for that system.

The quasi-static solution as given by equation (4) becomes

$$r_1^{qs} = -\frac{k_{12}}{k_{11}}v_{gA} - \frac{k_{13}}{k_{11}}v_{gB} \tag{12}$$

and equation (5), yielding the dynamic response, reduces to

$$\ddot{r}_1^d + 2\xi_1\omega_1\dot{r}_1^d + \omega_1^2 r_1^d = \left(\frac{k_{12}}{k_{11}} - \frac{m_{12}}{m_{11}}\right)\ddot{v}_{gA} + \left(\frac{k_{13}}{k_{11}} - \frac{m_{13}}{m_{11}}\right)\ddot{v}_{gB} \tag{13}$$

where

$$\begin{aligned} \omega_1 &= \sqrt{(k_{11}/m_{11})} \\ \xi_1 &= c_{11}/2m_{11}\omega_1 \end{aligned} \tag{14}$$

For the subsequent development, it is convenient to write equation (13) in the form

$$\ddot{r}_1^d + 2\xi_1\omega_1\dot{r}_1^d + \omega_1^2 r_1^d = -A\ddot{v}_{gA} - B\ddot{v}_{gB} \tag{15}$$

where

$$A \equiv -\left(\frac{k_{12}}{k_{11}} - \frac{m_{12}}{m_{11}}\right); \quad B \equiv -\left(\frac{k_{13}}{k_{11}} - \frac{m_{13}}{m_{11}}\right) \tag{16}$$

Let us now compare the maximum absolute value of dynamic response with the two simultaneous inputs as expressed by equation (15) with the average of the maximum absolute values of response produced by the two

inputs applied as rigid base inputs separately, i.e. the averages of the maximum absolute values of response derived from

$$\ddot{r}_1^d + 2\xi_1\omega_1\dot{r}_1^d + \omega_1^2 r_1^d = -(A+B)\ddot{v}_{gA} \tag{17}$$

$$\ddot{r}_1^d + 2\xi_1\omega_1\dot{r}_1^d + \omega_1^2 r_1^d = -(A+B)\ddot{v}_{gB} \tag{18}$$

Letting $S_a^{AA}(\xi, T)$ and $S_a^{BB}(\xi, T)$ represent the standard pseudo-acceleration response spectra for ground accelerations $\ddot{v}_{gA}$ and $\ddot{v}_{gB}$, respectively, the maximum absolute values for r_1^d as given by equations (17) and (18) will be

$$\frac{1}{\omega_1^2}(A+B)S_a^{AA}(\xi, T) \quad \text{and} \quad \frac{1}{\omega_1^2}(A+B)S_a^{BB}(\xi, T),$$

respectively. The average of these two maximum responses will be

$$\frac{1}{2\omega_1^2}(A+B)[S_a^{AA}(\xi, T) + S_a^{BB}(\xi, T)]$$

The quantity T introduced here is the fixed base structural period $2\pi/\omega_1$.

Consider now the maximum absolute value of response resulting from equation (15). It is convenient to designate inputs $\ddot{v}_{gA}$ and $\ddot{v}_{gB}$ so that $|A| \leq |B|$ and to introduce a participation factor ratio γ defined by

$$\gamma \equiv \frac{A}{B} \tag{19}$$

Because $|A| \leq |B|$, γ must always be in the range

$$-1 \leq \gamma \leq +1 \tag{20}$$

Using this participation factor ratio, equation (15) can be written as

$$\ddot{r}_1^d + 2\xi_1\omega_1\dot{r}_1^d + \omega_1^2 r_1^d = -B[\gamma\ddot{v}_{gA} + \ddot{v}_{gB}] \tag{21}$$

Defining $S_a^{AB}(\gamma, \xi, T)$ as the standard pseudo-acceleration response spectrum derived using $\frac{1}{2}[\gamma\ddot{v}_{gA} + \ddot{v}_{gB}]$ as the single input to the single degree of freedom system, the maximum absolute value of response resulting from equation (21) is $(2B/\omega_1^2)S_a^{AB}(\gamma, \xi, T)$.

A generalized dynamic response ratio $\Phi^d(\gamma, \xi, T)$ is now defined as the ratio of the maximum absolute value of response derived from equation (21) to the average of the maximum absolute values of response given by equations (17) and (18); thus $= \dfrac{2BS^{AB}}{\frac{1}{2}[A+B]S^{AA} + \frac{1}{2}[A+B]S^{BB}}$

$$\Phi^d(\gamma, \xi, T) \equiv \frac{4}{(\gamma+1)} \cdot \frac{S_a^{AB}(\gamma, \xi, T)}{[S_a^{AA}(\xi, T) + S_a^{BB}(\xi, T)]} \tag{22}$$

Note that as $\ddot{v}_{gA}(t)$ and $\ddot{v}_{gB}(t)$ approach full positive correlation with each other, $\Phi^d(1, \xi, T) \to 1$.

The generalized dynamic response ratio defined by equation (22) can be used effectively to measure the modified dynamic response resulting from the differences in the two simultaneous inputs $\ddot{v}_{gA}$ and $\ddot{v}_{gB}$. These differences obviously depend upon the distance between supports A and B as well as other factors.

Since $S_a^{AB}(1, \xi, T)$ and $S_a^{AB}(-1, \xi, T)$ are the pseudo-acceleration response spectra for single degree of freedom inputs $\frac{1}{2}[\ddot{v}_{gB} + \ddot{v}_{gA}]$ and $\frac{1}{2}[\ddot{v}_{gB} - \ddot{v}_{gA}]$, i.e. the in-phase and out-of-phase components, respectively, for motions at A and B, the normalized form of equation (22) given by

$$\Gamma(\gamma, \xi, T) \equiv \frac{(\gamma+1)}{2}\Phi^d(\gamma, \xi, T) = \frac{2S_a^{AB}(\gamma, \xi, T)}{[S_a^{AA}(\xi, T) + S_a^{BB}(\xi, T)]} \tag{23}$$

can be used for $\gamma = +1$ and $\gamma = -1$ to measure the intensity of in-phase motions and out-of-phase motions, respectively.

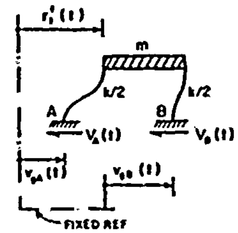

Figure 2. Simple shear frame with multi-support excitations

1. *Example No. 1 of the special case.* Consider the simple system shown in Figure 2 with support inputs at A and B as indicated. For this system, equations (4) and (6) become

$$r_1^s = \tfrac{1}{2}[v_{gA} + v_{gB}] \tag{24}$$

and

$$\ddot{r}_1^d + 2\xi_1\omega_1\dot{r}_1^d + \omega_1^2 r_1^d = -\tfrac{1}{2}[\ddot{v}_{gA} + \ddot{v}_{gB}] \tag{25}$$

where $\omega_1 = \sqrt{(k/m)}$ and ξ_1 is the fixed base damping ratio. Constants A and B as defined by equations (16) are both equal to $\frac{1}{2}$; thus $\gamma = +1$. The dynamic response ratio reduces to the form

$$\Phi^d(1, \xi, T) = \frac{2S_a^{AB}(\gamma, \xi, T)}{[S_a^{AA}(\xi, T) + S_a^{BB}(\xi, T)]} \tag{26}$$

and the shear forces are given by

$$V_A(t) = \frac{k}{2}\left[r_1^d + \left(\frac{v_{gB} - v_{gA}}{2}\right)\right]; \quad V_B(t) = \frac{k}{2}\left[r_1^d - \left(\frac{v_{gB} - v_{gA}}{2}\right)\right] \tag{27}$$

Let us now define two new acceleration spectra $S_A(\xi, T)$ and $S_B(\xi, T)$ by the relations

$$S_A(\xi, T) \equiv \omega_1^2\left|r_1^d + \left(\frac{v_{gB} - v_{gA}}{2}\right)\right|_{max}; \quad S_B(\xi, T) \equiv \omega_1^2\left|r_1^d - \left(\frac{v_{gB} - v_{gA}}{2}\right)\right|_{max} \tag{28}$$

Note that when $\ddot{v}_B = \ddot{v}_A$, $S_B(\xi, T) = S_A(\xi, T) = S_a^{AA}(\xi, T)$ and when $\ddot{v}_A = \ddot{v}_B$, $S_B(\xi, T) = S_A(\xi, T) = S_a^{BB}(\xi, T)$.

Defining a new generalized dynamic response ratio $\Phi^t(\xi, T)$ as the ratio of the average of the maximum absolute values of $V_A(t)$ and $V_B(t)$ produced by the multiple inputs as represented by equations (24) and (25) to the average of maximum absolute shears as produced by separate rigid base (single input) inputs $\ddot{v}_{gA}$ and $\ddot{v}_{gB}$, one finds

$$\Phi^t(\xi, T) = \frac{S_A(\xi, T) + S_B(\xi, T)}{S_a^{AA}(\xi, T) + S_a^{BB}(\xi, T)} \tag{29}$$

Note that for systems of the above type which are statically indeterminate through their supports, the forces produced by the quasi-static response are proportional to the out-of-phase ground displacement $(v_{gB} - v_{gA})/2$.

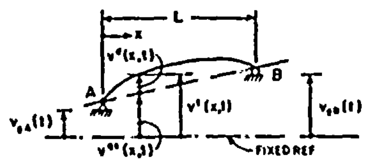

Figure 3. Simple beam with multi-support excitations

2. *Example No.* 2 *of the special case.* Consider the simple system shown in Figure 3 with support inputs at A and B as indicated. It is of interest to consider the absolute maximum response of a single mode vibration for simultaneous inputs $\ddot{v}_A(t)$ and $\ddot{v}_B(t)$ and to compare this maximum response with the average of the corresponding absolute maximum responses produced by rigid base inputs $\ddot{v}_A(t)$ and $\ddot{v}_B(t)$.

Considering the first mode, its dynamic response is given by

$$v^d(x,t) = r_1^d(t)\sin\frac{\pi x}{L} \tag{30}$$

and its quasi-static response is given by

$$v^{qs}(x,t) = v_{gA}(t) + \left(\frac{v_{gB}(t) - v_{gA}(t)}{L}\right)x \tag{31}$$

Adding equations (30) and (31), the total response is given by

$$v^t(x,t) = r_1^d(t)\Phi_1(x) + v_{gA}\Phi_2(x) + v_{gB}\Phi_3(x) \tag{32}$$

where

$$\Phi_1(x) = \sin\frac{\pi x}{L}$$

$$\Phi_2(x) = 1 - \frac{x}{L} \tag{33}$$

$$\Phi_3(x) = \frac{x}{L}$$

Using the principle of virtual work and standard finite element methods, one obtains

$$m_{11} = \frac{\bar{m}L}{2}; \quad m_{12} = m_{13} = \frac{\bar{m}L}{2}$$
$$k_{11} = \frac{\pi^4\overline{EI}}{2L^3}; \quad k_{12} = k_{13} = 0 \tag{34}$$

from which

$$\omega_1^2 = k_{11}/m_{11} = \frac{\pi^4\overline{EI}}{\bar{m}L^4}; \quad T_1 = 2\pi/\omega_1 \tag{35}$$

Substituting equations (34) into equations (16) gives $A = B = 2/\pi$; therefore, γ as defined by equation (19) equals 1. Since this structure is statically determinate through its supports, the quasi-static response produces no internal forces in the system, which is consistent with equation (4) giving $r_1^{qs} = 0$. It is quite clear now that the generalized dynamic response ratio given by equation (26) for $\xi = \xi_1$ and $T = T_1$ is a direct measure of the modified total force (or stress) response caused by the differences in the two inputs $\ddot{v}_A(t)$ and $\ddot{v}_B(t)$.

Considering the second mode response, equations (32) and (33) still apply except that

$$\Phi_1(x) = \sin\frac{2\pi x}{L} \tag{36}$$

This mode shape leads to

$$m_{11} = \frac{\bar{m}L}{2}; \quad m_{12} = \frac{\bar{m}L}{2\pi}; \quad m_{13} = -\frac{\bar{m}L}{2\pi}$$
$$k_{11} = \frac{8\pi^4\overline{EI}}{L^3}; \quad k_{12} = k_{13} = 0 \tag{37}$$

Thus,

$$\omega_1^2 = \frac{k_{11}}{m_{11}} = \frac{16\pi^4\overline{EI}}{\bar{m}L^4} \quad \text{(second mode frequency)} \tag{38}$$

Substituting equations (37) into equations (16) gives $A = 1/\pi$ and $B = -1/\pi$; therefore, γ as defined by equation (19) equals -1. From equation (26), it is seen that $\Phi^d(-1,\xi,T) = \infty$, the reason for this being that the second mode is excited only by the out-of-phase motion $(\ddot{v}_{gB} - \ddot{v}_{gA})/2$. In other words, the rigid base (in-phase) inputs produce no second mode response.

CORRELATIONS OF MULTI-SUPPORT EXCITATIONS

A. *Multiple components at one support*

Consider input accelerations $a_{rx}(t)$, $a_{ry}(t)$ and $a_{rz}(t)$ at support r in directions x, y and z, respectively. These motions can easily be transformed to any other orthogonal set of axes, say $\bar{x}$, $\bar{y}$ and $\bar{z}$, through a transformation matrix $\mathbf{a}$ which satisfies the condition $\mathbf{a}^T\mathbf{a} = \mathbf{I}$ (identity matrix); thus, we can write

$$\begin{Bmatrix} a_{r\bar{x}}(t) \\ a_{r\bar{y}}(t) \\ a_{r\bar{z}}(t) \end{Bmatrix} = \begin{bmatrix} a_{11} & a_{12} & a_{13} \\ a_{21} & a_{22} & a_{23} \\ a_{31} & a_{23} & a_{33} \end{bmatrix} \begin{Bmatrix} a_{rx}(t) \\ a_{ry}(t) \\ a_{rz}(t) \end{Bmatrix} \tag{39}$$

One can easily find that transformation giving the principal axes, i.e. the directions for which no cross correlations exist among the three transformed components of acceleration.[2] For small structures, the directions of the principal axes for all inputs would be approximately the same; however, for large structures significant differences could exist, particularly when the site conditions are complex.

B. *Uni-directional components at two supports*

Let $a_{ri}(t)$ and $a_{si}(t)$ be the recorded ground accelerations at stations r and s, respectively, in the ith coordinate direction ($i = x, y, z$) at time t. These motions can be separated into their in-phase and out-of-phase components as shown by

$$a_{ri}(t) = \left[\frac{a_{ri}(t) + a_{si}(t)}{2}\right] + \left[\frac{a_{ri}(t) - a_{si}(t)}{2}\right]$$
$$a_{si}(t) = \left[\frac{a_{ri}(t) + a_{si}(t)}{2}\right] - \left[\frac{a_{ri}(t) - a_{si}(t)}{2}\right] \tag{40}$$

The first term on the right-hand side of equations (40) represents the in-phase component while the second term represents the out-of-phase component. It is very informative to compare directly these two components for different pairs of stations and for different directions when studying the correlations of $a_{ri}(t)$ and $a_{si}(t)$. As pointed out previously, equation (23) can also be used for this same purpose by letting $\gamma = +1$ and $\gamma = -1$ and comparing the two results obtained.

Correlation studies of $a_{ri}(t)$ and $a_{si}(t)$ can also be carried out using the so-called 'moving window' technique. To develop this method, we make use of the Fast Fourier Transform algorithm to generate

$$a_{ri}(i\bar{\omega},t) \equiv \int_{t-(\Delta t/2)}^{t+(\Delta t/2)} a_{ri}(\alpha)e^{-i\bar{\omega}\alpha}\,d\alpha \tag{41}$$

$$b_{ri}(\bar{\omega},t,\alpha) \equiv \frac{1}{2\pi}\int_{\bar{\omega}-(\Delta\bar{\omega}/2)}^{\bar{\omega}+(\Delta\bar{\omega}/2)} a_{ri}(i\beta,t)e^{i\beta\alpha}\,d\beta \tag{42}$$

where α is a dummy variable for time t, Δt is the window width in the time domain, $\Delta\bar{\omega}$ is the window width in the frequency domain and β is a dummy variable for circular frequency $\bar{\omega}$. Time t in equation (41) can be

varied continuously for a fixed value of Δt resulting in a moving window in the time domain. Likewise, frequency $\bar{\omega}$ in equation (42) can be varied continuously for a fixed value of $\Delta\bar{\omega}$ resulting in a moving window in the frequency domain. Equation (41) is actually the Fourier Transform of $a_{rl}(t)$, but considering only its values over the time range Δt centred on t while equation (42) is the inverse Fourier Transform of $a_{rl}(i\bar{\omega}, t)$, but considering only its values over the frequency range $\Delta\bar{\omega}$ centred on $\bar{\omega}$. In some cases $a_{rl}(i\bar{\omega}, t)$ and $b_{rl}(\bar{\omega}, t, \alpha)$ are calculated for $\Delta t = \infty$ and $\Delta\bar{\omega}$ equal to a finite value, respectively; while in other cases, they are calculated for Δt equal to a finite value and $\Delta\bar{\omega} = \infty$, respectively. In certain special cases, finite values are used for both Δt and $\Delta\bar{\omega}$.

To continue with this moving window approach, generate the cross correlation coefficients (or functions) as defined by

$$\rho_{rl,sl}(\bar{\omega},t,\tau)\equiv\left(\int_{-\infty}^{\infty} b_{rl}(\bar{\omega},t,\alpha)\,b_{sl}(\bar{\omega},t,\alpha+\tau)\,d\alpha\right)\Big/\sqrt{\left[\int_{-\infty}^{\infty} b_{rl}(\bar{\omega},t,\alpha)^2\,d\alpha\right]}\sqrt{\left[\int_{-\infty}^{\infty} b_{sl}(\bar{\omega},t,\alpha+\tau)^2\,d\alpha\right]} \quad (43)$$

where τ is a time difference. By this definition, the cross correlation coefficients fall in the range

$$-1\leqslant\rho_{rl,sl}(\bar{\omega},t,\tau)\leqslant+1 \quad (44)$$

The use of equation (43) to study the cross correlation of motions $a_{rl}(t)$ and $a_{sl}(t)$ is described in the next section of this paper.

NUMERICAL RESULTS OF ANALYSES

A. *Directions of principal axes*

Directions of principal axes were determined for the ground accelerations produced at stations M02, M05 and M12 during the earthquake of 14 November 1980, and at stations C00, 106 and 009 during the earthquake of 29 January 1981. The directions of these axes when projected on a horizontal plane are shown in Figures 4 and 5 for eight different overlapping time segments of 4 s each. The crosses and dots indicate that the major and minor axes, respectively, are approximately vertical while the short and long solid lines indicate directions of the intermediate and major axes, respectively. The most significant of these results are those for time segments in the range $0<t<8$ s which covers the high intensity periods of the motions.

During this high intensity time range, the major principal axis for the earthquake of 14 November 1980 points downward towards the hypocentre located approximately 10 km S 16° E of the centre station of the array and at a depth of 62 km. This observation is consistent with high P-wave contributions to the ground

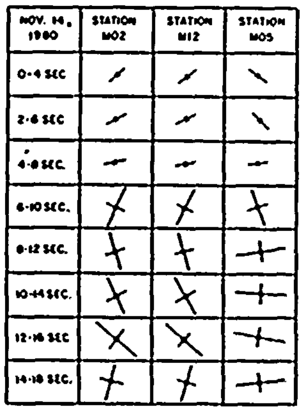

Figure 4. Directions of principal axes for ground motions produced by the earthquake of 14 November 1980

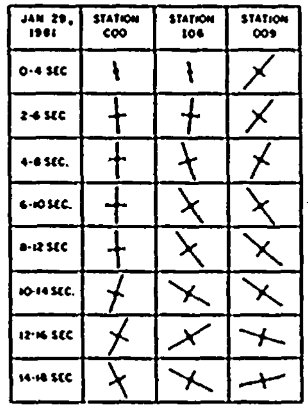

Figure 5. Directions of principal axes for ground motions produced by the earthquake of 29 January 1981

motions. During the time range $6<t<18$ s, the 4-s segments show the major principal axis to be approximately horizontal and usually pointing in the general direction of the epicentre.

For the earthquake of 29 January 1981, the major principal axis is approximately vertical only during the first 4-s segment at stations C00 and 106. For all other time segments, it is approximately horizontal. During the high intensity time range and considerably beyond, the directions of the major principal axis correlate reasonably well with direction to the epicentre located 30 km S 26° E of the array's centre station. The hypocentre depth for this earthquake was approximately 11 km. These observations are consistent with S-wave contributions to the high intensity motions.

B. *In-phase and out-of-phase components of uni-directional motions*

As defined by equation (40), in-phase and out-of-phase components of uni-directional motion at selected pairs of stations were calculated. Figures 6–9 show Fourier amplitude spectra for each of these components as recorded during the earthquakes of 14 November 1980 and 29 January 1981, respectively, for station pair C00 and 103. The in-phase component for the earthquake of 14 November 1980 is much stronger than the out-of-phase component except for frequencies in the approximate range 5–6 Hz. The large percentage of in-phase motion is consistent with coherent wave fronts of the P-wave type moving in an approximate vertical direction as indicated by the vertically oriented major principal axis previously described. The in-phase and out-of-phase components for the earthquake of 29 January 1981 are approximately equal in intensity if averaged over the entire frequency band $0<1/t<7$ Hz; however, there is a definite shifting of the intensity from one component to the other as a function of frequency. To illustrate this observation, notice the high percentage of out-of-phase motion for frequencies in the neighbourhood of 1, 3 and 5 Hz and the low percentage for frequencies in the neighbourhood of 2, 4 and 6 Hz. While some effort has been made to

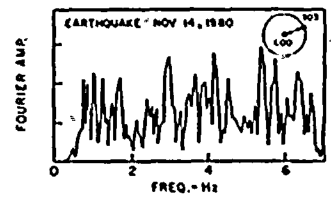

Figure 6. Fourier amplitude spectrum for E-W in-phase component of motion for station pair C00 and 103

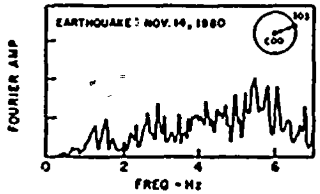

Figure 7. Fourier amplitude spectrum for E-W out-of-phase component of motion for station pair C00 and 103

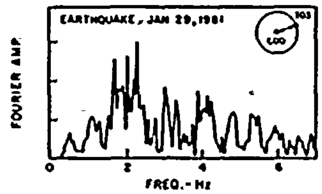

Figure 8. Fourier amplitude spectrum for E-W in-phase component of motion for station pair C00 and 103

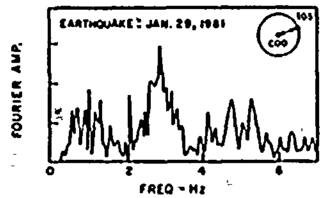

Figure 9. Fourier amplitude spectrum for E-W out-of-phase component of motion for station pair C00 and 103

rationalize the cause of this phenomenon, no explanation will be set forth at this time. Obviously, further study of these and other results are needed.

C. *Normalized dynamic response ratio*

The generalized dynamic response ratio $\Phi^d(\gamma, \xi, T)$ defined by equation (22) can be used to correlate the in-phase and out-of-phase components of uni-directional motions at station pairs when placed in its normalized form shown by equation (23) and when evaluated for $\gamma = +1$ and $\gamma = -1$. Plots of this normalized ratio against structural period T are shown in Figures 10–14 for $\xi = 0{\cdot}05$.

Figures 10 and 11 show plots of this ratio for station pairs C00 and 103 and C00 and 106, respectively, using $\gamma = +1$ which emphasizes the in-phase component of motion. Notice that the percentage of in-phase motion for the earthquake of 14 November 1980 is very high compared with the corresponding percentage for the earthquake of 29 January 1981 particularly as shown by the longer structural periods. This observation is quite similar for station pairs C00 and 103 and C00 and 106. Clearly, the results of Figures 10 and 11 are consistent with wide propagating P-waves for the 14 November 1980 earthquake and predominant S-waves propagating horizontally for the 29 January 1981 earthquake.

The normalized dynamic response ratio for $\gamma = +1$, $\xi = 0{\cdot}05$ and for station pair C00 and 103 is again plotted against structural period T in Figures 12 and 13. Also plotted in these figures is the same response ratio for $\gamma = -1$ which emphasizes the out-of-phase component of motion. Again notice the very high percentage of in-phase motion ($\gamma = +1$) for the earthquake of 14 November 1980 as compared with the earthquake of 29 January 1981. Comparing the curves in these same figures for $\gamma = -1$ shows a much higher percentage of out-of-phase motion for the earthquake of 29 January 1981 as compared with the earthquake

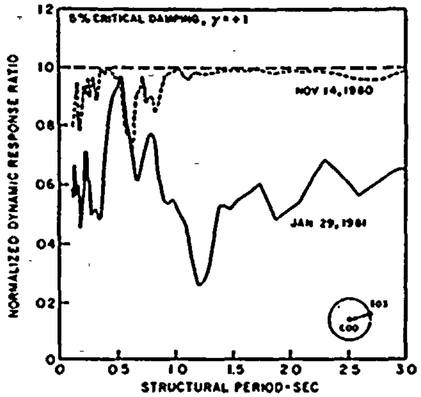

Figure 10. Normalized dynamic response ratio for E-W components of motion at stations C00 and 103

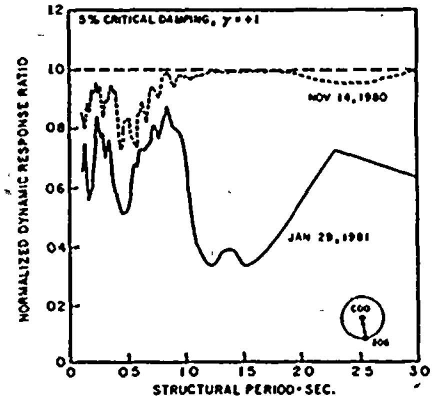

Figure 11. Normalized dynamic response ratio for E-W components of motion at stations C00 and 106

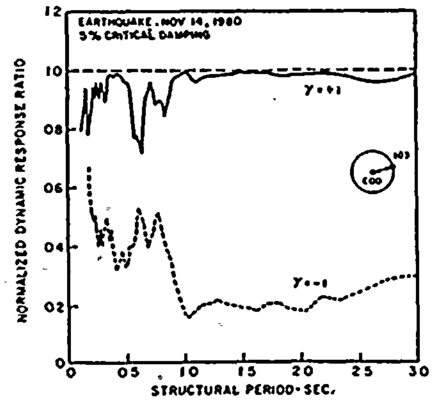

Figure 12. Normalized dynamic response ratio for E-W components of motion at stations C00 and 103

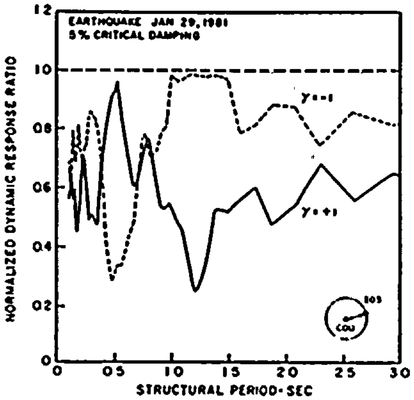

Figure 13. Normalized dynamic response ratio for E-W components of motion at stations C00 and I03

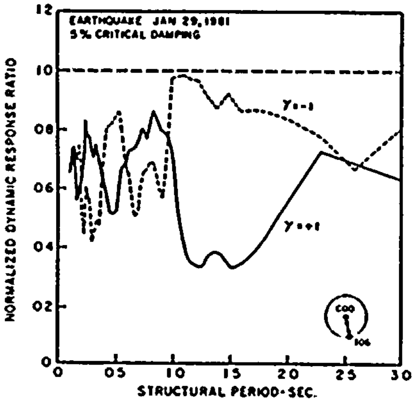

Figure 14. Normalized dynamic response ratio for E-W components of motion at stations C00 and I06

of 14 November 1980. The plots in Figure 14 correspond to those in Figure 13 except they represent station pair C00 and I06 instead of station pair C00 and I03. The results for both station pairs are quite similar.

The previously mentioned observation of an oscillatory shifting of the intensities of in-phase and out-of-phase motions with frequency for the earthquake of 29 January 1981 is again apparent in Figures 13 and 14.

D. *Shear ratio*

The generalized response ratio $\Phi'(\xi, T)$ defined by equation (29) (called the shear ratio here) is plotted in Figures 15 and 16 for the earthquakes of 14 November 1980 and 29 January 1981, respectively, using the recorded EW motions for station pair C00 and I03. The plot in Figure 15 showing the shear ratio to be nearly equal to 1 over the entire structural period range indicates a very large percentage of in-phase motion: in fact, so large a percentage that the rigid base input assumption usually made in engineering practice would be reasonably valid for this case. This observation is quite significant considering the fact that stations C00 and I03 are separated by 200 m.

The shear ratio plot in Figure 16 for the earthquake of 29 January 1981 is quite different from that in Figure 15. It shows a shear ratio considerably less than 1 over most of the structural period range which

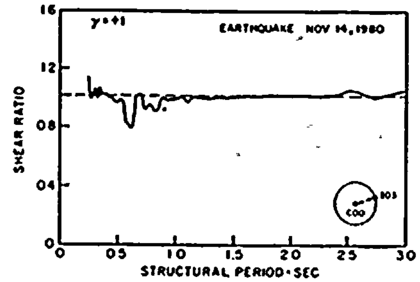

Figure 15. Shear ratio for E-W components of motion at stations C00 and I03

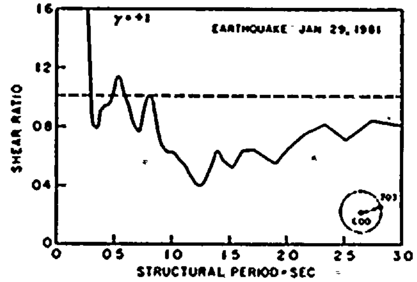

Figure 16. Shear ratio for E-W components of motion at stations C00 and I03

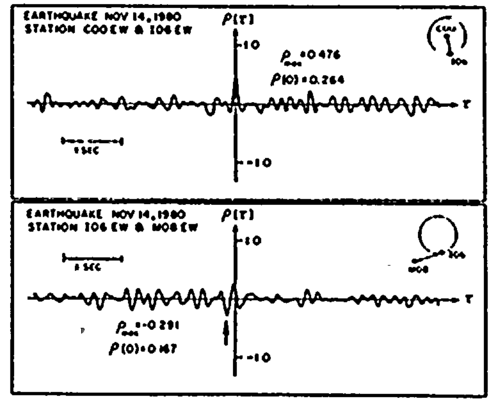

Figure 17. Cross correlation coefficient for E-W components of motion for station pairs C00 and I06 and I06 and M08

indicates the double-support input produces response considerably less than the average of the separate rigid base inputs. The out-of-phase components are obviously strong for this case causing a large reduction in structural response.

By definition, the shear ratio must approach infinity as the structural period approaches zero because the quasi-static forces approach infinity while the dynamic shear forces remain finite. This fact explains why the

shear ratio is larger than 1 for the shorter structural periods. The quasi-static response also increases the shear ratio above unity in the longer structural period range for the case of the earthquake of 14 November 1980 because of the large percentage of in-phase motion. One should note that the shear ratio is exactly unity when the motions at stations C00 and I03 are identically equal. This ratio can exceed unity only as a result of the quasi-static response caused by the out-of-phase motion.

E. *Cross correlation coefficients*

The cross correlation coefficient defined by equation (43) can be used to study the correlation of motions $a_{ri}(t)$ and $a_{si}(t)$ measured at stations r and s, respectively, in the ith direction. Letting Δt and $\Delta\bar{\omega}$ in equations (41) and (42), respectively, equal infinity, the cross correlation coefficient is a function of time difference τ only.

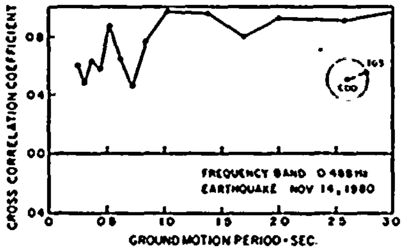

Figure 18. Cross correlation coefficient for E-W components of motion for stations C00 and I03 using frequency domain moving window

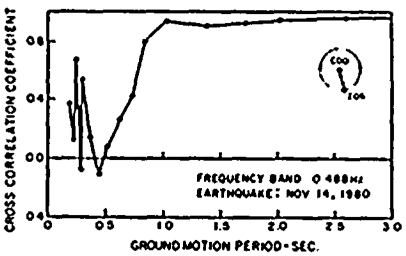

Figure 19. Cross correlation coefficient for E-W components of motion for stations C00 and I06 using frequency domain moving window

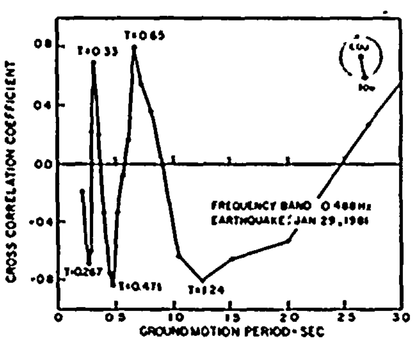

Figure 20. Cross correlation coefficient for E-W components of motion for stations C00 and I06 using frequency domain moving window

Figure 17 shows plots of this coefficient for the E-W components of motion at two station pairs, namely C00 and I06 and I06 and M08, as recorded during the earthquake of 14 November 1980. The maximum cross correlations for these two station pairs were found to be $+0.476$ and -0.291, respectively, while the corresponding cross correlations for zero time difference were found to be $+0.204$ and $+0.167$. These correlations are relatively low as their numerical values are dominated by the higher frequencies in the ground motions. The values of time difference τ associated with maximum values of correlation are now being used to assist in studies of wave transmission characteristics (wave type, velocity and direction). The results of these studies will be reported later.

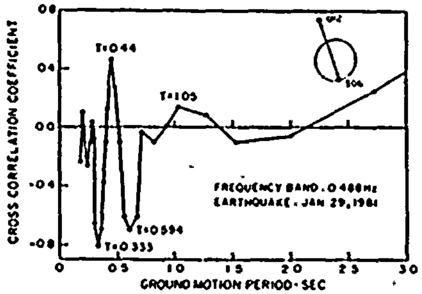

Figure 21. Cross correlation coefficient for E-W components of motion for stations I06 and O12 using frequency domain moving window

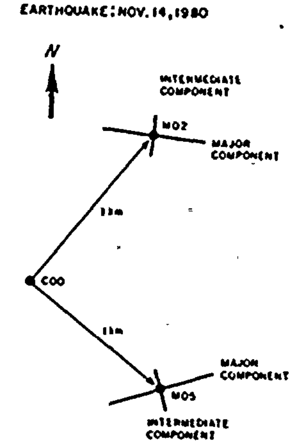

Figure 22. Direction of principal axes at stations M02 and M05 using both frequency and time domain moving windows

Because of the dominance of higher frequencies on the cross correlation coefficient and the differences in correlation which exist among frequencies, a moving window in the frequency domain was used to obtain cross correlation as a function of frequency $\bar{\omega}$ and time difference τ. In this case Δt was set equal to infinity.

Figures 18–21 show this correlation plotted against ground motion period $(2\pi/\bar{\omega})$ for $\tau = 0$ and for $\Delta f = \Delta\bar{\omega}/2\pi = 0.488$ Hz. East-west components of motion for stations C00, I03, I06 and O12 recorded during the earthquake of 14 November 1980 and 29 January 1981 were used as indicated. Figures 18 and 19 show the cross correlations to be very high for the longer periods of motion recorded during the earthquake of 14 November 1980 and they show a relatively fast drop in correlation with decreasing periods below 1 s. In

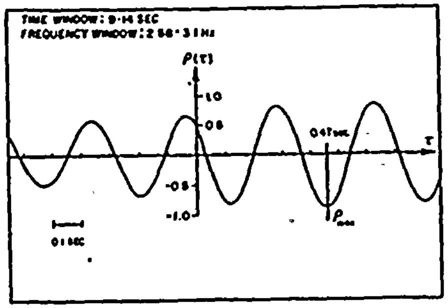

Figure 23. Cross correlation coefficient for major principal components of motion at stations M02 and M05

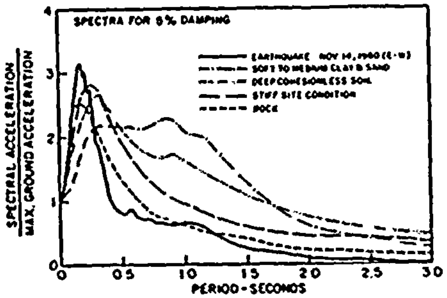

Figure 24. Normalized pseudo-acceleration response spectra

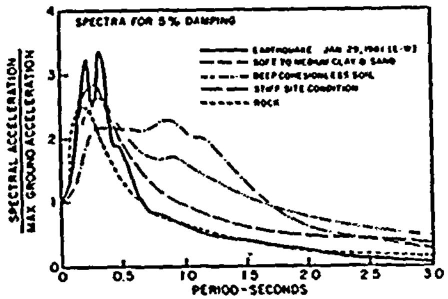

Figure 25. Normalized pseudo-acceleration response spectra

contrast, the cross correlations are relatively low over the entire period range for the motions recorded during the earthquake of 29 January 1981, as shown in Figures 20 and 21, except in the near neighbourhood of certain discrete periods. The significance of the oscillatory character of these cross correlation functions is now under investigation with no definitive conclusion having yet been reached.

Cross correlation coefficients have been generated for components of motion using both time and frequency moving windows. For example, it was generated for the major principal components of motion at stations M02 and M05 as recorded during the earthquake of 14 November 1980 within the time period 9–14 s and within the frequency band 2·6–3·0 Hz; see Figure 22. The resulting cross correlation is plotted against time difference τ in Figure 23. Because of the narrow band character of the components of motion and the

phase angles involved, this function has the appearance of a slowly varying harmonic with a 3·3 s period which peaks at about $\tau = 0{\cdot}47$ s where $\rho \simeq 0{\cdot}8$. The significance of this shape is now being correlated with other information to shed light on the wave transmission characteristics to be reported later.

F. *Pseudo-acceleration response spectra*

Standard normalized pseudo-acceleration response spectra were generated using 5 per cent of critical damping for the components of motion recorded during the earthquake of 14 November 1980 and 29 January 1981. The averages of these spectra for the E–W components of motion are shown plotted against structural period in Figures 24 and 25 where they can be compared with previously published average spectra representing four different soil types.[3] The average spectra for these two earthquakes have shapes which correlate best with the previously published averages for hard site conditions. This observation is not consistent with the relatively soft site conditions of the SMART 1 array which suggests dominant influences from the source mechanism.

CONCLUDING REMARKS

The SMART 1 strong motion array in Taiwan has provided an excellent data base for studying spatial variations of ground motions and their influences on large engineering structures. The methodologies and results presented herein represent the beginning of an expanding research effort in this important area. Much work needs to be done with special emphasis on interpretation of results. Hopefully, the present paper will provide a stimulus in this direction.

ACKNOWLEDGEMENTS

The authors express their sincere thanks and appreciation for the financial support received from the U.S. National Science Foundation and the National Science Council of Taiwan.

REFERENCES

1. B. A. Bolt, Y. B. Tsai, K. Yeh and M. K. Hsu, 'Earthquake strong motions recorded by a large near-source array of digital seismographs', *Earthquake eng. struct. dyn.*, 10, 561–573 (1982).
2. J. Penzien and M. Watabe, 'Characteristics of 3-dimensional earthquake ground motions', *Earthquake eng. struct. dyn.*, 3, 365–373 (1975).
3. H. B. Seed, C. Ugas and J. Lysmer, 'Site-dependent spectra for earthquake-resistant design', *Report No. EERC 74-12*, Earthquake Engineering Research Center, University of California, Berkeley, CA. November 1974.